

**STUDY ON WELD CORROSION OF X65QT PIPELINE
STEEL**

By

**VELU BALRAJ
COLLEGE OF ENGINEERING**

Submitted



**IN PARTIAL FULFILMENT OF THE DEGREE OF
DOCTOR OF PHILOSOPHY**

To

**UNIVERSITY OF PETROLEUM AND ENERGY STUDIES
DEHRADUN**

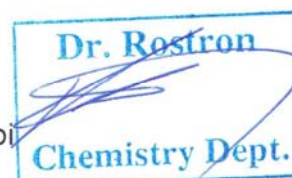
September 2015



CERTIFICATE

This is to certify that the thesis entitled “**Study on Weld Corrosion of X65QT Pipeline Steel**” submitted by **VELU BALRAJ** to University of Petroleum & Energy Studies (UPES), Dehradun for the award of the degree of Doctor of Philosophy is a bona fide record of the research work carried out by him under our joint supervision and guidance. The content of the thesis, in full or parts have not been submitted to any other Institute or University for the award of any other degree or diploma.

External Guide: **Dr. Paul Rostron**
Assistant Professor
Department of Chemistry
Petroleum Institute, Abudhabi
United Arab Emirates



Internal Guide: **Dr. Rajnish Garg**
Professor
Mechanical Engineering Department
UPES, Dehradun, India

Internal Co-Guide: **Dr. Mukesh Saxena**
Pro Vice Chancellor UTM, Shillong,
Ex Professor & Head
Mechanical Engineering Department
UPES, Dehradun, India

Place:

Date:

DECLARATION

I hereby declare that this submission is my own work and that, to the best of my knowledge and belief, it contains no material previously published or written by another person nor material which has been accepted for the award of any other degree or diploma of the university or other institute of higher learning, except where due acknowledgement has been made in the text.



(Balraj Velu)

Date:

ACKNOWLEDGEMENTS

I would like to thank *Prof. Dr. Rajnish Garg and Prof. Dr. Mukesh Saxena*, UPES and *Prof. Dr. Paul Rostron*, Petroleum Institute, Abudhabi, UAE who formed a part of my vision and taught me things which are most important in carrying out the experimental work and writing the research thesis. I would like to acknowledge *Dr. Meenu Mishra and Mr. Sugadaraj Paleri (ex staff) and Mrs. Rakhi Rahul*, UPES for their timely administrative help and advice. I would also like to acknowledge the administrative help extended by UPES staff during this research work.

I am very grateful to *Dr. Chinnapan Mani*, NDT Specialist-CCC, UAE who inspired, helped and guided me to do this study. I am grateful to *Dr. Abozour Mohamed*, GE, UAE who also guided me on experimental works.

I would like to thank *Mr. Sekar, Mr. Abudhahir*, Emirates Industrial laboratory, Abduahbi-UAE, and *Mr. Pramod*, Operations Manager, United Metal Works, Abudhabi-UAE for their help to conduct the experimental works.

I am indebted to my wife *Mrs. Indirani* who gave full support for all my efforts during the course of my research work and also during my entire professional career.

EXECUTIVE SUMMARY

The aim of this research is based on the welding consumable related issues at the pipe line construction sites which were experienced by the author of this thesis. Weld corrosion describes selective attack of the weld itself. The origin of this attack is usually a combination of a more active Weld Metal (the Weld Metal tends to be more susceptible to corrosion than the Base Metal) together with Galvanic Corrosion coupling to the Base Metal. The influence of coupling is accentuated by the poor area ratio, i.e. a small anode Weld Metal / large cathode Base Metal. Preferential Weld Metal corrosion of C-Mn steels has historically been a major problem. On the basis of various studies, early researchers concluded that the weldments of silicon killed C-Mn steels are the most electronegative (i.e. cathodic) and the unkilld steels with a low silicon content are the most electro positive. Weld Metal Zones of the welds made with the normal basic-coated electrodes exhibit most electro negative potential and with the acid types exhibit most electropositive whilst the potentials of the Weld Metal Zone of the welds made with rutile electrodes are placed in an intermediate position. The Weld Metals are usually more electronegative than the Base Metal depending upon relative silicon content. The operating conditions can change the weld behaviour from anodic to cathodic or vice versa at any stage during the process.

Preferential HAZ corrosion of a carbon steel weld occurs in a wide range of environments. The precise microstructural / electrochemical basis for the enhanced local activity of the HAZ is not fully clarified although it is known to be associated with hardened microstructures. It is considered that there are local micro cathodes formed on the surface in the HAZ which stimulate the corrosion process. However, this seems insufficient since the presence of such cathodes implies that this region is nobler than the Base Metal. In such situation, coupling to the Base Metal results in a coupled potential similar to that of the Base Metal itself, since the area of the HAZ is relatively small. An explanation is required on the basis of an increase in anodic activity of the HAZ rather than a simple cathodic activity. This is necessary since occurrence of failures in fairly high conductive solutions indicates that coupling to the Base Metal is effective.

The weld corrosion has been studied and reported by various authors in the recent past for specific applications. There are many reports available on corrosion prediction models to calculate the corrosion rate. But the models give differences in predicted corrosion rates and it all depends on how various parameters are treated and how much conservatism or assumptions are inbuilt in the model. For pipeline, all the operators now go for API X65/X65QT materials which provide added advantage over other lower grade materials due to higher strength which helps in reducing the wall thickness. Corrosion rate depends upon the electrochemical and mass transport processes that occur simultaneously on and close to the corroding metal surface. In this study, the corrosion of three different Weld Zones (Weld Metal Zone, HAZ and Base Metal) of the welds made by SMAW process using four different welding

electrodes (E7018, E8018G, E8018B2 and E8018B6) have been studied under aerated condition. The general and galvanic corrosion characteristics are studied under room temperature. In addition, the corrosion characteristics are studied at various temperatures with/without CO₂ environment. The results have shown that the hardness is insignificant for corrosion of these welds. The Heat Affected Zone (HAZ) shows minimum three times higher corrosion level than the Weld Metal Zone at room temperature. In general, addition of Si and Cr reduces corrosion resistance and the results reveal that these elements impart significant corrosion resistance comparable to that of Ni. The Weld Metal with high Cr content exhibits more anodic than the Weld Metal with high Ni content though Cr also reduces corrosion level. Also, Weld Metal with high Cr level exhibits more anodic than Weld Metal with low Cr level. The Weld Metal Zone of E7018 weld behaved anodic throughout the experiment till 80 °C . The HAZs of all the welds (except E7018 Weld Metal Zone) behaved as anodic up to 40 °C. The highest corrosion rate has been observed with E7018 electrode weld. The Base Metal behaved as anodic initially till 50 °C and then became cathodic. All other welds (E8018B2 and E8018G Weld Metals) resulted as cathodic at temperatures throughout the test duration. The overall corrosion behaviour of Weld Metal Zones of all the welds was cathodic under CO₂ environment which is a significant phenomenon at pH value of 5. The curve fitting was done using MINITAB statistical software and degree of fitness found very good. The equations formed by Polynomial regression analysis can be used to determine the corrosion rate for various temperatures under the absence or presence of CO₂ and aerated conditions.

TABLE OF CONTENTS

THESIS COMPLETION CERTIFICATE	ii
DECLARATION	iii
ACKNOWLEDGEMENTS	iv
EXECUTIVE SUMMARY	v
TABLE OF CONTENTS.....	viii
LIST OF FIGURES	xiv
LIST OF TABLES	xix
LIST OF ABRIVIATIONS.....	xx
CHAPTER 1. INTRODUCTION	1
1.1. Overview and motivation for the study	1
1.2. Research objectives.....	5
1.3. Research methodology	7
1.4. Thesis chapter scheme	8
CHAPTER 2. LITERATURE REVIEW	10
2.1. Introduction.....	10
2.1.1. Welding process-Shielded Metal Arc Welding (SMAW) .	10
2.1.2. Weld metal solidification.....	11

2.1.3. Gas and slag metal reaction	12
2.1.4. Heat flow and residual stress	13
2.1.5. Weld formation and microstructure	17
2.2. Corrosion – Theoretical background	20
2.2.1. Electro chemistry	20
2.2.2. Forms of corrosion.....	22
2.3. Material degradation mechanisms in oil and gas fields	22
2.3.1. General CO ₂ Corrosion	23
2.3.2. Wet Hydrogen sulphide	23
2.3.3. Elemental sulphur	23
2.3.4. Erosion corrosion.....	23
2.3.5. Microbiologically induced corrosion (MIC).....	25
2.3.6. Effect of Water, Oxygen and chloride	25
2.3.7. Under deposit corrosion.....	27
2.3.8. External Corrosion	27
2.3.9. General Galvanic Corrosion	28
2.3.10. Liquid metal embrittlement.....	29
2.3.11. Low temperature embrittlement.....	29
2.3.12. Types of Corrosion in pipelines	30
2.3.13. Bottom of line corrosion	30
2.3.14. Top of line corrosion.....	30
2.3.15. General Weld Corrosion	31
2.4. Conditions over field life	31
2.4.1. Declining reservoir pressure	31

2.4.2. Sulphide reducing bacteria.....	31
2.4.3. Particular operating conditions	32
2.4.4. Geometrical factors.....	32
2.5. CO ₂ Corrosion.....	32
2.5.1. Effect of pH.....	34
2.5.2. Effect of temperature	34
2.5.3. Effect of CO ₂ partial pressure	35
2.5.4. Effect of fluid flow.....	35
2.5.5. Effect of saturation.....	36
2.5.6. Corrosion product film formation.....	36
2.5.7. Preferential weld corrosion	39
2.5.8. Corrosion of welded line pipe.....	43
2.6. Types of weld corrosion in oil and gas industry	45
2.6.1. Galvanic Corrosion	45
2.6.2. Environmentally assisted cracking	46
2.6.3. Hydrogen induced cracking	46
2.6.4. Stress corrosion cracking	49
2.6.5. Corrosion rate calculation basis	49
3. EXPERIMENTAL PROCEDURE.....	51
3.1. Welding.....	51
3.1.1. Base Metal	51
3.1.2. Welding electrode	51
3.1.3. Welding power source	52
3.1.4. Weld samples	55

3.1.5. Chemical composition testing.....	55
3.1.6. Weld macro hardness testing	56
3.1.7. Weld metallography.....	58
3.2. Corrosion testing.....	58
3.2.1. Electrochemical testing methods	60
3.2.2. Corrosion testing cell-potentiostat and electrodes	61
3.2.3. Linear polarization resistance (LPR) method	62
3.2.3.1. Polarization resistance	66
3.2.3.2. Calculation of corrosion rate from corrosion current	67
3.2.3.3. IR compensation	69
3.2.3.4. Current and voltage conventions	71
3.2.4. Three electrode polarization resistance technique	72
3.2.4.1. Equipment used.....	72
3.2.4.2. Test procedure.....	73
3.3. Galvanic Corrosion current measurement	74
3.3.1. Test procedure.....	77
4. RESULTS	79
4.1. Welding test results.....	79
4.1.1. Chemical composition of Weld Metal	79
4.1.2. Micro Hardness Results	80
4.1.3. Weld Microstructure	81
4.2. Corrosion test results.....	89
4.2.1. General and Galvanic Corrosion at room temperature	89
4.2.2. Galvanic Corrosion at various temperatures.....	99

4.2.3. Galvanic Corrosion at various temperatures with CO ₂	104
4.3. Statistical analysis-Polynomial regression response model.....	113
4.3.1. Data analysis of variance	115
5.5. DISCUSSIONS.....	118
5.1. Weld Metal analysis.....	118
5.1.1. Chemical composition	118
5.1.2. Micro hardness.....	119
5.1.3. Weld microstructures	120
5.2. Corrosion test results.....	121
5.2.1. General and Galvanic Corrosion at room temperature	121
5.2.2. Galvanic Corrosion at various temperatures.....	127
5.2.3. Galvanic Corrosion at various temperatures under CO ₂ environment.....	129
5.3. Statistical analysis-Polynomial regression response model.....	134
6. CONCLUSIONS	135
LIMITATIONS AND FUTURE SCOPE OF WORK.....	138
1. Limitations	138
2. Future research.....	138
REFERENCES.....	139
PUBLISHED PAPERS.....	150
APPENDICES	151
APPENDIX A: Weld macro hardness test results	152
APPENDIX B: Corrosion testing - recorded traces.....	156

APPENDIX C: Polynomial Regression Analysis Curve Fitting

Graphs 199

APPENDIX D: Scholar profile 214

LIST OF FIGURES

- 1.1a. PWRC of 316 Stainless Steel
- 1.1b. Corrosion Failure at HAZ
- 1.2. PWRC of X65 Steel
- 1.3. Block Diagram of Experiment Plan
- 2.1. Schematic Diagram of SMAW Process
- 2.2. Weld Thermal Cycle in Carbon Steel (Typical)
- 2.3. Metallurgical Zones in a Typical Weld
- 2.4. Weld Cross Section (Typical Macro)
- 2.5. Color Micrograph (Klemm's I Tint Etching) of Weld Zones
- 2.6. Weld Metal – Fully Anodic.
- 2.7. Typical Weld Defects
- 2.8. PWRC of Failed Pipeline
- 2.9. Weld HAZ Corrosion
- 2.10. Cause and Effect Diagram for PWRC.
- 2.11. Effect of Micro Alloying Elements on Corrosion
- 3.1. Welding Rectifier
- 3.2. Welding Set Up.
- 3.3. Welded Samples
- 3.4. Etched Weld Specimens for Micro Hardness Testing
- 3.5. HV10 -Hardness Measurement Scheme as per NACE-MR 0175
- 3.6. Weld Samples Prepared for Corrosion Testing
- 3.7. Gamry Potentiostat Instrument
- 3.8. Corrosion Testing Cell set up

- 3.9. Tafel Plot
- 3.10. R_p - Slope of the Tangent at Zero Current
- 3.11. Data Input Pull Down Menu
- 3.12. Electric Circuit for Zero Resistance Ammeter
- 4.1. Micro Hardness Results
- 4.2. Base Metal X65QT Steel at 200X
- 4.3a. E8018G Weld Metal at 200X for 6-9 'O' clock position
- 4.3b. E8018G HAZ at 200X for 6-9 'O' clock position
- 4.3c. E7018 Weld Metal at 200X for 6-9 'O' clock position
- 4.3d. E7018 HAZ at 200X for 6-9 'O' clock position
- 4.3e. E8018B6 Weld Metal at 200X for 6-9 'O' clock position
- 4.3f. E8018B6 HAZ at 200X for 6-9 'O' clock position
- 4.3g. E8018B2 Weld Metal at 200X for 6-9 'O' clock position
- 4.3h. E8018B2 HAZ at 200X for 6-9 'O' clock position
- 4.4a. E8018G Weld Metal at 100X for 9-12 'O' clock position
- 4.4b. E8018G HAZ at 100X for 9-12 'O' clock position
- 4.4c. E7018 Weld Metal at 100X for 9-12 'O' clock position
- 4.4d. E7018 HAZ at 100X for 9-12 'O' clock position
- 4.4e. E8018B6 Weld Metal at 100X for 9-12 'O' clock position
- 4.4f. E8018B6 HAZ at 100X for 9-12 'O' clock position
- 4.4g. E8018B2 Weld Metal at 100X for 9-12 'O' clock position
- 4.4h. E8018B2 HAZ at 100X for 9-12 'O' clock position
- 4.5. Corrosion Rate Calculated by the Software
- 4.6. LPR Recording for E8018B2 Weld Metal

- 4.7. Galvanic Corrosion Tracing for E8018G Weld Metal
- 4.8. Galvanic Corrosion of E7018 Weld at Room Temperature
- 4.9. Galvanic Corrosion of E8018G Weld at Room Temperature
- 4.10. Galvanic Corrosion of E8018B2 weld at Room Temperature
- 4.11. Galvanic Corrosion of E8018-B6 at Room Temperature
- 4.12. Galvanic Corrosion of Weld Metals of Different Welds and Base Metal at Room Temperature
- 4.13. Galvanic Corrosion of HAZ of Different Welds at Room Temperature
- 4.14. Corrosion Tested Weld (E7018) with Lack of Root Fusion and Undercut
- 4.15. Corrosion Behaviour With / Without Defect -Weld E7018
- 4.16. Total Corrosion Rate for Base Metal and Weld Metal for Various Welds
- 4.17. Total Corrosion Rate for Weld Metal and HAZ for Various Weld
- 4.18. Galvanic Corrosion of E7018 weld at various temperatures
- 4.19. Galvanic Corrosion of E8018G weld at different temperatures
- 4.20. Galvanic Corrosion of E8018B2 weld at various temperatures
- 4.21. Galvanic Corrosion of E8018B6 weld at various temperatures
- 4.22. Galvanic Corrosion of Base Metal and Weld Metal Zones of Different Welds at Various Temperatures.
- 4.23. Galvanic Corrosion of Base Metal and HAZs of Different Welds at Various Temperatures.
- 4.24. Galvanic Corrosion of E7018 Weld in CO₂ Environment at Various Temperatures

- 4.25. Galvanic Corrosion of E8018G Electrode Weld in CO₂ Environment at Various Temperatures
- 4.26. Galvanic Corrosion of E8018B2 Electrode Weld in CO₂ Environment at Various Temperatures
- 4.27. Galvanic Corrosion of E8018B6 Electrode Weld in CO₂ Environment at Various Temperatures
- 4.28. Galvanic Corrosion of HAZs in CO₂ Environment at Various Temperatures for all the Welds
- 4.29. Galvanic Corrosion of Weld Metal Zones in CO₂ Environment at Various Temperatures
- 4.30. Effect of CO₂ and Temperature on the Corrosion of Base Metal
- 4.31. Effect of CO₂ and Temperature on the Corrosion of E7018 Weld Metal Zone
- 4.32. Effect of CO₂ and Temperature on the Corrosion of E8018G Weld Metal Zone
- 4.33. Effect of CO₂ and Temperature on the Corrosion of E8018B2 Weld Metal Zone
- 4.34. Effect of CO₂ and Temperature on the Corrosion of E8018B6 Weld Metal Zone
- 4.35. Effect of CO₂ and Temperature on the Corrosion of HAZ of E7018 weld
- 4.36. Effect of CO₂ and Temperature on the Corrosion of HAZ of E8018G weld

- 4.37. Effect of CO₂ and Temperature on the Corrosion of HAZ of E8018B2 weld
- 4.38. Effect of CO₂ and Temperature on the Corrosion of HAZ of E8018B6 weld
- 4.39. Regression Response Model for Weld Metal Zone of E8018G weld under CO₂ environment at various Temperatures
- 4.40 a. Plot for the Weld Metal Zone
- 4.40 b. Plot for the HAZ

LIST OF TABLES

Table 1.1	Responses to be Studied
Table 2.1	Factors Influencing Galvanic Corrosion
Table 3.1	Chemical Composition of Base Metal
Table 3.2	Chemical Composition of Electrodes
Table 3.3	Welding Parameters of E8018G Weld
Table 3.4	Welding Parameters of E7018 Weld
Table 3.5	Welding Parameters of E8018B6 Weld
Table 3.6	Welding Parameters of E8018B2 Weld
Table 3.7	Corrosion rate constants
Table 4.1	Weld Chemical Composition
Table 4.2	Heat Input and Micro Hardness of Different Weld Zones
Table 4.3a	Microstructure of different weld zones at 6-9 'O' Clock Position
Table 4.3b	Microstructure of different weld zones at 9-12 'O' Clock Position
Table 4.4	Heat Input and Corrosion Rate of Different Weld Zones
Table 4.5	Design Matrix Data for ANOVA Analysis

LIST OF ABBRIVIATIONS

ANOVA	–	Analysis of variance
API	–	American petroleum institute
ASME	–	American society of mechanical engineers
ASTM	–	American society for testing of materials
BSEN	–	British standard European norms
C.Eq.	–	Carbon Equivalent
CO ₂	–	Carbon di oxide
CR	–	Corrosion rate
CS	–	Carbon steel
CRA	–	Corrosion resistance alloy
EAC	–	Environmental assisted crack
EDM	–	Electric discharge machining
ERW	–	Electrical resistance welding
GC	–	Galvanic Corrosion
GMAW	–	Gas metal arc welding
GTAW	–	Gas tungsten arc welding
HFIW	–	High frequency induction welding
HIC	–	Hydrogen Induced cracking
H ₂ S	–	Hydrogen sulphide
H ₂	–	Hydrogen

HR _C	–	Rockwell hardness C scale
HV	–	Hardness Vickers
HAZ	–	Heat affected zone
LPR	–	Linear polarization resistance
N ₂	–	Nitrogen
NACE	–	National Association of Corrosion Engineers
O ₂	–	Oxygen
PWRC	–	Preferential weld root corrosion
PWHT	–	Post weld heat treatment
QT	–	Quenched and tempered
R _p	–	Polarization resistance
SCC	–	Stress corrosion cracking
SMAW	–	Shielded metal arc welding
SOHIC	–	Stress orientated hydrogen induced cracking
SAW	–	Submerged arc welding
SRB	–	Sulphide reducing bacteria
ZRA	–	Zero resistance ammeter

CHAPTER 1- INTRODUCTION

1.1. OVERVIEW AND MOTIVATION FOR THE STUDY

Onshore and offshore oil and gas facilities are constructed to satisfy ASME codes and API standards etc. The process piping and the equipments are fabricated using carbon steel products like seamless pipes & fittings, welded pipes, forgings and metals using material grades such as A106 Gr. B, A 516 Gr. 70 etc. For Pipelines, API X52, X60 and X65 materials are being used. As per NACE standard MR 0175 (ISO15156), the limitation is imposed on hardness as 22 HR_C to avoid stress corrosion cracking or Hydrogen induced cracking. In the recent past, operators prefer API X65QT material for pipelines due to various advantages though fabrication practice imposes additional care on welding and electrode selection as it has the typical chemical composition range. The quenched and tempered steels are normally supplied under heat treated conditions. It involves austenitizing, quenching and tempering to obtain high strength properties. This material normally consists of low carbon martensite and bainite microstructures. The major concerns are avoidance of martensite formation in the HAZ and strict low hydrogen welding practice in order to prevent cold cracking. Pipelines are welded using SMAW, SAW and GMAW processes. The matching electrodes are selected to satisfy the pipeline welding standard ‘API 1104–Welding of pipelines and related facilities’.

Material selection is carried out to suit the particular operating fluid temperature, pressure and composition etc. With any combination of these parameters, weld is more vulnerable for corrosion than the Base Metal. It is well known fact that the weld properties are different from that of Base Metal on many aspects due to the rate of heat input (rate of melting and solidification during welding). Hence the weld can act as anodic or cathodic depending upon the properties. The corrosion behaviour of carbon steel welds produced by fusion welding is dependent on number of factors. Corrosion of carbon steel welds can be due to metallurgical effects, such as preferential corrosion of the HAZ or Weld Metal, or it can be associated with geometrical aspects, such as stress concentration at the weld toe, or creation of crevices due to joint design, hardness level, impurities like Si, P, S and slag inclusions etc. Additionally, specific environmental conditions can induce localized corrosion such as temperature, conductivity of the corrosive fluid, or thickness of the liquid corrosive film in contact with the metal. In some cases, both metallurgical and geometric factors may influence corrosion behaviour, such as in stress corrosion cracking (SCC). Preferential weld root corrosion (PWRC) describes selective attack of the weld itself. The corroded and failed stainless steel pipe in one of the offshore platforms is shown in Figs.1.1a & b.

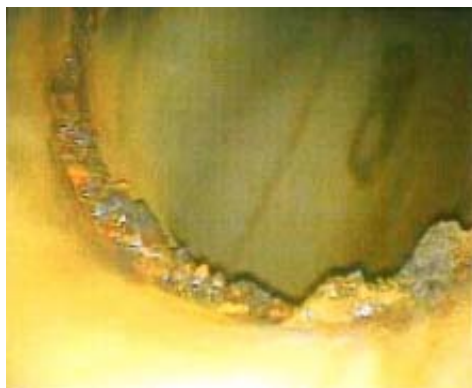


Figure 1.1a: PWRC of 316 Stainless Steel [1]



Figure 1.1b: Corrosion Failure at HAZ [1]

The above stainless steel (316L) pipe was hydro tested with sea water by mistake and was not flushed and treated properly immediately after the test. The stagnated water which contained chlorine led to preferential weld corrosion and failed. The corroded weld in one of the offshore carbon steel pipeline is shown in Fig. 1.2.



Figure 1.2: PWRC of X65 Steel [2]

The origin of this attack is usually a combination of a more active Weld Metal (the Weld Metal tends to be more susceptible to corrosion than the Base Metal in isolation) with galvanic coupling to the Base Metal. The influence of coupling is accentuated by the poor area ratio i.e. a small anode Weld Metal / large cathode Base Metal. Preferential Weld Metal corrosion of C-Mn steels has historically been a major problem. The following conclusions have been drawn by various studies [3-5]:

- In the welding of C-Mn steels, the silicon killed steels are the most electronegative (i.e. cathodic) and the unkilld steels with a low silicon content are the most electropositive (anodic).
- Of the Weld Metals, the normal basic-coated electrodes exhibit more electronegative potential and the acidic types exhibit the most electropositive whilst the potentials for the Weld Metal from rutile electrodes are placed in an intermediate position.
- The Weld Metals are usually more electronegative than the Base Metal depending upon the relative silicon content.
- The operating conditions can change the weld anodic or cathodic at any stage.

It has been reported that the low hydrogen electrodes give rise to enhanced corrosion of the Weld Metal [6]. The use of low alloy steel filler metals produces the weld which always behaves cathodic to the Base Metal. Nevertheless, corrosion of the HAZ still poses problem for some applications and depends on the rate of cooling and the level of Mn in the steel. These parameters affect the extent of martensite formation and the grain size, although the impact of the later on corrosion is likely to be marginal. The net effect is that the HAZ becomes anodic to the Base Metal.

Preferential HAZ corrosion of carbon steel weld has been reported to occur in a wide range of environments. The precise microstructural and electrochemical basis for the enhanced local activity of the HAZ is not fully clarified although it is known to be associated with hardened microstructures. It is considered that there are local micro cathodes formed on the surface in the HAZ which stimulates the corrosion process. However, this seems to be

insufficient since the presence of such cathodes also implies that this region is nobler than the Base Metal. If this is the case, coupling to the Base Metal results in a coupled potential similar to that of the Base Metal itself, since the area of the HAZ is relatively small. Hence, the reason for the increased anodic activity of the HAZ has to be explored. This seems to be necessary since failures occurring in solutions having fairly high conductivity indicate that coupling to the Base Metal is effective [7].

The weld corrosion has been studied and reported by various authors in the recent past for specific applications. Many mathematical models have been proposed on the prediction of corrosion rate. However, these models give various corrosion rate predictions depending on how various parameters are treated and how much conservatism or assumptions are inbuilt in the model. Corrosion rate depends upon the effect of electrochemical and mass transport process that occurs simultaneously on and close to the corroding metal surface [8].

Pipeline steel is selected in such a way that it reduces the material cost for the designed life. As API X65QT steel is favoured by the operators, this material is considered to study the corrosion characteristics.

1.2. RESEARCH OBJECTIVES

The welding electrodes are kept in ovens at sites. There are practical instances that the electrodes get mixed up at pipeline construction sites. Hence, four types of electrodes have been selected to find out the influence of these electrodes on corrosion characteristics of the weld. The detailed experimental plan is shown in Fig. 1.3.

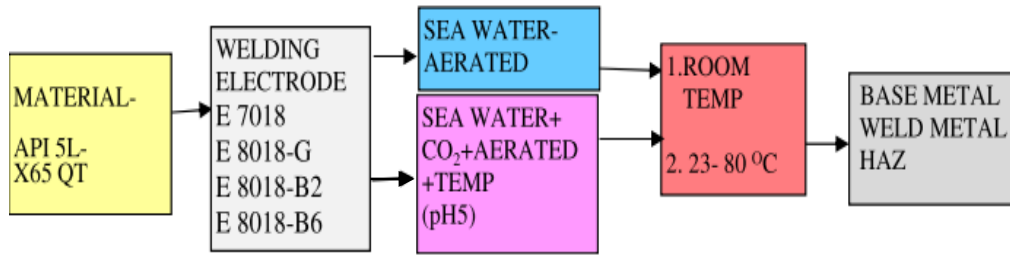


Figure 1.3: Block Diagram of Experiment Plan

The Table 1.1 lists the detail of the responses to be studied. This investigation has been taken to determine the corrosion characteristics of various welds in saline and CO₂ environment at various temperatures which is encountered in the actual field condition.

Table 1.1 - Responses to be Studied

Objectives	Responses to be Studied
1. General corrosion behaviour at room temperature.	1. Total corrosion 2. Galvanic Corrosion 3. Defective weld behaviour 4. Effect of Microstructure 5. Effect of Hardness 6. Effect of Composition
2. Effect of Temperature on Galvanic Corrosion (sea water aerated).	1. Galvanic Corrosion - aerated . 2. Effect of Microstructure 3. Effect of Hardness 4. Effect of Composition
3. Effect of Temperature on Galvanic Corrosion (sea water aerated + CO ₂ at pH 5).	1. Galvanic Corrosion -aerated CO ₂ . 2. Effect of Microstructure 3. Effect of Hardness 4. Effect of Composition

The objectives of present investigation are:

1. To determine the general and Galvanic corrosion characteristics of X65QT pipeline steel welds at room temperature.
2. To determine the corrosion characteristics of different weld zones of the welds prepared by SMAW process at different temperatures with / without CO₂ environment.
3. Corrosion mapping of different weld zones for four types of electrodes (E7018, E8018G, E8018B2 and E8018B6).
4. Statistical analysis of the experimental data using Surface Response Model.

1.3. RESEARCH METHODOLOGY

Corrosion data on carbon steel pipe works are well established. Many models also have been developed by NORSOK M506, De Waard, Gray and Nesic et.al [9, 10]. All these models are applicable only to the base material with some assumptions. The rate of attack under various environments is well established. However, there is a concern in the oil industry on the effect of electrodes for welding due to recurrence of preferential corrosion of welds in various environments. Corrosion attacks have been observed on the welds made using SMAW electrodes which have Ni or Ni / Cu as a part of composition. Most commonly used materials for pipelines and flow lines are ASTM A 106 Gr. B, API X60 / X65 etc. From the available published data till date, it is not possible to predict the rate of corrosion, the location of attack,

the effectiveness of corrosion inhibitors etc. The weld root corrosion characteristics reflect that once corrosion is initiated, it continues and propagates from the root. This localized corrosion at the weld root is not clearly understood. Considering the worst possible scenario in the field, the root weld corrosion has been studied with aerated sea water and CO₂ conditions at different temperatures as follows:

1. UNIFORM CORROSION at room temperature in aerated sea water.
2. GALVANIC CORROSION at room temperature in aerated sea water.
3. GALVANIC CORROSION at different temperatures (25 - 80 °C) in aerated seawater with an interval of 5 °C.
4. GALVANIC CORROSION at different temperatures (25 - 80 °C) in CO₂ + Aerated sea water at pH 5 with an interval of 5 °C.

1.4. THESIS CHAPTER SCHEME

The following chapters are laid out in sequence. The Chapter-1, describes the motivation of this study, research objectives and methodology and the thesis structure. Chapter-2 gives the literature review to get the overall insight to the corrosion issues in Oil and Gas field in present scenario. Chapter-3 gives the detail of research approach to the selected problem and the types of experiment to get meaningful result to quantify the weld corrosion. The results are presented to meet the objective of the research study in Chapter-4. The detailed discussion on the results are presented in Chapter- 5. The conclusions derived from experimental results are discussed in Chapter-6. The limitations

in conducting the experimental works and the scope for the future research work are discussed after conclusions. The list of references is given at the end of the thesis. The supporting documents for the detailed experimental works such as actual recordings etc. are provided as Appendices.

CHAPTER 2 - LITERATURE REVIEW

2.1. INTRODUCTION

The welding of pipelines is being carried out using mainly SMAW and GMAW processes. The process details of SMAW are described in this chapter as it is used for experimental work. There are three types of coated welding electrodes such as basic coated, cellulosic and rutile type. Generally, basic coated electrodes are being used in Oil and Gas facility constructions. The process details are discussed below.

2.1.1. SHIELDED METAL ARC WELDING (SMAW) PROCESS

The electrode consists of a metallic core which serves as the electrode conductor and supplies the filler metal and the coating contributes to the formation of a protective slag. The molten metal and slag volatilize in the arc plasma to stabilize the arc column. The process sketch is shown in Fig. 2.1.

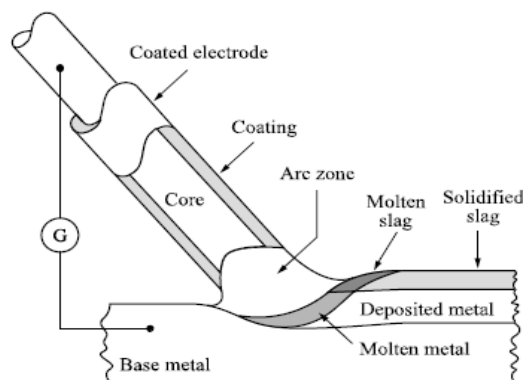


Figure 2.1: Schematic Diagram of SMAW Process

This process is also called electrode arc welding process as the electrode is consumed during welding. The electrode coating can be cellulosic (creates little slag but releases CO₂) by which the arc force is increased and good weld penetration is achieved. The rutile type electrode has titanium oxide in its coating which contributes to the desulphurization of molten metal during welding. The binding agents used in the coating releases hydrogen. The basic type coating has calcium carbonate which releases hydrogen but it is hygroscopic and so requires baking of electrodes at 300 °C. Rutile-Basic mixed coating or rutile-cellulosic type are also proposed for welding of piping and pipelines. These coatings contain metal powders to increase the deposition rate and alloying elements. A constant current is used in this welding process and process characteristic is termed as drooping arc characteristic.

2.1.2. WELD METAL SOLIDIFICATION

Solidification occurs spontaneously by equi-axial growth on the partially melted region. The factors such as temperature gradient, composition and rate of solidification are responsible for this growth. Pre or post weld heat treatment controls this solidification significantly. During growth of the solid in the weld pool, the shape of the solid–liquid interface controls the development of microstructural features [11]. The nature and the stability of the solid-liquid interface are mostly determined by the thermal and constitutional conditions that exist in the intermediate vicinity of the interface. The interface growth can be planar, cellular or dendritic. Solute

distribution during weld pool solidification is an important phenomenon resulting in segregation, microstructure and properties [12].

2.1.3. GAS AND SLAG METAL REACTION

Reactive gases (especially N_2 , O_2 and H_2) may be present in the arc atmosphere due to surface contamination, imperfect shielding etc. These gases dissociate in the arc and react rapidly with the turbulent liquid metal at high temperatures. Once dissolved in the metal, oxygen and nitrogen may combine with deoxidisers such as Si or Al. The resulting oxides or nitrides remain as small inclusions in the weld metal. Excess dissolved gases are rejected during solidification and may cause porosity. The dissolved hydrogen can develop cracks at the grain boundary and later, reacts with corrosion products [13].

Flux and slag interact with the molten metal. The cleanliness and properties of the weld metal depend upon the oxidation potential of the arc atmosphere and on the type of flux [14]. The basic type flux reduces the oxygen content level in the weld metal. Acidic flux tends to give higher oxygen contents and poor notch toughness. Through coating, the weld metal composition also changes by transfer of alloying elements from the molten slag to the liquid metal. Though inclusions are allowed to some limits in terms of number and size in the weld, the trapped slag inclusions can reduce the strength of the weld and may also act as sites for further degradation of the weld metal [15].

2.1.4. HEAT FLOW AND PROPERTIES

During fusion welding, the thermal cycles produced by the moving heat source cause physical state changes, metallurgical phase transformation, transient thermal stress and metal movement. Figure 2.2 shows the transformation details.

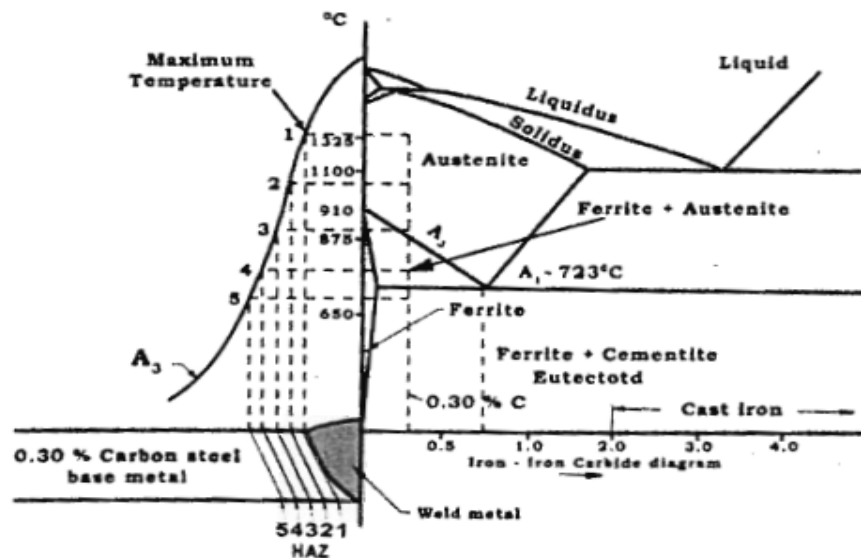


Figure 2.2: Weld Thermal Cycle in Carbon Steel (Typical) [16]

After welding is completed, the finished product may contain physical discontinuities due to rapid solidification or may have adverse microstructures due to inappropriate cooling or may have residual stress and distortion due to the existence of incompatible plastic strains. The welding heat source moves at a constant speed along a straight path. The end result, after either initiating or terminating the heat source, is the formation of a transient thermal state in the weld. At some point after heat-source initiation but before termination, the temperature distribution is stationary or in thermal equilibrium with respect to the moving coordinates. The origin of the moving coordinates coincides with the center of the heat source.

The intense welding heat melts the metal and forms a molten pool. Some of the heat is conducted to the base metal and some is lost either from the arc column or metal surface to the environment surrounding the joint [17]. Three metallurgical zones are formed in the metal upon completion of the thermal cycle; the Weld Metal Zone (WMZ), the Heat Affected Zone (HAZ), and the Base Metal (BM). The macro and micro samples are shown in Figs. 2.3 - 2.5.

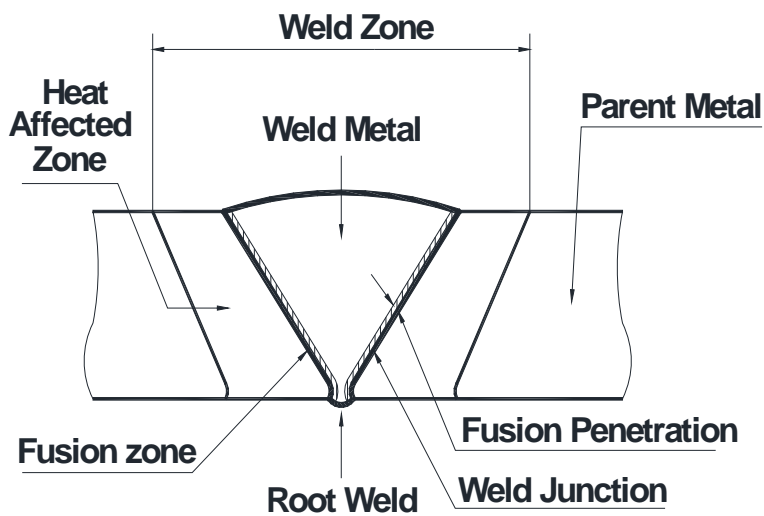


Figure 2.3: Metallurgical Zones in a Typical Weld

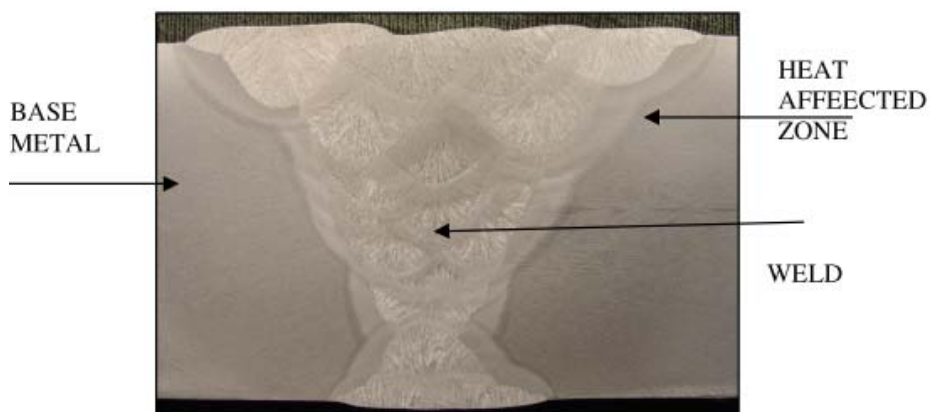


Figure 2.4: Weld Cross Section (Typical Macro)

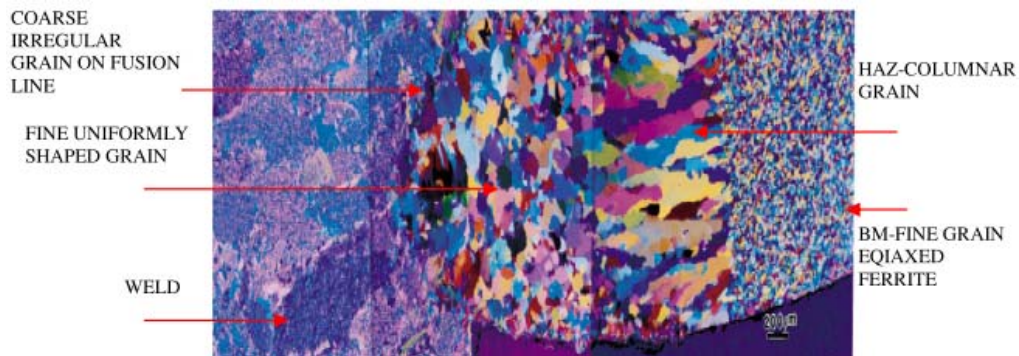


Figure 2.5: Color Micrograph (Klemm's I Tint Etching) of Weld Zones [18]

The Fig. 2.5 by Klemm's I tint color etching process shows three types of grains in the HAZ alone. The peak temperature and the subsequent cooling rates determine the HAZ microstructure, whereas the thermal gradients, the solidification rates determine the microstructure of the weld metal. The size and flow direction of the pool determine the amount of dilution (extent of molten electrode and base metal mixing in the weld pool) and weld penetration. Dilution is defined as the ratio of total weight of fused material over weight of parent metal melted and expressed in percentage. The material response in the temperature range near to melting temperature is primarily responsible for the metallurgical changes. Two thermal states; quasi-stationary and transient are associated with the welding process. The transient thermal response occurs during the source initiation and termination stages of welding. The termination stage of welding is of great metallurgical interest. Hot cracking usually begins in the transient zone, because of the non equilibrium solidification of the base metal. A crack that forms in the source-initiation stage may propagate along the weld if the solidification strains sufficiently multiply in the wake of the welding heat source. During source termination, the weld pool solidifies several times faster than the Weld Metal in the quasi-

stationary state. Cracks usually appear in the weld crater and may propagate along the weld. Rapid cooling results in a brittle HAZ structure and either causes cracking problem or creates a site for fatigue-crack initiation. The quasi-stationary thermal state represents a steady state thermal response of the weld with respect to the moving heat source. The significant thermal expansion and shrinkage in the base material occur during the quasi-stationary thermal cycle. Residual stress and weld distortion are the thermal stress and strain that remain in the weld after completion of the thermal cycle. In general, up to 25 mm thickness, a two dimensional heat flow and beyond this thickness, a three dimensional heat flow is considered. However, ASME 31.3 process piping code calls for heat treatment beyond 19 mm thickness to reduce the heat flow effects. Hence, the cooling rate has significant effect on the microstructure formation and induction of residual stresses. In a three dimensional heat flow, the base metal acts as a heat sink and the cooling rate is considered very high. For this reason, preheating and post heating are specified by the construction codes. The cooling rate influences the final microstructure and hardness in different regions of the weld. Generally, a fine grained soft structure is preferred. Hence, the hardness is limited to 22 HRC (248 BHN) by NACE MR 0175 (ISO 15156). Depending upon the environmental conditions, Weld Metal or HAZ or Base Metal is corroded. A typical preferential corrosion of weld is shown in Fig. 2.6, which is fully anodic [19].

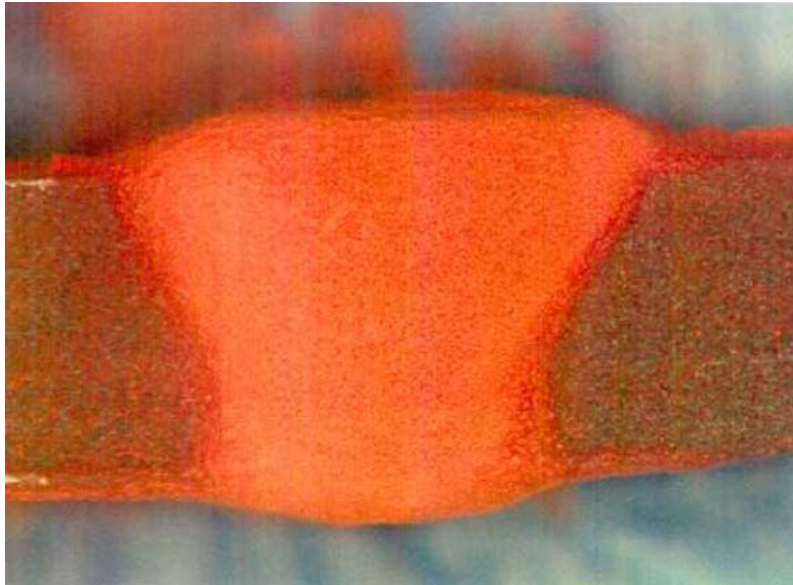


Figure 2.6: Weld Metal – Fully Anodic.

During welding, the Base Metal, HAZ, and underlying weld passes experience stresses due to thermal expansion and contraction. On solidification, residual stresses of high magnitude, often close to the material yield stress, are present as a result of weld shrinkage. Stress-concentration effects due to geometrical discontinuities such as weld reinforcement (excess Weld Metal) and lack of adequate weld penetration also becomes important due to the possibility of SCC in some environments [16].

2.1.5. WELD FORMATION AND MICROSTRUCTURE

Weld Metals inherently possess compositional and microstructural heterogeneities. It consists of transition from wrought Base Metal to solidified Weld Metal through HAZ. This includes five microstructural distinct regions such as fusion zone, the unmixed region, the partially melted region, the HAZ and the unaffected Base Metal. The unmixed region is a part of the fusion zone and the partially melted region is a part of the HAZ. The fusion zone is the result of melting the Base Metal and filler metal simultaneously leading to

a composition different from that of the Base Metal. Composition difference produces galvanic couple. A thin region within the fusion zone where the Base Metal melts and quickly solidifies is called unmixed (chilled) region. It has a composition similar to the Base Metal. The HAZ experiences peak temperature, high enough to produce solid state microstructural changes but too low for melting. In Every weld position, HAZ experiences a maximum temperature and cooling rate and may have its own microstructure and corrosion susceptibility. The unaffected Base Metal does not undergo any microstructural change. However, the Weld Metal may have residual shrinkage stress depending upon the restraint imposed on the weld. Microstructural gradient exists within the HAZ as shown in Fig. 2.5. The Weld Metal may have chemical composition variations due to micro-segregation during solidification [20]. The major defects or imperfections which may result in welds are shown in Fig. 2.7.

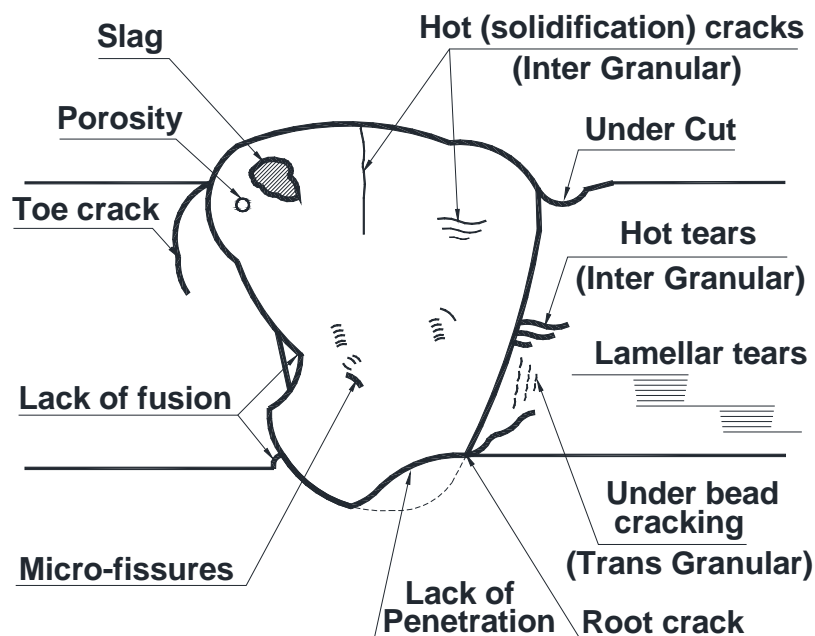


Figure 2.7: Typical Weld Defects

Apart from the microstructural effects, the weld defects also can be a source for corrosion initiation in various forms. The base metal undergoes various temperatures ranging from ambient at a distance away from the weld centre to the melting point at the fusion boundary during welding. Therefore, metallurgical transformations occur across the weld metal and HAZ. These microstructures can significantly alter the intrinsic corrosion rate of the steel. Due to the high cooling rate, fusion welding produces a weld metal that is effectively like a chill casting containing a high density of lattice defects and segregation. A wide range of microstructures can be developed in a weld based on cooling rates. These microstructures are dependent on energy input, preheat, metal thickness (heat sink effects), weld bead size, and reheating effects due to multi-pass welding [21].

As a result of different peak temperatures, chemical compositions, and weld inclusions (oxides and sulphides), Weld Metal Zone microstructures are usually significantly different from those of the HAZ and Base Metal. Similarly, corrosion behaviour can also vary, but where corrosion mitigation measures are correctly applied, for example, coating or cathodic protection or inhibition, preferential corrosion of carbon steel welds can be adequately prevented. Another important factor is that for a given composition, hardness levels is the lowest for high heat inputs, such as those produced by SAW welds, and highest for low-energy welds (with faster cooling rates) made by SMAW, GTAW, and GMAW etc. In SMAW process, depending upon the welding conditions, weld metal microstructures generally tend to be fine grained with basic flux and somewhat coarser with acid or rutile (TiO_2) flux compositions. Welding of process piping is done as per ASME IX [22]

welding code and pipelines are welded as per API 1104 [23] or equivalent BSEN standard. The essential and non-essential variables are almost the same though there are few distinct requirements to satisfy the particular standard such as AP 1104 etc.

2.2. CORROSION- THEORETICAL BACKGROUND

Corrosion is defined thermodynamically as a tendency of metals to convert to its origin. In other words, it can be specified as physio-chemical interaction between a metal and its environment leading to impairment of the function of the metal. The process usually involves electrochemical reaction, which cause the material to be removed from the metallic surface. Therefore the theoretical concept of corrosion process depends on the knowledge of electrochemistry and metallurgy.

2.2.1. ELECTROCHEMISTRY

Spontaneous electrochemical corrosion of metals requires two simultaneous half-cell reactions or processes; an oxidation reaction at the anode and a reduction reaction at the cathode [24]. Essentially, there are four components present in an electrochemical corrosion cell; an anode, a cathode, a conducting environment for ionic movement (electrolyte), and an electrical circuit between anode and cathode for electron flow. Absence of any one of the above components inhibit corrosion process. This is the fundamental principle for corrosion control.

The anodic process is the metal dissolution and is represented by:



The cathodic reaction depends on the environment and for aqueous media is represented by equation 2.2 or 2.3 as



In natural aqueous environments, hydrogen evolution and oxygen reduction are the most common cathodic processes. In general, the electrochemical reaction takes place in pipeline due to the presence of water. In other environments, other reactions may occur. Hydrogen evolution ($2\text{H}^+ + 2\text{e}^- \rightarrow \text{H}_2$) predominates in acid conditions. The equilibrium potential of hydrogen evolution depends on the pH level of electrolyte solution. The current density change of the reaction depends on composition and nature of the metal substrate [25].

Oxygen reduction ($\text{O}_2 + 2\text{H}_2\text{O} + 4\text{e}^- \rightarrow 4\text{OH}^-$) predominates in neutral and alkaline solutions. The driving force depends on pH level. However, the kinetics of the reaction is much slow due to low exchange current density and mass transfer limitations. The cathodic process consumes electrons produced in the anodic reaction. The rate of electron generation must match the rate of electron consumption i.e. no net build-up of electrons in the metal [26].

Sites of anodic and cathodic processes may be adjacent or some distance apart. An electrically conductive path must however exist between the electrodes via the metal and chemically conductive path through the electrolyte. Surface areas of anodic and cathodic sites also have impact on the corrosion process since it is the current density (number of electrons generated per unit area per unit time) that controls the dissolution rate. This is the basis at which corrosion rate can be calculated using Faraday's Law if

the corrosion current density is determined. The anodic and cathodic reactions vary for different alloys exposed to various environments. The corrosion phenomenon induces different forms of failure depending on alloy composition and environment [27].

2.2.2. FORMS OF CORROSION

Forms of corrosion are also referred to as modes or mechanisms of corrosion. Sub-forms can also be identified for these basic forms of corrosion [28]. A number of corrosion forms which are already known are:

- Uniform (or general) corrosion
- Pitting Corrosion
- Crevice corrosion
- Inter-granular corrosion
- Stress corrosion cracking
- Erosion corrosion
- Selective leaching
- Hydrogen embrittlement
- Galvanic corrosion
- Microbial corrosion

2.3. MATERIAL DEGRADATION MECHANISMS IN OIL AND GAS INDUSTRIES

Generally possible material degradation mechanisms for upstream oil and gas production facilities are related to material, medium and interphase parameters etc. There can be general corrosion or localized corrosion as per the operating conditions. The rate of general corrosion and the susceptibility to localized

corrosion mainly depends on the formation of protective, semi-protective or non protective corrosion products such as scales which are affected by temperature, CO₂ partial pressure, medium composition, pH, fluid velocity, alloy composition and mechanical stress [29].

2.3.1. GENERAL CO₂ CORROSION

Carbon dioxide (CO₂) itself is not corrosive at the temperatures encountered within oil and gas production systems but can be corrosive if dissolved in water. The overall reaction by which wet CO₂ corrodes steel is presented as follows:



The carbonic acid formed by the above reaction causes a reduction in pH of the water which makes it quite corrosive to carbon steel. In addition to the acidity produced by carbon dioxide, low molecular-weight organic acids such as acetic acid also contribute to the corrosion. These acids are seldom considered the primary cause of sweet corrosion. The important factors governing the solubility of the carbon dioxide are medium pressure, temperature and composition of the water. Medium pressure increases CO₂ solubility whereas temperature decreases the solubility. The dissolved minerals may buffer the water and prevent pH reduction. The partial pressure of CO₂ is the determining parameter for the corrosion rate. Using the partial pressure of CO₂ as a yard stick to predict corrosion, the following relationship has been found for vertical pipe and tubing:

Partial pressure > 2 bar usually indicates corrosion.

0.48 bar < Partial Pressure > 2 bar may indicate corrosion.

Partial Pressure < 0.48 bar is considered non-corrosive [30].

However, the salt water produced by a sweet oil well contains dissolved minerals and the above partial pressure relationship may not apply. In horizontal pipeline having pockets for water collection, corrosion occurs at a partial pressure of < 0.5 bar [14].

2.3.2. WET HYDROGEN SULPHIDE

Wet hydrogen sulphide can result in uniform and pitting corrosion of carbon steel. If wet H₂S is present, both carbon steel and CRA's get affected significantly. Also HIC and SOHIC of carbon steel can be a risk if H₂S is present [31].

2.3.3. ELEMENTAL SULPHUR

Most crude oils contain a certain amount of sulphur. Generally, sulphur is a chemically bonded part of hydrocarbon species. However, it is possible that the sulphur is either in the form of poly-sulphides or elemental sulphur. Elemental sulphur has a limited solubility in hydrocarbons depending on the temperature. If elemental sulphur is deposited on carbon steel, low temperature of the medium and liquid water creates severe under-deposit corrosion.

2.3.4. EROSION CORROSION

Sand in the production fluids can of course contribute to solid particle erosion and erosion-corrosion. Protective (carbonate) scales and other surface layers can be removed thus leading to high local corrosion rate. The entrained sand

particles on non-metallic materials, for instance GRE piping and internally coated separators, can generate significant level of erosion. However, there is no definite specification and standard reference to specify a limit for the sand content beyond which this issue becomes significant. This factor is considered when the fluid velocity calculation is carried out for erosion corrosion [32].

2.3.5. MICROBIOLOGICALLY INDUCED CORROSION (MIC)

Sulphate Reducing Bacteria (SRB) is the major contributor to microbiological induced corrosion inside piping or pipeline of oil and gas producing facilities. The bacteria colonies create hydrogen sulphide generation locally. The iron becomes iron-sulphide due to this reaction. The result can be severe pitting corrosion. SRB's are normally not present in an oil well and downstream production facilities, unless introduced during hydro testing or water injection in the well or wash-water process etc. Wash water is fresh water produced by passing seawater through deaeration and reverse osmosis units. The seawater is treated with biocides at the intake point and closer to upstream location of the deaerators. Because biocides are injected at two separate locations, the total amount of active (live) bacteria in the system is small. Furthermore, all pipelines are regularly cleaned by spearing to remove the debris which can harbour SRB colonies [33, 34].

2.3.6. EFFECT OF WATER, OXYGEN AND CHLORIDE

The most common type of corrosion, the rusting of steel, is an example of oxygen corrosion. The rate of oxygen corrosion may vary depending on various factors, such as temperature, erosion of the metal surfaces, corrosion films and availability & nature of electrolyte. Water is an important factor of

serving as electrolyte and the corrosion rate is affected by the concentration of oxygen and acidity. In every chemical reaction, the temperature can have a significant effect on the corrosion rate. Further the salinity, sulphate content and flow velocity can have a significant effect on the corrosion rate. Generally, oxygen is not naturally present in deep sub-surface water wells. Whenever present, it is introduced by contact with air due to leakage in the system. Therefore, reducing the supply of oxygen or preventing its entry into the system is a major task in reducing oxygen corrosion.

The corrosion rate of carbon steels in the presence of aqueous chlorides is fairly high as compared to other metals such as alloy steels. In acidic solutions, carbon steel is attacked very fast but in alkaline solutions, carbon steel can be a suitable material. The general corrosion rate for carbon steel in slowly moving natural seawater is considered about 0.2-0.3 mm / y. The pitting rate can be several times higher than this value [35].

For deaerated seawater the severe corrosion rate of carbon steel can be estimated by the Oldfield, Swales & Todd formula [36].

$$R = c / 189 * (v^7 / d)^{1/8} \exp(T / 42.6) \quad [2.6]$$

R- Corrosion rate in mm / y

c- Oxygen concentration in ppb

v- Flow velocity in m / s

d- Internal diameter in m

T- Temperature in °C

Generally, this formula is considered conservative due to the positive effects of scaling. However, this scaling can be disrupted locally by occasional higher oxygen content due to malfunctioning of the deaerator thus leading to pitting corrosion. Therefore, this formula is applied without any modification.

2.3.7. UNDER DEPOSIT CORROSION

Generally, no oxygen is expected in the hydrocarbon containing systems. However, it is possible that limited amount of oxygen is introduced through injection of drain fluids such as rainwater and deck washings. In addition, collection of sand and corrosion products in the pipelines may also be responsible for the introduction of oxygen. Under this kind of accumulated debris, under deposit corrosion is possible due to differential aeration. Further, it is likely that sulphate reducing bacteria are introduced unintentionally at a certain point during the process and can settle very easily in the debris. If localized corrosion under colonies of SRB's and other microbiological species have taken place, removing the debris become increasingly difficult. To avoid under deposit corrosion, it is required to clean pipelines regularly by pigging [37].

2.3.8. EXTERNAL CORROSION

External corrosion is related to the atmospheric conditions, such as humidity and salts. Since carbon steel can corrode due to atmospheric conditions, a suitable coating is applied. Hence, no additional corrosion allowance is provided for all carbon steel process equipment but specified internal corrosion allowance is required. Austenitic stainless steels do not corrode at atmospheric conditions but they are susceptible to chloride stress corrosion cracking at temperatures above 60°C. In order to minimize the risk of chloride stress cracking in the marine environment, all austenitic stainless steel piping and equipments are coated. To further minimize the risk for chloride ingress under insulation, chloride free insulation materials are used for stainless steel piping.

2.3.9. GENERAL GALVANIC CORROSION

Galvanic corrosion is due to the coupling of dissimilar materials in an electrically conductive environment. The more noble material for the specific environment and temperature acts as cathode and the less noble material acts as the anode. At the anode, generally metal ions go into solution. A large surface area of the cathode as compared to that of the anode can result in high local corrosion rates. For instance, the carbon steel casing of a pump can protect galvanically the 316 stainless steel impeller from pitting corrosion during downtime [38]. The factors which influence this galvanic corrosion are given in the Table 2.1.

Table 2.1 -Factors Influencing Galvanic Corrosion

Sl. No.	Primary Factors	Description
1	Reversible Electrode potentials	Potential differences
2	Reaction	Dissolution, Oxygen reduction, Hydrogen evolution, Kinetics
3	Metallurgical factors	Heat treatment, Mechanical working, Alloy composition, Intermetallic Inclusions
4	Mass transport	Migration, Diffusion, Flow effects
5	Surface condition	Surface defects like pores, undercuts, lack of fusion, Surface treatment, Passive film, Corrosion products, Microbes
6	Geometrical effects	Area, Distance, Position, Shape Orientation, Anodic to cathodic area ratio
7	Environmental effects	Forms of corrosion, Cyclic wet/dry Solar radiation, Climate, Seasonal variation, Soil type
8	Electrolyte properties	Ionic species, pH, conductivity Temperature, volume, flow rate oxygen content

2.3.10. LIQUID METAL EMBRITTLEMENT

Several combinations of solid metal in contact with molten metal can lead to liquid metal embrittlement e.g. austenitic stainless steel with zinc. The most important combination in this perspective is zinc embrittlement of stainless steel. If austenitic stainless steel is contaminated by zinc, rapid inter crystalline corrosion cracking occurs above 750 °C due to formation of a low melting temperature inter-metallic phase at this temperature.

In practice, under the following conditions, embrittlement damages can occur:

1. When zinc contaminated stainless steel operates above 750 °C, e.g. heater coils.
2. When zinc contaminated stainless steel is welded or hot formed above 750 °C.

Zinc contamination can happen in several ways, e.g. painting of stainless steel with zinc rich primers (but not zinc-phosphate pigmented primers), contact of stainless steel with galvanized tools, supports or racks and getting zinc dust on bare stainless steel. Also, it is possible that during a fire, zinc may drip off galvanized structures on uninsulated stainless steel piping or equipment. For this probable possibility, no galvanised items are installed on top of the Stainless Steel systems [39].

2.3.11. LOW TEMPERATURE EMBRITTLEMENT

The risk of possible brittle fracture due to low temperature embrittlement is fully acknowledged and incorporated in the mechanical design codes. The design code ASME section VIII Div. 1, Section UCS 66 and ASME B 31.3 are normally applied for process

equipment and piping respectively. Hence, the minimum operating temperature is considered from the design basis. The brittleness enhances sulphide stress corrosion cracking and hydrogen induced cracking.

2.3.12. TYPES OF CORROSION IN PIPELINES

There are almost three types of corrosion that can generally be experienced in a pipeline: i) Bottom of the line, ii) Top of the line corrosion and iii) General weld corrosion.

2.3.13. BOTTOM OF LINE CORROSION

In the wet fluid system, under certain conditions, the water drops out and accumulates on the bottom of pipeline. This part then becomes critical as corrosion may affect that area of the part. By injecting corrosion inhibitor on a continuous base, the probability of the condensed water to be inhibited is high provided i) the inhibitor is water soluble or dispersible and ii) no slug is formed with the condensed water to prevent the penetration of inhibitor into this part [40].

2.3.14. TOP OF LINE CORROSION

This type of corrosion mainly occurs in a wet gas system when condensation starts from the top of the line and flows down along the pipe wall towards the bottom of the pipe. Corrosion inhibitor does not reach the top of the line and consequently, this part is left uninhibited. However, it has been shown that the top of line corrosion rate decreases with time as a result of saturation of the condensed layer with FeCO_3 [41].

2.3.15. GENERAL WELD CORROSION

The weld corrosion can be the result of various factors such as difference in stress, variation in microstructure, variation in chemical composition, local turbulence and local carbonate scale formation. This is not a major issue where high viscosity and a wide range of fluid velocity exist within the system. The velocities in the lines have been determined by guidance and consideration described in API 14E [42]. This weld corrosion is considered in this study as this is more vulnerable than any other corrosion in the parts of piping or pipeline or equipment of the system.

2.4. CONDITIONS OVER FIELD LIFE

2.4.1 DECLINING RESERVOIR PRESSURE

Pressure declining is not considered relevant in the perspective of the calculation of the corrosion allowance of the pipelines and process facilities because this is based on the operating pressure and these do not change significantly over life time.

2.4.2. SULPHUR REDUCING BACTERIA

During commissioning and during the operational phase, the SRB is introduced which causes field souring. The introduction of SRB's has to be avoided via proper commissioning procedures. During the operation phase, the microbiological activity has to be monitored. Also, SRB's in the pipelines can result in pitting corrosion under colonies [43].

2.4.3. OPERATING CONDITIONS

Well acidizing is a possibility for the water injection wells only. It is not considered for the oil producing wells as this can be for relatively short time only. Therefore, no impact on the overall corrosion rate is envisaged due to well acidizing.

2.4.4. GEOMETRICAL FACTORS

It is recognized that excess root penetration can interrupt fluid flow close to the wall of a pipe during high-flow-rate operation leading to impingement corrosion at the downstream side of the weld. Alternatively, in low-velocity oil and gas systems where the water content is entrained in the bulk fluid, such excess penetration can cause flow disruption and water dropout. This allows pooling of water at the downstream side of the weld, which can lead to increased corrosion of the weld or adjacent base metal. There is a possibility that the weld root surface can be rough with crevices on the surface. These crevices can act as corrosion cell formation sites leading to localized corrosion [44].

2.5. CO₂ CORROSION

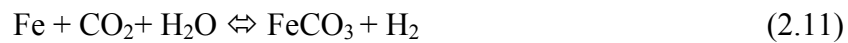
Carbon dioxide corrosion or "sweet corrosion" of carbon steel is a major problem in the oil and gas industry. The presence of dry CO₂ gas or only oil itself is not corrosive. However, it is the contact of the aqueous phase with the surface of the metal that leads to corrosion and subsequent failures. The basic CO₂ corrosion reactions have been well understood and accepted in the past few decades. The major chemical reactions include CO₂ dissolution and hydration to form carbonic acid as



It then dissociates into bicarbonate and carbonate ions in two steps:



CO₂ corrosion is an electrochemical reaction with the overall reaction given by:



Thus, CO₂ corrosion leads to the formation of a corrosion product FeCO₃. This gets precipitated and forms a protective or a non-protective scale depending on the environmental conditions [42, 43, 45]. The electrochemical reactions at the steel surface include the anodic dissolution of iron and two cathodic reactions [21, 22].



The cathodic reactions are proton reduction reaction and the direct reduction of carbonic acid:



Despite more than three decades of intense research, it is still not known which of the two reactions actually prevails on the surface [44-46]. Hence, many researchers have taken the net cathodic current to be the sum of the currents of the two reactions. It has been suggested that the direct reduction of bicarbonate ion becomes important at higher pH level [23]. It is anticipated that there are many environmental factors such as solution chemistry, flow velocity, temperature, pressure, pH etc. which influence the uniform CO₂

corrosion rate of carbon steel. The formation of the corrosion product scales due to the environmental conditions also has a significant impact on the corrosion rate of the metal. The effects of some of the important factors on CO₂ corrosion in the oil and gas industry are discussed in the following paragraphs.

2.5.1. THE EFFECT OF pH

The pH level of the solution is an indication of the ion concentration in the solution which is one of the main species involved in cathodic reaction of CO₂ corrosion process. It has been illustrated both experimentally and computationally that corrosion rate changes significantly with respect to pH level. At low pH (pH < 4) and low CO₂ partial pressure (≤ 1 bar), a flow sensitive direct reduction of H⁺ (equation 2.13) dominates the cathodic reaction. On the other hand, at higher pH (pH > 5) and higher CO₂ partial pressure (≥ 1 bar), the cathodic reaction is controlled by the direct reduction of H₂CO₃ (equation 2.14), which is related to the amount of dissolved CO₂. However, it is the indirect effect of pH on the formation of protective films (such as iron carbonate) which is the most important factor [46]. High pH level ensures a decreased solubility of iron carbonate that result in an increased precipitation rate and faster formation of protective films leading to a decrease in the corrosion rate.

2.5.2. EFFECT OF TEMPERATURE

Temperature accelerates all the processes involved in CO₂ corrosion including transport of species, chemical reactions in the bulk of the solutions and electrochemical reactions at the metal surface. It is reported that irrespective of

the solubility level of protective films (such as iron carbonate or other salts), temperature can either increase or decrease the corrosion rate [47, 48]. In the case of corrosion where protective films do not form (typically at low pH), corrosion rate increases with increasing temperature. However, at a higher pH where solubility of protective films is likely to be high, an increase in temperature accelerates the kinetics of precipitation and facilitates protective film formation thus, decreasing the corrosion rate. The corrosion rate is usually maximum somewhere in between 60 °C and 80 °C, depending on flow conditions and water chemistry.

2.5.3. EFFECT OF CO₂ PARTIAL PRESSURE

In the absence of protective films, an increase in CO₂ partial pressure increases the corrosion rate. At high CO₂ partial pressure, the direct reduction of H₂CO₃ (equation 2.8) is accelerated due to increase in H₂CO₃ concentration [49]. However, when other conditions are favourable for formation of protective iron carbonate films, high CO₂ partial pressure may facilitate the film formation. At a given high pH level, an increase in CO₂ partial pressure leads to an increase in CO₃²⁻ concentration and super saturation. This accelerates precipitation and film formation [50].

2.5.4. EFFECT OF FLUID FLOW

Flow affects corrosion through the mass transport process involved in CO₂ corrosion. High flow rates usually mean high turbulence and more effective mixing in the solution [45]. Depending on whether other conditions are favourable for protective film formation, flow affects CO₂ corrosion in a number of ways. Without protective films, turbulent flow accelerates the

transport of species between the anode and cathode surfaces which may increase the corrosion rate. Hence, this transport of species is the rate determining factor. On the other hand, when other conditions are conducive to formation of protective iron carbonate films, species transport in turbulent flow affects the surface concentration of species and consequently, affects the precipitation rate of iron carbonate. In many cases, less protective films are formed at higher flow velocities [47]. In some cases, where flow velocities are extremely high, flow can even mechanically remove the protective films that are already in place, resulting in an increase in corrosion rate.

2.5.5. EFFECT OF SATURATION

During the transportation of products such as oil and gas in the pipeline, the water phase accumulates as dissolved ferrous ions (Fe^{2+}) due to corrosion of the mild steel pipe wall. This considerable amount of Fe^{2+} in the downstream portion of the pipeline influences the formation of the iron carbonate scale. Increase in Fe^{2+} concentration can lead to high super saturation, thus increasing the precipitation rate of iron carbonate for more protective scale formation [45]. Corrosion also leads to an increase in pH which in turn, increases the CO_3^{2-} ion concentration. This leads to an increase in the super saturation and formation of iron carbonate film.

2.5.6. CORROSION PRODUCT FILM FORMATION

CO_2 corrosion of a metal strongly depends on the type of corrosion product film formed on the surface of the metal during the corrosion process. The stability, protectiveness, precipitation rate and the adherence of these films determine the nature (localized/uniform) and the rate of corrosion. Depending

on the environmental factors, corrosion films can be divided into following major classes:

a) Iron carbide (Fe₃C)

Iron carbide is the undissolved component of the mild steel, which is left behind from the corrosion process. It is conductive, very porous and non-protective [51]. Iron carbide films can either significantly decrease the corrosion rate by acting as a diffusion barrier or increase the corrosion rate due to:

- Galvanic coupling of the film to the metal.
- Increase in the true specimen surface area
- Acidification of the solution inside the corrosion product film

b) Iron carbonate (FeCO₃):

The reaction for formation of solid iron carbonate is given by:



The precipitation of solid iron carbonate occurs when the product of concentrations of Fe²⁺ and CO₃²⁻ exceed the solubility limit. However, the rate of precipitation of iron carbonate is so slow that most often the precipitation kinetics comes into consideration rather than the thermodynamics [52].

The equation for the rate of precipitation of the iron carbonate ($R_{\text{FeCO}_3(\text{s})}$) is given as:

$$R_{\text{FeCO}_3(\text{s})} = A / V \cdot f(T) \cdot K_{\text{sp FeCO}_3} \cdot f(S_{\text{FeCO}_3}) \quad (2.16)$$

Where Super saturation S is defined as:

$$S_{\text{FeCO}_3} = C_{\text{Fe}^{2+}} C_{\text{CO}_3^{2-}} / K_{\text{sp FeCO}_3} \quad (2.17)$$

A / V is ratio of surface area to volume and $K_{\text{sp FeCO}_3}$ is solubility limit of FeCO₃.

Since CO_3^{2-} ion concentration is dependent on the pH, it can be deduced that:

$$S = f(\text{Fe}^{2+}, \text{pH}) \quad (2.18)$$

When iron carbonate precipitates at the steel surface, it decreases the corrosion rate by [45]

- Presenting a diffusion barrier for the species involved in the corrosion process
- Blocking a portion of the steel and preventing electrochemical reactions from occurring.

The most important factors affecting the precipitation of iron carbonate are super saturation and the temperature.

c) Iron sulphide (FeS):

The formation of iron sulphide occurs only in the presence of H_2S . The reaction for formation of solid iron sulphide is given by:



It is assumed that the precipitation of solid iron sulphide occurs when the product of concentrations of Fe^{2+} and S^{2-} exceed the solubility limit of Fe. The equation for the rate of precipitation of the iron carbonate ($R_{\text{FeS(s)}}$) is given as [51]

$$R_{\text{FeCO}_3(\text{s})} = A / V \cdot f(T) \cdot K_{\text{spFeS}} \cdot f(S) \quad (2.20)$$

Where Super saturation S_{FeS} is defined as:

$$S_{\text{FeS}} = C_{\text{Fe}^{2+}} C_{\text{S}^{2-}} / K_{\text{spFeS}} \quad (2.21)$$

With K_{spFeS} = solubility limit of FeS

It is assumed that iron sulphide affects the CO_2 corrosion in the same way as iron carbonate (being a diffusion barrier and surface blockage). However, iron sulphide films being semi-conductive may lead to localized corrosion in some cases [52].

2.5.7. PREFERENTIAL WELD CORROSION

Weld has three primary regions- Base metal, HAZ and Weld Metal Zone as shown in the Fig. 2.4. HAZ has more than one region. For all practical purposes, HAZ can be considered as one region as the zone width is less as compared to other regions. A wide range of HAZ microstructures can be produced because being close to the fusion boundary, transformation to austenite on heating followed by subsequent cooling gives either a ferrite-carbide or martensite microstructure depending on material composition, peak temperature, and cooling rate. The material far from the Weld Metal Zone is exposed to a low peak temperature, so only partial reaustenization occurs. The areas heated below the ferrite-to-austenite transformation temperature (A_{c1}) are not affected significantly, except some carbide coarsening and tempering of the material. Irrespective of these variations, preferential HAZ corrosion is comparatively rare in majority of applications. An example of preferential weld corrosion of a carbon steel weld is shown in Fig. 2.8. The process conditions of the pipeline in Fig. 2.8 are 6% CO_2 gas phase at $93^\circ C$ with 85% water cut at 60 bar pressure of surrounding medium.



Figure 2.8: PWRC of Failed Pipeline

Preferential HAZ attack is more common in plain carbon & C-Mn steels as compared to high alloyed steels [2]. The HAZ corrosion is shown in the Fig. 2.9.

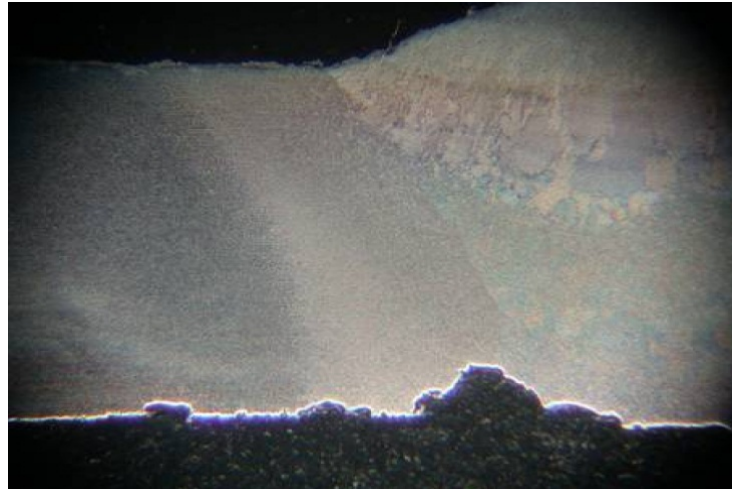


Figure 2.9: Weld HAZ Corrosion

This phenomenon has been observed in a wide range of aqueous environments. The common link being that the environments are fairly high in conductivity, while attack usually, but not invariably, occurs at pH values below 7. The factors for this type of corrosion are given in Fig. 2.10 [53-63].

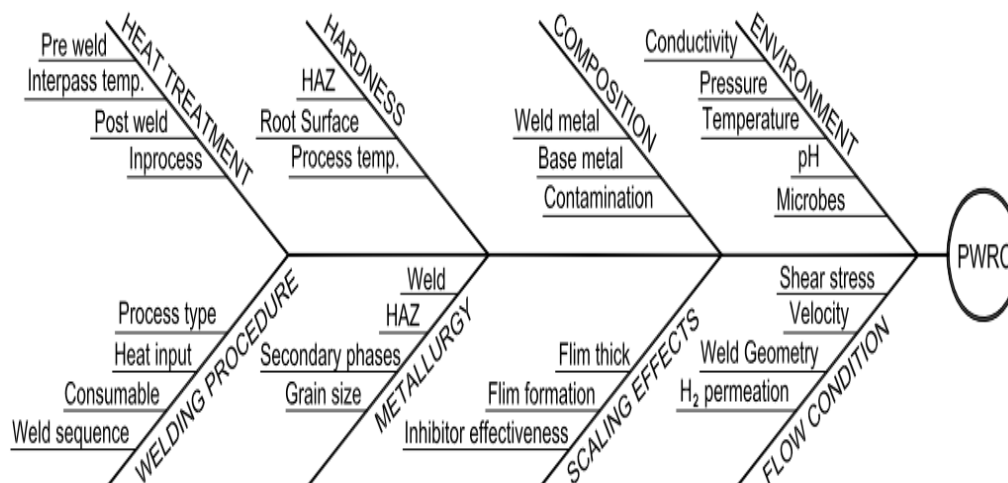


Figure 2.10: Cause and Effect Diagram for PWRC.

Preferential HAZ corrosion in seawater was reported in the 1960s and attributed to the presence of low-temperature transformation products such as martensite, lower bainite, or retained austenite [64]. Therefore, steel compositions favouring increased hardenability (e.g. increase in manganese content) may lead to higher level of localized corrosion, but micro alloyed steels are not susceptible. Tramline corrosion is a term applied to preferential HAZ corrosion concentrated at the fusion boundaries and has been observed in acidic aqueous environments such as acidic mine waters. It is clear that a microstructural dependence exists for enhanced corrosion level. Studies on HAZ show that corrosion is appreciably more severe with the hardened microstructures. These microstructures are formed due to material composition and welding parameters. It has been known for many years that hardened steel may corrode more rapidly in acidic conditions than fully tempered material because local micro cathodes on the hardened surface stimulate the cathodic hydrogen evolution reaction. The rate of corrosion is usually governed by the cathodic reaction when other limiting factors are not present and therefore, it is a significant factor in acidic environments but insignificant in neutral or alkaline conditions. On this basis, the water treatments which are ensuring alkaline conditions are less likely to induce HAZ corrosion. Even at a pH level of near 8, hydrogen ion (H^+) reduction can account for approximately 20% of the total corrosion current. The pH value substantially above this level is needed to suppress the corrosion effect completely. Furthermore, if such treatments are not useful to control preferential HAZ corrosion, corrections during design stage is more reliable to avoid such problems [65].

In some oil and gas production environments, preferential weld corrosion may lead to enhanced HAZ attack or Weld Metal corrosion. In the late 1980s, studies on the problems associated with preferential weld corrosion in sweet oil and gas production systems were undertaken [66]. In some cases, the HAZ was attacked, while in other cases, the Weld Metal was preferentially corroded. Wherever enhanced HAZ corrosion was observed, the composition was found to be more influential than the microstructure. The schematic representation of relative effects of micro alloying element is given in Fig. 2.11 [67]. However, hardened microstructures lead to increased corrosion level.

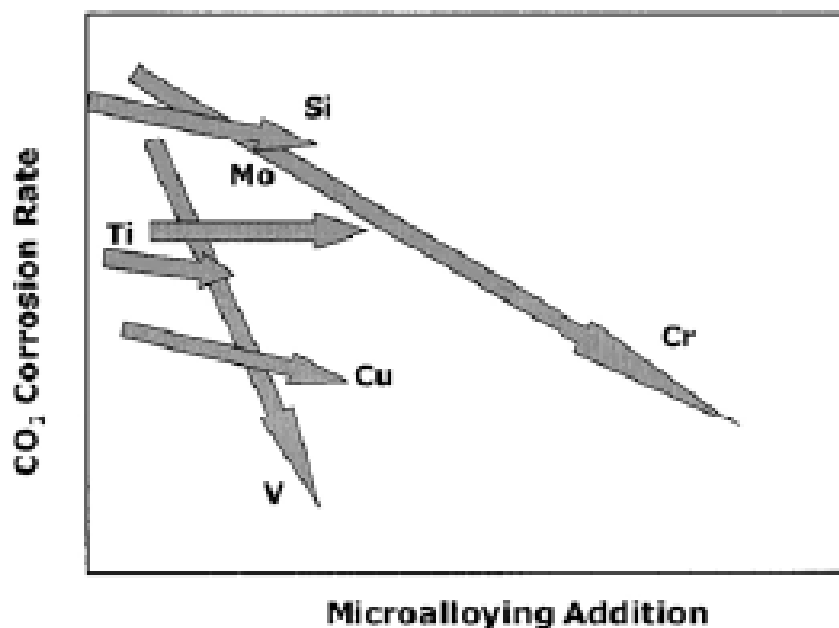


Figure 2.11: Effect of Micro Alloying Elements on Corrosion

The PWHT at 590 °C for stress relief is found to be beneficial in reducing HAZ attack [26]. The Weld Metal in C-Mn steel may suffer preferential corrosion, but again, if proper corrosion mitigation is in place for the main

structure, such as coating or cathodic protection, this preferential attack is normally prevented. However, there are cases where coating failure or inefficient inhibition can lead to localized corrosion [68].

It is probable that similar microstructural considerations should also apply to the preferential corrosion of Weld Metal. But in this case, the situation is further complicated by the presence of cathodic products, their type and quantity depending largely on the flux system employed. Electrode type plays a major role in determining Weld Metal corrosion rate; the highest rate of metal loss is normally associated with shielded metal arc electrodes having basic type coating. In seawater, for example, the corrosion rate for the Weld Metal of the weld made using a basic-flux-coated electrode may be three times as high as to that of the Weld Metal of the weld made using a rutile-flux-coated electrode. In SAW, relatively high corrosion rate of Weld Metal is expected as compared to the Base Metal. Preferential Weld Metal corrosion of carbon and low-alloy steels used for pipelines and process piping systems in carbon dioxide (CO₂) containing media has been observed in recent years particularly in manual metal arc (MMA) welds made using electrodes containing nickel or nickel plus copper. One comprehensive review has reported the link between preferential Weld Metal corrosion and electrode composition [65].

2.5.8. CORROSION OF WELDED LINE PIPE

Line pipe is generally welded using Electrical resistance welding and SAW processes. There is a particular case of preferential weld corrosion worth highlighting in respect to electric resistance welded / high frequency induction

welded (ERW / HFI) pipe where attack of the seam weld HAZ / fusion line occurred either in aqueous environment or when exposed to the water phase in a mixed-phase system due to flow conditions or water dropout at low points. The grooving corrosion has been attributed to inclusions within the pipe material being exposed at the pipe surface and modified by the weld thermal cycle. A normalizing heat treatment prevents such corrosion. However, the major remedial action is the selection of clean alloyed steel [62]. The corrosion reaction is due to electrochemical potential differences (galvanic corrosion) between the HAZ / fusion line and the Base Metal. This is attributed to the unstable MnS inclusions produced during the welding cycle. It is highlighted that the potential difference is of the order of 30 to 70 mV but low surface area ratio of anode to cathode results in high corrosion rates (between 1 to 10 mm per year). Mitigation against this form of corrosion was achieved through modified steel composition in the 1970s. The addition of copper reduces sulphur to minimize MnS formation and the addition of calcium, nickel or titanium stabilizes the remaining sulphur to eliminate the potential difference [67].

Generally, the corrosive environment encountered in OIL and Gas field are CO₂, H₂S, Brine, sea water etc. which are present alone or in combinations of various concentrations, pressures and temperatures etc. [69]. The corrosion reaction is so complex phenomenon that it is difficult to determine or pinpoint the responsible factors completely. But for all practical purposes, the testing methods and standards which are available as on date provide necessary data to control the corrosion effectively. Most of the studies carried out in the past were on general corrosion using the possible environment. Off late, due to the

unforeseen failures at welds, created necessity to study the preferential corrosion of welds. At present, attempts are being made by the leading world operators on this subject.

2.6. TYPES OF WELD CORROSION IN THE OIL AND GAS INDUSTRY

2.6.1. GALVANIC CORROSION

Detailed studies were undertaken in the late 1980s to assess more modern steels and welding electrodes in arctic waters in Canada [70]. Both HAZ and Weld Metal Zone attack were observed. It was concluded that steels having minimum yield strength of 235 to 515 MPa (34 to 75 ksi) and high manganese content (1.4%) result in enhanced preferential HAZ attack [44].

It is possible to reduce preferential HAZ attack by increasing heat input during welding. Generally, the rate of Weld Metal attack is dependent on the nickel and copper contents of the welding electrode and is slightly influenced by Base Metal composition. Although steel with copper, nickel, and chromium additions led to noble Base Metal and hence, accelerates Weld Metal attack. It has been reported that the Base Metal with low silicon content led to increased Weld Metal corrosion, supporting the earlier findings that silicon content < 0.2% can be detrimental. It has been highlighted that for the autogenously seam weld in ERW / HFI pipe, the difference in corrosion potential for the separated regions (Base Metal, HAZ, and Weld Metal) may be only a few tens of millivolts. Due to the low surface area ratio of anode to cathode in conductive solutions, the attack on the anodic Weld Metal or HAZ may be very high. Normally, for such Weld Metal attack which occurs in high-

conductivity media, ensuring the Weld Metal as cathodic (more noble) relative to the Base Metal has been successful. However, this may not be successful in different environmental conditions. Several case studies on galvanic corrosion failures had been presented elsewhere on A53 Gr. B and A285 Gr. C Base Metals within short period after commissioning [48]. It is reported that the examples demonstrate the necessity for testing each galvanic couple in the environment for which it is intended. In some cases, highly-alloyed filler metals are used to prevent rapid preferential weld corrosion.

2.6.2. ENVIRONMENTALLY ASSISTED CRACKING

Environmentally assisted cracking is common in the refining and power-generation industries where components frequently operate in aggressive environments. Environmentally assisted cracking or degradation can take many forms, ranging from local thinning caused by global corrosion attack to SCC and HIC etc. The form of cracking or degradation depends on number of factors such as material type, chemical composition, microstructure, Weld Metal & HAZ properties (including hardness), weld geometry, welding residual stresses, operating conditions, and environment [71].

2.6.3. HYDROGEN INDUCED CRACKING

Hydrogen can be present in the operating medium by cathodic reaction or due to welding conditions. The cracking has been observed in both high and low strength steels even under non-stressed conditions. This occurs primarily in the low-strength steels that are exposed to hydrogen containing process environment. Because of rapid cooling and solidification of weld pool, Weld Metal forms a structure of dendrites and oxide dispersed in the form of fine

globules. It has been confirmed that HIC does not occur in Weld Metals up to a hardness of 280 HV, which are welded even without a filler metal of specific weld chemistry as per material standard. In comparison, HIC has been observed primarily in the Base Metal and HAZ. HIC is also referred to as hydrogen-assisted cracking, cold cracking, delayed cracking, or under bead cracking. This is a phenomenon associated with carbon and low-alloy steel welds. This type of cracking results from the combined effects of four factors [72]:

- A susceptible (brittle) microstructure
- The presence of hydrogen in the Weld Metal
- Tensile stresses in the weld area
- A specific temperature range, 100 °C to 200 °C

Hydrogen-induced cracking occurs after cooling of weld (hence the term cold cracking) and is often delayed for many hours while hydrogen diffuses to areas of high tensile stress locations. At microstructural flaws in a tensile stress field, the hydrogen changes to its molecular form, causing cracking. Cracking may occur in the HAZ or Weld Metal, which may be longitudinal or transverse [67]. This crack occurs more likely in HAZ of carbon steel weld because carbon steel electrodes are usually low in carbon and the Weld Metal hardness is generally within the limits as per standards. There are exceptions that highly alloyed electrodes result in hard Weld Metal. In addition, HIC is possible under high dilution of carbon from the Base Metal in certain submerged arc welds.

The cracks also occur with excessive arc voltage and active fluxes that result in high manganese and / or silicon pickup from the flux. Cracks in the HAZ

are most often longitudinal. Under bead cracks lie more or less parallel to the fusion line. They do not normally extend to the surface and may therefore be difficult to detect. Under bead cracks can form at relatively low stress levels in martensite when hydrogen is present in high concentration [73].

Toe cracks and root cracks generate in areas of high stress concentration. Cracking may therefore occur in less susceptible microstructures or at relatively low hydrogen levels. This type of cracking is often delayed till the required level of hydrogen diffuses to the area. Transverse cracking in the HAZ is less common. It occurs in high-carbon martensite under conditions of high longitudinal stresses (for example, outside fillet welds on heavy metal). Weld Metal cracks may be longitudinal or transverse. Longitudinal cracks start due to stress concentrations at the root of the weld. Transverse cracking starts at hydrogen containing defects with the influence of longitudinal stresses. Weld Metal cracks do not always extend to the surface. In submerged arc Weld Metal made with damp fluxes, a unique crack morphology known as chevron cracking occurs. Here the cracks lie at 45° angle to the weld axis. One of the serious problems with hydrogen induced cracking is the difficulty in detecting the presence of a crack. The delayed nature of some of the cracks cannot be found immediately after the weld completion, especially in welds that has externally applied stresses when put in service. The major preventative measures to avoid cold cracking are [44]:

- Preheat, including maintenance of proper inter pass temperature
- Heat input control
- Post weld heat treatment
- Bead tempering

- Use of low-hydrogen processes and electrodes
- Use of alternate filler materials

2.6.4. STRESS CORROSION CRACKING

Stress-corrosion cracking is a term used to describe service failures in engineering materials that occur by environmentally assisted crack (EAC) propagation in slow phase. The observed crack propagation is the result of the combined and synergistic interaction of mechanical stress and corrosion reactions. There is no doubt that residual welding stresses can contribute to SCC in specific environments in which such failure may represent a hazard. This failure is due to the active path and hydrogen embrittlement mechanisms. Under the presence of residual stress, failure is likely to occur in low-heat-input welds because of the enhanced susceptibility to form hardened microstructures inevitably [62].

It is not unusual to find the welding residual stresses equal to that of yield strength of the material. As discussed above, proper welding practices can minimize or eliminate such failures. In the industry, still there are failures occurring knowingly or unknowingly as the welding procedures are implemented under various practical constraints.

2.6.5. CORROSION RATE CALCULATION BASIS

If the polarization behaviour of a metal in an environment is known, the measurement of the corrosion potential in that environment can be used to determine the corrosion rate. The magnitude of the anodic current at the measured potential is directly related to weight loss of the metal.

The corrosion rates have been calculated based on process data sheets (fluid list) and parameters including pipeline data, operating condition i.e. temperature, operating pressure, CO₂ content, gas flow rate, oil flow rate, water flow rate, water analysis and also corrosion control by inhibition etc. The inhibited corrosion rate is calculated with a default inhibited corrosion rate of 0.1 mm / yr. The inhibitor availability is set at 95%, meaning that the inhibitor has been appropriately tested for its efficiency and present at the internal surface for 95% of the time. The total predicted corrosion rate is then calculated as follows:

$$CR_{predicted} = 95\% \times CR_{inhibited} (mm / yr) + 5\% \times CR_{uninhibited} (mm / yr) \quad (2.22)$$

The corrosion rate calculations are for general corrosion purpose only and pitting corrosion is not considered. Pitting is expected to occur if oxygen enters the process plant and deposits settles in uninhibited areas [74].

CHAPTER 3 - EXPERIMENTAL PROCEDURE

3.1. WELDING

3.1.1. BASE METAL

Welding was carried out on 60.3 mm outside diameter and 8.7 mm wall thickness pipe of API X 65 QT Steel. The chemical composition is given in Table 3.1.

Table 3.1- Chemical Composition of Base Metal

Elements	C	Si	Mn	S	P	Ni	Cr	Mo	C.Eq.
Composition	0.1	0.29	1.32	0.003	0.013	0.17	0.07	0.01	0.37

3.1.2. WELDING ELECTRODE

The chemical composition and carbon equivalent (calculated as per IIW formula) of welding electrodes used in present investigation are given in Table 3.2 [75]. The important elements which have significant effect on corrosion are highlighted there.

The electrodes were selected under the following conditions.

1. Electrodes are being used at present in the pipeline construction field.
2. The intended elements like Cr, Mo, Ni, and Si must be there in the Weld Metal in appropriate proportions.

Table 3.2 - Chemical Composition of Electrodes

Elements	Composition of Welding Electrodes (Wt. %)			
	E7018G	E8018G	E8018B2	E8018 B6
C	0.05	0.05	0.094	0.1
Si	0.68	0.20	0.279	0.24
Mn	1.2	1.120	0.773	0.92
S	0.004	0.009	0.008	0.008
P	0.013	0.017	0.022	0.011
Ni	0.02	0.890	0.02	0.04
Cr	0.04	0.050	1.251	4.82
Mo	<0.01	0.380	0.595	0.58
Cu	< 0.01	0.030	0.012	0.03
V	0.01	0.020	0.005	0.011
Nb	0.01	-	-	0.006
C. Eq.	0.27	0.39	0.466	1.34

3.1.3. WELDING POWER SOURCE

Welding rectifier Miller – Gold Star, Model No.402 was used for welding.

The power source is shown in Fig. 3.1.



Figure 3.1: Welding Rectifier

Pipe material was welded using SMAW process following the qualified welding procedure as per API 1104 requirements [76]. The welding was carried out at 5G position as shown in Fig. 3.2. Before the start of welding process, the current levels were selected from the heat input calculation of the ampere range for the electrode diameter. The heat input was maintained as per the qualified procedure. The welding speed was selected accordingly from the calculation. The recorded welding parameters are given in Tables 3.3 to 3.6.



Figure 3.2: Welding Set Up.

Table 3.3 - Welding Parameters of E8018G Weld

Weld	Electrode	Dia. mm	Weld Pass	A	V	Welding Speed (mm / min)	Heat Input KJ / mm
E8018G	E8018G	2.5	Root	75	21	66.67	1.41
		2.5	Fill-1	79	22	97.2	1.08
	E8018G	3.25	Fill-2	82	22.4	75	1.469
			Fill-3	74	23	60	1.7
			Fill-4	78	22	66	1.65
			Fill-5	80	21.8	60	1.62
			Fill-6	79	22.3	48	1.47

Table 3.4 - Welding Parameters of E7018 Weld

Weld	Electrode	Dia. mm	Weld Pass	A	V	Welding Speed (mm / min)	Heat Input KJ / mm
E7018	E7018	2.5	Root	76	20	50	1.82
	E7018	2.5	Fill-1	82	22	100	1.08
		3.25	Fill-2	102	24	95.23	1.54
			Fill-3	80	22	40	2.6

Table 3.5 - Welding Parameters of E8018B6 Weld

Weld	Electrode	Dia. mm	Weld Pass	A	V	Welding Speed (mm / min)	Heat Input KJ / mm
E8018B6	E8018B6	2.5	Root	76	20	51	1.8
		2.5	Fill-1	79	22	61	1.7
	E8018-B6	3.25	Fill-2	105	24	95.5	1.6
			Fill-3	101	23	120	1.2
			Fill-4	103	24	117	1.3
			Fill-5	104	24	141	1.6

Table 3.6 - Welding Parameters of E8018B2 Weld

Weld No	Electrode	Dia. Mm	Weld Pass	A	V	Welding Speed (mm / min)	Heat Input KJ / mm
E8018B2	E8016B2	2.5	Root	72	22	70	1.35
		2.5	Fill-1	78	22	75	1.37
	E8018-B2	4.0	Fill-2	133	25	79.5	2.5
			Fill-3	138	24	166	1.2
			Fill-4	135	25	174	1.17

Due to manual welding, small pipe diameter and 5G-horizontal weld position, It is difficult to maintain a constant heat input as the position changes from 6 'O' clock to 12 'O' clock continuously. Pipe size of 60.3 mm (outer diameter) was chosen to create a difficult welding condition which is normally experienced during actual welding at site.

3.1.4. WELD SAMPLES

The test samples were prepared as shown in Fig.3.3.

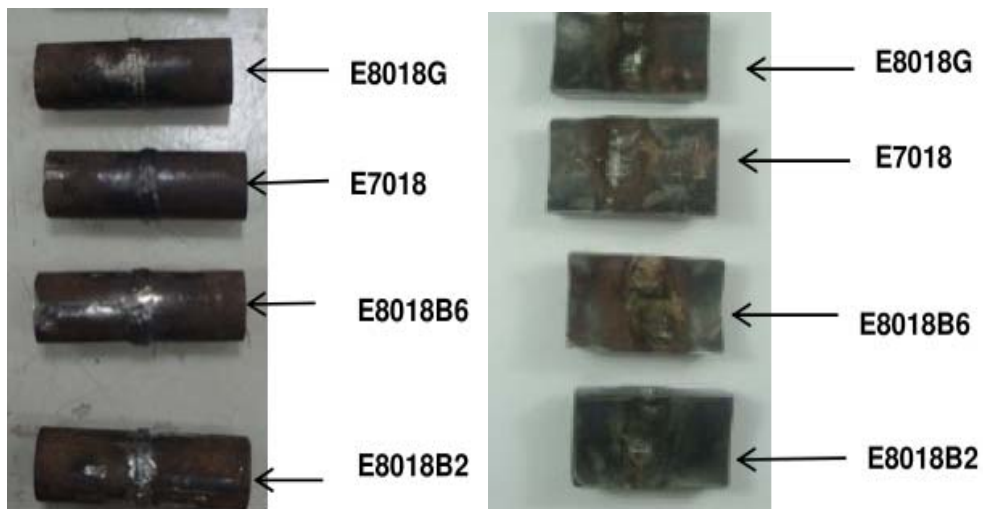


Figure 3.3: Welded Samples

Normally, defects occur at 2nd and 3rd quarter of the pipe weld. Hence, the samples are selected from these regions. The defects like excess penetration and root undercut are observed in welds E8018G, E8018B6 and E8018B2 which are shown in Fig. 3.3.

3.1.5. CHEMICAL COMPOSITION TESTING

The chemical composition was tested using Optical Emission Spectrometry equipment- Spectro Lab, Type-LAVWA 18A. The samples were prepared as per ASTM E 415 standard [77]. A controlled discharge is produced between the flat surface of the specimen and the counter electrode. The radiant energy of selected analytical lines are converted into electrical energy by photo-multiplier tubes and stored on capacitors. The discharge is terminated at a predetermined level of accumulated radiant energy or after a fixed exposure time. At the end of the exposure period, the charge on each capacitor is

measured and recorded as concentration. The test surface was polished with aluminum oxide sand paper of grade 60 using a polishing machine. The sample was placed in a fixture and evaporated by spark discharge inside the container. In this process, the released atoms and ions are excited to emit light. This light is directed into the optical system and measured using light sensitive electronic detector converting light into electric charges.

3.1.6. WELD MICRO HARDNESS TESTING

The etched specimens which were prepared for micro hardness testing are shown in the Fig. 3.4.

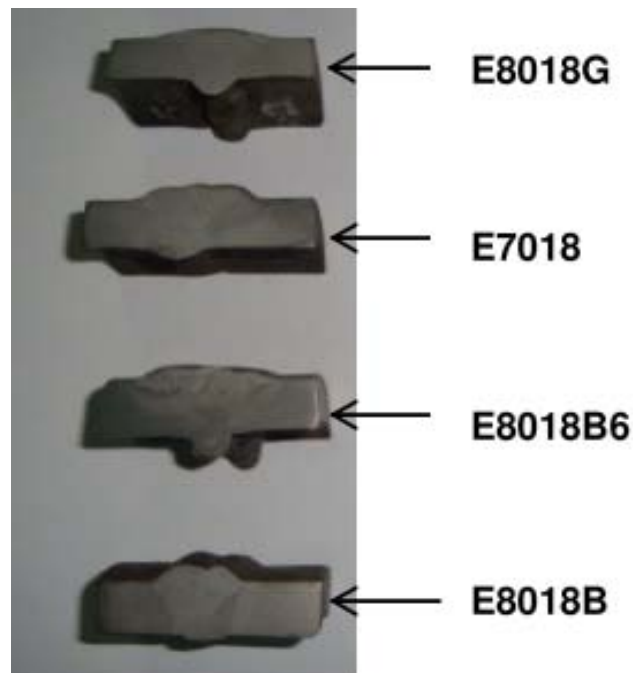


Figure 3.4: Etched Weld Specimens for Micro Hardness Testing

The weld samples were prepared as per ASTM E340 [78]. The samples were cut using wire electrical discharge machining (EDM) process. This process is an electro thermal production process in which a thin strand metal wire in conjunction with de-ionized water (used to conduct electricity) allows the wire to cut through metal by the medium of heat from electrical sparks.

The surface was polished using 600 grit paper and extended up to 1000 grit abrasive paper to get the weld zone transition lines to be seen clearly. 2% Nital (ethanol 98% and Nitric acid 2%) solution was used for etching the specimens.

Vickers hardness testing (HV10) was carried out as per the guidelines given in NACE MR 0175 [79] standard measuring scheme and is shown in the Fig.3.5.

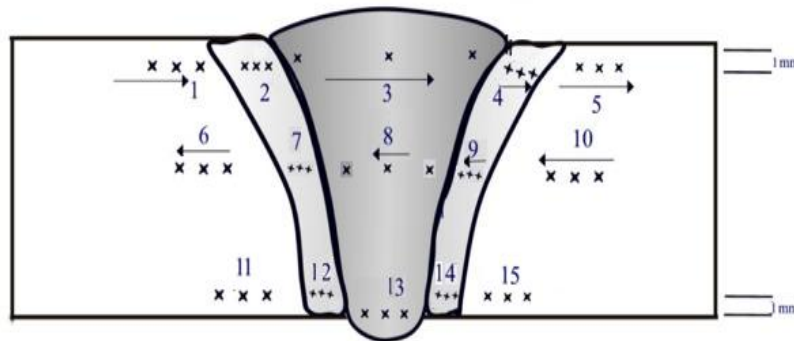


Figure: 3.5. HV10 -Hardness Measurement Scheme as per NACE-MR 0175

The Vickers hardness test (HV10) is an indentation hardness test using calibrated machines to force a square-based pyramidal diamond indenter having specified face angles, under a predetermined force, into the surface of the material under test and to measure the diagonals of the resulting impression after removal of the force. Force is applied as per the predetermined load (10kg) and released smoothly without shock or vibration. The time of application of the full test force is 10 to 15 seconds, unless otherwise specified and the angle between the indenter and the specimen surface is $90 \pm 1^\circ$. Spacing between indentations is as per the NACE standard guide lines. The center of the each impression was maintained at a distance equal to three times the length of diagonal of impression from any edge of the test specimen or from other surrounding impressions. The individual hardness number was recorded at the respective location. The Impression was made

such that both diagonals of the impression were measured and their mean value was used as a basis for calculation of the Vickers hardness number. The measurement was made with the impression centred as close as possible in the field of the microscope. The number of indentations was taken more than the standard requirements to have better data to analyse the hardness as it may influence the corrosion behaviour significantly. Additional hardness measurements were taken at the root edge as it is exposed to atmosphere like cap weld.

3.1.7. WELD METALLOGRAPHY

The weld microstructure analysis was carried out using optical microscope Model No. AXIOVERT. Two samples were cut; one at 6-9 'O' clock position and the other at 9-12 'O' clock position of the weld for comparison. Generally, difference in heat input is expected between 6 'O' clock position (high heat input due to slow welding speed to overcome gravitational forces) and 12 'O' clock position (low heat input due to fast welding speed). The positional difference also influences the Weld Metal properties. The samples were, etched with 2% Nital solution and examined at 100x & 200x magnification.

3.2. CORROSION TESTING

The corrosion tests were conducted in three parts as noted below. The first two experiments were conducted to understand the basic corrosion behavior of the weld zones as per the standard practice. General Corrosion using Linear Polarization Resistance and Galvanic Corrosion methods were used to determine:

- The total (general and galvanic) corrosion behavior in aerated seawater at room temperature.
- Galvanic Corrosion at various temperatures in aerated seawater
- Galvanic Corrosion at various temperatures in aerated seawater with CO₂ at pH 5.

The samples were prepped for corrosion studies. A 5 mm dia and 6 mm depth hole was drilled for soldering the wires. The samples with wire and epoxy sealing around the wire is shown in Fig. 3.6. The counter electrode is also shown as well.



Figure 3.6: Weld Samples Prepared for Corrosion Testing

For all corrosion testing, GAMRY series- Reference 600 Potentiostat was used. According to the current convention of Gamry Framework software, anodic-oxidation current is denoted as positive [80]. The potentiostat used in present study is shown in Fig. 3.7.



Figure 3.7: Gamry Potentiostat Instrument

3.2.1. ELECTROCHEMICAL TESTING METHODS

Most metal corrosion occurs via electrochemical reactions at the interface between the metal and an electrolyte solution. Corrosion normally occurs at a rate determined by equilibrium between opposing electrochemical reactions. The first is the anodic reaction, in which a metal is oxidized, releasing electrons to the cathode through electrolyte. The other one is the cathodic reaction, in which a solution species (often O_2 or H^+) is reduced, absorbing the electrons from electrolyte. When these two reactions are in equilibrium, the flow of electrons from each reaction is balanced, and no net electron flow (electrical current) occurs. These two reactions (anodic & cathodic) can take place on the same metal surface or on two dissimilar metals (or metal sites) that are electrically connected. The general corrosion behavior was tested using LPR method and the effect of metallurgical properties was evaluated by Galvanic Corrosion method [81].

3.2.2. CORROSION TESTING CELL- POTENTIOSTAT AND ELECTRODES

The electrodes (working electrode, counter electrode and reference electrode) were immersed in an electrolyte (an electrically conductive solution). The collection of the electrodes, the solution, and the container holding the solution are referred as an electrochemical cell. The combination of electrochemical cell and potentiostat constitutes the corrosion testing setup as shown in Fig. 3.8.

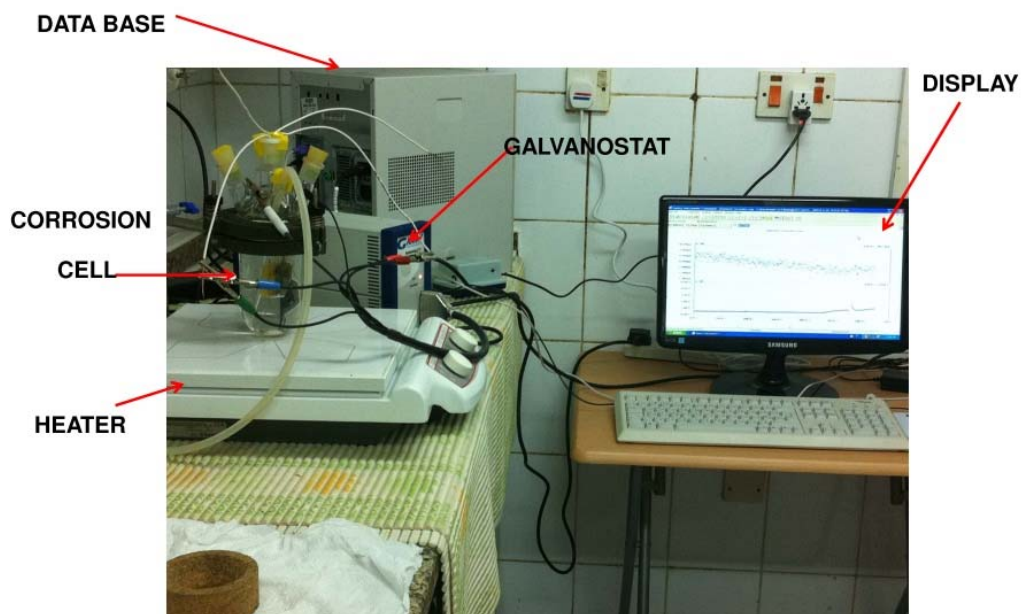


Figure 3.8: Corrosion Testing Cell set up.

A potentiostat is an electronic instrument that controls the voltage difference between a working electrode and a reference electrode which are placed in the same cell. The potentiostat implements this control by injecting current into the cell through an auxiliary or counter electrode. In almost all applications, the potentiostat measures the current flow between the working and counter electrodes. The controlled variable in a potentiostat is the cell potential and the measured variable is the cell current. The working electrode is the electrode

where the potential is controlled and the current is measured. In corrosion testing, the working electrode is a sample of the corroding metal. Generally, the working electrode is not the actual metal structure being studied. Instead, a small sample is used to represent the structure. This is analogous to testing using weight loss coupons. The working electrode can be bare metal or coated. The reference electrode is used in measuring the working electrode potential. A reference electrode has a constant electrochemical potential as long as no current flows through it. The reference electrode – silver / silver chloride (Ag / AgCl) electrode was used in LPR experiments (three electrode techniques). The counter or auxiliary electrode is a conductor that completes the cell circuit. The counter electrode in lab cells is generally an inert conductor like platinum or graphite. In this study, the working electrode material was used as counter electrode. This was cut from the same pipe material. The current that flows into the solution via the working electrode leaves the solution via the counter electrode. The corrosion cell was heated by surrounding water which was kept inside the container. This container was placed directly on the heater. The corrosion current was measured at 5 °C interval. The pH value of natural sea water which was used for the experiments was 7.7 at 25 °C. The chemical composition of water was analyzed using various test methods as given in the Appendix - B, Table B1.

3.2.3. LINEAR POLARIZATION RESISTANCE TESTING (LPR) METHOD

As I_{corr} cannot be measured directly, in many cases, it can be estimated from current versus voltage data. The log current versus potential curve over a range of about half volt was measured. The voltage scan was centred on E_{oc} .

The model of the corrosion process assumes that the rates of both the anodic and cathodic processes are controlled by the kinetics of the electron transfer reaction at the metal surface. An electrochemical reaction under kinetic control obeys equation-3.1, the Tafel equation [82].

$$I = I_0 e^{[2.3 (E - E^\circ) / \beta]} \quad (3.1)$$

In this equation,

I - is the current resulting from the reaction

I_0 - is a reaction dependent constant called the exchange current

E - is the electrode potential

E° - is the equilibrium potential (constant for a given reaction)

β - is the reaction's Tafel constant (constant for a given reaction)

Beta has units of volts / decade. The Tafel equation describes the behaviour of one isolated reaction. In a corrosion system, we have two opposing reactions; anodic and cathodic. The Tafel equations for both the anodic and cathodic reactions in a corrosion system can be combined to generate the **Butler - Volmer Equation** (Equation 3.2).

$$I = I_a + I_c = I_{\text{corr}} \left\{ e^{[2.3 (E - E_{\text{oc}}) / \beta_a]} - e^{[-2.3 (E - E_{\text{oc}}) / \beta_c]} \right\} \quad (3.2)$$

Where

I - is the measured cell current in amps

I_{corr} - is the corrosion current in amps

E - is the electrode potential

E_{oc} - is the corrosion potential in volts

β_a - is the anodic Beta Tafel Constant in volts / decade

β_c - is the cathodic Beta Tafel Constant in volts / decade

A log I versus E plot is called a Tafel Plot. The Tafel plot generated directly from the Butler - Volmer equation is shown in the Fig. 3.9.

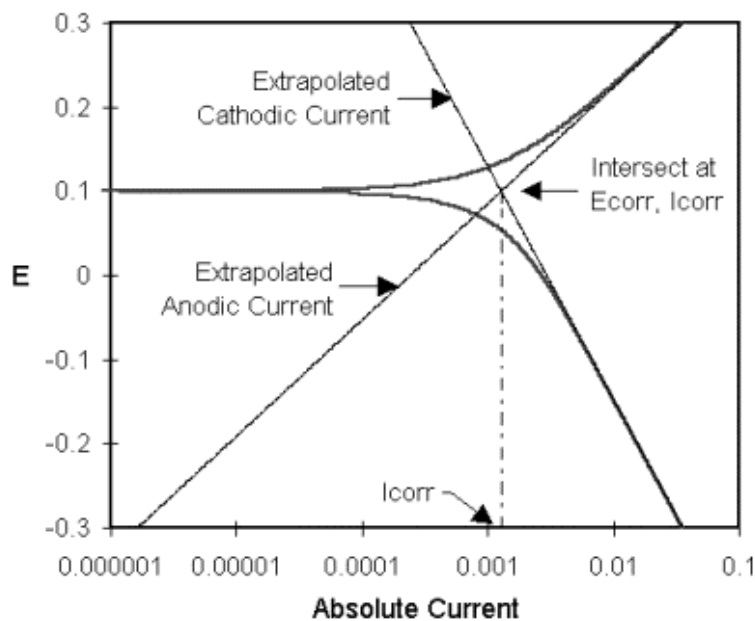


Figure 3.9: Tafel Plot

The following factors were considered in this experiment to determine the corrosion current.

1. Concentration polarization, where the rate of a reaction is controlled by the rate at which reactants arrive at the metal surface. Often cathodic reactions show concentration polarization at high currents, when diffusion of oxygen or hydrogen ion is not fast enough to sustain the kinetically controlled rate.
2. Oxide formation, which may or may not lead to passivation, can alter the surface of the sample being tested. The original surface and the

altered surface may have different values for the constants in equation 3.2.

3. Other effects which alter the surface such as preferential dissolution of one alloy component can also cause variations in the results.
4. A mixed control process where more than one cathodic or anodic reaction occurs simultaneously may complicate the reaction activity. An example of mixed control is the simultaneous reduction of oxygen and hydrogen ion.
5. The potential drop as a result of cell current flowing through the resistance of cell solution cause errors. This effect is not too severe and is correctable via IR compensation in the potentiostat.

The above factors may cause non-linearity in the Tafel plot. The classic Tafel analysis is performed by extrapolating the linear portions of a log current versus potential plot back to their intersection as shown in the Fig. 3.9. The value of either the anodic or the cathodic current at the intersection is I_{corr} . Many real world corrosion systems do not provide a sufficient linear region to permit accurate extrapolation. Most modern corrosion test software performs a more sophisticated numerical fit to the Butler - Volmer equation. The measured data is fit to equation 3.2 by adjusting the values of E_{corr} , I_{corr} , β_a , and β_c . The curve fitting method has the advantage that it does not require a fully developed linear portion of the curve.

3.2.3.1. Polarization Resistance

Equation 3.2 can be further simplified by restricting the potential to be very close to E_{oc} . Near E_{oc} , the current versus voltage curve approximates a straight line. The slope of this line has the units of resistance (ohms). The slope is, therefore, called the polarization resistance, R_p . An R_p value can be combined with an estimate of the Beta coefficients to yield an estimate of the corrosion current [83].

The output data shown in the Fig. 3.10 is used to calculate both the polarization resistance R_p and the corrosion current I_{corr} .

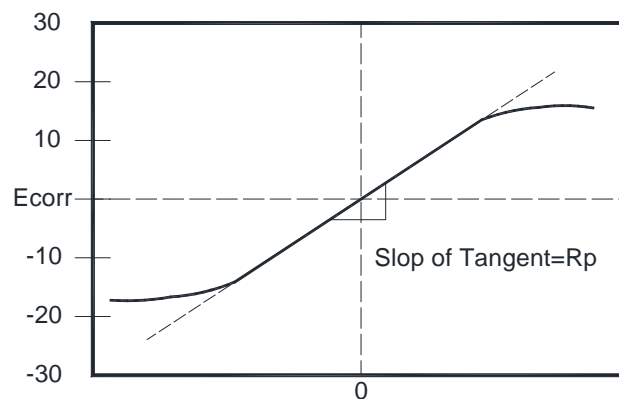


Figure 3.10: R_p - Slope of the Tangent at Zero Current.

The slope of the line is the change in potential (y axis values) divided by corresponding change in current. If we approximate the exponential terms in equation 3.2 with the first two terms of a power series expansion ($e^x = 1 + x + x^2/2\dots$) and simplify, we get one form of the Stern-Geary equation:

$$I_{corr} = \beta_a \beta_c / 2.3 R_p (\beta_a + \beta_c) \quad (3.3)$$

In a polarization resistance experiment, current versus voltage curve is recorded. The cell voltage is swept over a small range of potential that is very near to E_{oc} (generally ± 10 mV). A numerical fit of the curve yields a value for the polarization resistance R_p . Polarization resistance data does not provide any information about the values for the beta coefficients. Therefore, to use equation 3.3 beta values have to be determined. These can be obtained from a Tafel Plot.

By selecting a point, the corrosion current is calculated using the GAMRY software. This can be found by placing the cursor at the required point and the value will be shown automatically in the display. The recorded LPR tracing with calculated values by the software are given in the Appendix B. The corrosion current – maximum, minimum and average can be obtained with different units (A / cm^2 , mills / year etc.) by selecting the desired icons.

3.2.3.2. Calculation of Corrosion Rate from Corrosion Current

The numerical result obtained by fitting corrosion data to a model is generally the corrosion current. The corrosion rate is calculated with more useful units of rate of penetration, such as millimeters per year. Assume an electrolytic dissolution reaction involving a chemical species, S:



The current flow can be related to mass via **Faraday's Law**.

$$Q = nFM \quad (3.5)$$

where

Q - is the charge in coulombs resulting from the reaction of species S

n - is the number of electrons transferred per molecule or atom of S

F - is Faraday's constant = 96,486.7 coulombs/mole

M - is the number of moles of species S reacting

A more useful form of equation 3.5 requires the concept of equivalent weight.

The equivalent weight (E_w) is the mass of species S that reacts with one Faraday of charge. For an atomic species, $E_w = A_w / n$ (where A_w is the atomic weight of the species).

Recalling that $M = W / A_w$ and substituting into equation 3.5 we get:

$$W = E_w Q / F \quad (3.6)$$

Where, 'W' is the mass of species that has reacted.

In cases where the corrosion occurs uniformly across a metal surface, the corrosion rate can be calculated in units of distance per year. This calculation is valid only for uniform corrosion. It underestimates the calculation when localized corrosion occurs.

Conversion from a weight loss to a corrosion rate (CR) is straight forward.

We need to know the density, d, and the sample area, A. Charge is given by $Q = I T$, where T is the time in seconds and I is the current. We can substitute in the value of Faraday's constant. Modifying equation 3.6:

$$CR = I_{corr} K E / d A \quad (3.7)$$

Where, CR - The corrosion rate. Its units are given by the choice of K

(see Table 3.7),

I_{corr.} - The corrosion current in amps

K - A constant that defines the units for the corrosion rate

E_w - the equivalent weight in grams/equivalent

d- Density in grams/cm³

A- Sample area in cm²

Table 3.7 shows the value of K used in equation 3.7 for corrosion rates in the units of choice.

Table 3.7 - Corrosion rate constants

Corrosion Rate-units	K
mm / year (mm / y)	3272 mm / (amp-cm-year)
milli-inches / year (mpy)	1.288 x 10 ⁵ milli-inches / (amp-cm-year)

3.2.3.3. IR Compensation

In an electrochemical experiment, the potential measurement is the potential of a metal specimen (called the working electrode) versus a reference electrode. Generally, potential drop due to solution resistance is not considered for the potential measurement. Careful placement of the reference electrode can compensate for some of the IR drop resulting from the cell current, I, flowing through the solution resistance, R. IR error is proportional to the distance between the electrodes. The close distance between the electrodes makes the measurement free from IR errors. However, complete IR

compensation cannot be achieved in practice through placement of the reference electrode, because of the finite physical size of the electrode. The portion of the cell resistance that remains after placing the reference electrode is called the uncompensated resistance, R_u .

The potentiostat in the system use current interruption technique for IR dynamic compensation to correct uncompensated resistance errors. In the current interrupt technique, the cell current is periodically turned off for a very short time. With no current flowing through the solution resistance, its IR drop disappears instantly. The potential drop at the electrode surface remains constant for a determined duration set in the system. The difference in potential with and without the flow of current is a measure of the uncompensated IR drop. The potentiostat makes a current interrupt measurement immediately after each data point is acquired. It actually takes three potential readings such as E1 before the current is turned off, and E2 and E3 when current is turned off. Normally, the latter two are used to extrapolate the potential difference, ΔE , back to the exact moment when the current was interrupted. The timing of the interruption of current depends on the cell current. The interrupt time is 40 microseconds in the high current range. In low current range, the interruption lasts longer.

In controlled potential modes, the applied potential can be dynamically corrected for the measured IR error in one of several ways. In the simplest of these, the IR error from the previous point is applied as a correction to the applied potential. For example, if an IR free potential of 1 volt is desired, and the measured IR error is 0.2 volts, the potentiostat apply 1.2 volts. The correction is always one point behind, as the IR error from one point is applied

to correct the applied potential for the next point. In addition to this normal mode, the Gamry PC4 offers more complex feedback modes in which the two points on the decay curve are averaged.

By default in the controlled potential mode, the potential error measured via current interrupt is used to correct the applied potential. In the controlled current mode, no correction is required. If IR compensation is selected, the measured IR error is subtracted from the measured potential. All reported potentials are therefore free from IR error.

3.2.3.4. Current and Voltage Conventions

Current polarities in electrochemical measurements can be inconsistent. The current value of -1.2 mA indicates different meaning to the workers in different areas of electrochemistry or in different countries or even to different potentiostats [81]. To an analytical electrochemist it represents 1.2 mA of anodic current. To a corrosion scientist it represents 1.2 mA of cathodic current. For the convenience of the users around the world, Gamry potentiostat manufacturer provide the current polarity in preferred polarity convention as per the users requirement with a simple software command.

The polarity of the potential can also be a source of confusion. In electrochemical corrosion measurement, the equilibrium potential assumed by the metal in the absence of electrical connections to the metal is called the open circuit potential, E_{oc} . The term corrosion potential, E_{corr} , is the potential when there is no current flow as determined by a numerical fit of current versus potential data. In an ideal case, these E_{oc} and E_{corr} voltages may differ

as the changes occur at the electrode surface during the scan due to the deposition of corrosion products on the surface.

With most modern potentiostats, all potentials are specified or reported as the potential of the working electrode with respect to either the reference electrode or the open circuit potential. The former is always labeled as "E vs E_{ref} " and the later is labeled as "E vs E_{oc} ". The equations used to convert from one form of potential to the other are:

$$E \text{ vs. } E_{oc} = (E \text{ vs. } E_{ref}) - E_{oc} \quad (3.8)$$

$$E \text{ vs. } E_{ref} = (E \text{ vs. } E_{oc}) + E_{oc} \quad (3.9)$$

Regardless of whether potentials are versus E_{ref} or versus E_{oc} , one sign convention is used. The positive and negative potentials indicate whether the electrode is anode or cathode respectively. A positive potential accelerates oxidation at the working electrode. Conversely, a negative potential accelerates reduction at the working electrode.

The general corrosion was determined using LPR (ASTM G5-94) [83] testing at room temperature. This offers both practical and theoretical advantages for measuring the corrosion rate. It involves the potentiostatic measurement of the voltage - current curve in the immediate vicinity of the open - circuit potential E_{oc} .

3.2.4. THREE ELECTRODES POLARIZATION TECHNIQUE

3.2.4.1. Equipment Used

The various systems such test cell, potentiostat, data acquisition system, reference electrode, and counter electrode were used to conduct the experiments.

3.2.4.2. Test Procedure

1. Set up the instruments connections as shown in Fig.3.5.
2. Begin polarization **20** mV more negative than the free-corrosion potential.
3. For polarization, a typical potential step sequence in steps of 5 mV and holding for **30** seconds at each potential step is used before recording the current and proceeding to the next potential step.
4. Continue to change the potential of the working electrode as described in step 3 until a potential of approximately **40** millivolts more positive than the initial potential is reached (this produces a scan from **-20** mV to **+20** mV around the free corrosion potential. If nonlinear behavior is observed, the scan range may be reduced to plus or minus **10** mV of the corrosion potential or the data at potentials greater than **+ 10** mV can be ignored). The experiment was repeated five times to determine the reproducibility of the linear portion of the curve.
5. Plot the potential vs. current density.
6. Determine the slope of the potential vs. current curve (dE / dI) near the free-corrosion potential and use the slope in equation 3.3 to predict the corrosion current density.

All the above six steps are pre-programmed and the corrosion current or corrosion rate is calculated by selecting from the pull down menu of Echem Analyst software. In addition, the open circuit voltage, minimum and maximum corrosion current level in various units (mils per year, amp/cm² etc.) can be obtained from the pull down menu as shown in the Fig. 3.11. If there is some curvature to the potential-vs.-current plot, dE / dI is taken as the slope of the tangent of the curve at the free-corrosion potential. The selection

of the line is shown in Fig. 3.10 with a star mark on the tracing with thick line. By selecting this point as slope, the corrosion current was calculated using the GAMRY software.

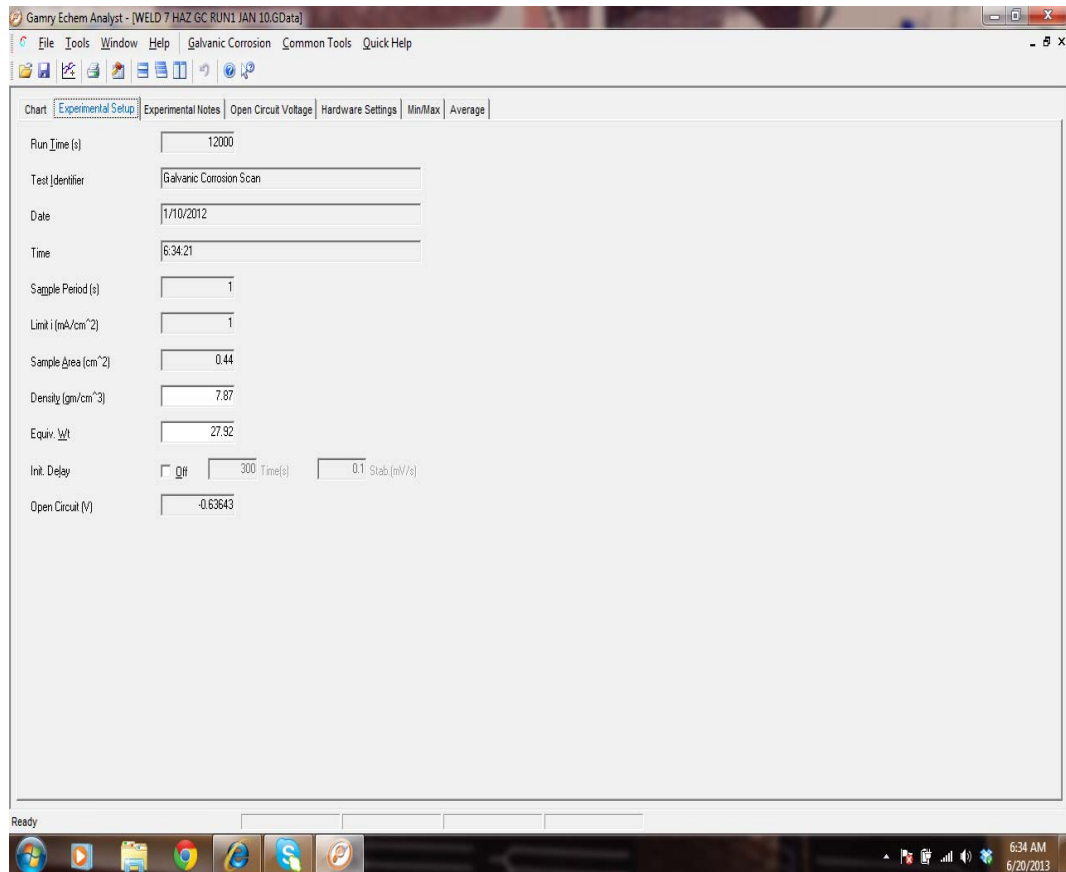


Figure 3.11: Data Input Pull Down Menu.

3.3. GALVANIC CURRENT MEASUREMENTS

The measurement of current flow in an electrochemical test arrangement must be performed so that no interference occurs with the electrochemical processes being examined. The current measurement device is inserted between the counter electrode and the working electrode output of the potentiostat. The device is isolated to prevent ground loops. A Zero Resistance Ammeter (ZRA) is the current measurement device used in the working electrode portion of the

circuit. The voltage drop measurement is the standard method used in multimeters for current measurements. This measurement across a precision resistor is an effective way of monitoring the current flow. The current flow direction is indicated with a positive reading on the voltmeter. A negative reading indicates the flow of current in the opposite direction.

Measuring the corrosion current directly is not usually feasible as described in section 2.7.8. The galvanic current measurement was carried out using ZRA. When the electrodes are immersed in solution, a natural voltage (potential) difference exists between the electrodes. The current is generated due to the rate of corrosion which is occurring on the most active surface of the electrode couple. The ZRA is an electronic instrument used to measure the current flowing in a circuit without introducing the additional voltage drop as associated with a standard ammeter. In potentiostat, the main functional component of the ZRA is an operational amplifier. It is an electronic component designed to supply any current necessary at its output terminal to maintain zero potential difference between two input terminals. Additionally, the operational amplifier is designed so that no current flows into or out of its input terminals. The potentiostat mode circuit is shown in the Fig. 3.12. In this mode, the voltage difference between the reference electrode and working sense leads is the feedback to the control panel. In ZRA mode, the feedback is from a differential amplifier measuring the difference between the counter sense and the working sense leads of the cell. Based on these two properties, the operational amplifier circuit perform the function of a ZRA.

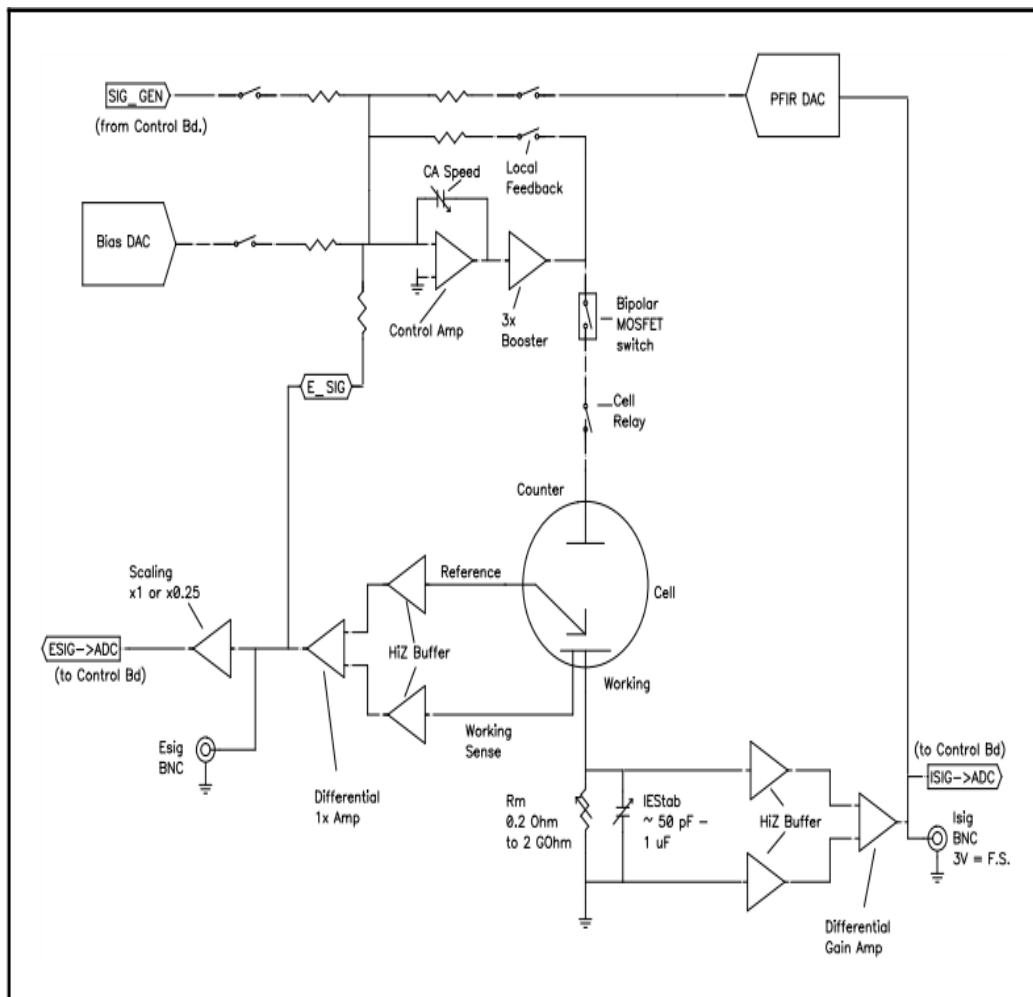


Figure 3.12: Electric Circuit for Zero Resistance Ammeter

The positive current flow is from the positive lead to the negative lead through the ammeter and the ammeter indicates the positive reading. The ZRA is employed when there is no IR drop permitted in the measuring circuit. The experimental procedure is followed as per ASTM G71, sec.6 [84] and GAMRY instrument Operation manual 'Gamry-Reference 600'. This instrument theoretically resolve current changes as small as 1 femo-amp (1×10^{-15} amps = 6000 electrons / sec). The voltage signal is measured below the 'x' axis and the current signal is recorded above the 'x' axis. The system "electronically shorts" these specimens and measures the current flow between

them. At the same time, the potentials of the specimens were measured with respect a reference electrode. The rms (root mean square) value of both the current and potential are calculated. The data curves from a ZRA mode test is current level and potential level versus time. The corrosion currents were recorded and the corrosion rate was calculated using the Fig. 3.11. The recorded galvanic corrosion tracings are attached in the Appendix B2 – B4. The galvanic current was recorded for 60 seconds. The experiment was terminated when the corrosion current started reducing significantly. The calculated corrosion was obtained in A/cm^2 by using the inbuilt software.

3.3.1. TEST PROCEDURE

1. Set the experimental arrangement as shown in Fig. 3.8
2. Immerse the two metal specimens in the solution and measure the corrosion potential of each metal in the uncoupled, isolated condition (switch open).
3. Allow a steady state potential to be attained for each specimen, i.e. a potential change of less than 2 millivolts in five minute duration.
4. Complete the couple of the two metal specimens by closing the switch and monitor current flow using the ZRA and employing the data acquisition system.
5. Note the direction of the current. The current leaves the anodic (more negative potential) member and flows through the solution to the cathode (more positive potential). A positive ZRA current is recorded with the low (negative) lead of the ZRA connected to the anode (more negative potential) and the high (positive) lead connected to the cathode (more positive potential).

6. To check consistency between current and potential of the metals comprising the couple, disconnect the couple. Measure the potential with respect to a reference electrode of the individual, isolated specimen comprising the couple. The potentials are maintained to be consistent with the direction of current (step 5). The type of testing technique is selected from the pull down menu of GAMRY Frame work software.
7. The corrosion current and corrosion rate were calculated using the Echem Analyst software which is inbuilt in the data acquisition system.
Galvanic current was recorded for minimum 60 seconds and the actual recordings are presented in the Appendix B.

CHAPTER 4 - RESULTS

4.1. WELDING TEST RESULTS

The mechanical properties are ensured as per the applicable welding code by maintaining the heat input within the qualified welding parameters. The heat input was maintained from 1.35 to 1.95 kJ/mm as per the qualified welding procedure to minimize the variations in mechanical and chemical properties.

The results are as follows.

4.1.1. CHEMICAL COMPOSITION OF WELD METAL

The chemical composition test results for the Weld Metal are given in Table 4.1.

Table 4.1 - Weld Chemical Composition

Weld	Elements (Wt. %)										C. Eq.
	C	Mn	Si	P	S	Cr	Ni	Mo	Cu	V	
E8018G	0.02	1.41	0.31	0.20	0.015	0.08	0.92	0.02	0.02	0.003	0.345
E7018	0.04	1.10	0.68	0.01	0.004	0.06	0.10	0.05	0.09	0.009	0.263
E8018B6	0.07	1.06	0.29	0.01	0.007	4.63	0.05	0.52	0.06	0.002	1.290
E8018B2	0.05	0.98	0.38	0.02	0.005	0.98	0.10	0.51	0.05	0.005	0.524

The elements of interest are Si, Cr, Mo and Ni which influence the corrosion characteristics. Though influence of Cu is also significant, it is not considered for observation purposes as the amount of Cu is very less as compared to other

elements. The carbon equivalent (C.Eq) is also calculated using International Institute of Welding (IIW) standard. The Cr and Mo content are significant for the welds made with E8018B6 and E8018B2 welds. Si is present at significant level in all the welds. Ni is highest for weld E8018G and lowest for E7018. The carbon equivalent is observed to be lowest for E7018 weld and highest for E8018B6 weld.

4.1.2. MICRO HARDNESS

The detailed hardness data are given in Appendix - A, Tables A1 - A4. The average hardness values are shown in the Fig. 4.1 for comparison among different weld zones.

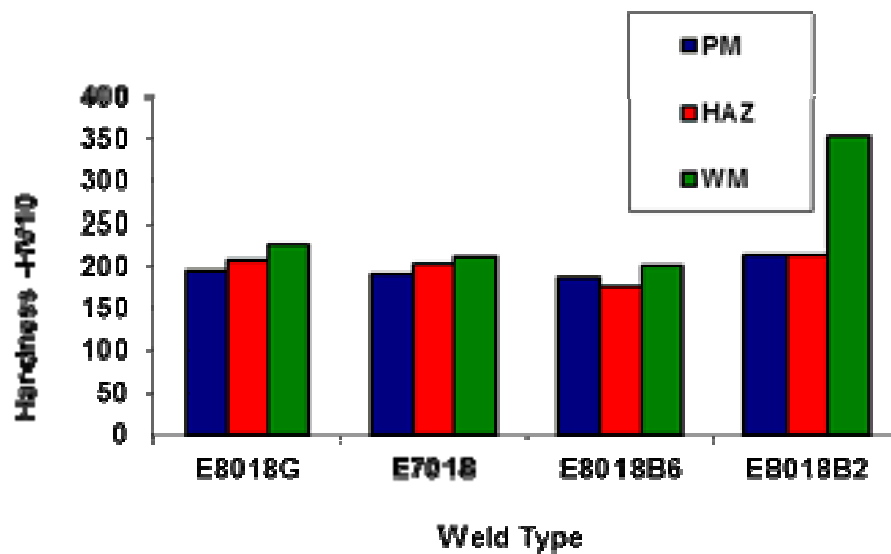


Figure 4.1: Micro Hardness Results

The heat input and the average hardness values are given in Table 4.2 to evaluate the influence of heat input on hardness levels.

Table 4.2 - Heat Input and Micro Hardness of Different Weld Zones

Sample ID	Heat Input (kJ / mm)	Avg. Hardness - HV10		
	Root weld	Base Metal	Weld Metal	HAZ
E 7018	1.82	193	204	212
E 8018G	1.95	212	224	207
E 8018B2	1.35	190	354	214
E 8018B6	1.8	192	202	175

There is no significant difference in hardness levels of Base Metal and HAZs but a significant difference is there in the hardness level of Weld Metal Zones of different welds. Weld Metal Zone of E8018B2 electrode weld shows a very high hardness of 354 in comparison to 202 for the Weld Metal Zone of E8018B6 electrode weld.

4.1.3 WELD MICROSTRUCTURE

The micrograph for the Base Metal is shown in Fig. 4.2. The micrographs for different weld zones (Weld Metal and HAZ) of all the welds are shown in Fig. 4.3 (a-h) and Fig. 4.4 (a-h) for all the welds for 6-9 'O' clock and 9-12 'O' clock positions respectively. The details of the observed microstructures are described in Tables 4.3 a and 4.3 b.

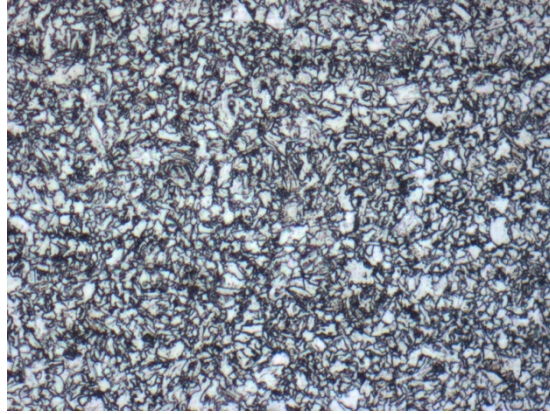


Figure 4.2: Base Metal X65QT Steel at 200X



Figure 4.3a: E8018G Weld Metal at 200X for 6-9 'O' clock position

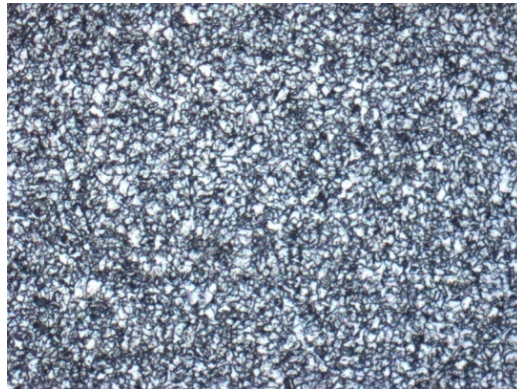


Figure 4.3b: E8018G HAZ at 200X for 6-9 'O' clock position

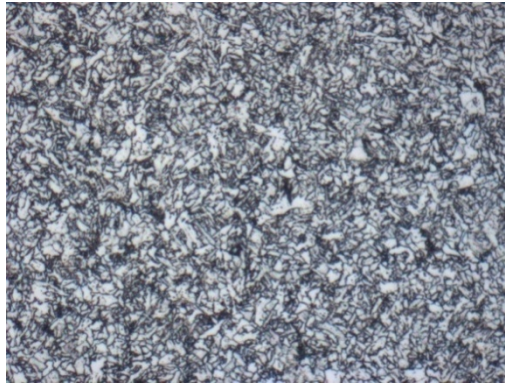


Figure 4.3c: E7018 Weld Metal at 200X for 6-9 'O' clock position

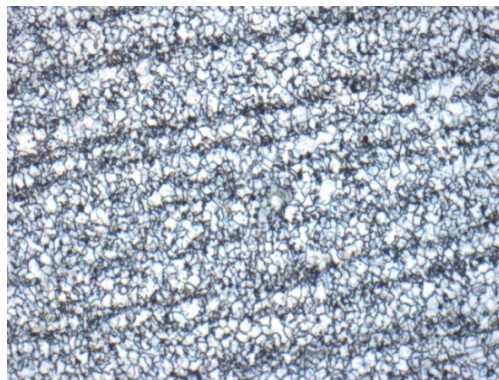


Figure 4.3d: E7018 HAZ at 200X for 6-9 'O' clock position



Figure 4.3e: E8018B6 Weld Metal at 200X for 6-9 'O' clock position

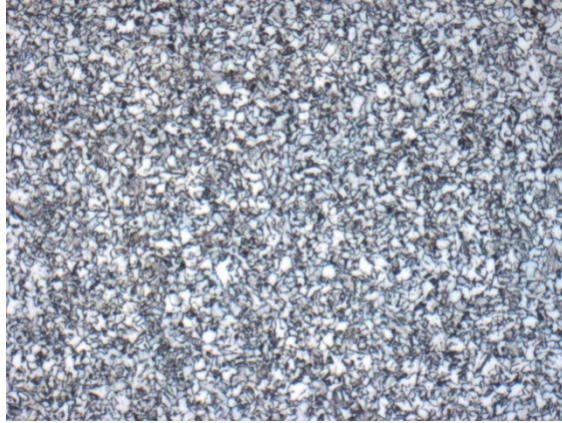


Figure 4.3f: E8018B6 HAZ at 200X for 6-9 'O' clock position

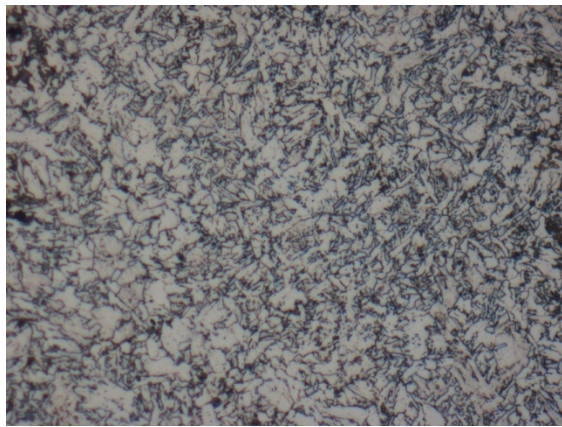


Figure 4.3g: E8018B2 Weld Metal at 200X for 6-9 'O' clock position



Figure 4.3h: E8018B2 HAZ at 200X for 6-9 'O' clock position

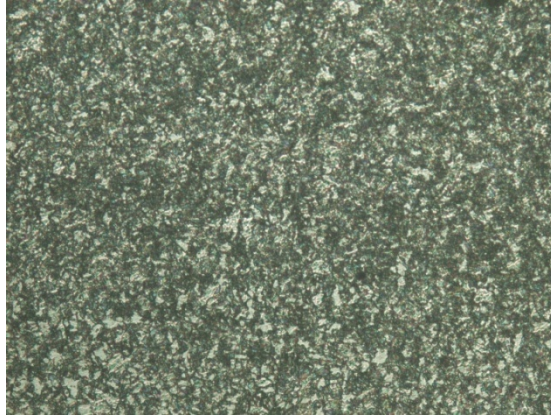


Figure 4.4a: E8018G Weld Metal at 100X for 9-12 'O' clock position

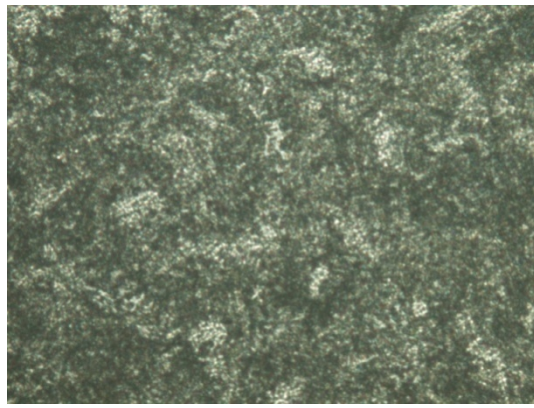


Figure 4.4b: E8018G HAZ at 100X for 9-12 'O' clock position

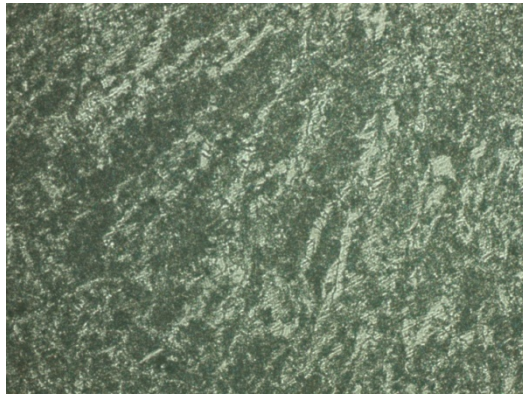


Figure 4.4c: E7018 Weld Metal at 100X for 9-12 'O' clock position

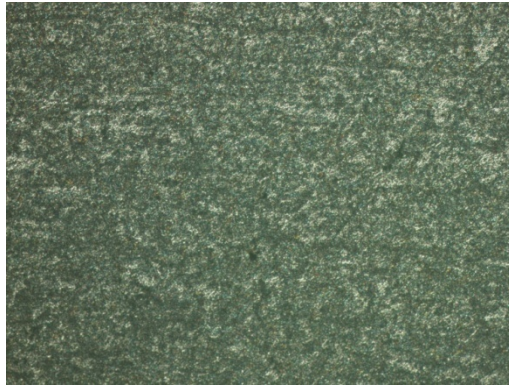


Figure 4.4d: E7018 HAZ at 100X for 9-12 'O' clock position

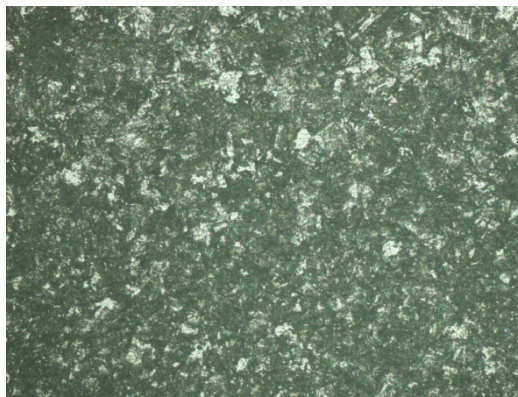


Figure 4.4e: E8018B6 Weld Metal at 100X for 9-12 'O' clock position

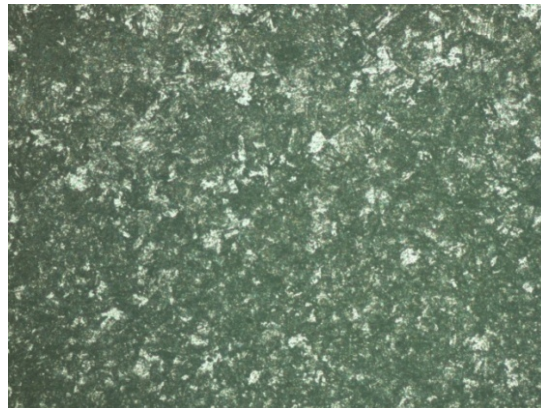


Figure 4.4f: E8018B6 HAZ at 100X for 9-12 'O' clock position

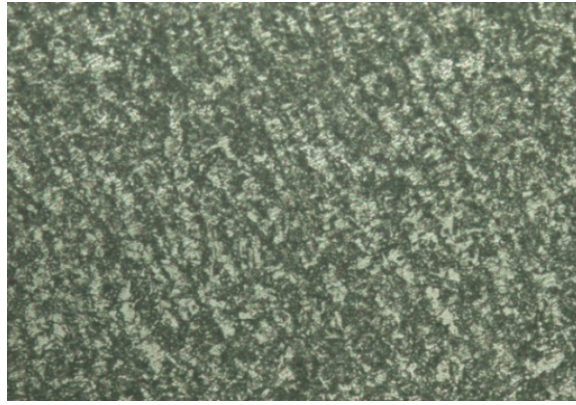


Figure 4.4g: E8018B2 Weld Metal at 100X for 9-12 'O' clock position

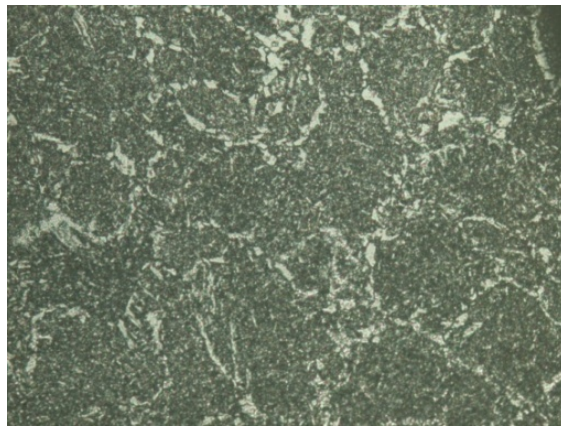


Figure 4.4h: E8018B2 HAZ at 100X for 9-12 'O' clock position

Table 4.3a - Microstructure of different weld zones at 6-9 'O' Clock Position

WELD	Microstructures		
	BM	HAZ	WELD METAL
E8018G	Fine bainite and acicular bainite	mixed grain of feathery and acicular bainite	columnar grain of ferrite and pearlite
E7018	Ferrite and pearlite	Mixed grain of fine bainite	Coarse columnar grain of ferrite and pearlite
E8018B6	Fine Bainite	Mixed grain structure of bainite& acicular bainite	Uniformly distributed feathery bainite and fine acicular bainite
E8018B2	Fine bainite and acicular bainite	Network of fine ferrite with bainite	Columnar grain with feeble bainite

Table 4.3b- Microstructure of different weld zones at 9-12 'O' Clock Position

WELD	Microstructures		
	BM	HAZ	WELD METAL
E8018G	Pearlite in ferrite matrix	Refined ferritic grain structure	Polygonal & Widmanstatten ferrite growth from grain boundary ferrite with coarse acicular ferrite
E7018	Pearlite in ferrite matrix	Refined ferritic grain structure	Polygonal & Widmanstatten ferrite growth from grain boundary ferrite with coarse acicular ferrite
E8018B6	Pearlite with ferrite matrix	Refined ferritic grain structure	Polygonal & Widmanstatten ferrite growth from grain boundary ferrite with coarse acicular ferrite
E8018B2	Pearlite banding in ferrite matrix	Refined ferritic grain structure	Polygonal & Widmanstatten ferrite growth from grain boundary ferrite with coarse acicular ferrite

The same Base Metal when subjected to different heat input has different microstructures. High heat input results in bainite structure whereas low heat input results in pearlite and ferrite microstructures.

4.2. CORROSION TEST RESULTS

4.2.1. GENERAL AND GALVANIC CORROSION AT ROOM TEMPERATURE

General corrosion was determined using linear polarization resistance (LPR) method. The experimental recording for the Base Metal with calculated value by the software that appears at the bottom of graph is shown in Fig. 4.5. The corrosion current is also shown in micro amps / cm² on X axis. The selection of the line is shown with a star mark on the tracing with thick line. Few recorded graphs show the dispersion of tracing points which is acceptable. This is due to the disturbances in the testing medium. The LPR recordings for Weld Metal, Heat Affected Zone (HAZ) of all the welds are attached in Appendix B.

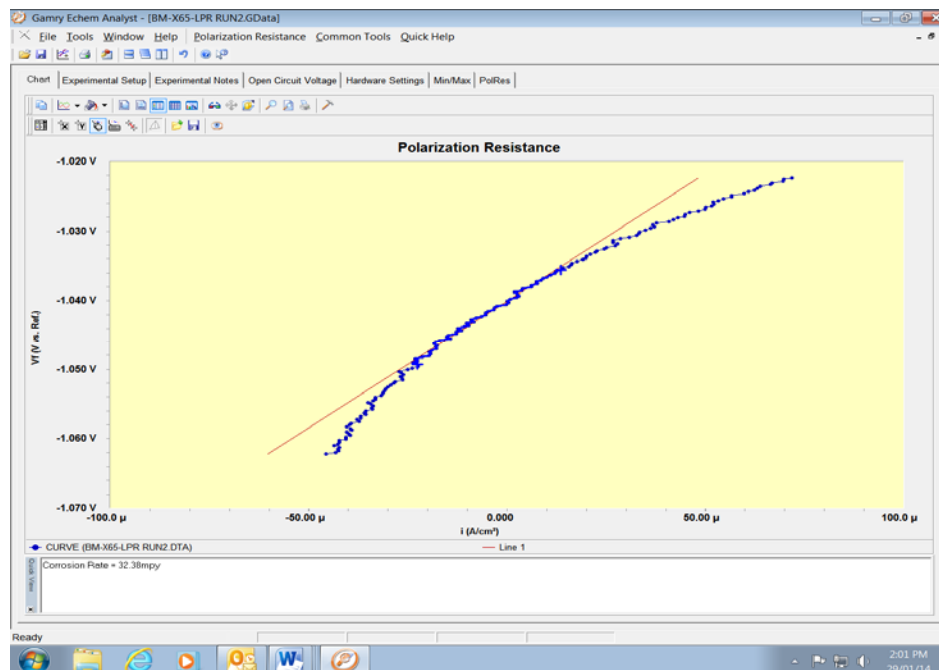


Figure 4.5: Corrosion Rate Calculated by the Software

The corrosion rate of different weld zones i.e. Base Metal, Weld Metal and HAZ for all the welds is calculated in mm / year and given in Table 4.4.

Table 4.4- Heat Input and Corrosion Rate of Different Weld Zones.

Sample ID	Heat Input (kJ / mm)	Corrosion Rate (mm / y)		
	Root weld	BM	Weld	HAZ
E7018	1.82	1.271	0.844	2.666
E 8018G	1.95	1.271	0.787	4.369
E8018B2	1.35	1.271	9.4×10^{-8}	5.134
E 8018B6	1.8	1.271	1.172	3.164

The Fig. 4.6 shows the galvanic corrosion current for the Weld Metal of E8018B2 electrode weld which becomes almost constant after the initiation of the corrosion process. Using the inbuilt software, the average corrosion current density (minimum and maximum) is determined.

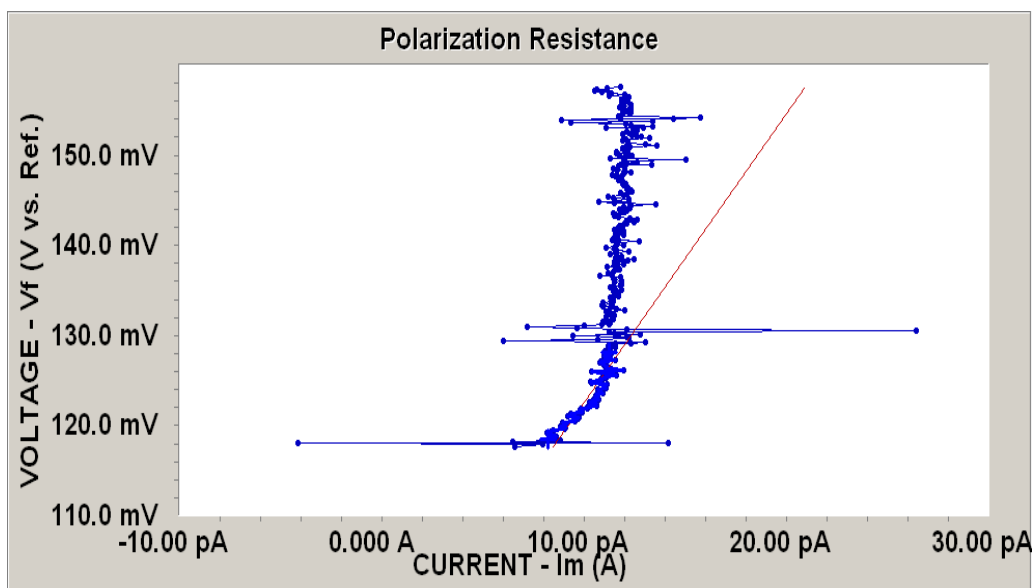


Figure 4.6: LPR Recording for E8018B2 Weld Metal

The galvanic current recording for the Weld Metal of the 8018G electrode weld is shown in Fig. 4.7. The blue colour trace represents the corrosion current and green colour trace represents the voltage. The calculated corrosion

value (average, minimum and maximum) appears at the bottom window of the trace. The galvanic corrosion recordings for different zones of all the welds are attached in the Appendix B.

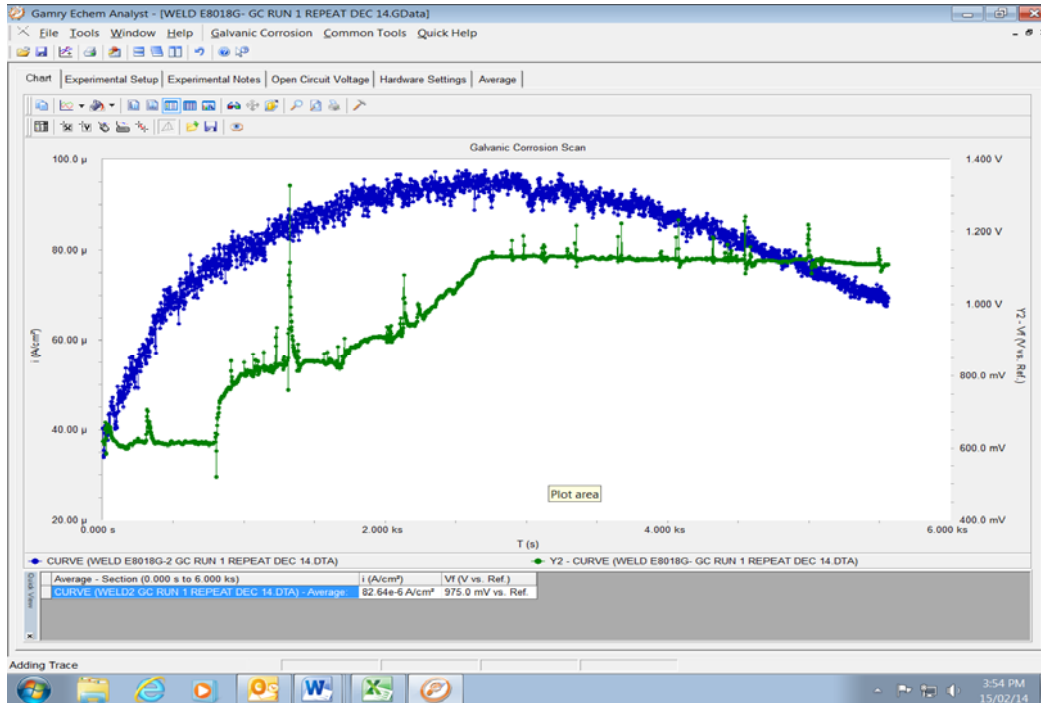


Figure 4.7: Galvanic Corrosion Tracing for E8018G Weld Metal

The corrosion characteristics of individual weld zone for various welds are determined by plotting the corrosion rate against time at an interval of 500 sec. Figure 4.8 shows the galvanic corrosion behaviour of different weld zones for E7018 weld at room temperature. The corrosion rate is highest for Weld Metal and lowest for the Base Metal. The corrosion rate of Weld Metal and Base Metal becomes constant towards the end of experiment. The corrosion rate of HAZ decreases at one point and then increases continuously for the remaining period to attain an intermediate level in between the Weld Metal and Base Metal.

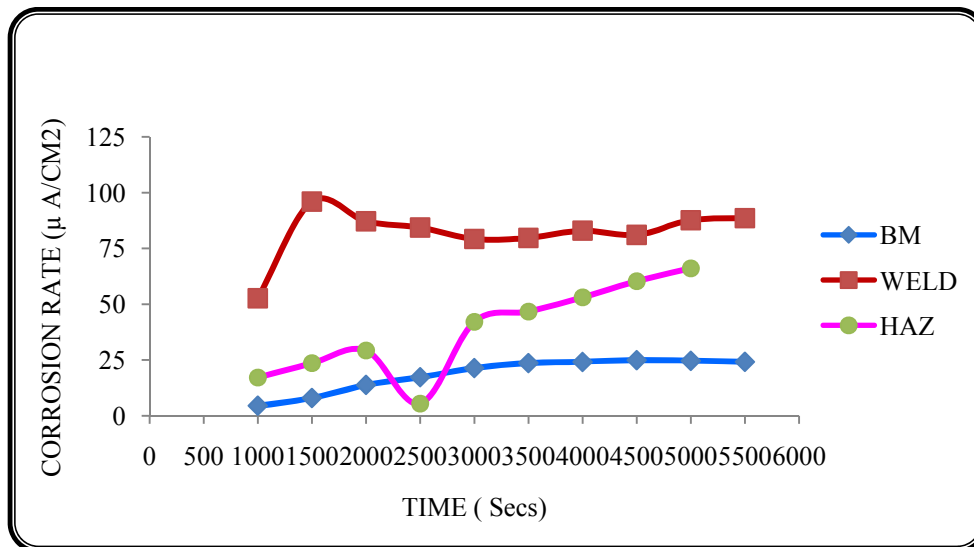


Figure 4.8: Galvanic Corrosion of E7018 Weld at Room Temperature

The corrosion current density for different weld zones of E8018G electrode weld at room temperature is shown in Fig. 4.9. The corrosion current density is highest for HAZ and lowest for Base Metal. The corrosion current density of HAZ and Base Metal increases continuously for the whole duration of experiment. The corrosion current density of Weld Metal increases initially to reach maximum in 2500 sec and then decreases continuously for the remaining duration of the experiment.

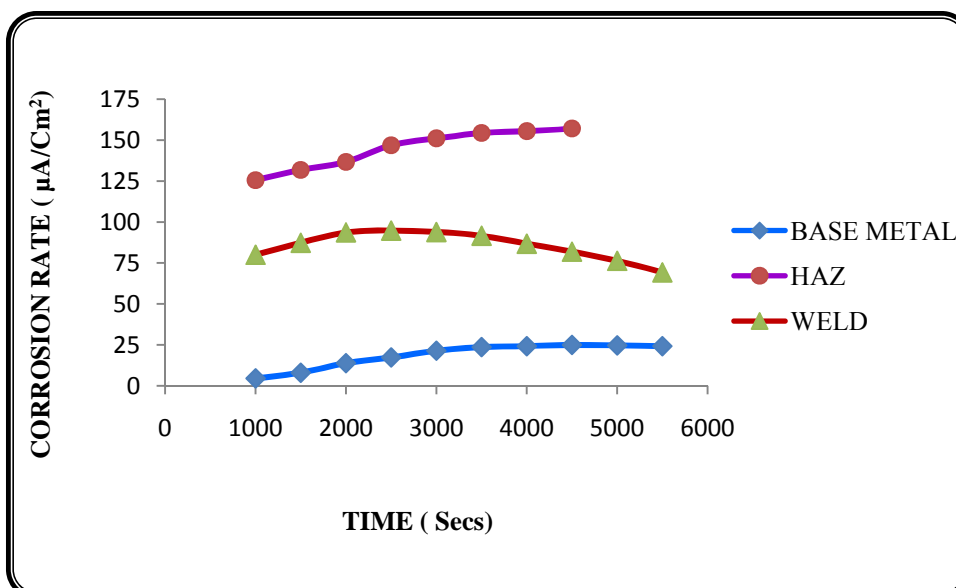


Figure 4.9: Galvanic Corrosion of E8018G Weld at Room Temperature

The corrosion current density for different weld zones of E8018B2 electrode weld at room temperature is shown in Fig. 4.10. The corrosion current density of HAZ for E8018B2 weld varies drastically by starting from the highest level and then fluctuates to become cathodic and anodic within the duration of experiment. The corrosion current density of Weld Metal is negative throughout the experiment i.e. it is passive and it increases slightly during the experiment. The corrosion current density of Base Metal increases continuously during the experiment and becomes constant towards the end of the experiment.

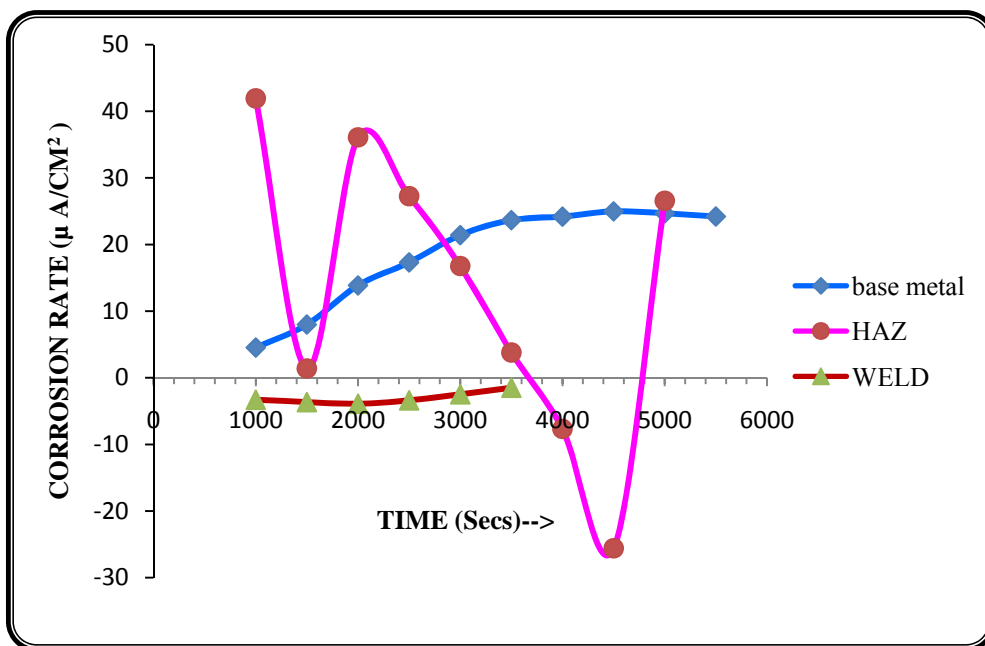


Figure 4.10: Galvanic Corrosion of E8018B2 weld at Room Temperature

The corrosion current density for different weld zones of E8018B6 electrode weld at room temperature is shown in Fig. 4.11.

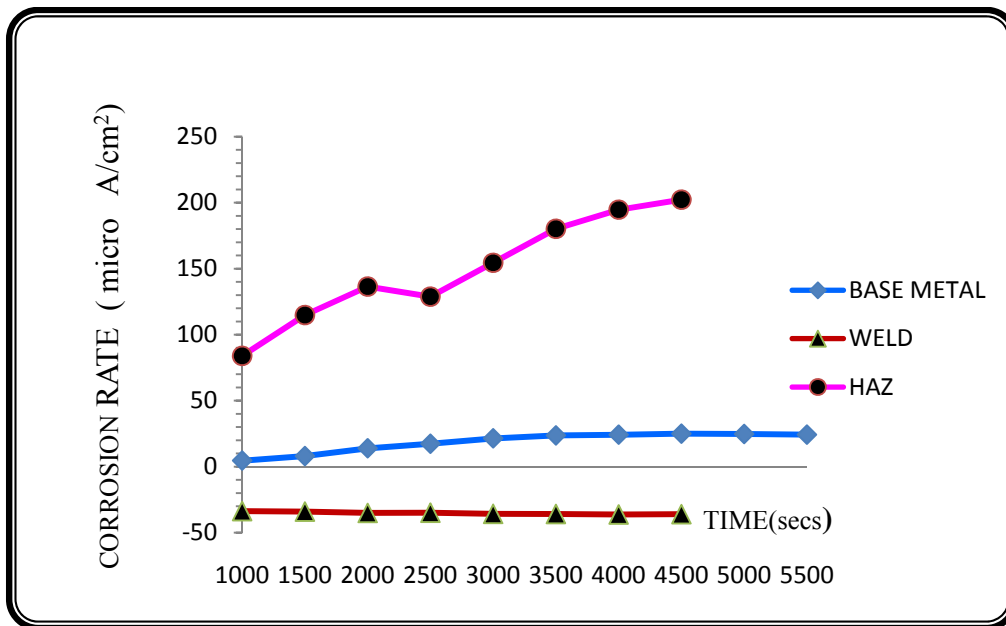


Figure 4.11: Galvanic Corrosion of E8018-B6 at Room Temperature

The corrosion current density of HAZ is highest and it increases continuously throughout the experiment except a drop at one point of time. The corrosion current density of Weld Metal is lowest and negative i.e. it is passive and it remains nearly constant throughout the experiment. The corrosion current density of Base Metal increases continuously and becomes constant at the end of the experiment.

The galvanic corrosion of Weld Metal of different welds along with Base Metal is compared as shown in Fig. 4.12. The corrosion current density of Weld Metals of E7018 and E8018G welds is positive i.e. these are active whereas the corrosion current density of Weld Metals of E8018B2 and E8018B6 is negative i.e. these are passive. The corrosion current density of Base Metal is positive i.e. it is active throughout the experiment. The corrosion current density of Weld Metal of E7018 weld continuously decreases after attaining maxima at 2400 sec but corrosion current density of

Weld Metals of other welds and Base Metal increases continuously throughout the experiment and becomes constant towards the end of the experiment.

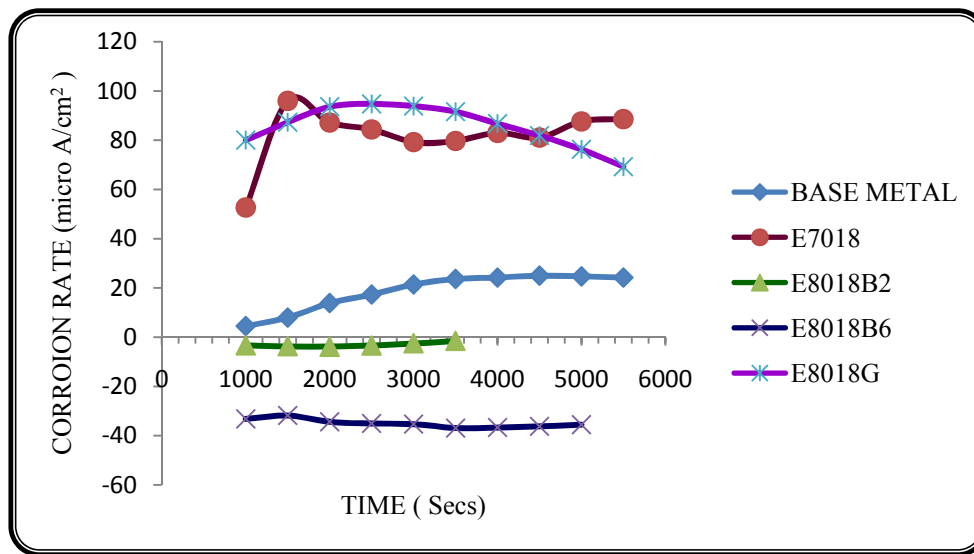


Figure 4.12: Galvanic Corrosion of Weld Metals of Different Welds and Base Metal at Room Temperature

The corrosion current density of Weld Metals and Base Metal is low and steady. The highest level of corrosion is observed for Weld Metals of E7018 and E8018G welds which are almost at the same level.

The galvanic corrosion of HAZ of different welds along with Base Metal is compared as shown in Fig. 4.13. The corrosion current density of HAZ of all the welds is positive i.e. these are active. The corrosion current density of HAZ of E7018 is initially negative but becomes positive after 1500 sec. The corrosion current density of E8018B2 is positive initially but becomes slightly negative between 3000 to 4500 sec. i.e. it is passive in this duration and then again becomes positive. The corrosion current density of Base Metal is positive i.e. it is active throughout the experiment. The corrosion current density of HAZ of E7018 weld continuously decreases after attaining maxima

at 2000 sec but corrosion current density of HAZ of E8018B6 increases continuously throughout the experiment.

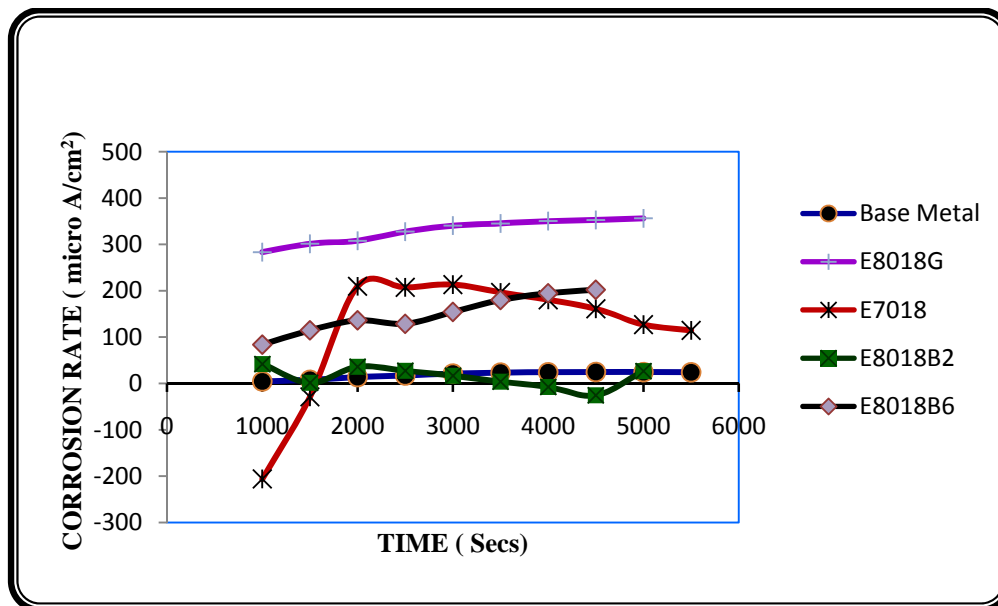


Figure 4.13: Galvanic Corrosion of HAZ of Different Welds at Room Temperature

The corrosion current density of HAZ of other welds and Base Metal remain nearly constant during the experiment. The corrosion current density of HAZ of all welds is relatively high in comparison to Base Metal but steady. The highest level of corrosion is observed for HAZ of E8018G weld and lowest for HAZ of E8018B2 weld.

The effect of welding defects like lack of fusion and undercut on corrosion behaviour of the Weld Metal is also investigated. Initially, the corrosion current density of the Weld Metal of defective weld is higher than that of the Weld Metal of weld without defect. The corrosion initially started at the defect locations as shown in the Fig.4.14. It attains maxima after 3000 sec whereas corrosion current density of the Weld Metal of the weld without defect continuously increases during the experiment and both become equal

after 4500 sec. The corrosion level of the defective weld is higher than the weld without defect as clearly shown in Fig. 4.15.



Figure 4.14: Corrosion Tested Weld (E7018) with Lack of Root Fusion and Undercut

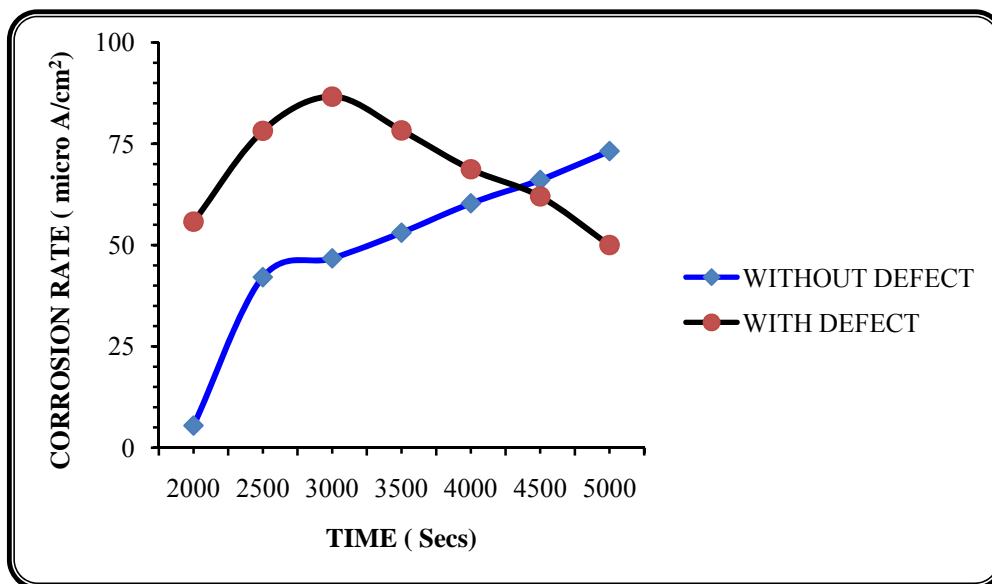


Figure 4.15: Corrosion Behaviour With / Without Defect -Weld E7018

The consolidated corrosion levels of Base Metal and Weld Metal for various welds are shown in Fig. 4.16. Figure 4.17 shows the consolidated corrosion levels of Weld Metal and HAZ. The galvanic corrosion test was conducted for

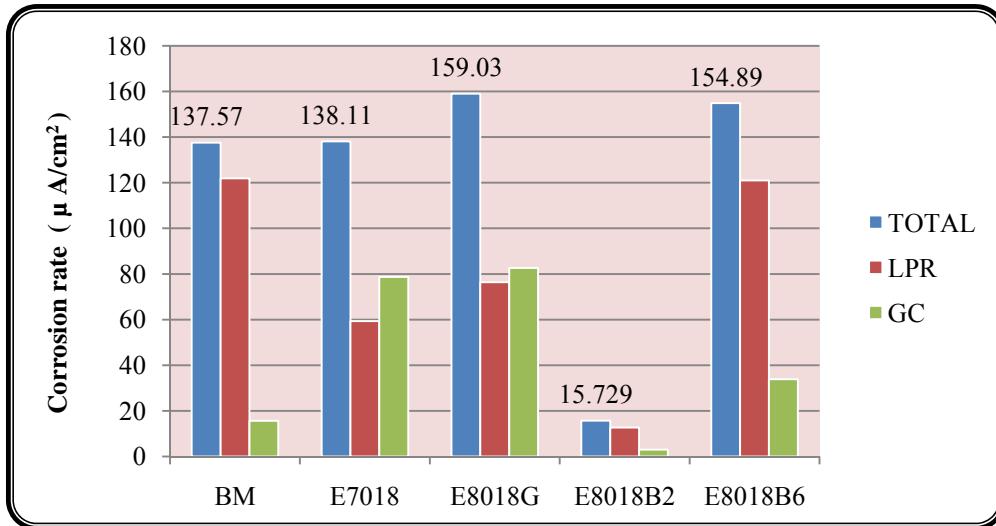


Figure 4.16: Total Corrosion Rate for Base Metal and Weld Metal for Various Welds

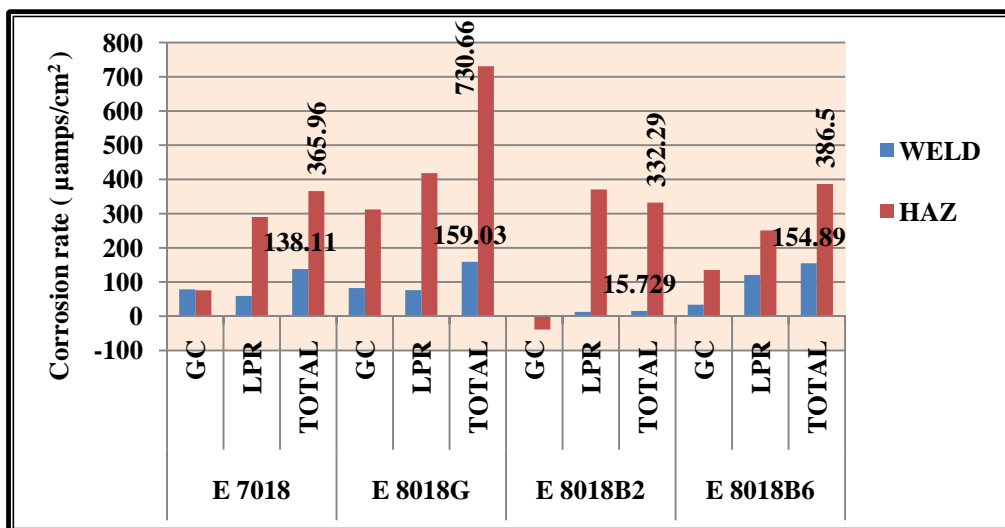


Figure 4.17: Total Corrosion Rate for Weld Metal and HAZ for Various Weld

Base Metal, Weld Metal and HAZ of all the welds. It is revealed that galvanic corrosion current of Weld Metal of E8018B2 electrode weld is lowest. Galvanic Corrosion current of HAZs is highest among all the weld zones except HAZ of E8018B2 electrode weld which is negative (below zero). General corrosion of HAZ is also highest among all the weld zones. It is observed that the total corrosion current is significantly low for Weld Metal of

E8018B2 electrode weld. Total corrosion current is highest for HAZ of E8018G electrode weld. The overall corrosion rate (Base Metal + Weld Metal + HAZ) is highest for E8018G electrode weld and lowest for E8018B2 electrode weld.

4.2.2. GALVANIC CORROSION AT VARIOUS TEMPERATURES

Experiments were conducted for the Base Metal and other zones of all the four types of (E7018, E8018G, E8018-B2 and E8018-B6) welds to determine the effect of temperature on corrosion reaction. The corrosion behaviour of E7018 weld is shown in Fig. 4.18.

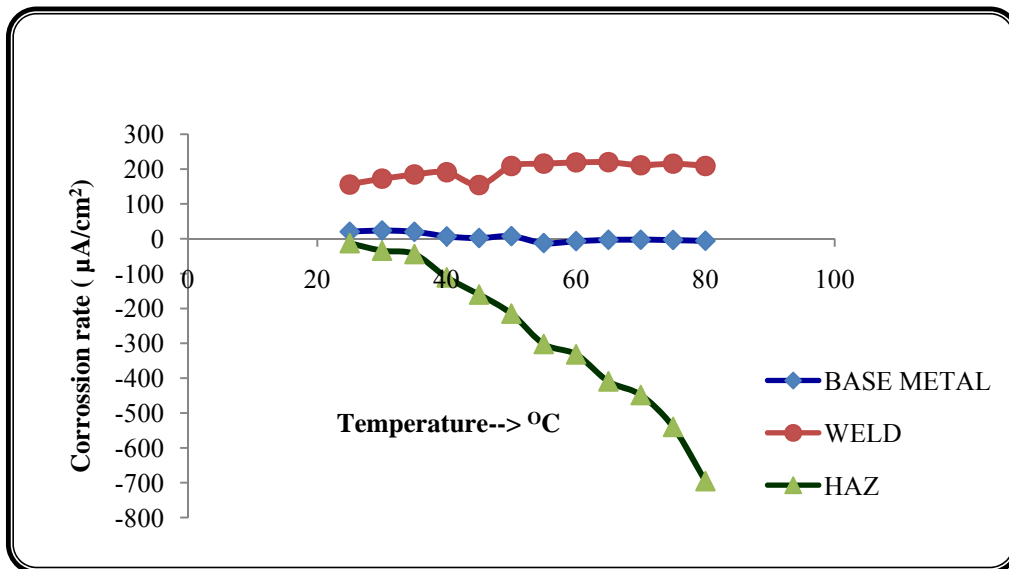


Figure 4.18: Galvanic Corrosion of E7018 weld at various temperatures

In this weld, HAZ seems to be more cathodic than Weld Metal and Base Metal whereas the Weld Metal is more anodic than the Base Metal. Corrosion rate of Base Metal remains nearly constant with temperature. Cathodic behaviour of HAZ increases drastically with increase in temperature but anodic behaviour of Weld Metal increases slightly with temperature. In other words, HAZ is most sensitive and Base Metal is least sensitive to temperature. The overall corrosion rate of E7018 electrode weld increases with temperature.

In general, increase in temperature accelerates the corrosion process. In the case of E8018G weld, HAZ behaves more cathodic as compared to the Base Metal and Weld Metal as shown in Fig. 4.19. Base Metal behaves anodic throughout the entire temperature range but Weld Metal and HAZ initially behave anodic and become cathodic after 30 °C for the remaining temperature range.

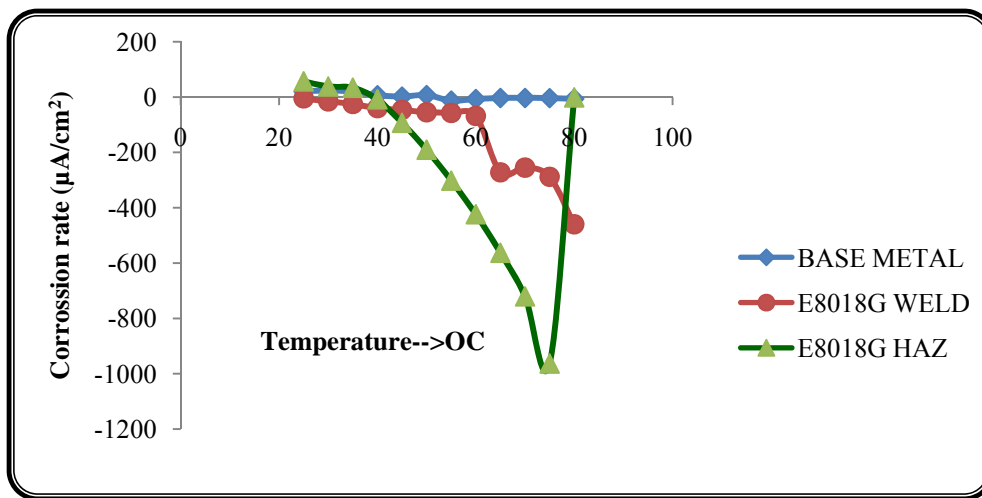


Figure 4.19: Galvanic Corrosion of E8018G weld at different temperatures

The corrosion behaviour of E8018B2 electrode weld at different temperatures is shown in Fig. 4.20.

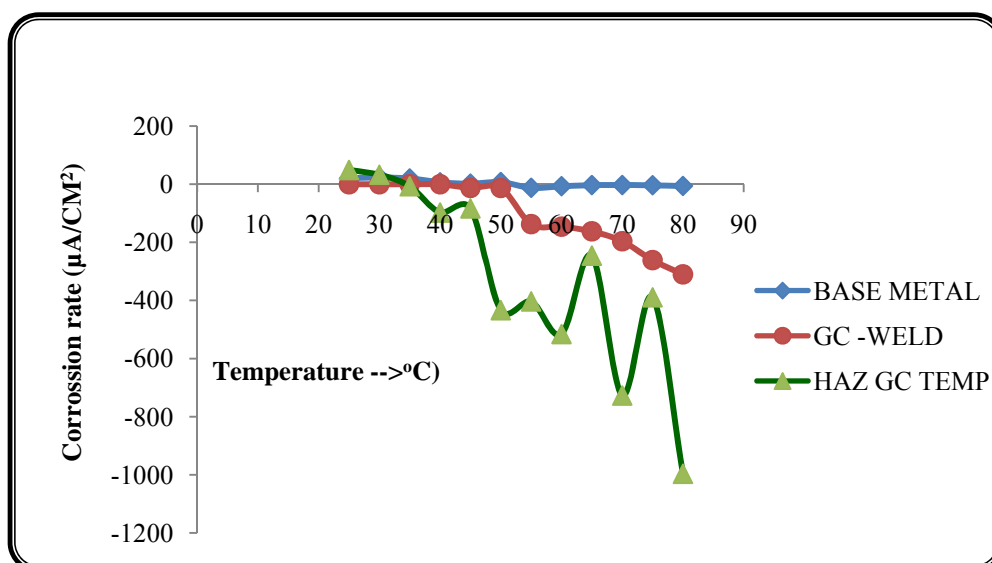


Figure 4.20: Galvanic Corrosion of E8018B2 weld at various temperatures

The HAZ of this weld is observed to be very active as compared to other zones. The Base Metal behaves anodic for the complete temperature range but Weld Metal and HAZ are slightly anodic during initial stages of temperature range but both become cathodic after 40 °C till the remaining temperature range. The corrosion current of HAZ was unstable after 50 °C and considerable change in current level was observed at every 5 °C interval.

The corrosion behaviour of E8018B6 electrode weld with increasing temperature is shown in Fig. 4.21.

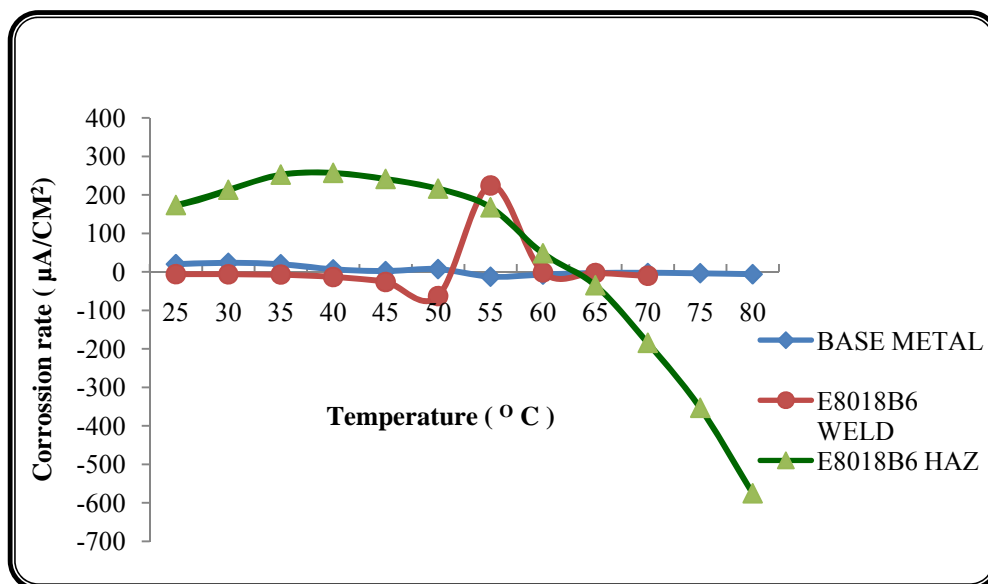


Figure 4.21: Galvanic Corrosion of E8018B6 weld at various temperatures

The Base Metal remains anodic throughout the entire temperature range. The Weld Metal behaves very differently as it is slightly passive initially till 35 °C and then becomes cathodic till 50 °C. It exhibits transition from cathodic to anodic between 50 °C to 60 °C and then again becomes passive for the remaining temperature range. The HAZ behaves anodic for most of the temperature range and then show transition from anodic to cathodic at 65 °C to become very active towards the end of the temperature range i.e. 80 °C. In this

weld, the Weld Metal behaves very similar to Base Metal except at two temperatures i.e. at 50 °C where it is more active than Base Metal and at 55 °C, where it is more passive than Base Metal. The Corrosion rate of individual zone at various temperatures is compared for all the welds using bar chart. Figure 4.22 shows the corrosion rate of Base Metal and Weld Metal zones of all the welds at different temperatures whereas Fig. 4.23 shows the corrosion rate of Base Metal and HAZs of all the welds at different temperatures.

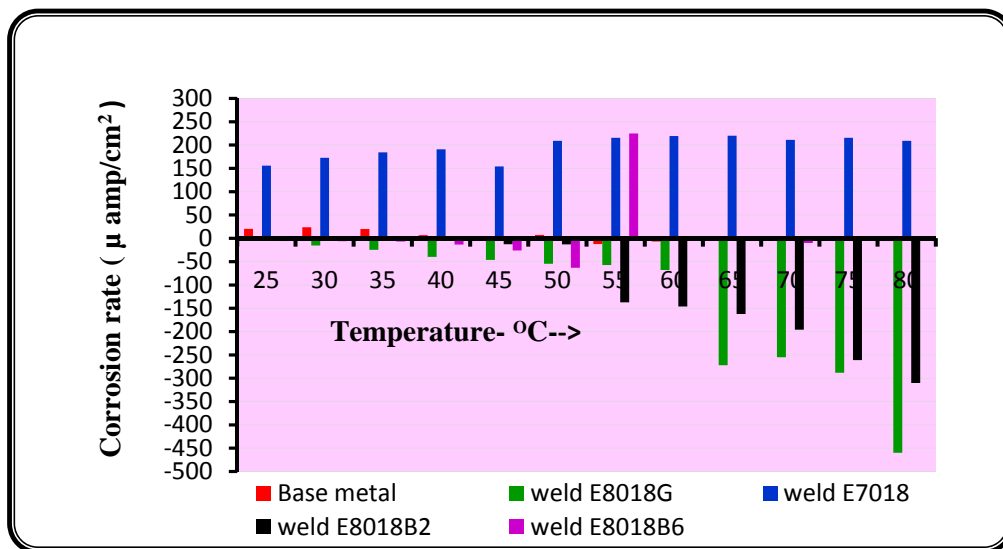


Figure 4.22: Galvanic Corrosion of Base Metal and Weld Metal Zones of Different Welds at Various Temperatures.

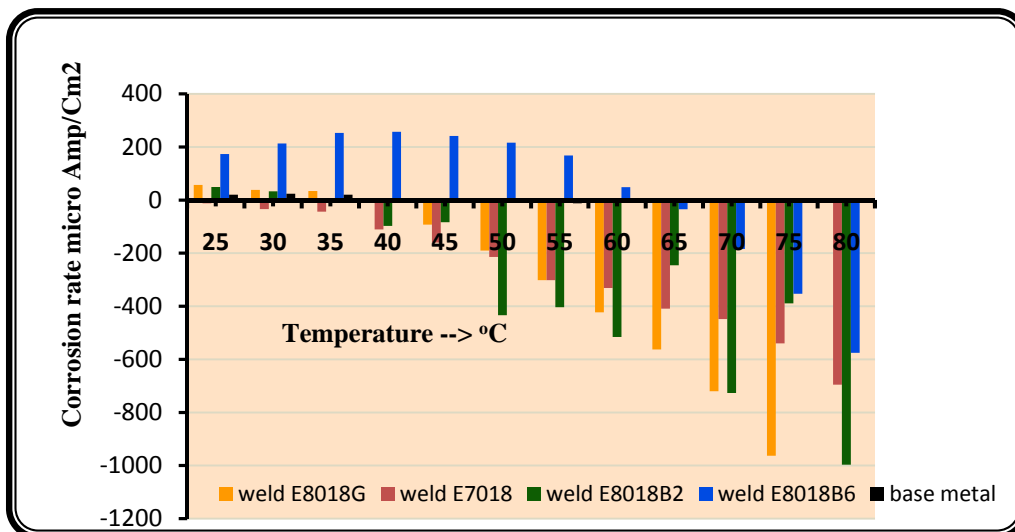


Fig.4.23: Galvanic Corrosion of Base Metal and HAZs of Different Welds at Various Temperatures.

It is clear that the Base Metal is anodic till 55 °C, and then becomes passive but the corrosion current is very low. The Weld Metal zone of E7018 electrode weld is fully anodic throughout the experiment. The Weld Metal zones of E8018G and E8018B2 electrode welds remain cathodic throughout the experiment but Weld Metal zone of E8018G electrode is more cathodic than the Weld Metal zone of E8018B2 electrode weld at low and high temperature whereas Weld Metal zone of E8018B2 electrode weld is more cathodic than Weld Metal zone of E8018G electrode weld at intermediate temperatures. The Weld Metal zone of E8018B6 electrode exhibits cathodic to anodic transition between 50 °C to 60 °C and then again becomes passive for the remaining temperature range. The Weld Metal zones of E7018 electrode weld and E8018B6 electrode weld are most active around 55 °C and Weld Metal zones of E8018G electrode weld and E8018B2 electrode weld are most passive towards the end of the experiment i.e. at around 80 °C.

The HAZ of E8019B6 electrode weld is anodic up to 60 °C and then becomes passive. Heat affected zone of E8018G is also initially active till 35 °C and then exhibits transition between 35 °C to 45 °C to become passive. The HAZs of all the welds become passive beyond 60°C. Passivity of all HAZs increases with increase in temperature. HAZs of E8018G electrode weld and E8018B2 weld are most passive whereas HAZ of E8018B6 electrode weld is least passive at high temperatures.

4.2.3. GALVANIC CORROSION AT VARIOUS TEMPERATURES WITH CO₂

Experiments were conducted on the Base Metal and different zones of all the four types of welds (E7018, E8018G, E8018-B2 and E8018-B6) to determine the combined effect of temperature and CO₂ environment on corrosion reaction. The corrosion behaviour of all the zones of E7018 electrode weld is shown in Fig. 4.24. The Weld Metal zone of this weld behaves fully cathodic throughout the experiment. The Base Metal and HAZ of this weld also behave cathodic during most of the temperature range but with one cathodic to anodic transition around 30 °C and 55 °C respectively.

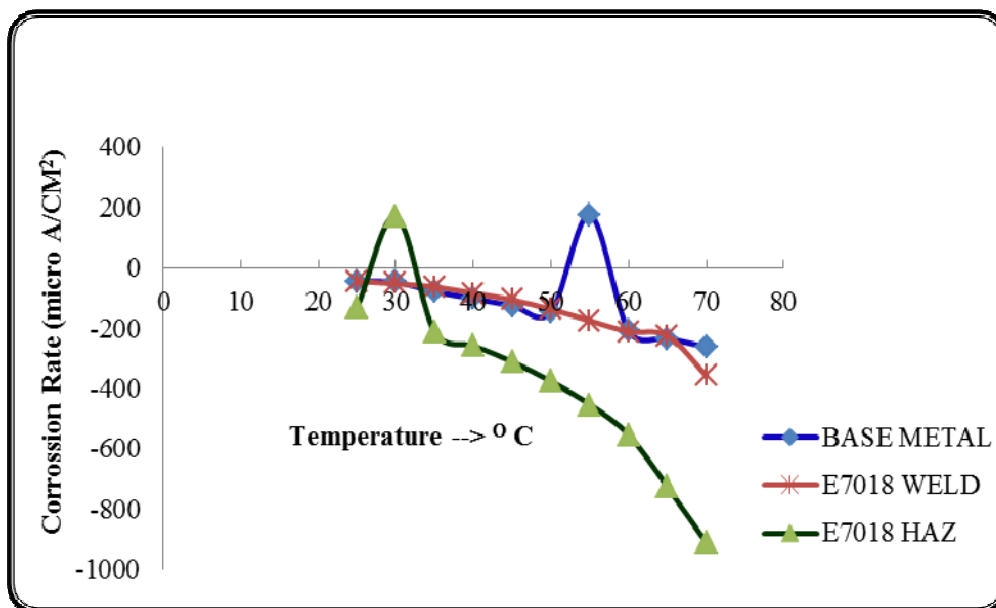


Figure 4.24: Galvanic Corrosion of E7018 Weld in CO₂ Environment at Various Temperatures

The corrosion rate of all the zones of E8018G electrode weld is shown in Fig. 4.25. All the zones are passive except Base Metal which exhibits cathodic to anodic transition between 50 °C to 60 °C.

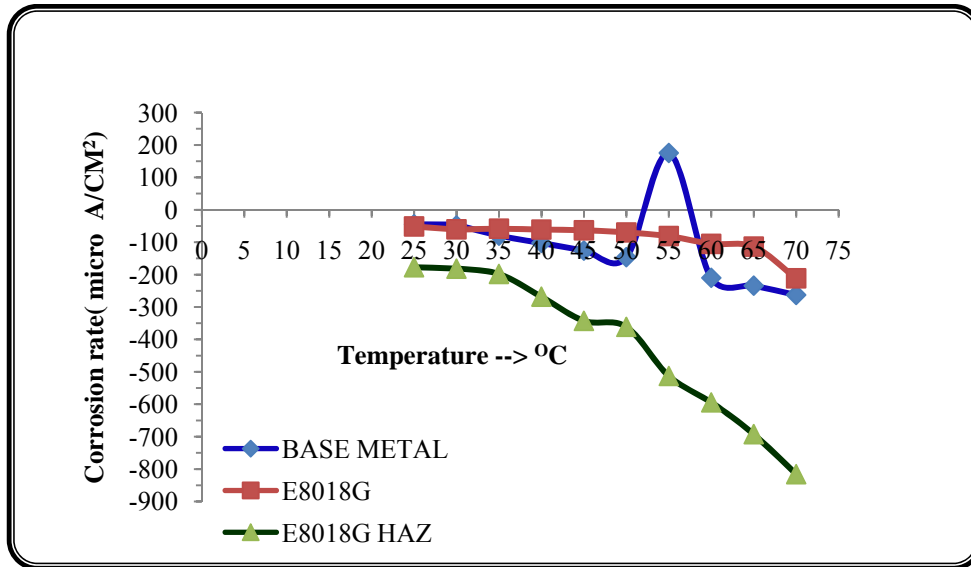


Fig. 4.25: Galvanic Corrosion of E8018G Electrode Weld in CO₂ Environment at Various Temperatures

The Weld Metal zones and HAZs of E8018B2 and E8018B6 electrode welds also remain passive throughout the experiment as shown in Fig. 4.26 and Fig. 4.27.

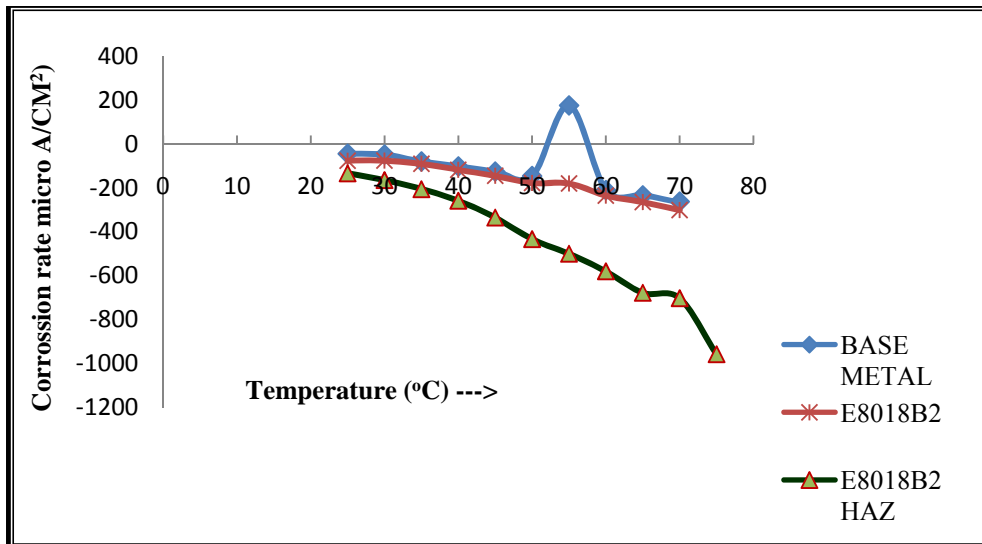


Fig. 4.26: Galvanic Corrosion of E8018B2 Electrode Weld in CO₂ Environment at Various Temperatures

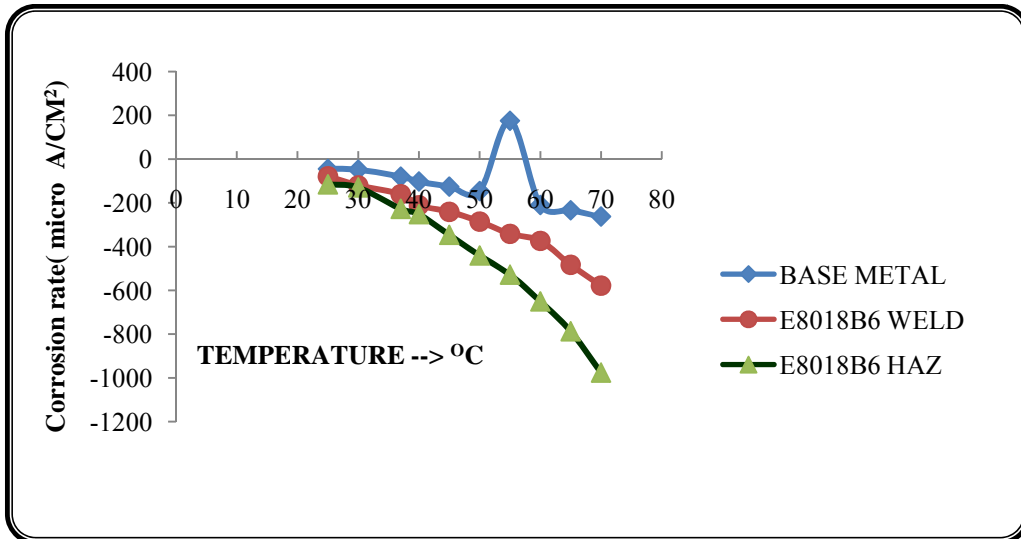


Fig.4.27: Galvanic Corrosion of E8018B6 Electrode Weld in CO₂ Environment at Various Temperatures

In all the welds, HAZ exhibits higher passivity as compared to the Weld Metal Zone and Base Metal. The corrosion characteristics of HAZs of all the welds are shown in Fig. 4.28.

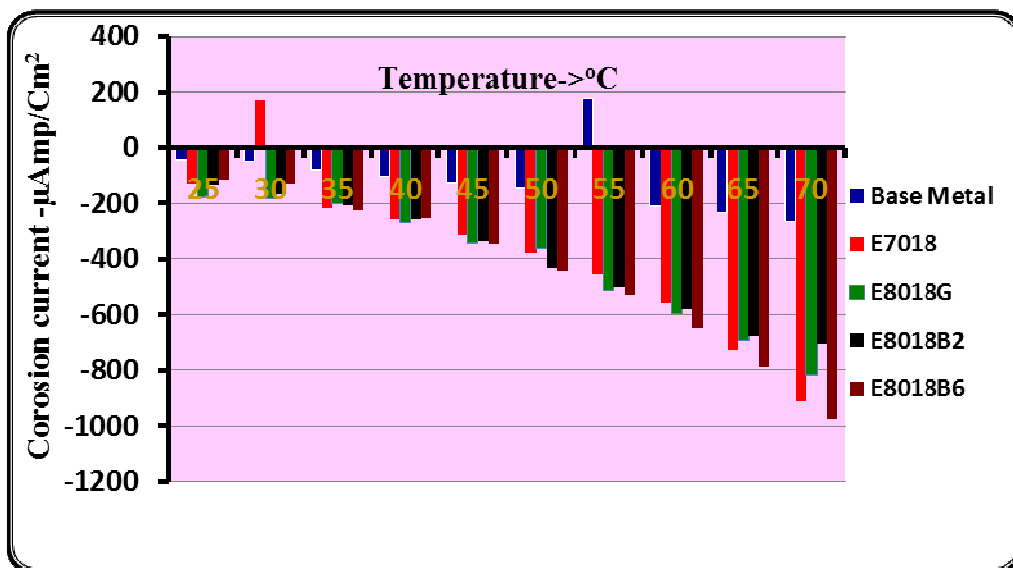


Fig.4.28: Galvanic Corrosion of HAZs in CO₂ Environment at Various Temperatures for all the Welds

The HAZ of E8018G electrode weld shows the highest passivity at low temperatures whereas HAZ of E8018B6 weld shows highest passivity at high

temperatures among HAZs of all the welds. The passivity of HAZ increases with temperature for all the welds.

Base Metal and the Weld Metal Zone show almost similar corrosion characteristics. The bar chart in Fig.4.29 shows the corrosion level of Weld Metal Zones for all the welds. The highest passivity is observed for Weld Metal of E8018B6 electrode weld and lowest for Weld Metal of E8018G electrode weld. The passivity of Weld Metal Zone also increases with temperature for all the welds.

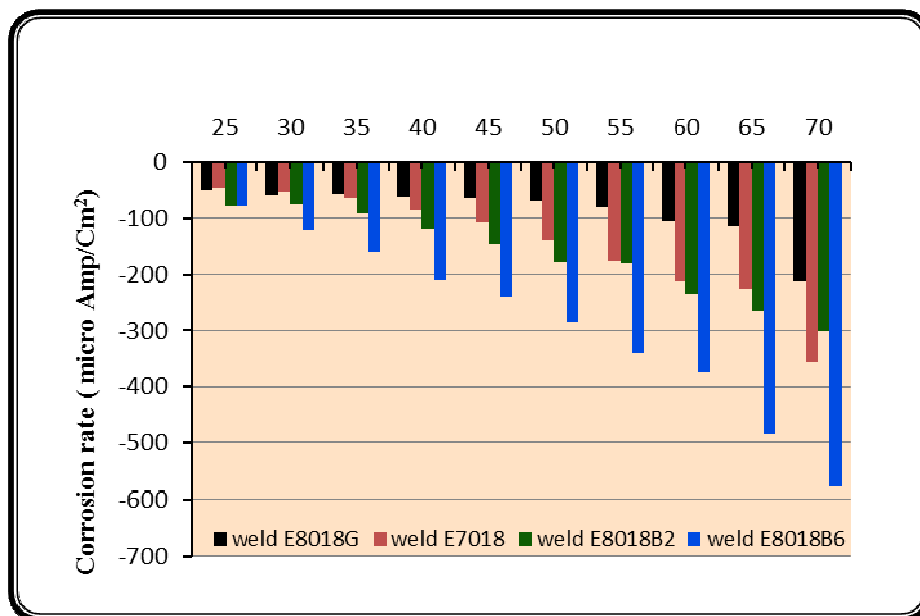


Fig. 4.29: Galvanic Corrosion of Weld Metal Zones in CO₂ Environment at Various Temperatures

The Base Metal and the Welds Metal Zones of E7018 and E8018G electrode welds are observed to be active at the small temperature range but other two welds are observed to be passive throughout the experiment. Except the Base Metal which shows relatively low passivity during most of the temperature range (up to 50 °C), the passivity of Weld Metal Zone and HAZ increases many folds with increase in temperature for all the welds.

The effect of temperature with or without CO₂ on Base Metal is shown in Fig. 4.30. Base metal is slightly active throughout in absence of CO₂ but in CO₂ environment, it is passive at all the temperatures except 55 °C.

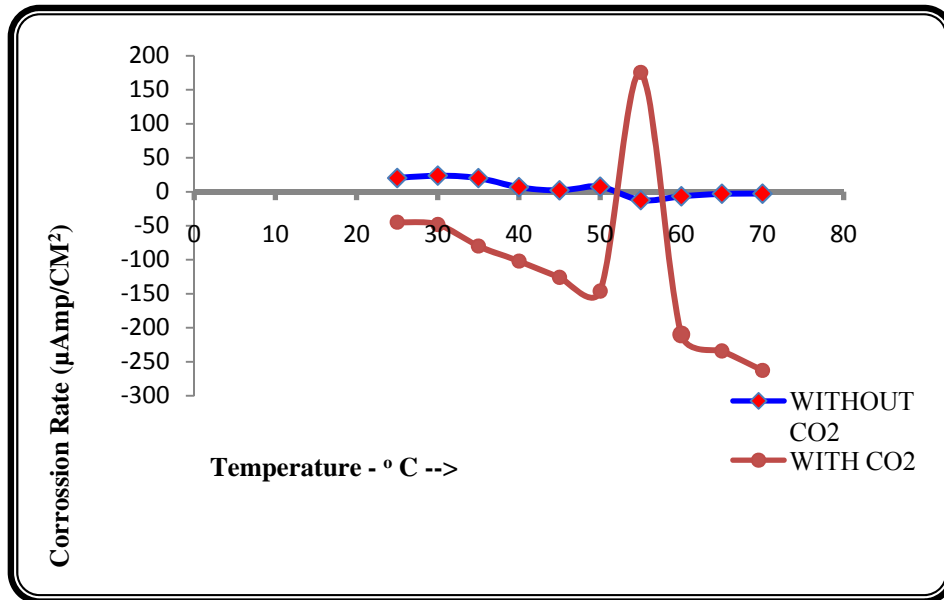


Fig.4.30: Effect of CO₂ and Temperature on the Corrosion of Base Metal

The effect of temperature with or without CO₂ on Weld Metal Zone for all the welds is shown in Figs 4.31 – 4.34. Weld Metal Zone of E7018 electrode weld is active in absence of CO₂ whereas the Weld Metal Zones of E8018G electrode and E8018 B6 electrode welds are passive. There is significant difference among these four welds. Weld made with E8018G is passive under both environments as shown in the Fig.4.31. However, in the presence of CO₂, the passive effect increases steadily with increase in temperature.

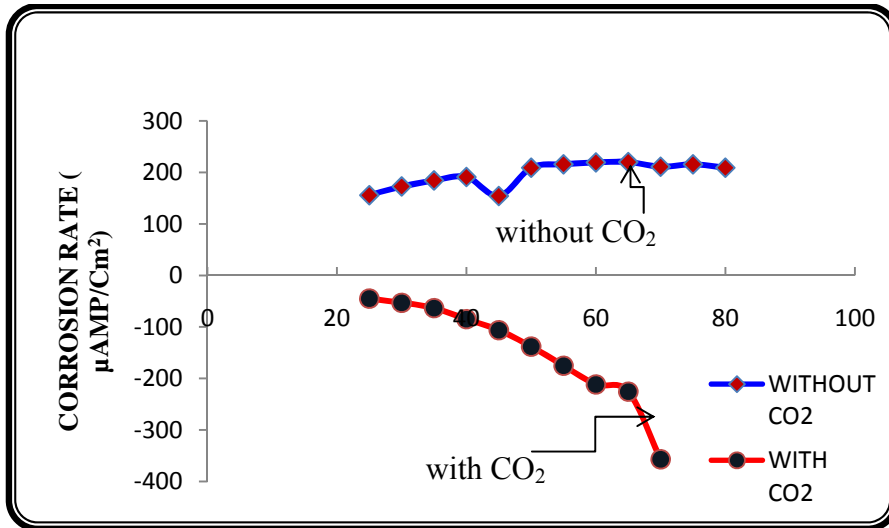


Fig.4.31: Effect of CO₂ and Temperature on the Corrosion of E7018 Weld Metal Zone

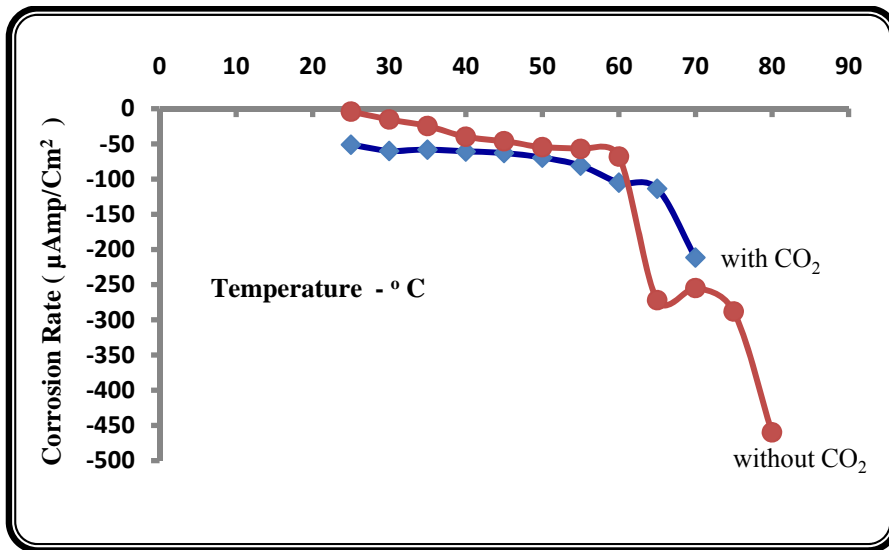


Fig.4.32: Effect of CO₂ and Temperature on the Corrosion of E8018G Weld Metal Zone

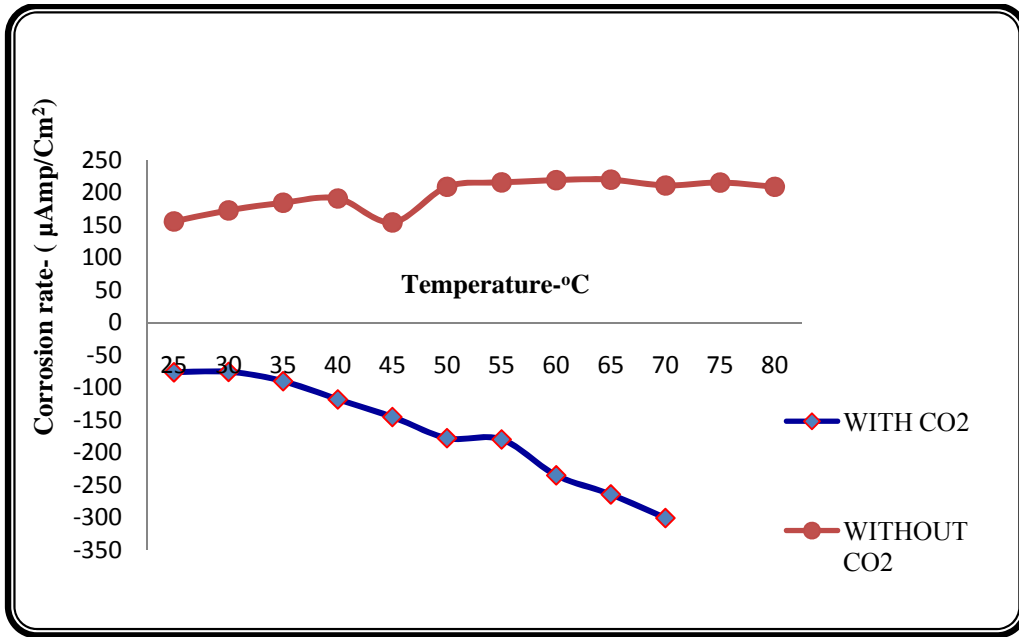


Fig.4.33: Effect of CO₂ and Temperature on the Corrosion of E8018B2 Weld Metal Zone

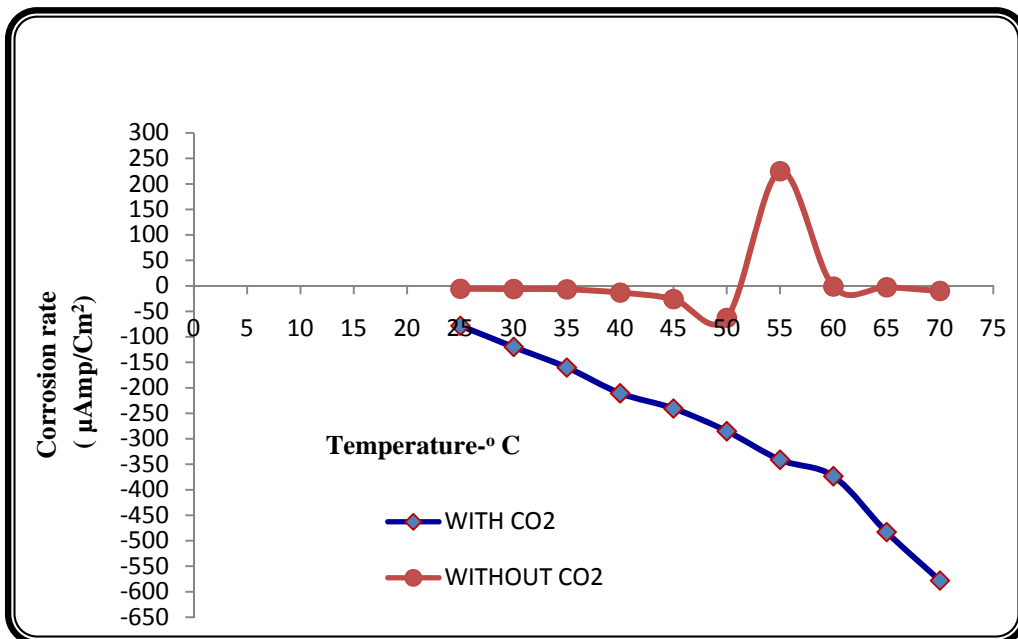


Fig.4.34: Effect of CO₂ and Temperature on the Corrosion of E8018B6 Weld Metal Zone

The effect of CO₂ on various HAZs is shown in the Figs. 4.35- 4.38. The HAZ of E7018 electrode is active around 30 °C and becomes passive afterwards till

the end of the experiment at 75 °C. In the absence of CO₂, the HAZ behaves completely cathodic as shown in the Fig.3.35.

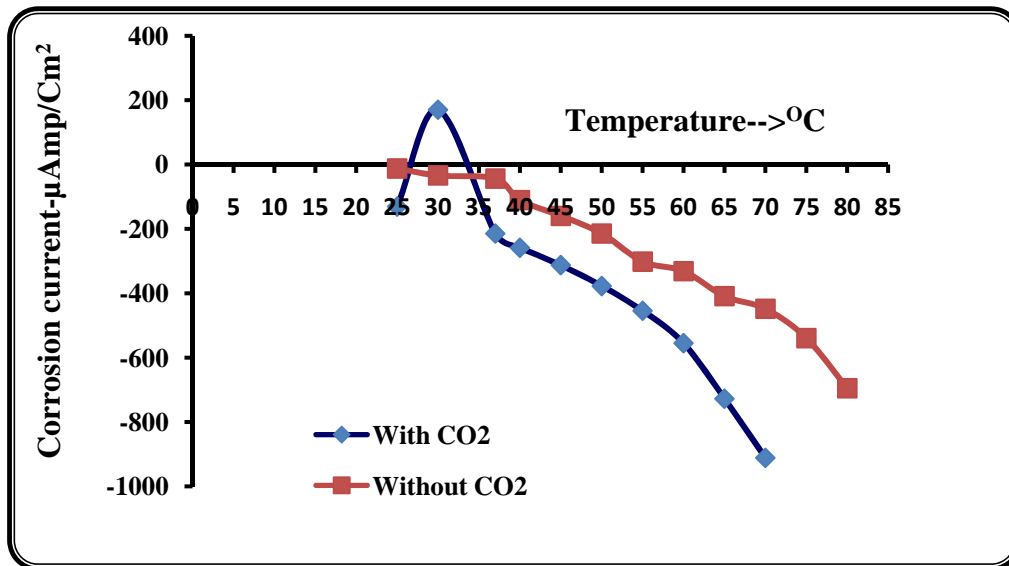


Fig. 4.35: Effect of CO₂ and Temperature on the Corrosion of HAZ of E7018 weld

In the case of E8018G electrode weld, HAZ is anodic till 40 °C and then becomes passive till 70 °C in absence of CO₂ environment. Beyond 70 °C, again the passivity is reduced and reaches close to anodic region. The HAZ behaves completely cathodic under CO₂ environment as shown in Fig. 4.36.

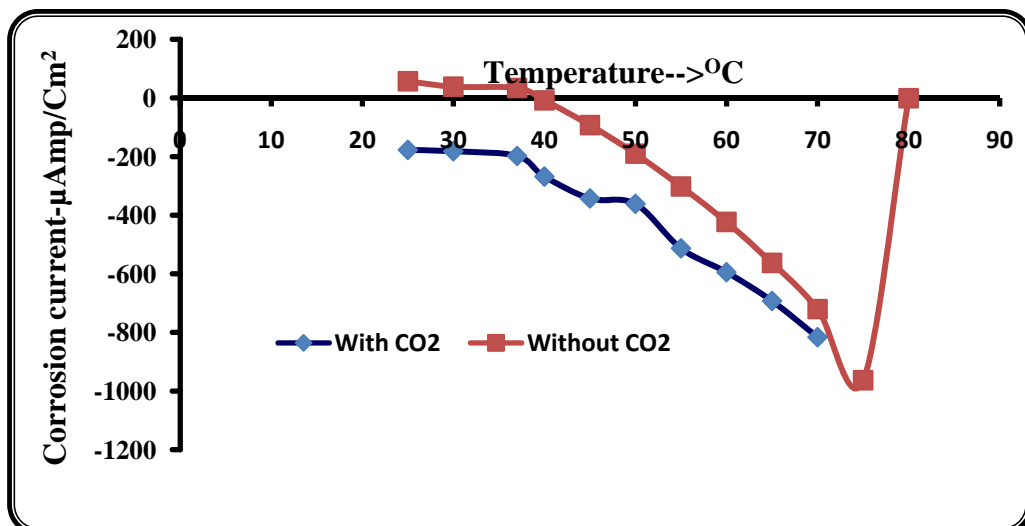


Fig. 4.36: Effect of CO₂ and Temperature on the Corrosion of HAZ of E8018G weld

The Fig. 4.37 shows the effect of CO₂ environment on corrosion behaviour of HAZ of E8018B2 weld at various temperatures. In the absence of CO₂, HAZ is fully passive but the variation in passivity is significant. The presence of CO₂ results in continuous increase in cathodic behaviour of HAZ.

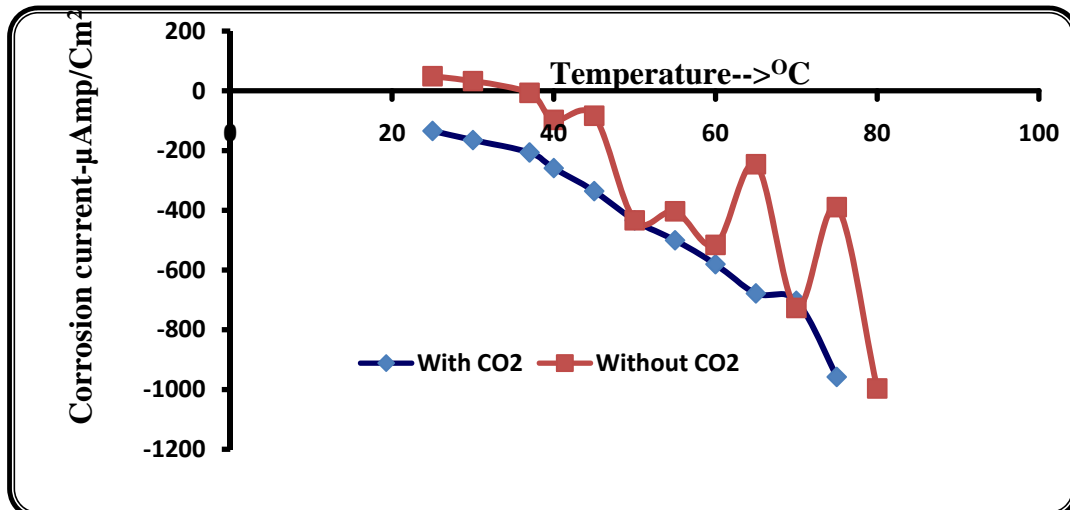


Fig. 4.37: Effect of CO₂ and Temperature on the Corrosion of HAZ of E8018B2 weld

The effect of temperature and CO₂ environment on corrosion behaviour of HAZ of E8018B6 weld is shown in Fig. 4.38. Under CO₂ environment, the HAZ is fully passive but in absence of CO₂, HAZ behaves anodic till 60 °C and then becomes passive till the end of the experiment.

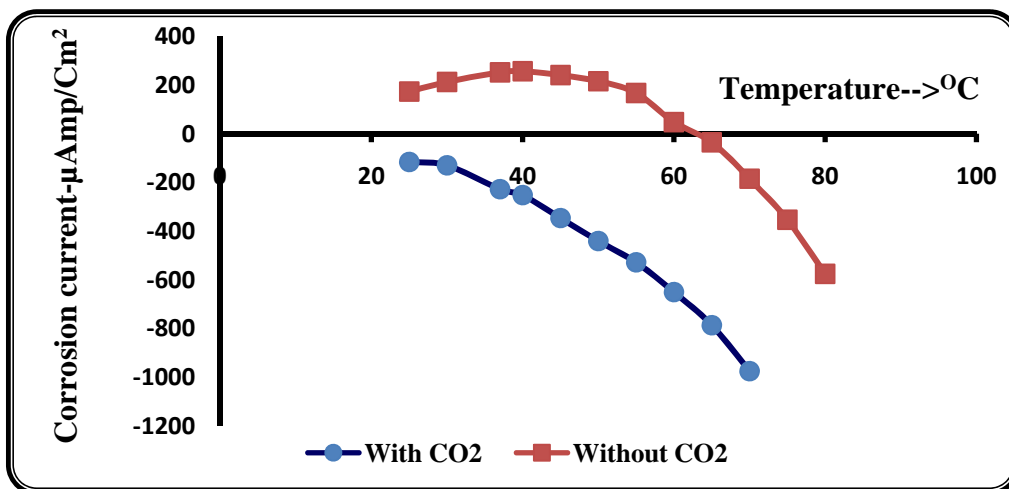


Fig. 4.38: Effect of CO₂ and Temperature on the Corrosion of HAZ of E8018B6 weld

4.3. STATISTICAL ANALYSIS - POLYNOMIAL REGRESSION RESPONSE MODEL

This regression model is a simple function, such as linear, quadratic or higher degree polynomial, fitted to the data obtained from the experiments. This function is called a response surface, and the approach is called the response surface method. It consists of a group of mathematical and statistical techniques to develop an adequate functional relationship between a response of interest and number of associated control variables (input) for empirical model building [85]. For one variable, this model is expressed as follows-

$$y = \beta_0 + \beta_1 X + \beta_2 X^2 + \beta_3 X^3 + \dots + \beta_n X^n \quad (4.4)$$

In this polynomial model, the mean of the dependent variable is a function of a single dependent variable. Even though the independent variables in a multiple regression model may be related to each other, typically they are not assumed to be function of one another. The degree (or order) of an individual term in a polynomial is defined as the sum of the powers of the independent variables in the term. The degree of the entire polynomial is defined as the degree of the highest degree term. The higher degree polynomial models provide increased flexibility in the response surface. This flexibility of the higher degree polynomials allows any true model to be approximated to the desired degree of precision. This model has been proved to be extremely useful for summarizing the relationships and is useful in situations where the curvilinear effects are present in the true response. Also, it is useful as approximating function to unknown and complex nonlinear relationships. The experimental data was analysed using this regression model.

Generally, a well curve fitting regression model results in predicted values close to the observed values. The mean model uses the mean for every predicted value if there are no informative predictor variables. The fit of a proposed regression model is better than the fit of the mean model. The curve fitting was done using MINITAB statistical software. The results have been in line with the experimental values. This has the useful property that its scale is intuitive. It ranges from zero to one. Zero indicates the proposed model does not improve prediction over the mean model and one indicates perfect prediction.

The degree of fitness is around 0.99 for all the samples which reflects that the fitness level is good. The regression model is given in the form of equation which is applicable only for a particular weld zone. The experimental data was analysed using this regression model. A typical sample curve fitting of Weld Metal Zone of E8018G weld is shown in the Fig. 4.39.

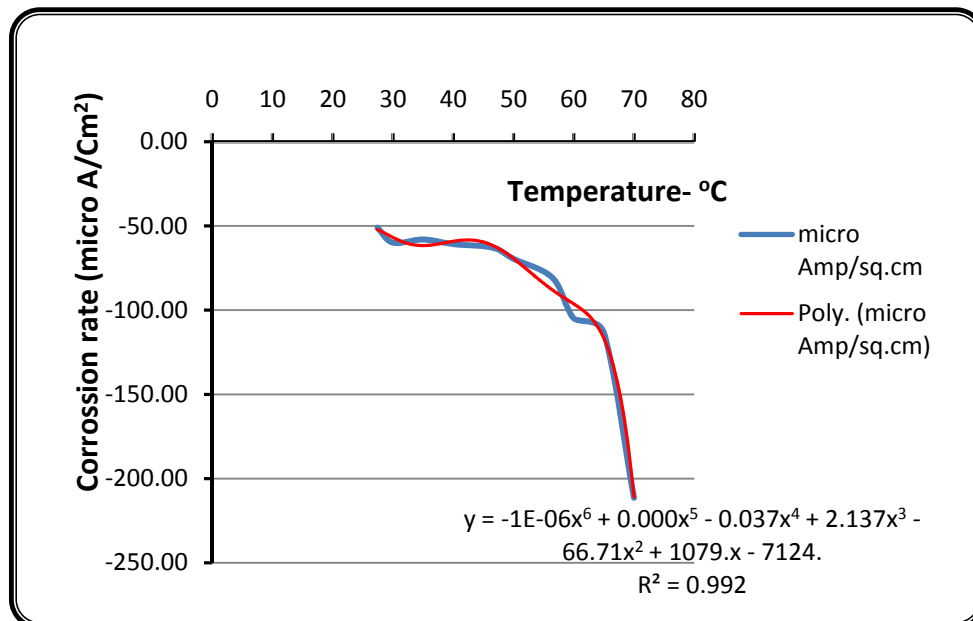


Fig.4.39: Regression Response Model for Weld Metal Zone of E8018G weld under CO₂ environment at various Temperatures

The other results are given in the Appendix-C with R-square values. The R-square value has been determined for different weld zones of all the tested welds and found to be around 0.9 which is considered as good fitting.

The equations are given below for other welds-E7018, E8018B2 and E8018B6 which can be used to calculate the corrosion rate (y) at any temperature (x).

Equations for Weld Metal Zone and HAZ of E7018 weld:

$$y = -2E^{-06}x^6 + 0.0006x^5 - 0.0652x^4 + 3.7395x^3 - 117.81x^2 + 1932.2x - 12922 \quad (4.5)$$

$$(R^2 = 0.998)$$

$$y = -2E^{-05}x^6 + 0.004x^5 - 0.557x^4 + 35.48x^3 - 1239.x^2 + 22460x - 16454 \quad (4.6)$$

$$(R^2 = 0.985)$$

Equations for Weld Metal Zone and HAZ of E8018B2 weld:

$$y = 0.0009x^3 - 0.1963x^2 + 6.9094x - 136.76 \quad (4.7)$$

$$(R^2 = 0.990)$$

$$y = -2E^{-06}x^6 + 0.0005x^5 - 0.053x^4 + 3.113x^3 - 100.56x^2 + 1689x - 11616 \quad (4.8)$$

$$(R^2 = 0.997)$$

Equations for Weld Metal Zone and HAZ of E8018B6 weld:

$$y = -0.006x^3 + 0.7274x^2 - 36.584x + 479.98 \quad (4.9)$$

$$(R^2 = 0.996)$$

$$y = -0.000x^4 + 0.069x^3 - 4.923x^2 + 140.0x - 1479 \quad (4.10)$$

$$(R^2 = 0.999)$$

The experimental data was validated using polynomial regression model and found fitted well with the experimental results.

4.3.1. DATA ANALYSIS OF VARIANCE

The existing methods of data analysis are Analysis of variance (ANOVA), half normal plots, t-tests, stepwise regression and other variables selection

techniques etc. These are done to determine the significant effects which influence the responses. After identification of the significant effects, a model is determined using these effects. In this study, the effects are studied in three stages and detailed data have been analysed to determine the responses. The equations obtained by regression analysis (curve fitting) can be considered as optimum setting of factors involved. The important factors with / without CO₂ and the effect of temperature were analysed for the Weld Metal Zone and HAZ of E8018G electrode weld by analysis of variance method. This method was used to determine the impact of independent variables on the dependent variable in the regression analysis. The design matrix and the data are provided in Table 4.5.

Table 4.5- Design Matrix Data for ANOVA Analysis

Std. Order	Run Order	Pt. Type	Blocks	Temp	Time	Medium
2	1	1	1	1	1	2
6	2	1	1	2	1	2
7	3	1	1	2	2	1
3	4	1	1	1	2	1
5	5	1	1	2	1	1
1	6	1	1	1	1	1
8	7	1	1	2	2	2
4	8	1	1	1	2	2

This is used to analyse the differences between the means. Under the column – temp, time 1 represents minimum and 2 represents maximum. Under the column medium, 1 represents without CO₂ condition and 2 represents with CO₂ condition. Since E8018G electrode is being used for welding procedure qualification for the actual jobs, this weld was used for the analysis to simulate the practical situation. Moreover, the response trends are almost same for

other electrodes. The ANOVA plot for both Weld Metal Zone and HAZ are shown in the Fig.4.40 a & b.

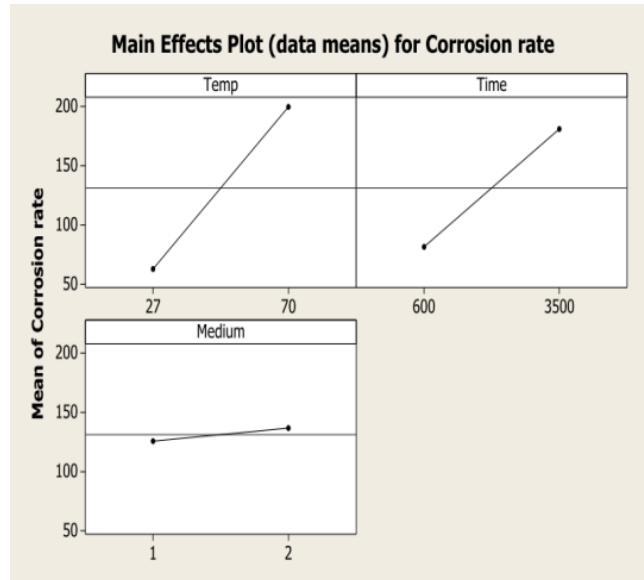


Fig.4.40 a: Plot for the Weld Metal Zone

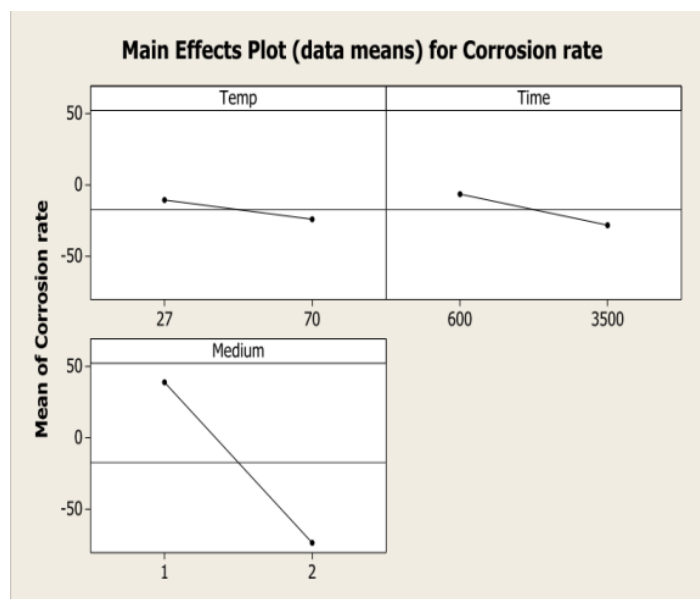


Fig.4.40 b: Plot for the HAZ

CHAPTER 5 - DISCUSSION

5.1. WELD METAL ANALYSIS

5.1.1. CHEMICAL COMPOSITION

The important elements which influence the corrosion characteristics are Si, Cr, Mo and Ni. Si promotes fast slag formation by lowering melting point and improves tensile strength of steel. Further, it promotes graphitization i.e. decomposition of Iron Carbide (Fe_3C) into metallic Fe and graphite. Si is present in significant amount in all the welds. Cr being strong carbide former improves wear resistance and somewhat increases resistance to softening during tempering. When present in solid solution, Cr stiffens ferrite and decreases ductility. It improves corrosion resistance largely by formation of Cr enriched protective scale [86]. Mo has remarkable effect on hardenability. When present in solid solution, Mo stiffens ferrite and decreases ductility. It also improves high temperature corrosion resistance. The Cr and Mo content are significant for the welds made with E8018B6 and E8018B2 electrodes. Ni is the highest for weld E8018G and lowest for weld E7018. Ni improves fatigue properties and hardenability. When present in solid solution, it has the ability to impart strength at lower carbon contents. It improves weldability and plasticity. In addition, it improves low temperature toughness and corrosion resistance. The change in carbon content is not much and the film formation is expected without much change in all the welds. Hence, this

element is not considered for the analysis. But it influences the corrosion characteristics as chromium depletion takes place by formation of chromium carbide in the welds. The mechanical properties are determined by the composition. The weldability and hardenability of the material is determined by the carbon equivalent which is given in the Table 4.1b. Each alloying element is given a coefficient relating to its influence to that of the equivalent amount of carbon. Many oil and gas operators specify this equivalent of 0.42 as maximum for carbon steels. If the level is more than this limit, hardness, brittleness and fraction of hard microstructure of the weld get increased. This equivalent value is important which decides the weld corrosion characteristics. In practice, the pre and post heat treatment requirements are determined on the basis of this equivalent level to avoid formation of hard microstructure during welding.

5.1.2. MICRO HARDNESS

There is not much variation in the hardness of Base Metals and HAZs of the welds. A significant variation was there in the hardness of Weld Metal Zones of the welds. The Weld Metal Zone of E8018B2 showed a very high hardness of 354 in comparison to other Weld Metal Zones having hardness in the range of 202 to 226.

Hardness is a measure of the ease with which solids can be plastically deformed. There are two types of hardness such as Physical and chemical [87]. The theory of chemical and physical hardness is useful because it unifies understanding of various properties and it connects the behaviour of molecules with those of liquids and solids. Physical hardness is proportional or sometimes

equal, to the chemical hardness. Chemical hardness is an energy parameter that measures the stabilities of molecules, atoms etc. This electronic chemical hardness is the derivative of the electronic chemical potential i.e. the internal energy with respect to the number of valence electrons. The electronic chemical potential itself is the change in total energy of a molecule with a change in the number of valence electrons. The corrosion characteristics are related to chemical hardness. Chemical potential is another name for total internal energy. During corrosion process, the exchange of electrons through the medium depends upon this chemical potential. One of the chemical hardness properties is polarizability which depends upon the valence electron density. This property requires electron be excited from the valence to the conduction band. This is what happens during polarization due to corrosion process. In this aspect, hardness also plays important role in corrosion process.

5.1.3. WELD MICROSTRUCTURES

The micrographs for the different zones are shown in Figs. 4.2 (a-h) & 4.3 (a-h) for all the welds. The variations can be due to the magnification level and difficulties in interpretation etc. [88]. High resolution electron microscope at high magnification can provide precisely microstructural variations among different zones of all the welds. It is reported that HAZ of Quenched and Tempered steels normally has martensitic and bainitic structures. In this investigation, only ferritic and bainitic structure is obtained. This may be due to controlled heat input during welding. The Base Metal is not affected by heat input and so similar microstructures were obtained.

The metallurgical properties of Weld Metal Zone are mainly influenced by heat input, cooling rate and type of electrode [89]. All the Weld Metal Zone micrographs reveal the presence of pearlite, coarse columnar or coarse acicular ferrite with feeble bainite. The observed variation in microstructures of Weld Metals of different welds may be due to different chemical compositions of electrodes, different heat input during welding and largely cooling rate during solidification of the weld pool. Generally, microstructural features like grain size and increase in aligned second phase, phases like cementite, martensite etc. lead to preferential weld corrosion [90-92]. During multi pass welding, the weld gets refined after the root weld whereas the root weld is exposed to atmosphere and the surface becomes unrefined compared to subsequent weld passes. Hence, the weld root surface has the tendency for preferential corrosion. In addition, the surface roughness also alters the corrosion action [93].

5.2. CORROSION TEST RESULTS

5.2.1. GENERAL AND GALVANIC CORROSION AT ROOM TEMPERATURE

A clear difference is observed in the polarization resistance curve with E8018B2 electrode compared to other electrodes. The corrosion current was very less even at aerated condition (in peco amps) and almost constant. Though little noise had been observed, the slope is almost zero at E_{corr} . To get closer approximation on corrosion rate, a tangent was drawn as shown in the Fig.4.6 which is a common practice to find the slope other than E_{corr} location. Every element is having its own property to influence the characteristics like corrosion resistance, ductility, machinability etc. There can be little difference

in corrosion rates according to the line drawn on the tracing keeping the zero as the centre point. Galvanic corrosion is mainly influenced by the composition. The distinct difference in the influence on corrosion behaviour has been observed with Cr, Ni, Cu and Mo. Some of the elements influence the grain size, final microstructure, weld hardness such as Al, Ti, V and Boron etc. The elements like Cu, Al and V assist in the formation of protective film. PWRC describes selective attack of the Weld Metal Zone. Weld Metal Zones are usually more electronegative than the Base Metal depending upon relative Si content. Generally, Si content improves metal fluidity during welding but it forms SiO₂ inclusion which may act as sites for the initiation of corrosion [22]. Hence, addition of this element is made with caution though it helps the Weld Metal Zone to become cathodic.

In general, the elements like Ni and Cr possess very good resistance to oxidation and corrosion. Chromium is a solid solution strengthener and carbide former [94]. Mo tends to help steel to resist softening at high temperatures and increases creep strength. There are conflicting reports on the influence of various elements on corrosion [95]. The effect of thermal cycle on corrosion is ring worm corrosion in HAZ. This has the shape of a ring and is located a few inches from the pipe upset. The ring can either be very smooth or may have severe pitting. Ring worm corrosion is caused by the upsetting process, in which the heat required for upsetting creates two different grain structures; One in the upset (A part at the end of tubulars such as drill pipe, casing or other tubing, which has extra thickness and strength to compensate for the loss of metal in the threaded ends) and another in the rest of the pipe [96]. The welding parameters significantly contribute to the heating and

cooling cycle, chemical composition, and microstructure transformation and in turn on corrosion characteristics. It is a proven fact that Ni addition up to 1% increases corrosion resistance and beyond 1%, it enhances the preferential corrosion. This limit is also emphasized by MR-0175 but the limit is somewhat arbitrary [79]. Though this is satisfactory for many applications, there are instances that severe preferential weld corrosion has been reported in sweet (CO₂) environments under certain conditions even at less than 1% Ni level [16]. Ni alloyed weld reduces the risk of PWC but only in low conductivity environment [9]. Ni is an austenite stabilizer and depresses ferrite and martensite formation temperatures. It contributes beneficial effect on steel transformations similar to manganese. It lowers the austenite transformation temperatures and improves toughness. It also provides solid solution hardening effect. Hence, changes in any one of the conditions like environment, Base Metal composition, deposited Weld Metal Zone composition and the welding procedure (thermal cycle) may influence the corrosion characteristics either way. In SMAW process, the Weld Metal Zone is deoxidised by the flux coating. The slag and gas metal reaction promotes acceptable properties of Weld Metal Zone by increasing or decreasing the content of various elements. The oxide inclusion in combination with Mn and Si can lead to corrosion attack. It has been reported that Si is also equally detrimental like more than 1% Ni [9]. Solution resistance also influences the local corrosion rate. It limits the anodic area to a narrow band adjacent to the weld bead. The Base Metal revealed pearlite in the ferrite matrix. All the welds revealed polygonal & widmanstatten ferrite growth from grain boundary ferrite along with coarse acicular ferrite. During this process, the

corrosion scale formation takes place which in turn reduces the corrosion action. It means that the electrons which were generated at the anode were unable to reach the cathode surface as the formed scale slow down the reaction hence, cathodic activity is reduced. Later, when the formed scale breaks down, the corrosion current again increases.

Generally, if there is a disturbance on the corrosion film, a change in corrosion level is observed. The corrosion current is reduced as the passive film builds up. It is clearly shown in the Fig. 4.7. At 1.085 ks, there is a break in the tracing and the current level comes down by about 15% and then again started increasing but could not reach to that level which was observed at the start of the experiment. The negative sign indicates that the weld is passive. The Base Metal shows lowest level of corrosion as compared to the Weld Metal Zone and HAZ. The Weld Metal showed highest level of corrosion. The Weld Metal Zone of E7018 electrode weld behaved less cathodic than its HAZ. The same characteristic was observed with E8018G weld. The HAZ and Base Metal of E8018B6 weld showed high corrosion current and the Weld Metal Zone behaved fully passive because the exposed HAZ is very narrow, the corrosion film formation is very fast and became passive after 6 minutes of the test.

It is shown that the weld properties especially the composition is very strong factor in controlling the corrosion action. The hard microstructures lead to higher corrosion than any other microstructure. The corrosion currents of Weld Metal Zones of E7018 and E8018G electrode welds are almost close to each other. Welds Metal Zones of E8018B2 and E8018B6 electrode welds were cathodic. The HAZ of all the welds behaved as anodic at different levels of corrosion current.

The highest corrosion current was observed with HAZ of E8018G electrode weld. Any reduction in corrosion current level is due to corrosion film formation. This phenomenon is primarily due to microstructure of HAZ. The highest level of corrosion was observed with E8018G electrode weld. The corrosion rates of Weld Metal Zone of E7018 and E8018G electrode welds show almost same level though the chemical compositions differ slightly except the Ni content. The Si content of E7018 electrode weld is almost double to that of E8018G weld which is contributing to this effect.

The experimental results exhibit higher corrosion current levels for the sample which has the lack of fusion defect as compared to samples without defect. Wherever, surface defects (like undercut, lack of penetration etc.) exist, the corrosion reaction is found to be more pronounced compared to remaining weld surface [97] which is clear from the corrosion film formed at the lack of fusion area as shown in Fig. 4.13. It is reported that such weld defects even creates catastrophic failure such as grooving corrosion since the corrosion activity gets initiated at these surface defect locations. Surface roughness due to weld bead ripples also increase the corrosion reaction [98].

The consolidated corrosion levels for various weld zones are shown in Figs. 4.15 and 4.16. Though welding codes allow certain amount of defects and the welds are accepted after non-destructive testing like radiography and ultrasonic methods, still there is a possibility for initiation of corrosion from these surface defects at the weld root. The average corrosion current (general and galvanic corrosion) is highest for E8108G electrode weld. This reflects that the effect of Si content is comparable to the effect of Ni content. Though the Si content is reported detrimental for corrosion protection, there seems to

be no other reason except the microstructure. Hence, in case the E7018 electrode got mixed up with 8018G, only the strength (particularly toughness) of the weld is a concern. But the Si content may vary up to 0.75% maximum in various commercial electrodes of same specification as per AWS A5.1. Hence, the same level of Si content cannot be expected in all the commercial electrodes of same specification. The observed difference in corrosion rate is due to high Ni content. The higher corrosion rate in HAZ as compared to other zones of all the welds proves that HAZ is anodic to nearby Weld Metal and Base Metal Zones. The effect of weld root hardness seems to be less significant on corrosion rate under the present experimental conditions as the differences in hardness levels are not much significant. This is due to the control of heat input. During welding the root side is exposed to atmosphere and hence normalizing effect is expected. The hardness cannot be directly measured on the root surface under as welded condition due to ripples / roughness etc. Hence, the hardness was measured as close as possible inside the root in the cross sectioned weld as per NACE MR 0175. The Weld Metal Zone reflects distinct difference in corrosion rate. There is no difference in weld microstructures of 8018B2 and 8018B6 electrode welds. There is considerable variation in Cr and less variation in Ni content. All other elements are almost at close level. Being the same microstructure, Cr level plays major role on corrosion. Composition of 1% Cr weld is nobler than 5% Cr (E8018B6) weld. The Weld Metal Zones of E7018 and E8018G electrode welds are cathodic and HAZ of all the welds are more anodic to Base Metal. The Weld Metal Zone of E8018B2 electrode weld is more cathodic as compared to Weld Metal Zones of all other welds. A clear difference can be

observed between the Weld Metal Zones of welds which has 1% Cr with less Ni and 1%Ni with very less Cr. The Weld Metal Zone of the weld with Cr is more anodic than Weld Metal Zone of Ni content weld. Another interesting observation is that the Weld Metal Zone of high Cr (4.6 %) content is more anodic than Weld Metal Zone of 1% Cr. This result is contradicting the general understanding of Cr effect.

The galvanic corrosion test was conducted for different zones of all the welds including the Base Metal and HAZ. It was observed that the total corrosion current was significantly low with high chromium level E8018B6 electrode. HAZ showed high level of corrosion current. The corrosion current of Weld Metal Zone made with high Cr content electrode E8018B6 is significantly low. The galvanic corrosion test for E8018B2 shows negative (below zero) and the Weld Metal Zone corrosion is almost zero.

5.2.2. GALVANIC CORROSION AT VARIOUS TEMPERATURES

Generally, liquid phase generates more corrosion than gas phase. The corrosion behaviour under temperature depends upon wet or dry environment. General trend is that the corrosion rate increases with increase in temperature [99]. Temperature is analogues to potential. A potential difference creates current flow. In similar manner, a temperature difference creates heat flow and both are measure of energy. In general, corrosion increases exponentially with increase in temperature. As temperature increases, oxygen solubility decreases so that oxygen tends to leave the liquid. In the closed system, oxygen cannot escape. As the temperature increases, the water vapour pressure increases which tend to maintain the oxygen concentration in the medium. The

corrosion rate (mass transfer rate) continues to increase with temperature. Also, increase in temperature can affect corrosion by changing the pH from neutral to acidic value. The medium temperature can affect the polarity of galvanic corrosion. It affects electrochemical reaction, chemical reaction, mass transfer etc. As the temperature increases, the corrosion products form a film on the surface and the corrosion process is slowed down. This is a common phenomenon observed in most of the carbon steel material. This protective layer is called siderite (FeCO_3) layer [100]. Also the Fe_3C (cementite) present in the original steel microstructure is often incorporated in the formed layer along with siderite. The size and distribution of this cementite determines the protectiveness of the layer [101]. The corrosion potential of the anode might be more sensitive to temperature than that of the cathode. The anode potential can become noble with respect to cathode. In the E7018 electrode weld, HAZ behaved more cathodic than the Weld Metal Zone and Base Metal but the Weld Metal Zone exhibited more anodic than the Base Metal. In the case of E8018G weld, the HAZ exhibited more cathodic compared to the Weld Metal Zone and Base Metal as shown in Fig 4.18. It confirms clearly that the composition plays major role on corrosion behaviour. Since, the microstructures are almost similar, the effect of microstructure seems to be less as compared to composition.

The Weld Metal Zone of E8018B2 electrode weld exhibited cathodic behaviour. In this case, though the weld has high alloy content (Cr & Mo), HAZ exhibited more cathodic means comparatively microstructure plays the major role. The HAZ has fine ferritic grain and fine grain always gives less corrosion as compared to coarse grain. The Weld Metal Zone behaved similar

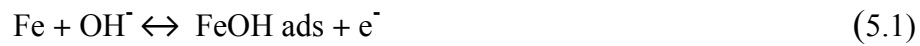
to the Base Metal till 50°C and then the Weld Metal Zone became more cathodic due to scale formation. The variations seen on the HAZ shows the frequent break down of the formed scale. Base Metal corrosion slowly increased with increase in temperature and then remained almost constant. The Weld Metal Zone of E8018B6 electrode weld also exhibited cathodic behaviour with respect to the Base Metal and HAZ. The HAZ was very active compared to other zones.

The HAZs of E8018B2 & E8018B6 welds which have the same refined ferritic grains behaved differently. The HAZ of E8018B2 weld is cathodic and of E8018B6 weld is anodic. Hence, the general belief that the fine ferritic structure provides good corrosion resistance is still questionable. The Weld Metal of E7018 electrode weld is fully anodic throughout the experiment while that of E8018G electrode weld is fully cathodic. The HAZ of E8018B6 electrode weld is anodic up to 60 °C and then became passive. The Base Metal initially active and then slowly became passive after 45°C. HAZs of E7018 and E8018G electrode welds were passive. In general, though the HAZ microstructure results in more corrosive (anodic), the individual weld zones show different corrosion behaviour. In spite of almost similar microstructure of the HAZs, the heterogeneities in this area creates different behaviours.

5.2.3. GALVANIC CORROSION AT VARIOUS TEMPERATURES UNDER CO₂ ENVIRONMENT

CO₂ corrosion is influenced by parameters related to interface, materials and medium. Interface related parameters are temperature, flow rate, condensation and presence of scales. Materials related parameters are alloy composition, microstructure and heat treatment. The medium related parameters are pH,

CO₂ partial pressure, solution chemistry and the presence of oxygen. All the parameters are independent and influence the CO₂ corrosion in different ways. The formation of corrosion product layers on the metal surface during corrosion reaction control the corrosion rate. At low temperature range (below 60 °C) formation of protective film may not be significant due to high solubility of FeCO₃ [103]. Above this temperature, solubility of FeCO₃ decreases considerably and high saturation leads to FeCO₃ precipitation and dense protective film may form. In the presence of chloride, the anodic dissolution takes place in three steps.



The mechanism of equation 5.3 is always fast and the reaction 5.1 is in equilibrium at low pH. The reaction 5.2 is the rate determining under active dissolution. The high hydroxyl concentration speeds up the rate of reaction. Deward and Milliams [9] concluded that two parallel cathodic reactions take place in CO₂ corrosion; one is reduction of hydrogen ions and the other is reduction of carbonic acid which is electro-active. H₂CO₃ can be directly reduced and H₂CO₃ dissociation can serve as the source of H⁺ ions [103]. The elements present in small concentrations are strongly enriched at the corroding surface after the exposure to the medium. Spots at the metal surface which are rich in Cr, Ni, Cu and S have the influence on both electron transfer and the catalysis of CO₂ to carbonic acid. Galvanic corrosion is essentially a multi-electrode system with each zone of material having individual corrosion characteristics. In conducting media, the corrosion potential (coupling

potential) is uniform over the surface and determined by the corrosion activity and the relative area ratios of the individual zones. For materials in the passive state, coupling of a nobler Base Metal to a less noble and more susceptible section of the different zones of the weld, e.g. the Weld Metal Zone itself, raise the potential of the later with the result that localized attack is ensured. For an isolated material suffering localized attack, the corrosion potential tends to drop as corrosion developed and results in a decrease in the corrosion rate. However, coupling to the large area of the Base Metal means that the coupled potential does not decrease significantly as localized corrosion develops in the Weld Metal Zone. For carbon steels in the active state (no protective passive film), the main concern is when regions of the weld are electrochemically more active than the Base Metal. For carbon steels which actively corrodes (no protective passive film), the Base Metals are more active (lower potential) than the other regions of the weld which becomes cathodic [104-106]. Since the area ratio of the Weld Metal Zone and the Base Metal is small, the electrode potential of the Base Metal is not modified significantly by the Weld Metal. Correspondingly, the electrochemical driving force on the Base Metal remains unchanged. However, the effective area ratio involved in corrosion reaction depends on the potential drop in the solution. Generally, the rate of Weld Metal attack is dependent on the Ni and Cu contents of the welding electrode and is less influenced by Base Metal composition. Although steel with copper, nickel, and chromium additions led to nobler Base Metal, acceleration of Weld Metal attack is possible. It has been reported that the Base Metal with low silicon content leads to increased Weld Metal corrosion, supporting the earlier findings that silicon $< 0.2\%$ can be detrimental, but the

opposite was observed here for silicon in the Weld Metal. Several case studies on galvanic corrosion failures are presented elsewhere on carbon steels within short period after commissioning [44]. It is reported that the examples demonstrate the necessity for testing each galvanic couple in the environment for which it is intended. Hence, higher alloy filler metals are used to prevent rapid preferential weld corrosion. The galvanic corrosion of Weld Metal and HAZ for all the welds revealed that at pH 5 level, Base Metal of all the welds acted as passive at all temperatures except around 50-60 °C where it became active for a short period. The corrosion layers play an important role as the non-corroding part of the weld is covered with a thick protective layer of iron carbonate [107]. The HAZ of E7018 electrode weld was active between 30-35 °C, and then became passive. The Base Metal corrosion film breaks and the corrosion level becomes anodic around 55 °C. The HAZ exhibited more cathodic than the Weld Metal indicating that the microstructure effect is not significant. Base Metal and the Weld Metal showed almost same corrosion characteristics. The E8018G electrode weld showed that the HAZ was more passive compared to the Base Metal and the Weld Metal. The lowest passivity was observed with HAZ of E8018G electrode weld and the highest level with HAZ of E8018B6 electrode weld.

The reason for the lowest level of passivity of E8018G electrode is due to high Ni content and moderate Si level. It is normally expected that E7018 weld results in very low passivity compared to other welds as the protective alloy elements are very low compared to other welds. The passivity level of E7018 weld is almost closer to E8018B2 weld. The Base Metal and the Weld Metal of E7018 and E8018G electrode welds behaved active at the small temperature

range while for the Weld Metals of other two welds were observed as passive throughout the experiment. Except the Base Metal which exhibited low passivity up to 50 °C, all the HAZs showed almost same passivity level. This is due to the rate transfer kinetics under CO₂ medium at this pH level and also by the contribution of associated microstructure. The active and passive dissolution varies though the experimental conditions are same except the individual zone characteristics. The presence of CO₂ does not seem to affect the anodic reaction significantly at the used pH level. The primary factors which increase Weld Metal Zone corrosion are microstructure, composition, aligned second phases and the inclusions. Hence, the effect of temperature with or without CO₂ was investigated for each Weld Metal Zone including the Base Metal. The Weld Metal Zones of E8018G and E8018B6 electrode welds behaved passive. There are significant differences among these four welds. Weld Metal Zone of E8018G electrode weld is passive under both environments. This is a significant phenomenon as compared to other welds. Under the condition of varying temperature without CO₂ this weld shows highest passivity after 60 °C. This shows that the protective film formation is so effective to influence the cathodic reaction. In the presence of CO₂, the passivity is less initially and then increased after the same temperature. However, in presence of CO₂, the passive effect is steadily increases with the increase in temperature. The Weld Metals of all other welds behaved differently in the absence of CO₂, being active with the increasing temperature. The Weld Metal Zone of E7018 electrode weld follows a clear anodic trend. This shows the composition effect when compared to other welds with low alloy elements. The HAZ of all the four welds exhibited little

difference in the level of passivity whereas the Weld Metal Zones of all the welds show distinct difference in passivity level. This may be due to the composition effect. Generally, the passive nature of corrosion reaction is due to the pH level of the electrolyte. The lower level of pH may result more active compared to the tested level. The Weld Metal Zone of E8018B6 electrode weld showed higher level of passivity which may be due to the higher Si and Cr content. As the temperature increased, the passivity was also found to increase. This may be due to the scaling effect at higher temperatures. The primary factors for the difference between the HAZ and the Weld Metal Zone are composition and the microstructure. Almost all the Weld Metal Zones exhibited acicular ferrite and the HAZs resulted with ferrite grain structures. Hence the effect of microstructure is comparatively uniform under CO₂ environment at this pH level. But this is not the case, when it is tested at room temperature and various temperatures with natural sea water. There were distinct differences in general and galvanic corrosion characteristics [9].

5.3. STATISTICAL ANALYSIS-POLYNOMIAL REGRESSION RESPONSE MODEL

The degree of fitness varies from 0.78 to 0.99 for all the weld samples reflecting the good fitness level except the sample which had the weld defect. This is because of the changes in corrosion current at faster rate. The regression model which is given in the form of equation is applicable only for the particular zone of the weld. The experimental data was analysed using this regression model and found to match well with the experimental results. The derived equations are useful to determine the corrosion level.

CHAPTER 6- CONCLUSIONS

1. The General Corrosion of Weld Metal Zone of E8018B6 electrode weld is highest and almost at same level to that of Base Metal and Weld Metal Zone of E8018B2 electrode weld is lowest whereas General Corrosion is highest for HAZ of E8018G electrode weld and lowest for HAZ of E8018B2 electrode weld under the room temperature test conditions.
2. The Galvanic Corrosion of the Weld Metal Zone of E8018B2 electrode weld is lowest and the for the Weld Metal Zone of E8018G electrode weld is highest whereas Galvanic Corrosion is lowest for the HAZ of E8018B2 electrode weld and highest for HAZ of E8018G electrode weld under the room temperature test conditions.
3. The Total Corrosion (General and Galvanic) of Weld Metal Zone of E8018G electrode weld is observed to be the highest and of Weld Metal Zone of E8018B2 weld is observed to be the lowest among all the welds under room temperature test conditions.
4. The Total Corrosion of HAZ of E8018G electrode weld is the highest and of HAZ of E8018B2 electrode weld is the lowest among HAZs of all the welds under room temperature test conditions. HAZs of all the welds shows minimum three times higher corrosion level as compared to other Zones (Base Metal and Weld Metal Zone) under room temperature test conditions.

5. The Total Corrosion level at room temperature is the lowest for E8018B2 electrode weld and the highest for E8018G electrode weld.
6. The Weld Metal Zone of the weld made with E7018G electrode is fully active at all temperatures. All other Weld Metal Zones are completely passive throughout the tested temperature range. The Base Metal is active till 35°C and then became passive. This is due to the formation of protective film.
7. The HAZ of E8018B6 electrode weld is active till 60°C and HAZ of E8018G electrode weld is active till 35°C both then become passive due to the formation of protective film. The HAZs of other two welds are completely passive under the tested temperature range.
8. The HAZ of high Cr (E8018B6) weld exhibits high passivity as compared to HAZs of all other welds hence, confirms the influence of Cr on corrosion resistance of steels under CO₂ environment.
9. Passivity of the Weld Metal Zones increases with temperature in CO₂ environment, as the galvanic corrosion current is negative throughout the experiment. HAZs of all the welds also behaved passive throughout the temperature range except HAZ of E7018 weld which behaves slightly active up to 30°C.
10. The passivity of Weld Metal Zones of E7018 and E8018G electrode welds are comparable at low temperatures but differ significantly at high temperatures. The high Ni content of E8018G electrode may be the primary factor for this characteristics as up to 1% addition of this element improves the corrosion resistance at high temperatures. There

is no much variation in hardness level of Weld Metal Zones of these welds hence; effect of hardness on corrosion is not significant.

11. The Weld Metal Zone of high Cr content weld prepared with E8018B6 electrode behaves more anodic than the Weld Metal Zone of high Ni content weld prepared with E8018G electrode. Also, high Cr content Weld Metal Zone behaves more anodic than low Cr content Weld Metal Zone.
12. The chemical composition seems to be the primary factor for Weld Metal Zone corrosion characteristics as there is insignificant variation in microstructures and significant variation in chemical compositions of Weld Metal Zones of the welds.
13. The microstructure seems to be the primary factor for HAZ corrosion characteristics as chemical composition is nearly same being a part of Base Metal but microstructures of HAZs differ significantly for different welds.
14. The experimental data was validated using polynomial regression model and found to be well fitted with the experimental results. The derived equations can be used to determine the corrosion level at specific set of controlling parameters and conditions used but not investigated in this study.

LIMITATIONS AND FUTURE SCOPE FOR RESEARCH

1. LIMITATIONS

- (i) The electrodes which are commercially available in the market are used in the present investigation. It is very difficult to get electrodes with desired composition level of Cr, Ni, or Mo etc. Hence, the composition effect on corrosion behaviour is not consistent in this study. However, the available variations in electrode composition used in this study provide meaningful result.
- (ii) Since the HAZ is very narrow, masking the other areas by paint may not give 100% protection as the paint/ lacquer may be porous. More accurate result can be obtained with epoxy moulded sample as higher contact area with the fluid is possible.

2. FUTURE RESEARCH

- (i) Specially made electrodes with distinct composition level may still give better results.
- (ii) Effect of heat input and the influence of resulting microstructure, grain size and secondary phases can be studied.
- (iii) The corrosion study can be carried out under controlled environment simulating the field process conditions such as CO₂ partial pressure, pH level, and other flow conditions etc.

REFERENCES

1. Velu Balraj et.al, "Failure Analysis of Stainless Steel Piping at an Offshore Platform", pp-62-65, NACE International, -Material Performance, May 2008.
2. Internal Report "Risk Assessment Study Report ", No.3291-W-RP-001.
3. M.B. Kermaniet.al., "Development of low alloy C-Mo steels with exceptional corrosion resistance for oil field applications", conference paper no. 01065, NACE International, Corrosion 2001.
4. Tatyana et.al., "The effect of micro structure and non-metallic inclusions on corrosion behavior of low carbon steel in chloride containing solution, Corrosion science, Vol.80, ,pp 299-308,Elsevier publication, March 2014.
5. T. Kushida, "Effects of metallurgical factors and test conditions on neutral pH SCC of pipeline steels", conference paper no. 01213, NACE International, Corrosion 2001.
6. Regis Blondeau, "Metallurgy and Mechanics of Welding", First Edn. Wiley Publication,2010.
7. Davis, Joseph R. "Corrosion-Understanding the Basics", pp 39-41, ASM International, 2000.
8. C.C. Chen and Abe, " Influence of welding on steel weldments properties", pp 416-428, ASM International, 1993.
9. C.de. Waard and D.E. Milliams,"Carbonic acidcorrosion of steel", Corrosion no.5, vol 31, NACE International, 1975.

10. NORSOK standard M506, "CO₂Corrosion rate calculation model" Rev.2, 2005.
11. H. Granjon, "Fundamentals of Welding Metallurgy", Abington Publishing, 1991.
12. D. Sefranet.et.al. "The Metallurgy of Welding", Chapman and Hall, London, 1962.
13. T. Rogne, et.al, Corrosion conference paper No.48 (10), 864-870, NACE International, 1992.
14. George Vander Voort, "Welding Metallurgy", Bohler Technical Notes, Vol.4, issue no. 3, 2004.
15. Study Material "Welding Engineering", Published by Welding Research Institute, India.
16. "Welding Hand Book", Published by American Welding Society, Vol-1, 9th edn. 2001.
17. Hand Book "Welding, Brazing and Soldering" ASM, Vol. 6. Edn.1993.
18. Hand Book "Metallography and Microstructures", ASM, Vol. 9. Edn. 1993.
19. N.G. Harmandas and P.G. Koutsoukos, "The formation of iron sulphides in aqueous solutions", Journal of Crystal Growth, p.719, 1996.
20. S.A. David and J.M. Vitek," Correlation between solidification parameters and weld microstructures, International Material Reviews,Maney publication, vol 34, issue 1, p 213-245, Jan 1989.
21. S. Murugan et.al. "Temperature distribution during multi pass welding of plates" International journal of pressure vessels and piping" ELSEVIER, vol 75, issue 12, pp 891-905, October 1998.

22. ASME sec IX, Boiler and Pressure vessel code, "Welding, brazing, October 1998.
23. API standard, API 1104, "Welding of Pipelines and Related Facilities", American Petroleum Institute, 25th edn. 2013
24. Fontana M.G., "Corrosion Engineering", McGraw-Hill publication, 3rd edition, chapter 2, 2005.
25. R.Winston Revie and Herbert H.Uhlig, "Corrosion and corrosion control", John Wiley publication, fourth edn. 2008
26. Einer Bardal, "Corrosion and protection", Springer publication, pp 53-61, 2004.
27. Qian linWn et.al. " Corrosion behavior of low alloy steel contain 1% Cr in CO₂ environment " Corrosion Science journal, pp 400-408, 75, 2013.
28. R.nyborg, "Initiation and Growth of Mesa Corrosion Attack during CO₂ Corrosion of Carbon Steel", CORROSION/98, conference paper no.48, NACE International, 1998.
29. Gunter Schmit and Michaela Horstemeies, "Fundamental aspects of CO₂ metal loss corrosion, part II, conference paper no.06112, Corrosion NACE expo 2006.
30. R.nyborg, A.Dugstad, "Mesa Corrosion Attack in Carbon Steel and 0.5% Chromium Steel", CORROSION/98, conference paper no.29, NACE International, 1998.
31. R. Torella et.al. , "Influence of microstructures on SSC and SOHIC in base material and welded joints of high strength sour service steels", Technical Steel Research, Report No.EVR 21906EN, 2006.

32. A. Bhatia, "Material properties and Corrosion", course manual no.T06-001, page 24.
33. NACE International publication "Internal corrosion for pipelines basic" version 1.00, July 2014.
34. Brenda S. Little et.al, "Microbiologically influenced corrosion" Wiley VCH, Verlog GMBH, BIZTEC consultant publication.
35. ASM International - Hand Book of Corrosion, 2nd edition, 1997, pp 685-686.
36. A.Dugstad, "Mechanism of Protective Film Formation during CO₂ Corrosion of carbon Steel", CORROSION /98, conference paper No.31 NACE International, 1998.
37. Samuel Bradford, " Corrosion Control", Casti publishing Inc., second edn. p- 126, 2001.
38. A Van Bennekomet.al., "Pump impeller failures-compendium of case studies", vol.8, issue 2, pp 145-156, April 2001.
39. R. Winston Revie," Herbert H. Uhlig," Corrosion and Corrosion Control", John Wiley & Sons Inc., p 160, 2008.
40. Boyun Guo," Offshore pipelines- design, installation and maintenance", second edn. ELSIVER, 2014.
41. Mark E. Orazen, " Underground pipeline corrosion-Detection, Analysis and prevention, Wood Head publishing, ELSIVIER, 2014.
42. API standard- API RP 14E, "Recommended Practice for Design, & Installation of offshore products platform piping systems", section 5, edition 2013.

43. Kathy Riggs Larson, "A closer look at microbiologically Influenced Corrosion", NACE -Material Performance, vol.53, no 1, pp 32-40
44. Oldfield et.al," Corrosion of metals in de-aerated sea water", Inco Europe limited report, Birmingham, UK.
45. L.G.S Gray et.al," Effect of pH and temperature on the Mechanism of carbon Steel Corrosion by Aqueous Carbon Dioxide", Corrosion/90, paper no.40, NACE International, 1990.
46. B.F.M. Pots, "Mechanistic models for the prediction of CO₂ corrosion rates under multi-phase flow conditions", conference paper no. 137, CORROSION/95, NACE International, 1995.
47. S.Nesic, M.Nordsveen, R.Nyborg and A.Stangeland, "A Mechanistic Model for CO₂ Corrosion with Protective Iron Carbonate Films", CORROSION/2001, conference paper no. 40, Houston, TX: NACE International, 2001.
48. W. Nimmo et.al "Evaluation of Techniques for measuring the Corrosion Activity of carbon steel Welds" National Physical laboratory Publication, Report No. MATC (A) 34, October 2001.
49. S. Nesic and K.J. Lee, "The mechanistic model of iron carbonate film growth and the effect on CO₂ corrosion of mild steel", conference paper No.237, CORROSION/02, NACE International, 2002.
50. E.W.J. Van Hvnnik," The formation of FeCO₃ Corrosion product layer in CO₂corrosion", conference paper no 6, Corrosion 96, NACE international, 1996.

51. Arne Dugstad, "Fundamental aspects of CO₂metal loss corrosion mechanism, part I, Corrosion 2006, conference paper no.6111, NACE International, 2006.
52. Srdjan et.al. "A mechanistic model of Iron carbonate film growth and the effect on CO₂ corrosion of mild steel", NACE-international, Conference paper No. 02237, NACE International, 2002.
53. M. Stephen and P.C. Pistorious" Localized corrosion of carbon steel welds" Corrosion journal, vol. 56, No.12,pp 1272-1279, NACE International Dec 2000.
54. David Queen et.al," Guidelines for the prevention, control and monitoring of preferential weld corrosion of ferritic steels in wet hydrocarbon production systems containing CO₂", SPE-87552-MS, SPE international symposium on Oilfield corrosion, UK, May 2004.
55. C.M.Lee et.al, " Preferential weld corrosion effect of weldment microstructure and composition", Conference paper no.5277, CORROSION /2005, NACE International, 2005.
56. T.G. Gooch," The Effect of Welding on material Corrosion behaviour"- CORROSION Seminar on Process Industries, NACE International, 1986.
- 57.J.L. Robinsion, "Preferential Corrosion of welds" The Welding Institute ,UK ,Research Bulletin, Vol 20, 1979.
58. J.S. Smart, "Weld Corrosion in line deserves Closer attention", Pipeline gas Industries, Vol. 79, June 1996.
59. Uhllig-Corrosion Hand Book, second edition, John Wiley and sons, 2000.

60. ASM Hand Book, Vol. 13," Corrosion", edn. 1993
61. C.G. Arnold, "Galvanic Corrosion Measurement of Welds", conference paper no.71.CORROSION /80, NACE-International, 1980.
62. M.B. Kermani et.al, "Corrosion Control in OIL and Gas Production" European Federation of Corrosion, publication 23, 1997.
63. R.J. Brigham et.al, "Evaluation of Weld zone Corrosion of shipbuilding Steel metals for use in the Arctic environment ", Canadian Metal Journal, Vol. 27. 1998.
64. "The procedure hand book of arc welding ", Lincoln Electric, 12th end., 1973.
65. Alibaba Kr, "Preferential weld corrosion-a case study" Material Performance, NACE-International, pp 58-62, March 2008.
66. B.A. Graville, "Cold Cracking in welds in HSLA steels ", Conference Proceedings, American society of Metals, 1976.
67. D.A.Lopez et.al.," The influence of microstructure and chemical composition of carbon and low alloy steels in CO₂ Corrosion-A state of the art appraisal," Material and Design, vol 24, pp 561-575, 2003.
68. Charles G. Munger, "Corrosion Prevention by protective coating", NACE -International publication, pp 347-376, edn.1984.
69. Jose E. Ramaire Christopher, D.Tailor, "Preventing Corrosion Failures", Advanced Materials &Process, pp15-17, August 2014.
70. J.R. Davis, "Corrosion of Welds", ASM International publication, edn. 2006.
71. David Tolbot, James Talbot, "Corrosion Science and Technology", CRC Press, 1997.

72. W.F. Savage, "New insight into weld cracking and a new way of looking at welds", *Welding Design Engineering*, Dec.1969.
73. Padhy Girish kumar, Komizoyu-ichi," Diffusible Hydrogen in steel weldments", *Transaction of JWRI*, vol 42, no.1, pp-39-62, 2013.
74. J. Soltis, "Passivity breakdown, pit initiation and propagation of pits in metallic materials-Review", *Corrosion Science*, ELSEVIER Publication, 90, pp 5-22, 2015.
75. API standard -API 5L," Specification for line pipe", 3rd .edn.2004.
76. Mark E. Orazem, "Understanding underground pipeline corrosion-detection, analysis and prevention", Wood head publishing (ELSEVIER), Part 1, 2014
77. ASTM E415, "Standard Test Method for Atomic Emission Vacuum Spectrometric Analysis of Carbon and Low-Alloy Steel", edition 2005.
78. ASTM E 340, "Standard test method for Macro etching metals and Alloys ASTM International.
79. NACE-MR 0175/ISO 15156, "Petroleum and natural gas industries-Materials for use in H₂S-containing environments in oil and gas production," NACE International, edition 2007.
78. Oldfield et.al, "Corrosion of Metals in De-aerated Seawater", Inco Europe limited, Birmingham, UK.
80. GAMRY Ref. 600, Operators manual
81. Neil G. Thompson et.al." Corrosion test made easy-DC electrical test methods", NACE –International publication, 1998.
82. Allen J. Bard, "Electrochemical methods-Fundamentals and Applications", John Wiley & sons, second edn, 2009.

83. ASTM G5-94, "Standard Reference test Method for making potentiodynamic polarization resistance measurements", edition 1994.
84. D.M. Drastic, "Iron and its Electrochemistry in an Active State" in Corrosion Mechanisms, Vol. 19, p-79, Plenum press, 1989.
84. ASTM standard G71- Standard Guide for Conducting and Evaluating Galvanic Corrosion Tests in Electrolytes, 2013.
85. John O. Rawlings et.al. " Applied Regression Analysis: A Research Tool", Springer publication, 2ndedn., 1998.
86. Egil Gulbrandsen, "Effect of steel micro structural and composition on inhibition of CO₂"Conference paper No, 23, CORROSION 2000, NACE-International, 2000.
87. John.J. Gilman, "Chemistry and Physics of Mechanical Hardness", John Wiley & Sons publication, pp 189-196, 2009.
88. S. Al-Hassen, et.al. "Effect of steel microstructure on corrosion of steels in aqueous solutions containing carbon dioxide", Corrosion journal No 57, pp 369-378, 2001 .
89. S. Turgoose et.al, "Preferential weld corrosion of 1% Ni welds- effect of solution conductivity and corrosion inhibition", Conference paper no. 5275, CORROSION 2005, NACE International, 2005.
90. H.B.Luft et.al, "Designing welding procedures for preferential corrosion resistance in cold marine environments", Conference paper No. 304, CORROSION 89, NACE-International, 1989.
91. .Lancaster, "Metallurgy of Welding" London, U.K, Chapman & Hall, 1962.

92. Lorenz and K.Heusler, “Anodic Dissolution of Iron Group Metals”, in Corrosion Mechanisms, edn.F.Mansfeld, Marcel Dekker, Newyork, 1987.
93. T.K. Ross, R.K. Badhwar, “The effect of surface roughness upon electrochemical processes” ,Corrosion Science, ELSEVIER publication, Pages 29-38,Volume 5, Issue 1, 1965.
94. K. Denpo and H.Ogawa, “ Effects of Ni and Chromium on corrosion rate of line pipe steel”, Corrosion Science (ELSEVIER),vol.35, pp 285-288, 1993.
95. “Corrosion Control”, NACE Publication, P-69, edn.1979.
96. Robert Heidersbach, “Metallurgy and Corrosion Control in Oil and Gas Production”, Jhon Wiley and sons Inc. p-89, 2011.
97. Mohamed Hanafy, “Grooving Corrosion of a 24-in seam welded pipeline”, Material Performance, NACE-International, vol. 53, No6, pp 62-70, June 2014.
98. Andrew Cosham , “ The assessment of Corrosion in pipelines-Guidance in the pipeline”, Guidance in the pipeline defect Assessment Manual(PDAM), Penspen Integrity,Pipeline Pigging and Integrity Management Conference17-18th, May 2004 – Amsterdam, The Netherlands.
99. Domnic Paisley et.al. “ Pipeline Failure: The roles played by corrosion, flow and metallurgy” Corrosion 99, Conference paper no.18, NACE-International, 1999.
100. M.KO et.al., "In situ synchrotron x-ray diffraction study of the effect of microstructure and boundary layer condition on CO₂ corrosion of pipeline, Corrosion science, ELSIVIER, 90, pp-192-201, 2015.

101. M. Kimura, Y. Nakano, "Effect of alloying elements on corrosion resistance of high strength line steel pipe steel in wet CO₂ environment, Corrosion 94, NACE-International paper no 8, 1994.
102. Videm Ketil, "The Influence of composition of carbon steels on anodic and cathodic Reaction rate in CO₂ Corrosion", Corrosion 98, paper no. 30, NACE International, 1998.
103. Masakatsu & Hideki Takabe, "Effect of Environmental Factor and Microstructure on Morphology of Corrosion Products in CO₂ environments", Corrosion 99, paper no.13, -NACE International, 2009.
104. M.B. Kermani, A. Morshed, " Carbon di-oxide corrosion in Oil and Gas production", Corrosion 59, No.8, pp 659-683, NACE-International, 2003.
105. S. Nestic and L. Lunde, " Carbon di-oxide corrosion of carbon steel in two phase flow", Corrosion 50, pp 717-727, NACE International, 1994.
106. A Dugstd, H. Hemmer , " Effect of steel micro structure upon corrosion rate and protective Iron carbonate film formation, Corrosion 2000, paper no. 00024, NACE –International, 2000.
107. D.A. Lopez, T. Perez, S.N. Simison "The influence of microstructure and chemical composition of carbon and low alloy steels in CO₂ Corrosion-A state of art appraisal", Material Design, pp 561-575, vol.24, 2003.

PUBLISHED PAPERS

1. Balraj Velu, Rajnish Garg, Mukesh Saxena and Paul Rostron, “ Welding Consumable issues on Corrosion of X65QT Steel” , NACE-International Journal, Material Performance, Vol. 53, No.8, Aug 2014.
2. Balraj Velu, Rajnish Garg and Paul Rostron,“ Evaluation of weld root Corrosion of X65QT Material”, International journal of Current Research, Vol.5.Issue 04, pp871-875, April, 2013.

APPENDICES

APPENDIX A: Weld macro hardness test results

APPENDIX B: Corrosion testing - recorded traces

APPENDIX C: Polynomial Regression Analysis Curve Fitting Graphs

APPENDIX D: Scholar profile

APPENDIX –A : WELD MACRO HARDNESS TEST RESULTS

Table A1. Hardness Survey Results- Weld E7018

Hardness Values in HV10

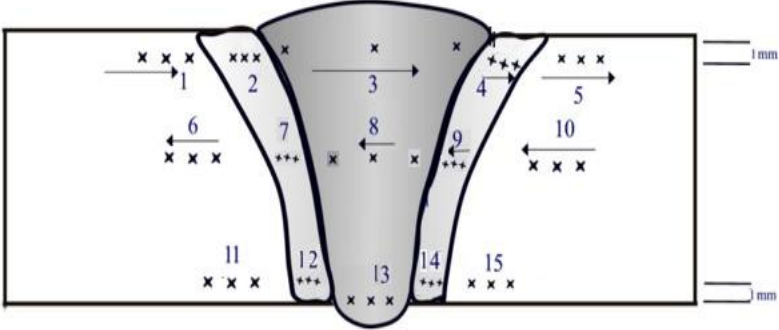
Macro ID	E7018	Maximum Hardness Value (HV 10)	217											
														
Illustrative Sketch														
Cap					Mid					Root				
1	2	3	4	5	6	7	8	9	10	11	12	13	14	15
PM	HAZ	Weld	HAZ	PM	PM	HAZ	Weld	HAZ	PM	PM	HAZ	Weld	HAZ	PM
193	216	204	215	191	193	210	205	211	192	191	215	204	211	196
191	217	206	212	196	197	214	202	214	196	194	214	206	211	194
194	214	203	214	194	196	213	202	213	193	195	214	203	212	193

Table A2. Hardness Survey Results- Weld E8018B

Hardness Values in HV10

Macro ID		E8018B6			Maximum Hardness Value (HV 10)					204				
Illustrative Sketch														
Cap					Mid					Root				
1	2	3	4	5	6	7	8	9	10	11	12	13	14	15
P	HAZ	Weld	HAZ	PM	PM	HAZ	Weld	HAZ	PM	PM	HAZ	Weld	HAZ	PM
M	HAZ	Weld	HAZ	PM	PM	HAZ	Weld	HAZ	PM	PM	HAZ	Weld	HAZ	PM
190	171	202	175	193	193	176	201	174	192	191	176	201	176	191
192	176	204	174	191	193	177	203	173	192	193	174	203	174	194
191	174	203	174	192	192	174	202	174	194	191	174	204	177	193

Table A3. Hardness Survey Results- Weld E8018B2

Hardness Values in HV10

Macro ID		E8018B2			Maximum Hardness Value (HV 10)					366				
Illustrative Sketch														
Cap					Mid					Root				
1	2	3	4	5	6	7	8	9	10	11	12	13	14	15
PM	HAZ	Weld	HAZ	PM	PM	HAZ	Weld	HAZ	PM	PM	HAZ	Weld	HAZ	PM
183	246	366	239	188	184	242	362	239	192	189	193	351	237	191
186	244	358	236	192	188	238	357	237	193	191	189	359	239	186
184	243	354	238	191	187	239	360	236	188	187	192	353	234	189

Table A4. Hardness Survey Results- Weld E8018G

Hardness Values in HV10

Macro ID		E8018G			Maximum Hardness Value (HV 10)					229				
Illustrative Sketch														
Cap					Mid					Root				
1	2	3	4	5	6	7	8	9	10	11	12	13	14	15
PM	HAZ	Weld	HAZ	PM	PM	HAZ	Weld	HAZ	PM	PM	HAZ	Weld	HAZ	PM
215	210	228	206	214	216	206	227	209	214	211	209	229	205	212
212	209	226	209	214	214	208	224	210	212	214	210	224	206	212
214	208	229	208	213	213	207	228	207	215	213	208	226	206	215

APPENDIX- B: CORROSION TESTING RECORDED TRACES

1.0. INTRODUCTION

The corrosion testing was carried out using natural sea water collected from the Arabian sea near one of the OIL Process platform and the results are shown in the Table No. B1.

Table B1. Water chemistry analysis data

TESTS	METHODS	RESULTS
pH value @ 25°C	APHA 45001113	7.7
Electrical Resistivity, Ω.m @25°C	APHA 2510 B	0.16
Calcium g/L	APHA 3111 B	654
Magnesium, mg / L	APHA 3111 B	1537
Sodium, mg / L	APHA 3111 B	13581
Potassium, mg /L	APHA 3111 B	750
Chloride, mg /L	APHA 4500 Cl ⁻ B	24718
Sulfate, mg /L	APHA 4500 SO ₄ ²⁻ C	3280
Carbonate, mg/L	APHA 2320 B	< 1
Bicarbonate, mg/L	APHA 2320 B	189
Iron, mg /L	APHA 3111 B	0.3
Total Dissolved Solids, mg/L	APHA 2540 B	45100
Total Alkalinity as CaCO ₃ , mg/L	APHA 2320 B	155
Total Hardness as CaCO ₃ , mg/L	APHA 2340 B	7958
Dissolved Oxygen, mg/l (Direct)	APHA 4500 0 C	5.7
Dissolved Oxygen mg/l (After 1 hr. aeration)	APHA 4500 0 C	6.0

ATTACHMENTS

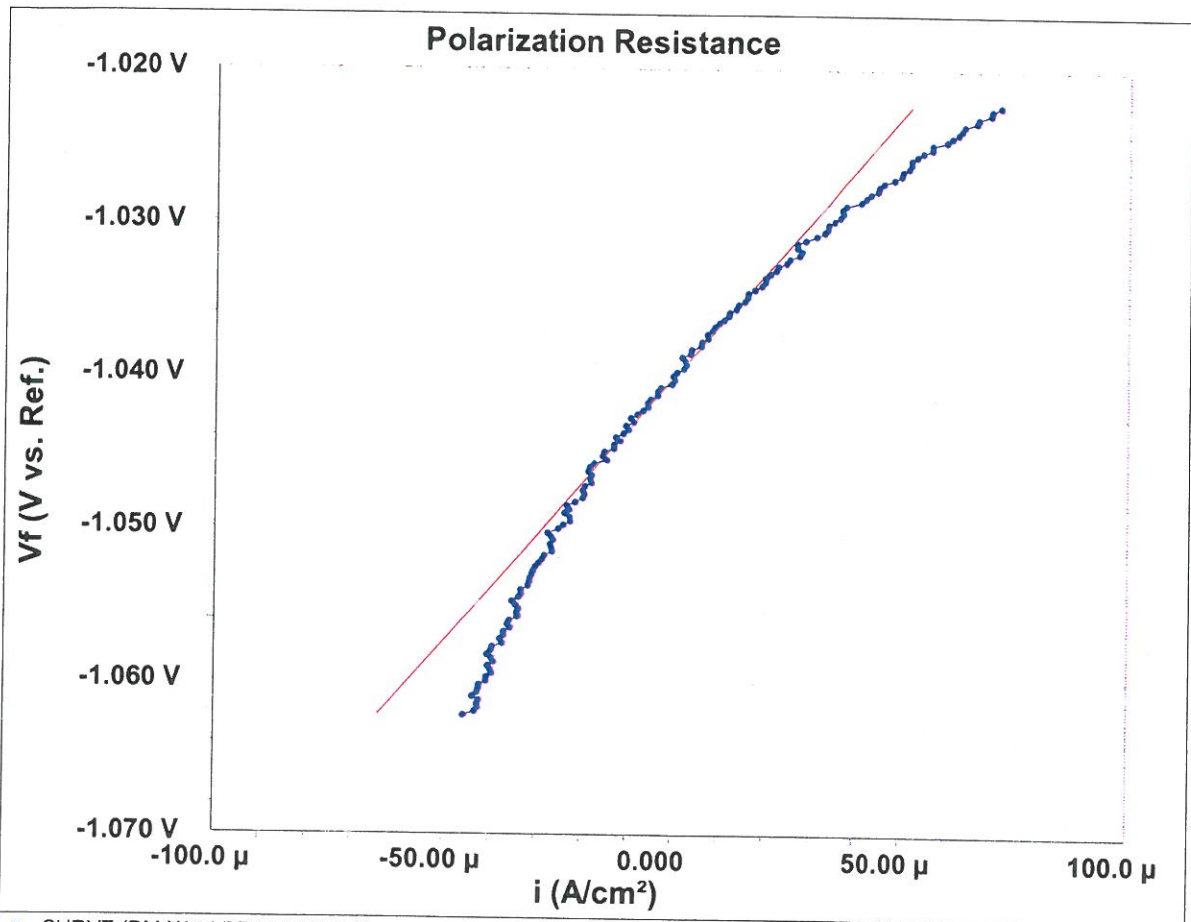
B1-LPR recordings

B2 - Galvanic current recordings at room temperature

B3 - Galvanic current recordings at various temperatures

B4 - Galvanic current recordings at various temperatures with CO₂

B1 - LPR Recordings



● CURVE (BM-X65-LPR RUN2.DTA)

— Line 1

EXPERIMENTAL PARAMETERS

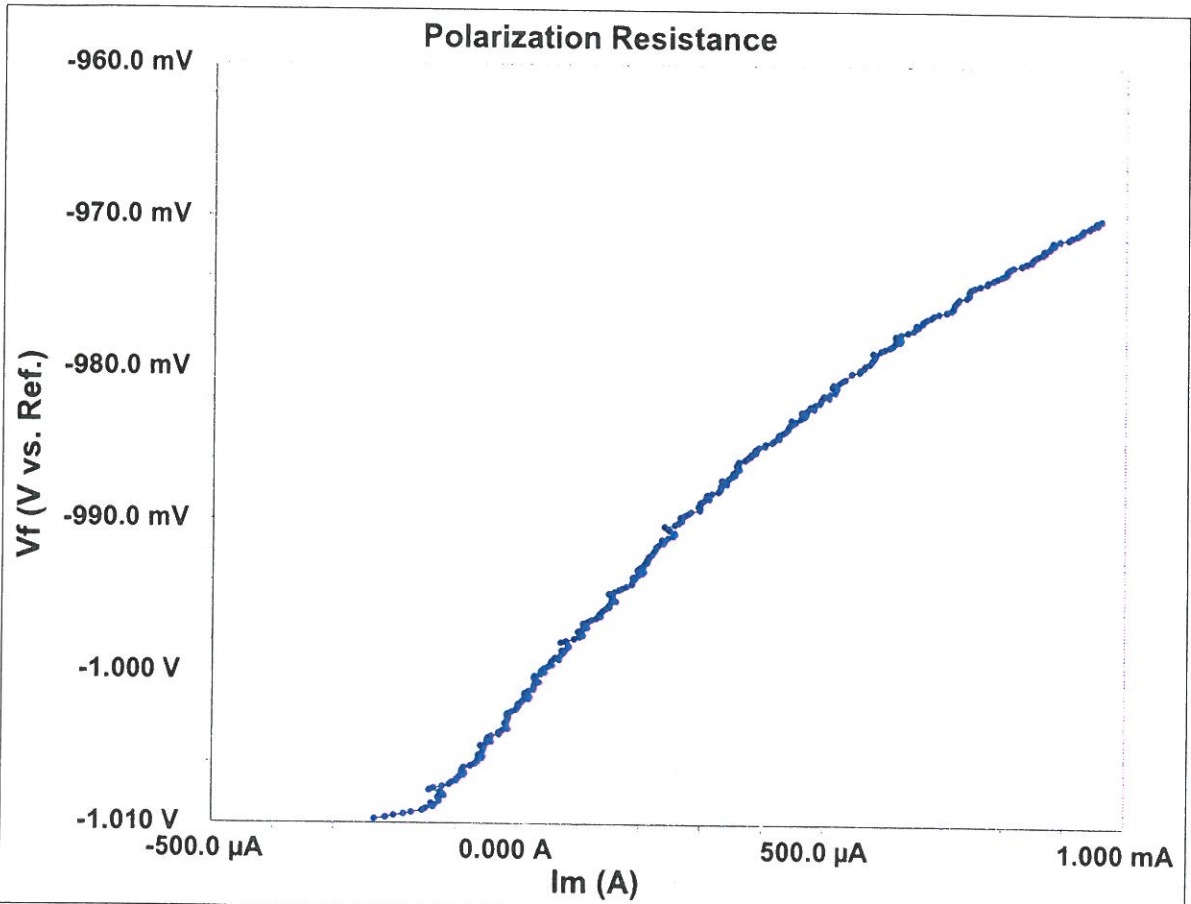
Initial E (V): -0.02 vs. Eoc
 Final E (V): 0.02 vs. Eoc
 Polarization Resistance
 11/29/2011
 13:43:21
 Scan Rate (mV/s): 0.125
 Sample Period (s): 2
 Sample Area (cm²): 9
 Density (gm/cm³): 7.87
 Equiv. Wt: 27.92
 Conditioning: Off
 Init. Delay: Off
 Open Circuit (V): -1.04213

EXPERIMENTAL DETERMINATIONS

Beta An. (V/Dec): 0.12
 Beta Cat. (V/Dec): 0.12
 Icorr (A): 7.581984E-05
 Ecorr (V): -1.04004
 Corrosion Rate (mpy): 34.64491

EXPERIMENTAL NOTES

29 NOV



● CURVE (WELD E7018- LPR RUN1 .DTA)

EXPERIMENTAL PARAMETERS

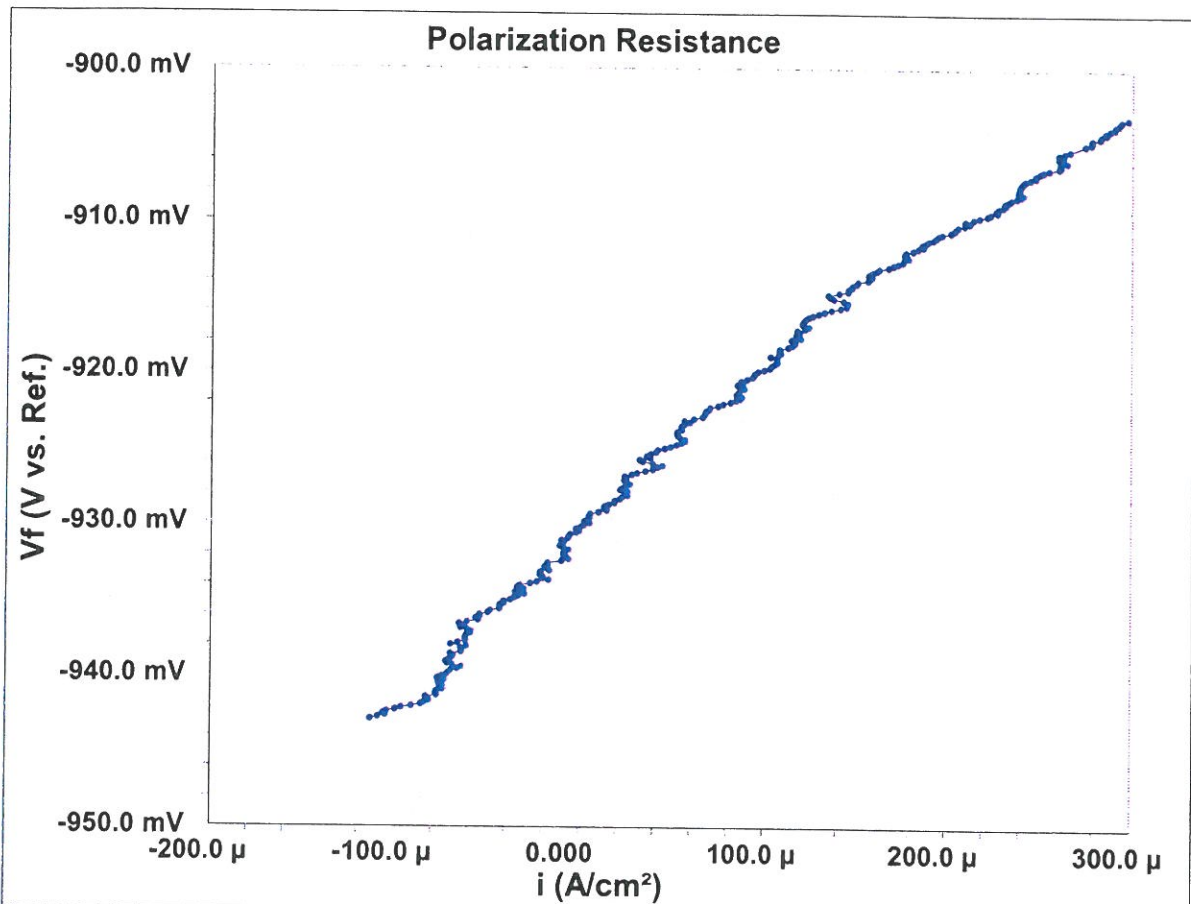
Initial E (V): -0.02 vs. Eoc
 Final E (V): 0.02 vs. Eoc
 Polarization Resistance
 11/30/2011
 9:17:37
 Scan Rate (mV/s): 0.125
 Sample Period (s): 1
 Sample Area (cm²): 2.2
 Density (gm/cm³): 7.87
 Equiv. Wt: 27.92
 Conditioning: Off
 Init. Delay: Off
 Open Circuit (V): -0.98999

EXPERIMENTAL DETERMINATIONS

Beta An. (V/Dec): 0.12
 Beta Cat. (V/Dec): 0.12
 Icorr (A): 5.260428E-04
 Ecorr (V): -1.00239
 Corrosion Rate (mpy): 109.2584

EXPERIMENTAL NOTES

NOV 30



● CURVE (WELD E7018--HAZ LPR RUN 2 DEC29 .DTA)

EXPERIMENTAL PARAMETERS

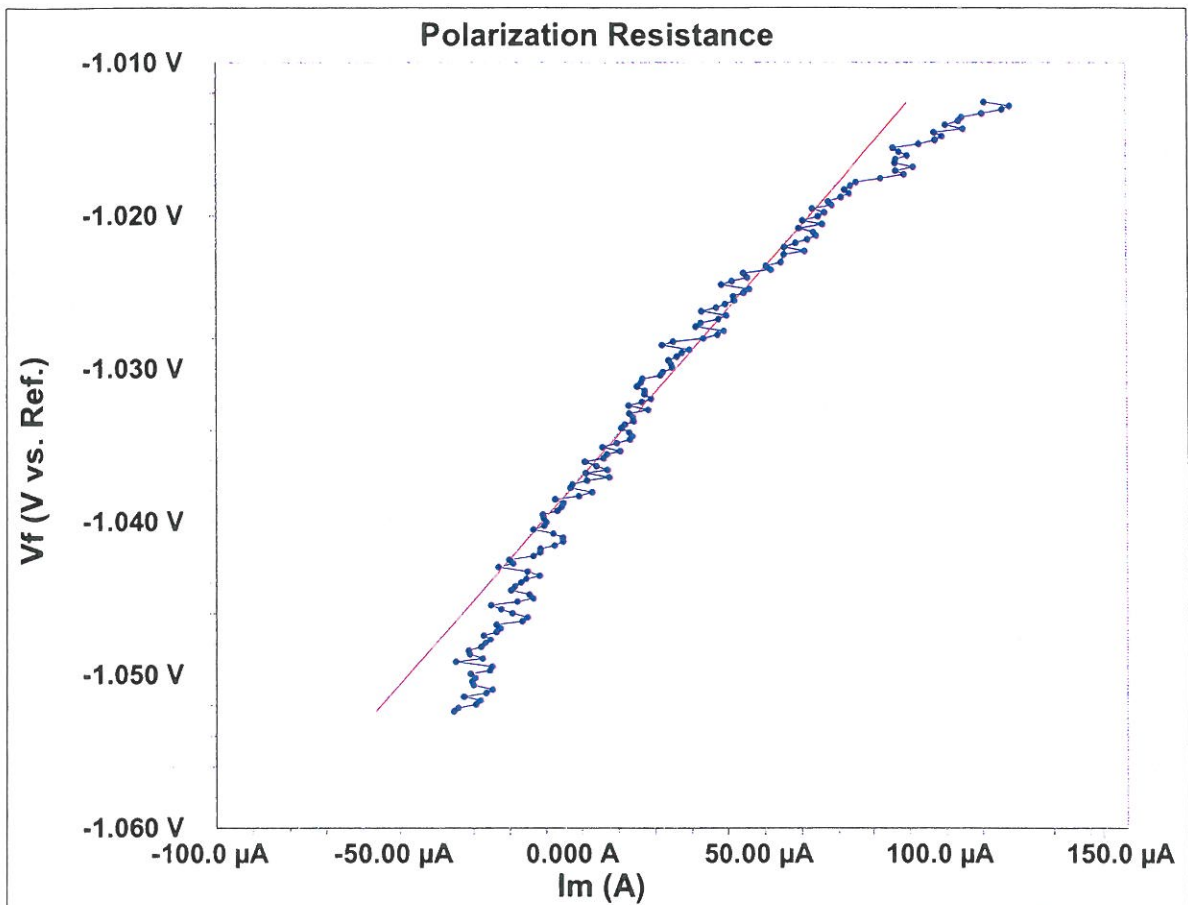
Initial E (V): -0.02 vs. Eoc
 Final E (V): 0.02 vs. Eoc
 Polarization Resistance
 12/29/2011
 8:27:25
 Scan Rate (mV/s): 0.125
 Sample Period (s): 1
 Sample Area (cm²): 0.2
 Density (gm/cm³): 7.87
 Equiv. Wt: 27.92
 Conditioning: Off
 Init. Delay: Off
 Open Circuit (V): -0.92341

EXPERIMENTAL DETERMINATIONS

Beta An. (V/Dec): 0.12
 Beta Cat. (V/Dec): 0.12
 Icorr (A): 0.000001
 Ecorr (V): -0.930227
 Corrosion Rate (mpy): 0

EXPERIMENTAL NOTES

DEC 29-AERATED



● CURVE (WELD 8018G- LPR RUN1 .DTA)

— Line 1

EXPERIMENTAL PARAMETERS

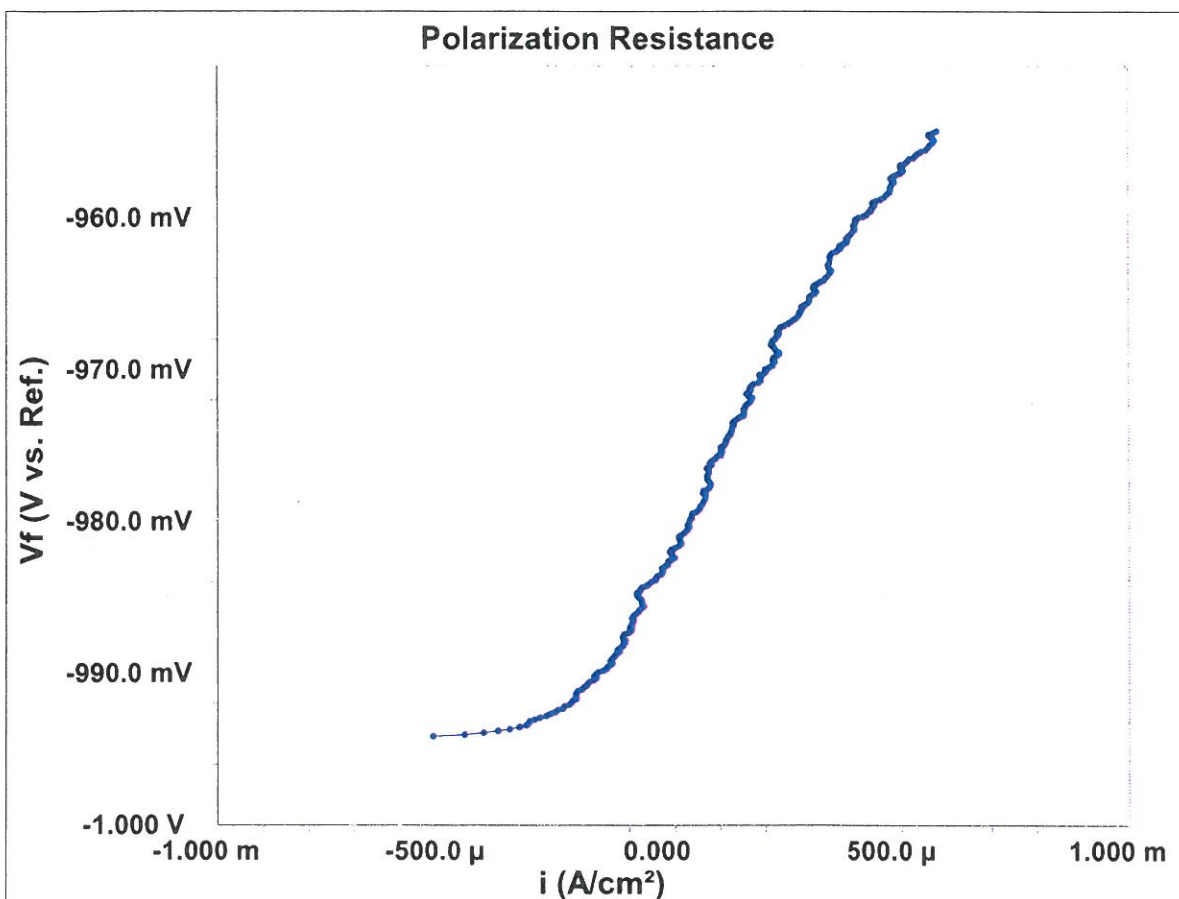
Initial E (V): -0.02 vs. Eoc
 Final E (V): 0.02 vs. Eoc
 Polarization Resistance
 11/30/2011
 8:37:07
 Scan Rate (mV/s): 0.125
 Sample Period (s): 2
 Sample Area (cm²): 1
 Density (gm/cm³): 7.87
 Equiv. Wt: 27.92
 Conditioning: Off
 Init. Delay: Off
 Open Circuit (V): -1.03235

EXPERIMENTAL DETERMINATIONS

Beta An. (V/Dec): 0.12
 Beta Cat. (V/Dec): 0.12
 Icorr (A): 9.582047E-05
 Ecorr (V): -1.03831
 Corrosion Rate (mpy): 43.78394

EXPERIMENTAL NOTES

NOV 30



● CURVE (WELD E8018G-HAZ LPR RUN 1 DEC29 .DTA)

EXPERIMENTAL PARAMETERS

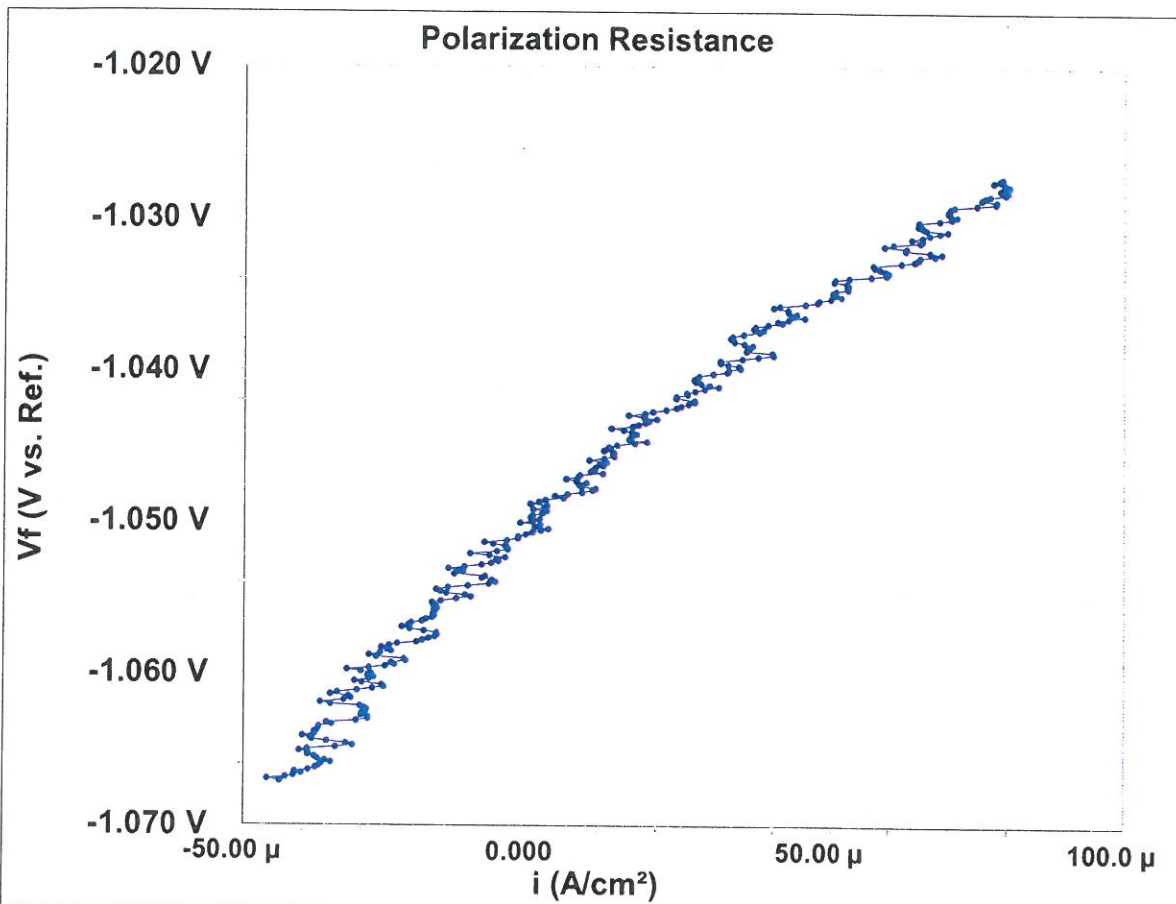
Initial E (V): -0.02 vs. Eoc
 Final E (V): 0.02 vs. Eoc
 Polarization Resistance
 12/29/2011
 7:27:54
 Scan Rate (mV/s): 0.125
 Sample Period (s): 1
 Sample Area (cm²): 0.2
 Density (gm/cm³): 7.87
 Equiv. Wt: 27.92
 Conditioning: Off
 Init. Delay: Off
 Open Circuit (V): -0.97435

EXPERIMENTAL DETERMINATIONS

Beta An. (V/Dec): 0.12
 Beta Cat. (V/Dec): 0.12
 Icorr (A): 4.734911E-04
 Ecorr (V): -0.981754
 Corrosion Rate (mpy): 216.3557

EXPERIMENTAL NOTES

DEC 29-AERATED



● CURVE (WELD E8018B6- LPR RUN 2 .DTA)

EXPERIMENTAL PARAMETERS

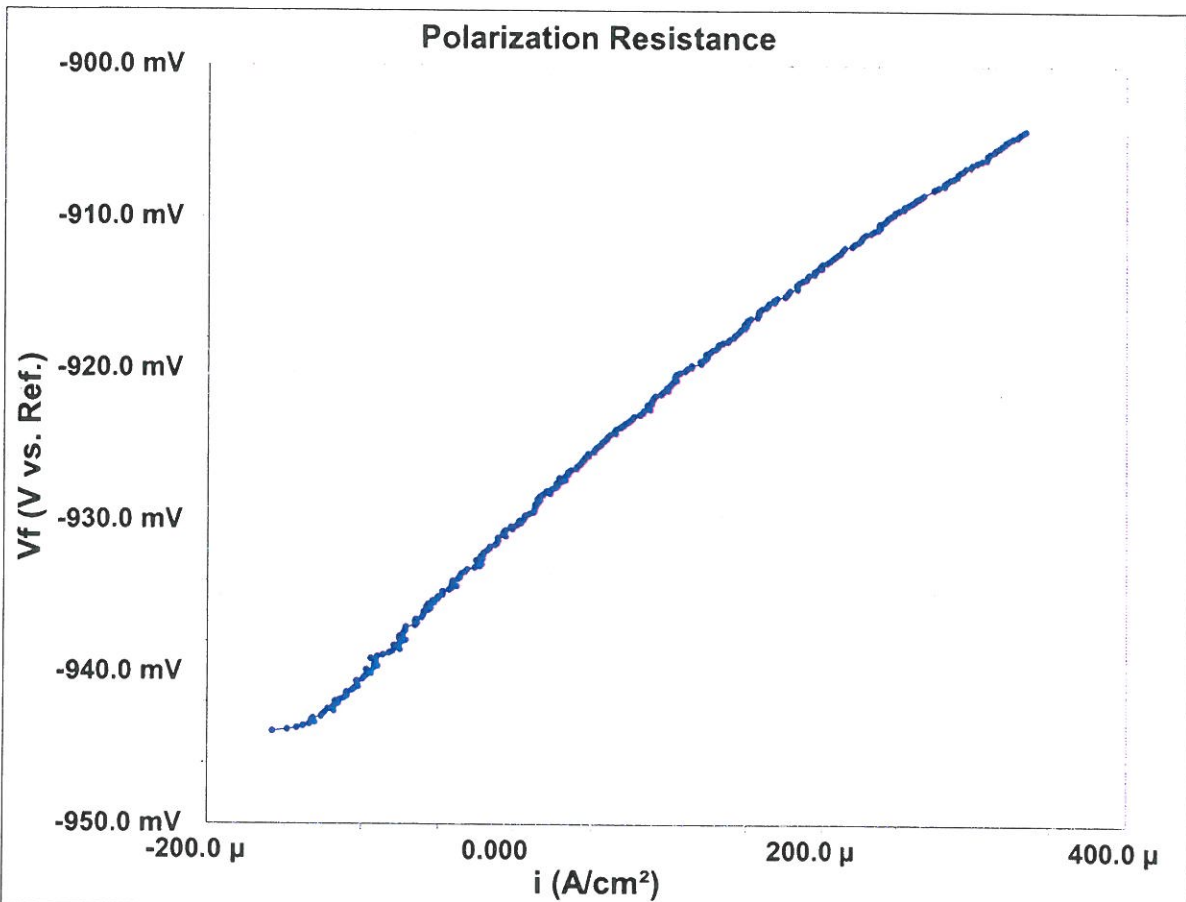
Initial E (V): -0.02 vs. Eoc
 Final E (V): 0.02 vs. Eoc
 Polarization Resistance
 12/14/2011
 12:14:01
 Scan Rate (mV/s): 0.125
 Sample Period (s): 1
 Sample Area (cm²): 1
 Density (gm/cm³): 7.87
 Equiv. Wt: 27.92
 Conditioning: Off
 Init. Delay: Off
 Open Circuit (V): -1.04748

EXPERIMENTAL DETERMINATIONS

Beta An. (V/Dec): 0.12
 Beta Cat. (V/Dec): 0.12
 Icorr (A): 0.000001
 Ecorr (V): -1.04867
 Corrosion Rate (mpy): 0

EXPERIMENTAL NOTES

DEC 14-AERATED



● CURVE (WELD E8018B6-HAZ LPR RUN 2 DEC29 .DTA)

EXPERIMENTAL PARAMETERS

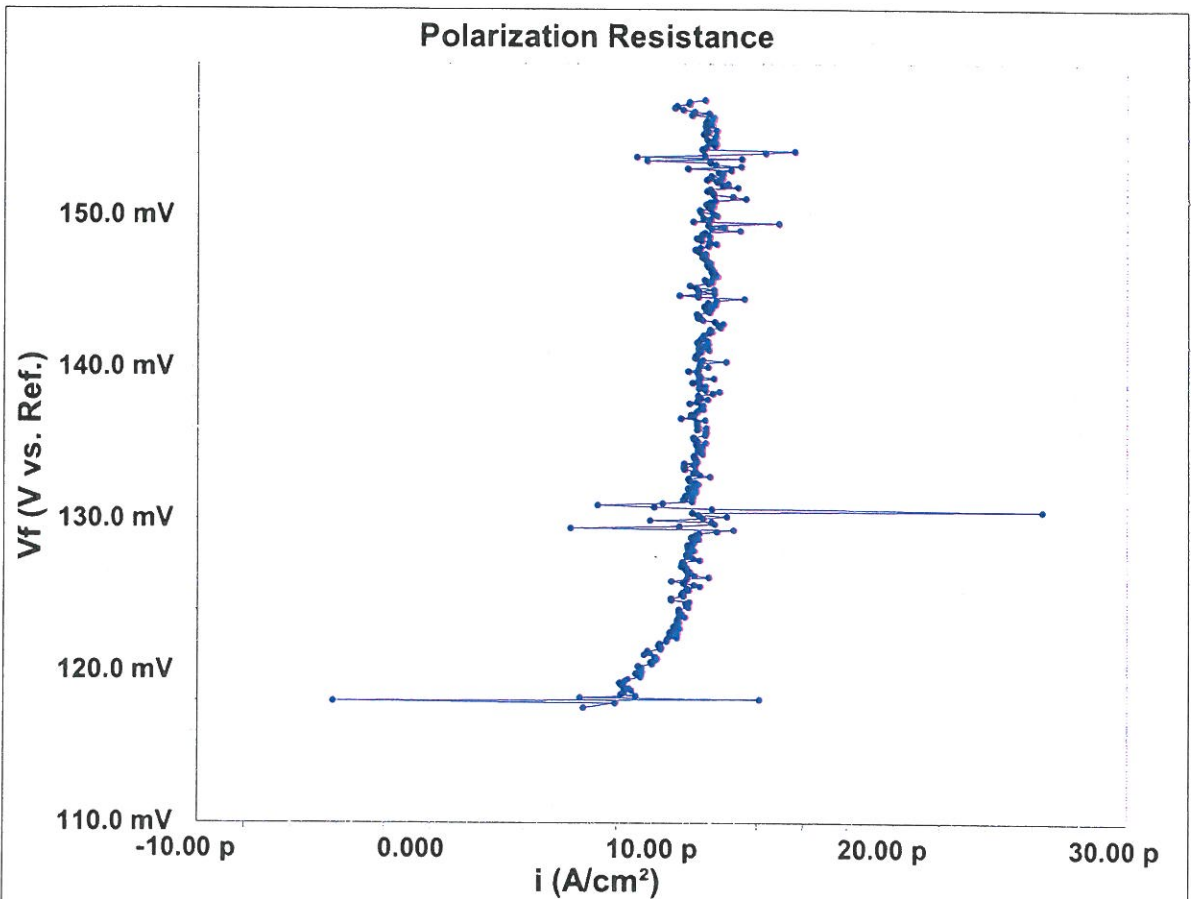
Initial E (V): -0.02 vs. Eoc
 Final E (V): 0.02 vs. Eoc
 Polarization Resistance
 12/29/2011
 9:12:29
 Scan Rate (mV/s): 0.125
 Sample Period (s): 1
 Sample Area (cm^2): 0.2
 Density (gm/cm^3): 7.87
 Equiv. Wt: 27.92
 Conditioning: Off
 Init. Delay: Off
 Open Circuit (V): -0.924368

EXPERIMENTAL DETERMINATIONS

Beta An. (V/Dec): 0.12
 Beta Cat. (V/Dec): 0.12
 Icorr (A): 0.000001
 Ecorr (V): -0.930542
 Corrosion Rate (mpy): 0

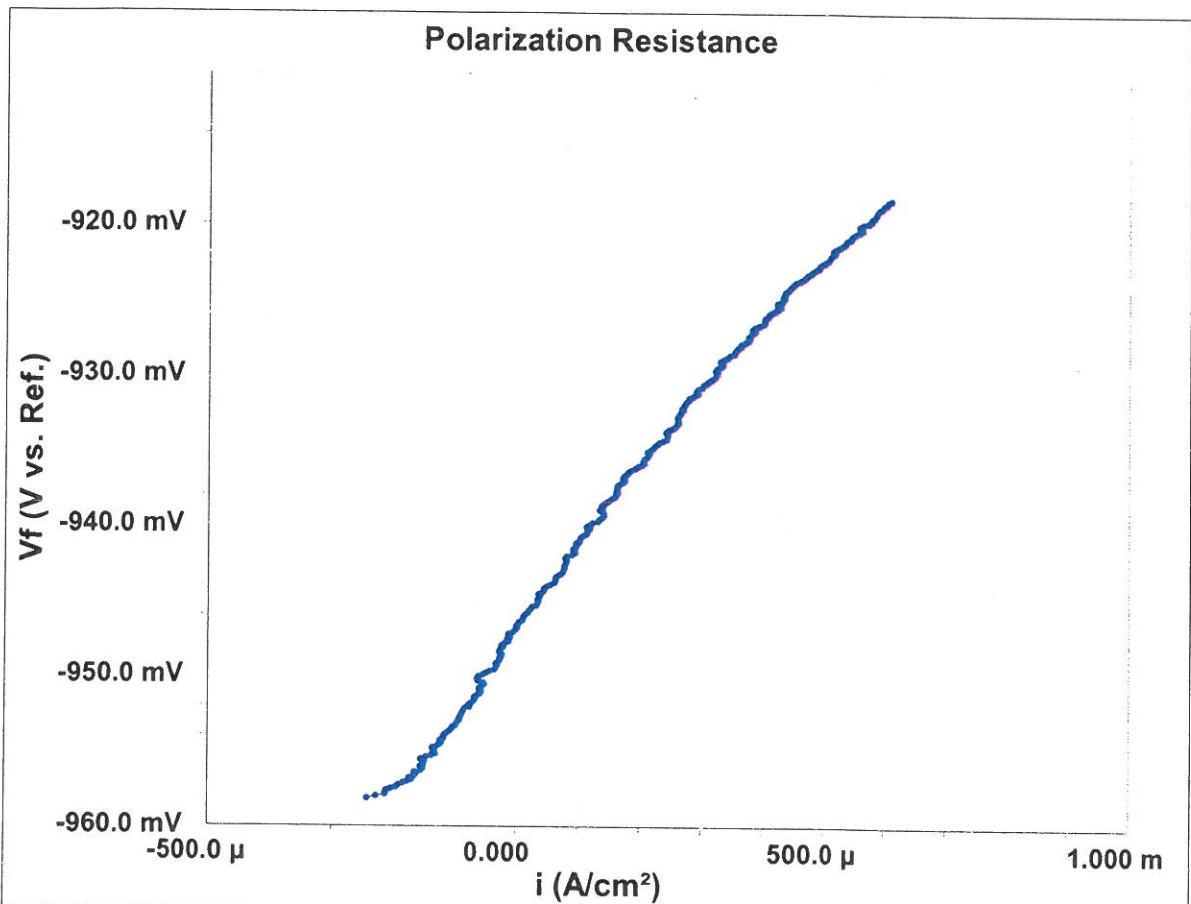
EXPERIMENTAL NOTES

DEC 29-AERATED



● CURVE (WELD E8018B2- LPR RUN1 .DTA)

EXPERIMENTAL PARAMETERS	EXPERIMENTAL NOTES
<p>Initial E (V): -0.02 vs. Eoc Final E (V): 0.02 vs. Eoc Polarization Resistance 11/30/2011 10:03:01 Scan Rate (mV/s): 0.125 Sample Period (s): 1 Sample Area (cm²): 1 Density (gm/cm³): 7.87 Equiv. Wt: 27.92 Conditioning: Off Init. Delay: Off Open Circuit (V): 0.137553</p> <p>EXPERIMENTAL DETERMINATIONS</p> <p>Beta An. (V/Dec): 0.12 Beta Cat. (V/Dec): 0.12 Icorr (A): 0.000001 Ecorr (V): 0.118031 Corrosion Rate (mpy): 0</p>	<p>NOV 30</p>



CURVE (WELD E8018B2-HAZ LPR RUN 2 DEC29 .DTA)

EXPERIMENTAL PARAMETERS

Initial E (V): -0.02 vs. Eoc
 Final E (V): 0.02 vs. Eoc
 Polarization Resistance
 12/29/2011
 8:48:16
 Scan Rate (mV/s): 0.125
 Sample Period (s): 1
 Sample Area (cm²): 0.2
 Density (gm/cm³): 7.87
 Equiv. Wt: 27.92
 Conditioning: Off
 Init. Delay: Off
 Open Circuit (V): -0.93848

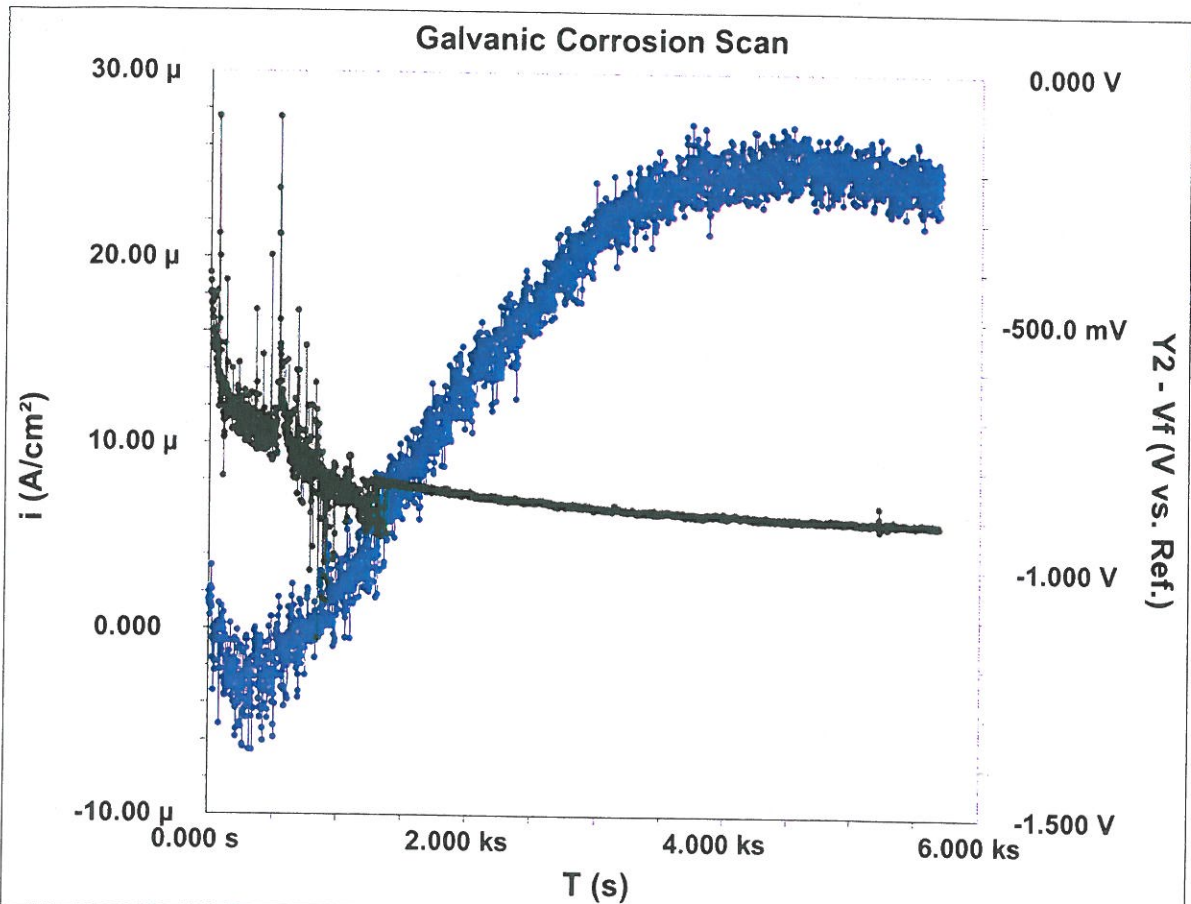
EXPERIMENTAL DETERMINATIONS

Beta An. (V/Dec): 0.12
 Beta Cat. (V/Dec): 0.12
 Icorr (A): 0.000001
 Ecorr (V): -0.946666
 Corrosion Rate (mpy): 0

EXPERIMENTAL NOTES

DEC 29-AERATED

B2 – Galvanic Current Recordings at Room Temperature



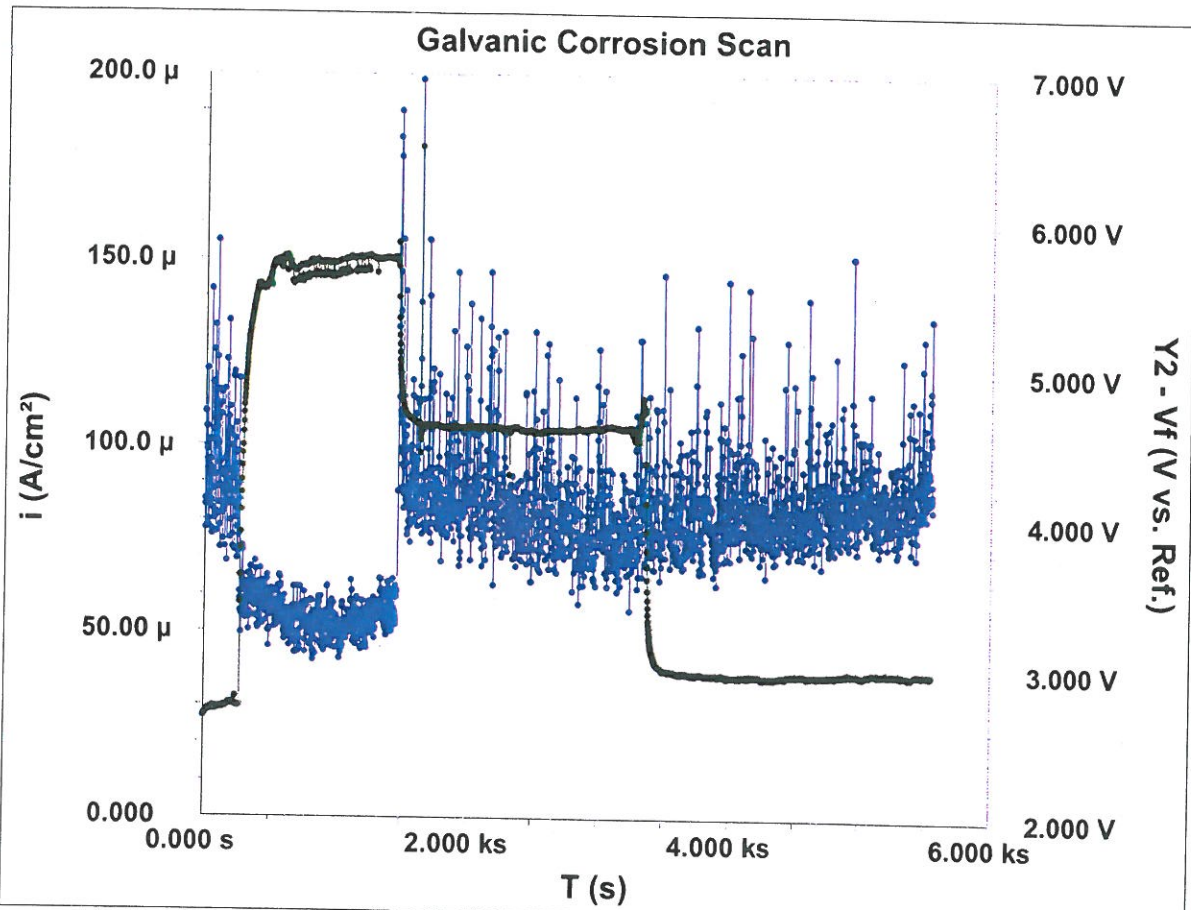
● CURVE (BM GC RUN 1 DEC 14.DTA) ● Y2 - CURVE (BM GC RUN 1 DEC 14.DTA)

EXPERIMENTAL PARAMETERS

Run Time (s): 12000
 Galvanic Corrosion Scan
 12/14/2011
 13:22:55
 Limit i (mA/cm^2): 1
 Sample Period (s): 2
 Sample Area (cm^2): 10
 Density (gm/cm^3): 7.87
 Equiv. Wt: 27.92
 Init. Delay: Off
 Open Circuit (V): -0.319299

EXPERIMENTAL NOTES

NOV 30



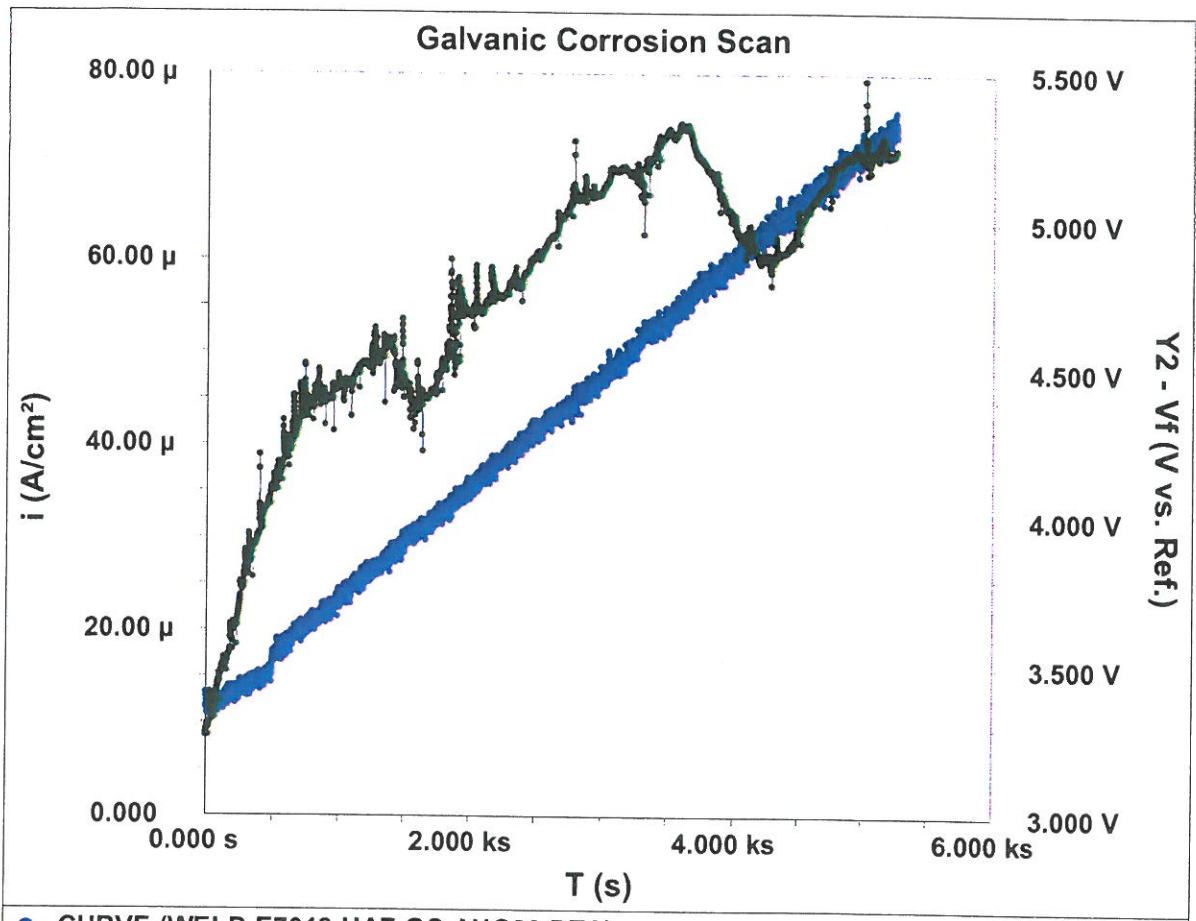
● CURVE (WELD E7018- GC RUN 1 DEC 14.DTA)

EXPERIMENTAL PARAMETERS

Run Time (s): 12000
 Galvanic Corrosion Scan
 12/14/2011
 17:01:50
 Limit i (mA/cm^2): 1
 Sample Period (s): 2
 Sample Area (cm^2): 1
 Density (gm/cm^3): 7.87
 Equiv. Wt: 27.92
 Init. Delay: Off
 Open Circuit (V): 2.68491

EXPERIMENTAL NOTES

DEC 14

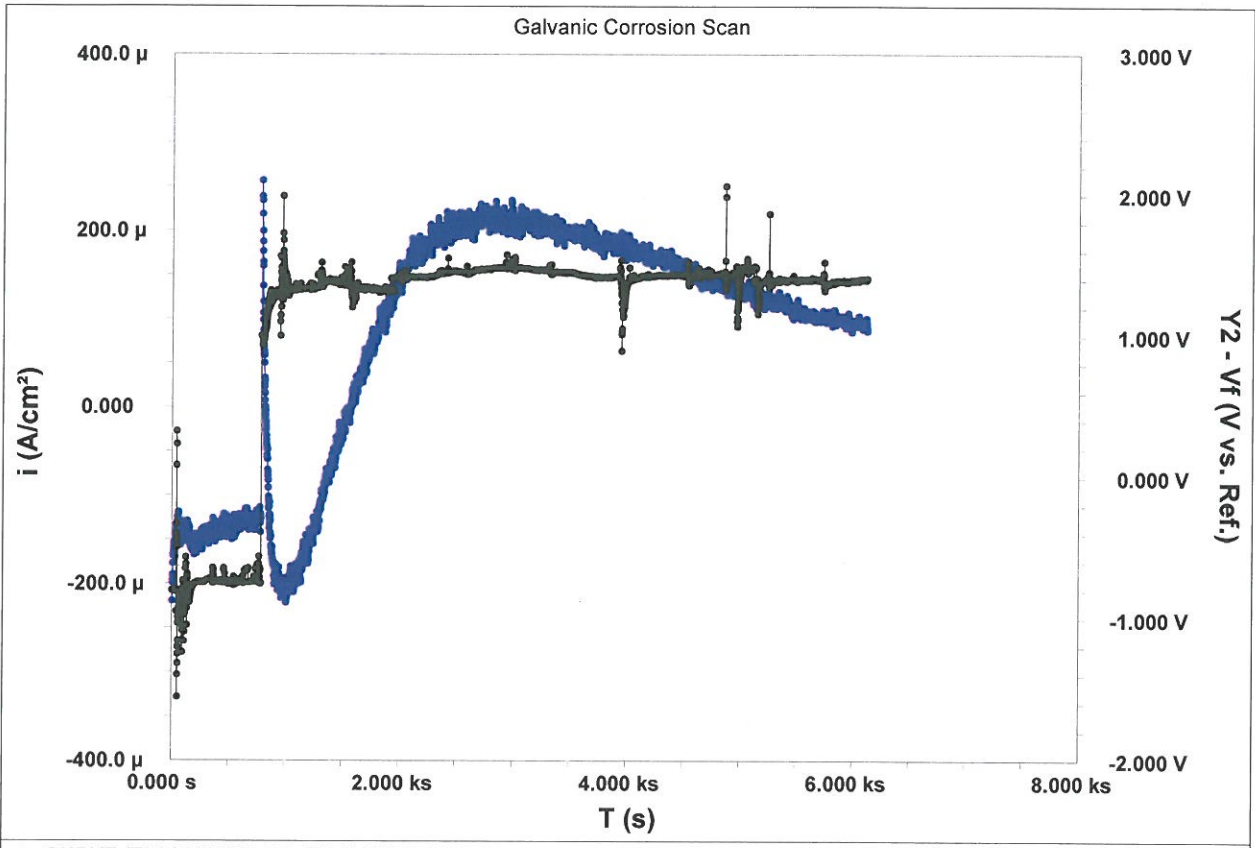


● CURVE (WELD E7018-HAZ-GC-AUG20.DTA)

EXPERIMENTAL PARAMETERS

Run Time (s): 12000
 Galvanic Corrosion Scan
 8/20/2012
 13:42:55
 Limit i (mA/cm^2): 1
 Sample Period (s): 1
 Sample Area (cm^2): 1
 Density (gm/cm^3): 7.87
 Equiv. Wt: 27.92
 Init. Delay: Off
 Open Circuit (V): 3.27328

EXPERIMENTAL NOTES



● CURVE (E7018-WELD-GC-WITH DEFECT.DTA)

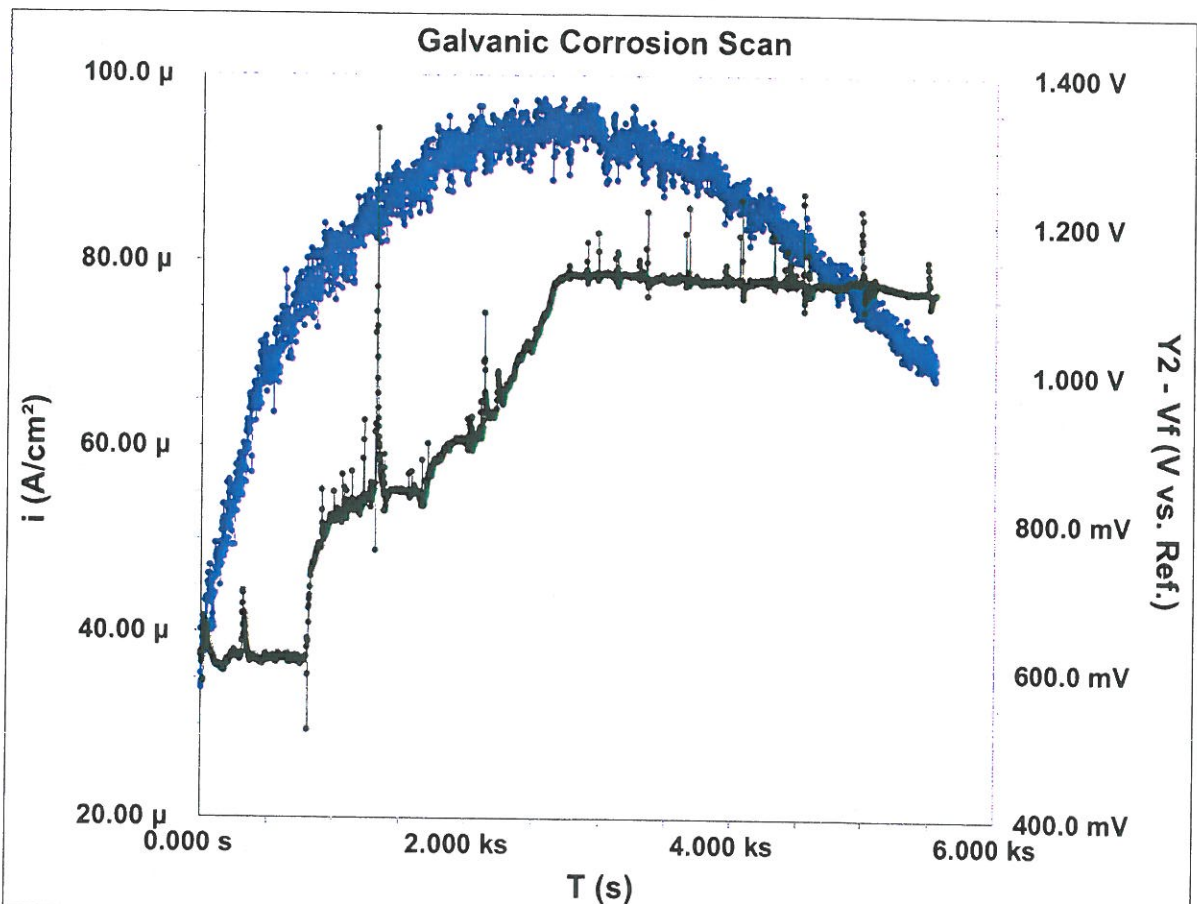
● Y2 - CURVE (E7018-WELD-GC-WITH DEFECT.DTA)

EXPERIMENTAL PARAMETERS

Run Time (s): 12000
 Galvanic Corrosion Scan
 11/28/2011
 10:57:28
 Limit i (mA/cm^2): 25
 Sample Period (s): 1
 Sample Area (cm^2): 0.4
 Density (gm/cm^3): 7.87
 Equiv. Wt: 27.92
 Init. Delay: Off
 Open Circuit (V): -0.813226

EXPERIMENTAL NOTES

28-11-11



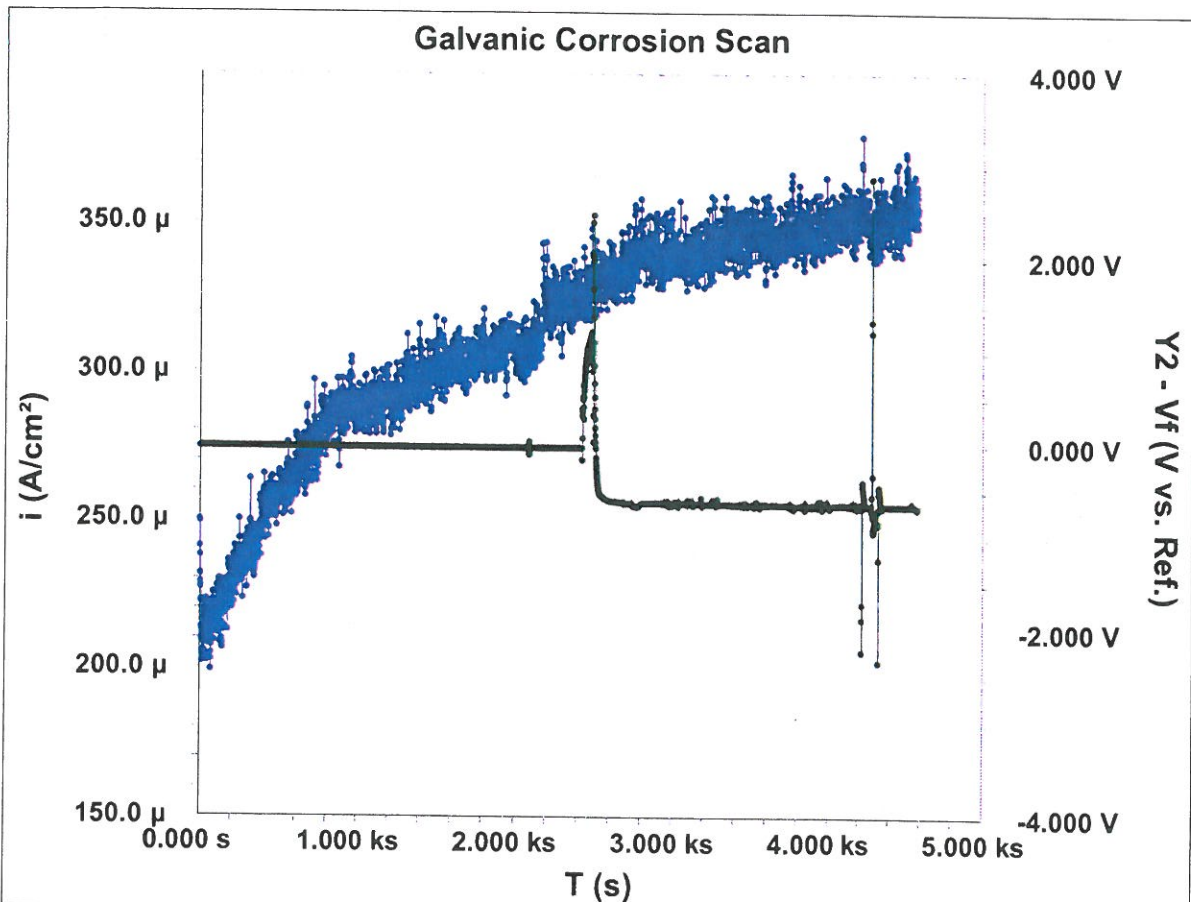
● CURVE (WELD E8018G- GC RUN 1 REPEAT DEC 14.DTA)

EXPERIMENTAL PARAMETERS

Run Time (s): 12000
 Galvanic Corrosion Scan
 12/14/2011
 15:20:11
 Limit i (mA/cm^2): 1
 Sample Period (s): 2
 Sample Area (cm^2): 2.2
 Density (gm/cm^3): 7.87
 Equiv. Wt: 27.92
 Init. Delay: Off
 Open Circuit (V): 0.624744

EXPERIMENTAL NOTES

DEC 14

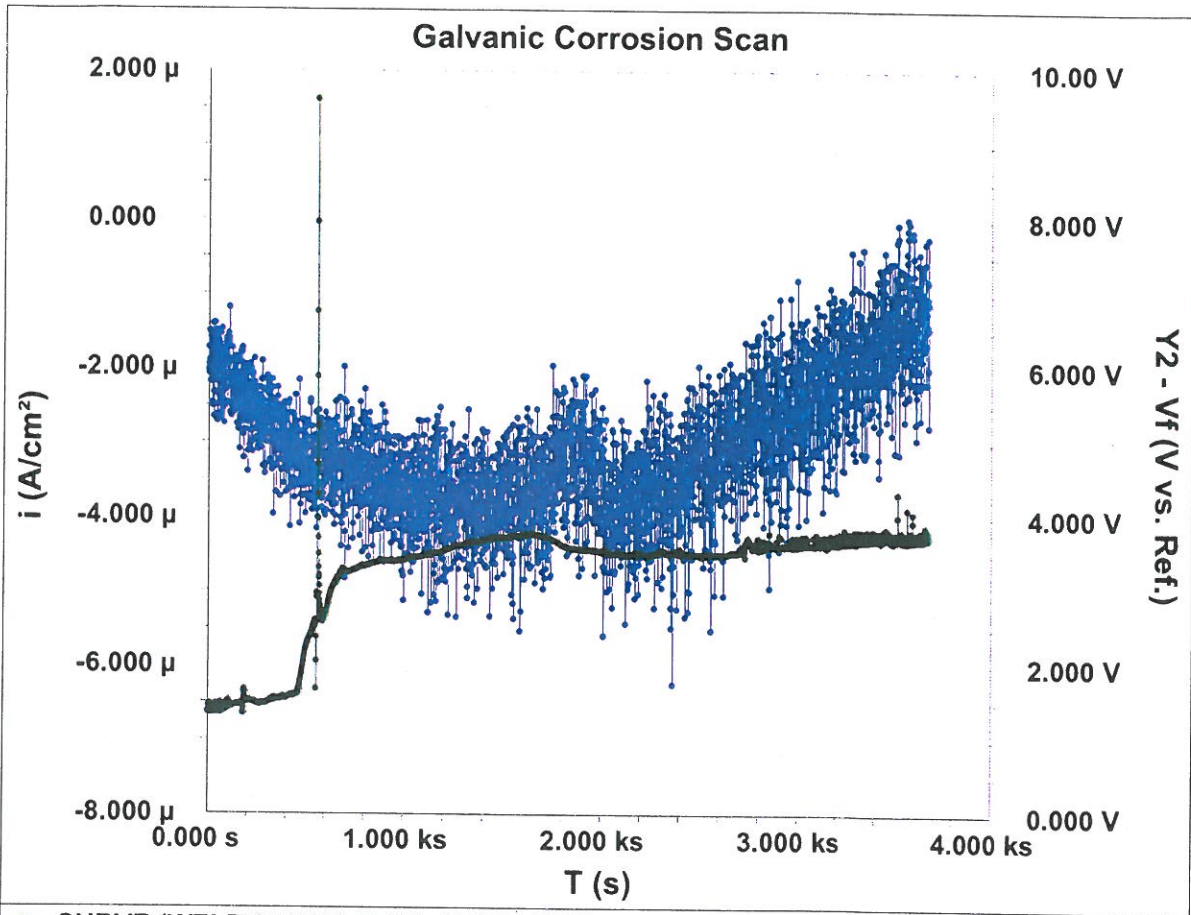


● CURVE (WELD E8018G- HAZ GC RUN1 JAN4.DTA)

EXPERIMENTAL PARAMETERS

Run Time (s): 12000
 Galvanic Corrosion Scan
 1/4/2012
 7:01:42
 Limit i (mA/cm^2): 1
 Sample Period (s): 1
 Sample Area (cm^2): 0.44
 Density (gm/cm^3): 7.87
 Equiv. Wt: 27.92
 Init. Delay: Off
 Open Circuit (V): -0.000108

EXPERIMENTAL NOTES

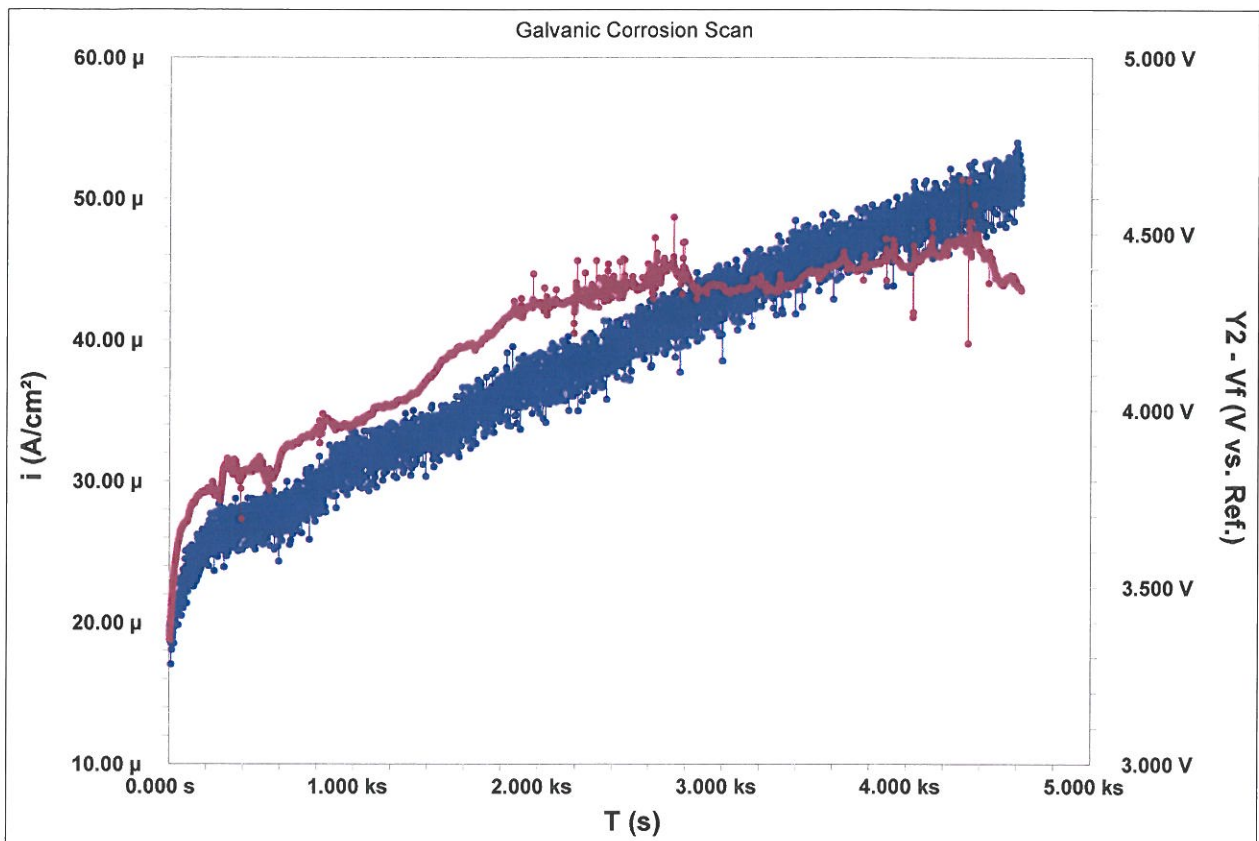


● CURVE (WELD 8018B2-M-GC-AUG24.DTA)

EXPERIMENTAL PARAMETERS

Run Time (s): 12000
 Galvanic Corrosion Scan
 8/24/2012
 17:45:27
 Limit i (mA/cm²): 1
 Sample Period (s): 1
 Sample Area (cm²): 0.3
 Density (gm/cm³): 7.87
 Equiv. Wt: 27.92
 Init. Delay: Off
 Open Circuit (V): 1.37743

EXPERIMENTAL NOTES



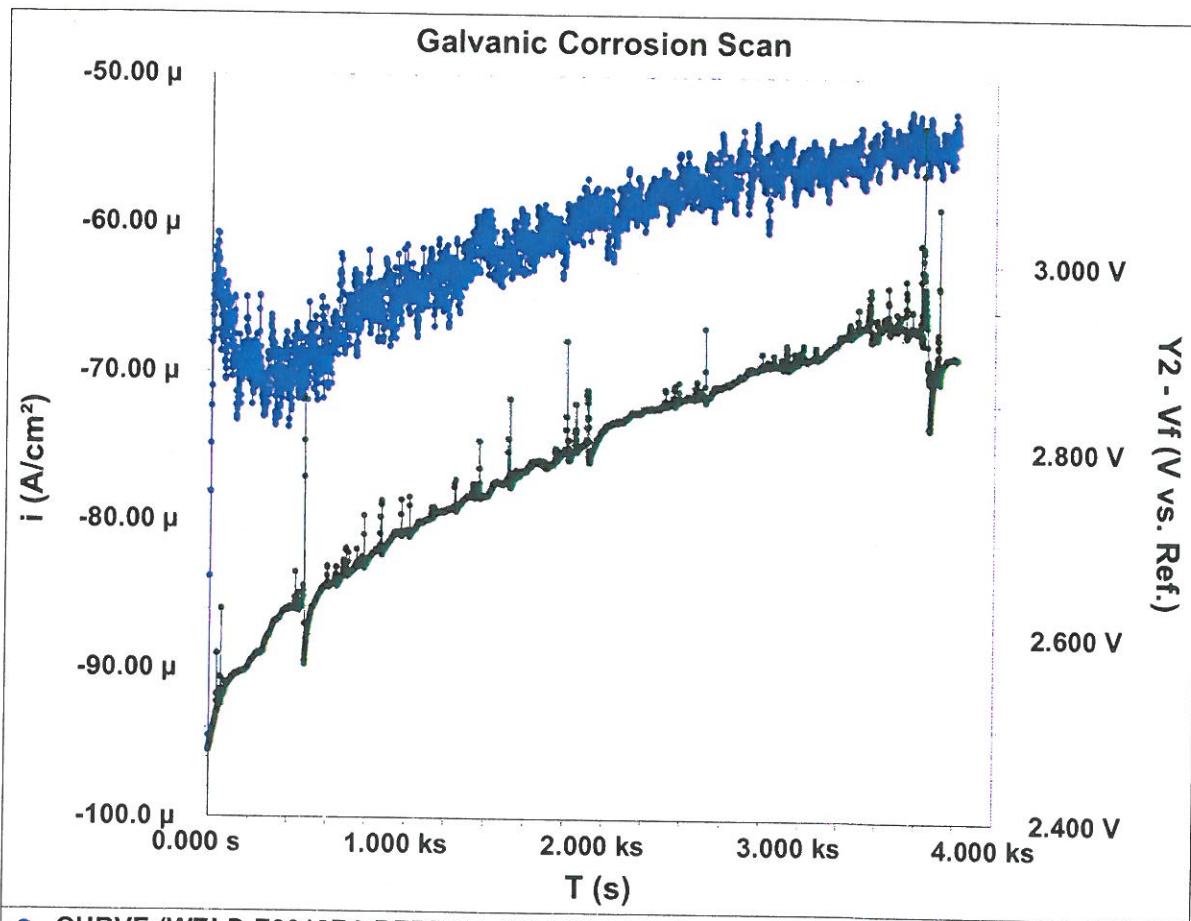
● CURVE (WELD-E8018B2-HAZ-M-GC-AUG24.DTA)

● Y2 - CURVE (WELD 6M-HAZ-GC-AUG24.DTA)

EXPERIMENTAL PARAMETERS

Run Time (s): 12000
 Galvanic Corrosion Scan
 8/24/2012
 18:47:54
 Limit i (mA/cm²): 1
 Sample Period (s): 1
 Sample Area (cm²): 0.3
 Density (gm/cm³): 7.87
 Equiv. Wt: 27.92
 Init. Delay: Off
 Open Circuit (V): 3.3023

EXPERIMENTAL NOTES



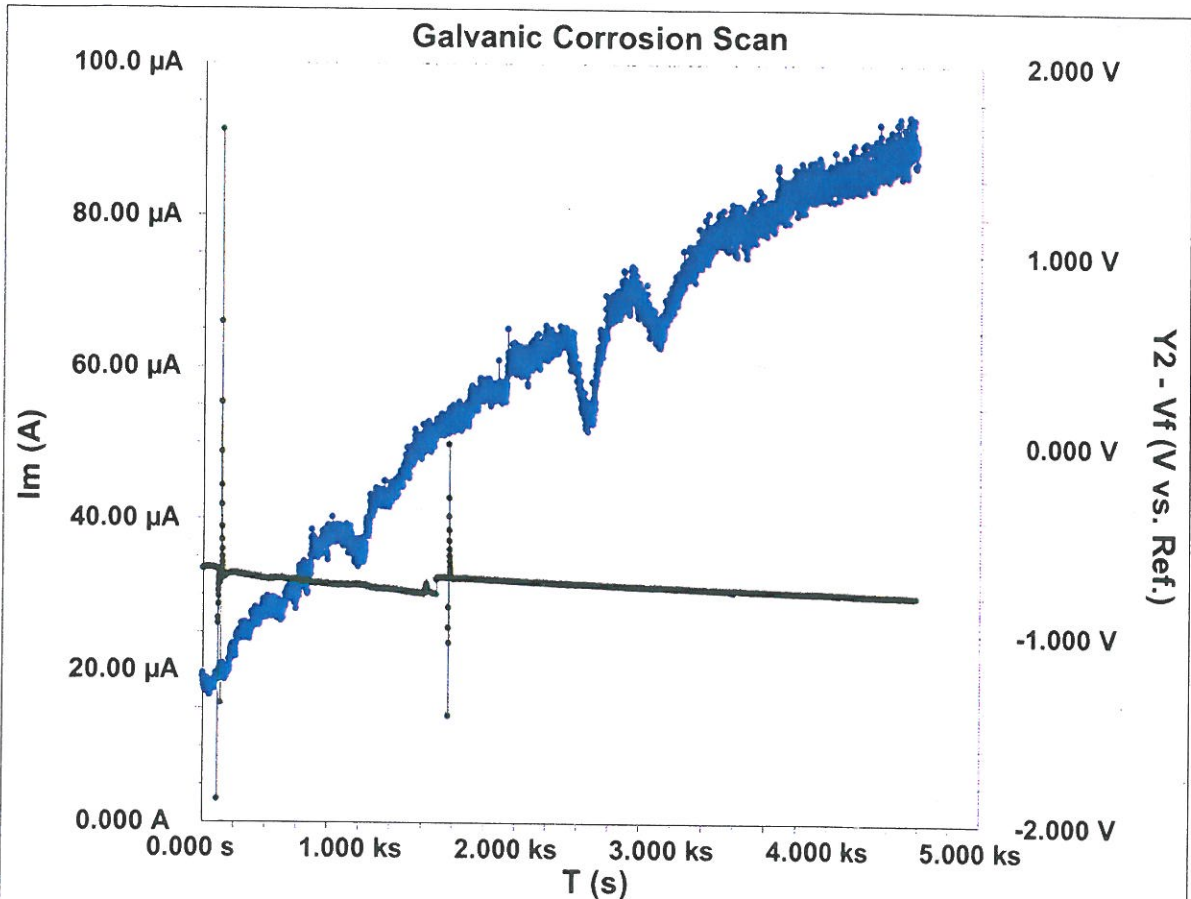
● CURVE (WELD E8018B6-REPEAT -DC-RUN2.DTA)

EXPERIMENTAL PARAMETERS

Run Time (s): 12000
 Galvanic Corrosion Scan
 11/29/2011
 16:11:43
 Limit i (mA/cm^2): 1
 Sample Period (s): 1
 Sample Area (cm^2): 1.5
 Density (gm/cm^3): 7.87
 Equiv. Wt: 27.92
 Init. Delay: Off
 Open Circuit (V): 2.4345

EXPERIMENTAL NOTES

29-11-11



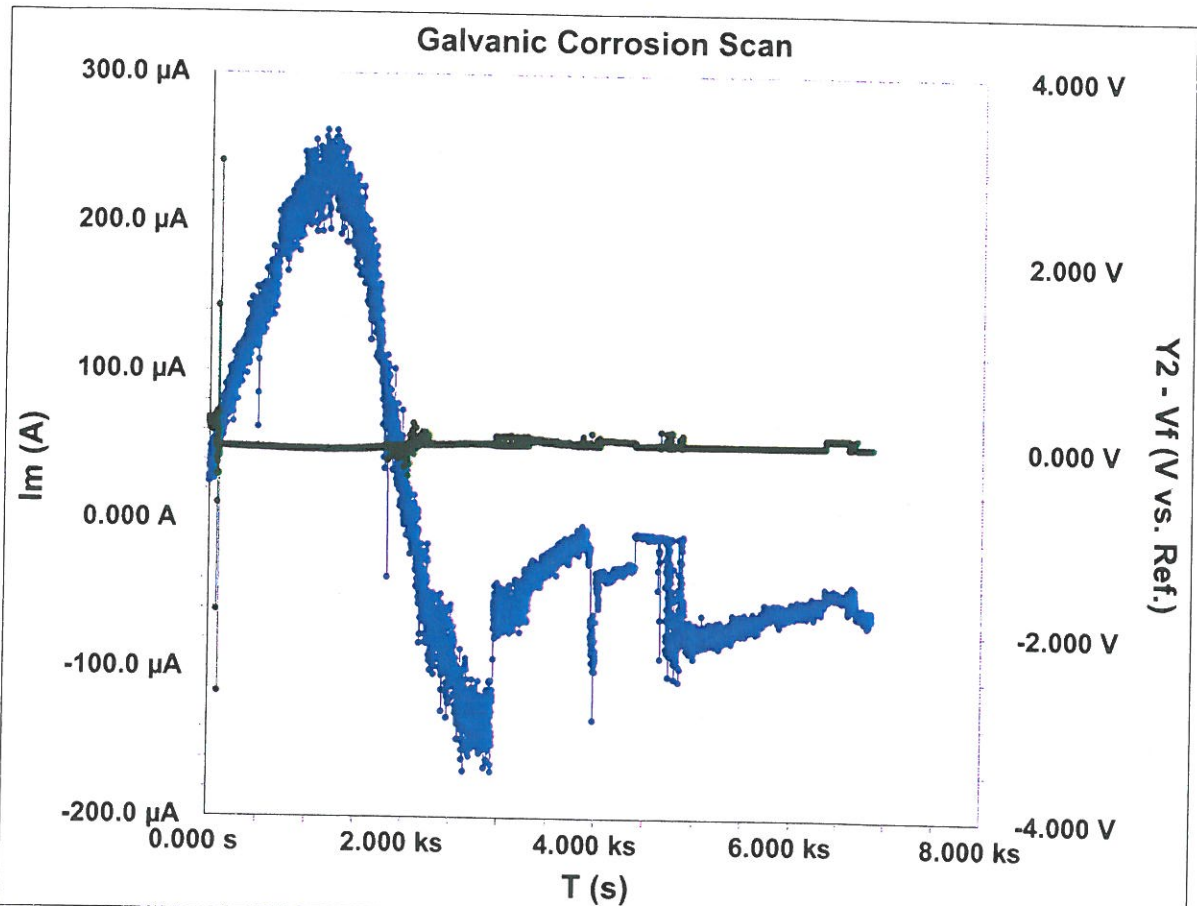
● CURVE (WELD B8018B6- HAZ GC RUN1 JAN 10.DTA)

EXPERIMENTAL PARAMETERS

Run Time (s): 12000
 Galvanic Corrosion Scan
 1/10/2012
 6:34:21
 Limit i (mA/cm²): 1
 Sample Period (s): 1
 Sample Area (cm²): 0.44
 Density (gm/cm³): 7.87
 Equiv. Wt: 27.92
 Init. Delay: Off
 Open Circuit (V): -0.63643

EXPERIMENTAL NOTES

B3 – Galvanic Current Recordings at Various Temperatures



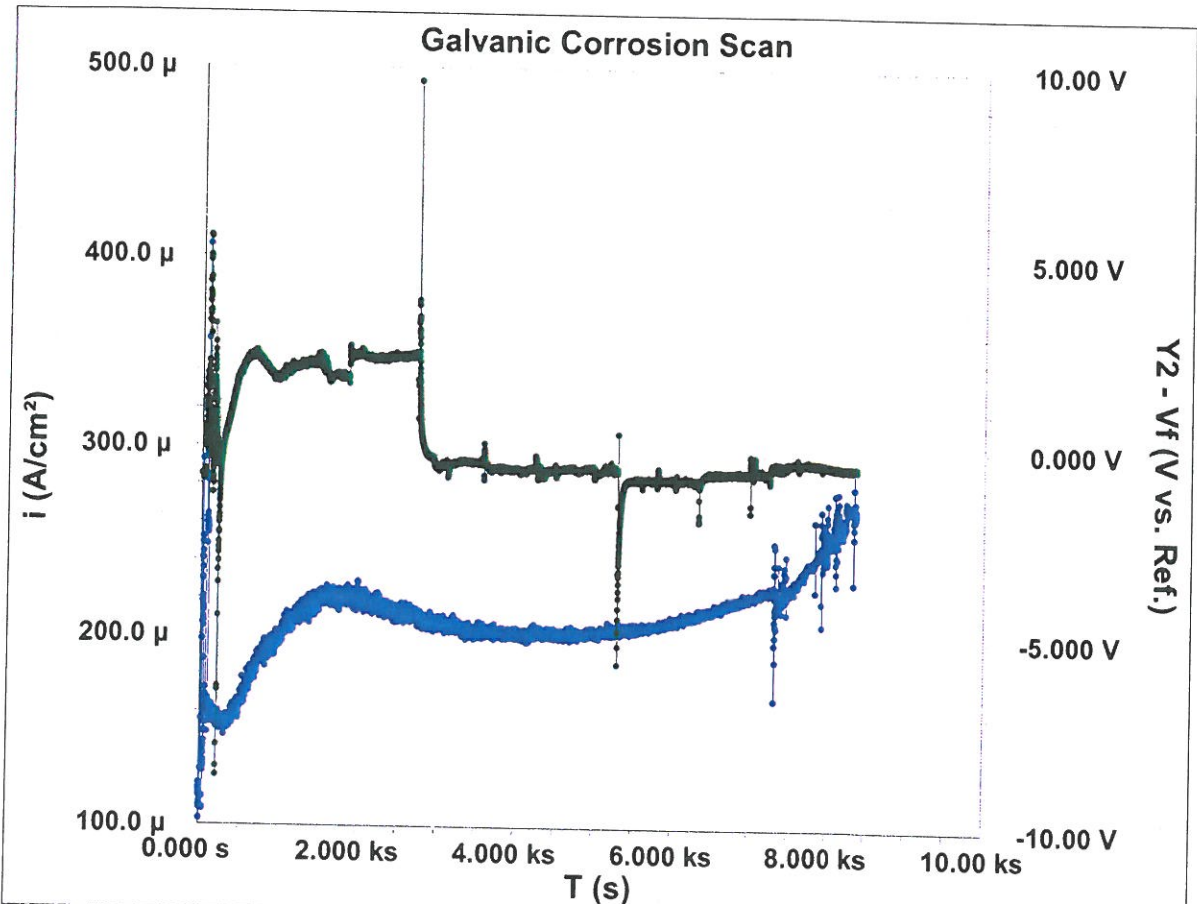
● CURVE (BM TEMP GC RUN 1 DEC 22.DTA)

EXPERIMENTAL PARAMETERS

Run Time (s): 12000
 Galvanic Corrosion Scan
 12/22/2011
 7:08:10
 Limit i (mA/cm²): 1
 Sample Period (s): 1
 Sample Area (cm²): 10
 Density (gm/cm³): 7.87
 Equiv. Wt: 27.92
 Init. Delay: Off
 Open Circuit (V): 0.244535

EXPERIMENTAL NOTES

DEC 20



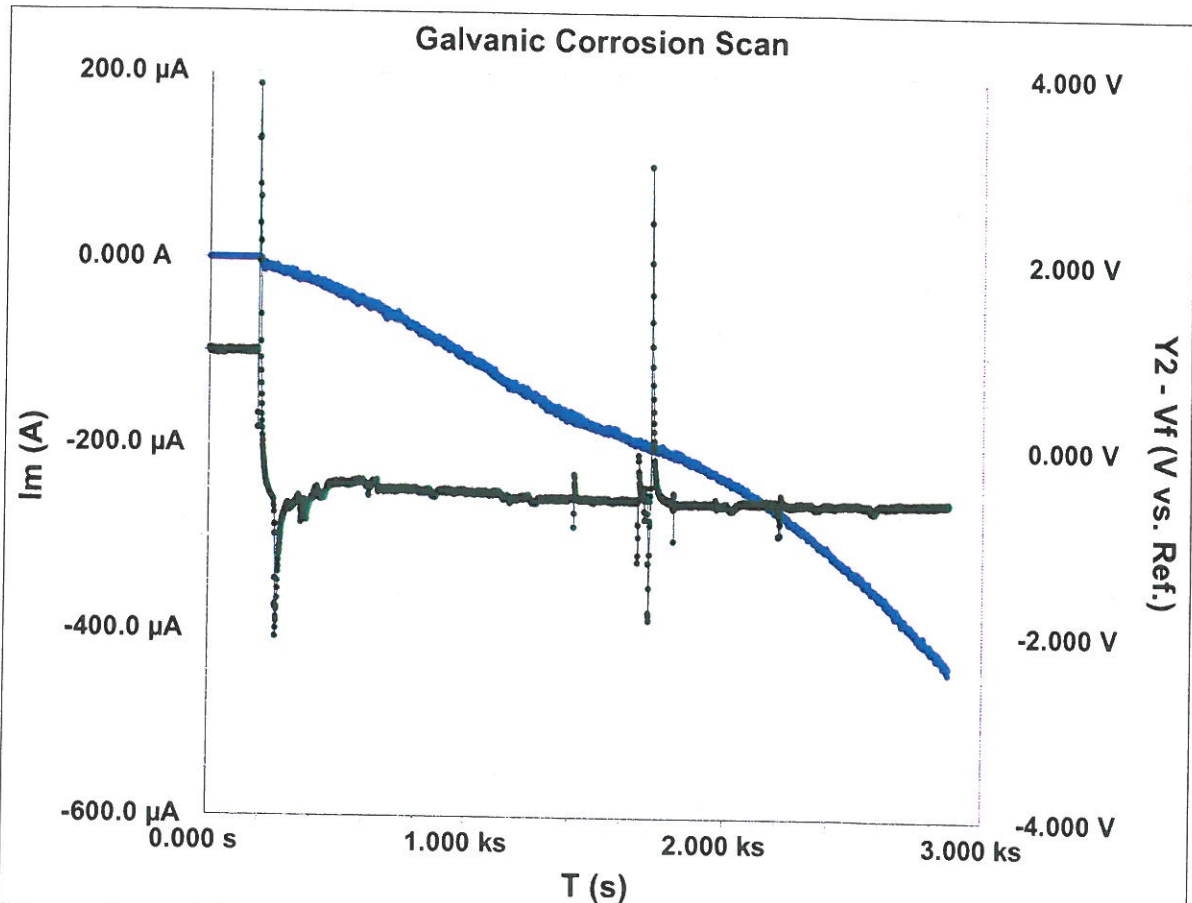
● CURVE (WELD E7018 temperature run 2.DTA)

EXPERIMENTAL PARAMETERS

Run Time (s): 12000
 Galvanic Corrosion Scan
 11/16/2011
 15:11:12
 Limit i (mA/cm²): 25
 Sample Period (s): 1
 Sample Area (cm²): 2.2
 Density (gm/cm³): 7.87
 Equiv. Wt: 27.92
 Init. Delay: Off
 Open Circuit (V): -0.695943

EXPERIMENTAL NOTES

this weld root has a significant defect.

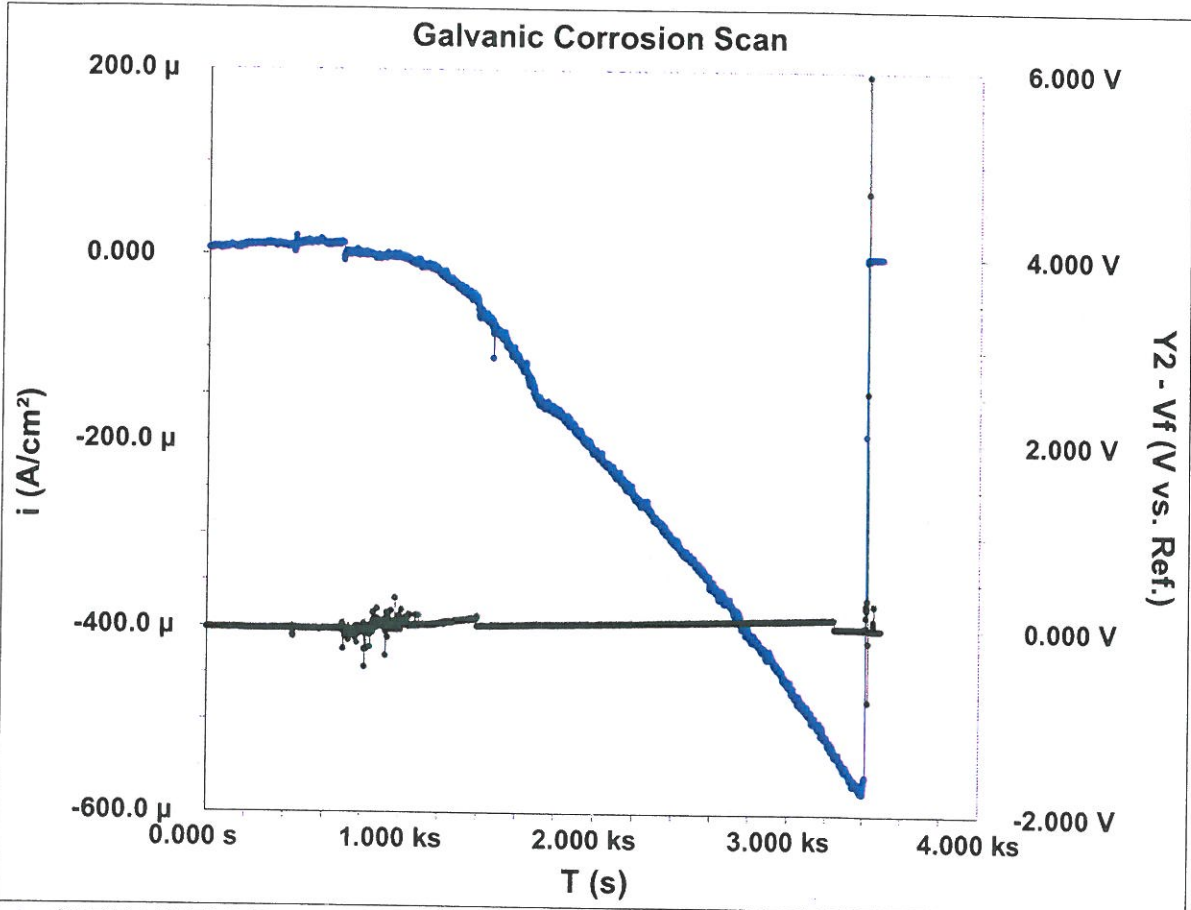


● CURVE (WELD E7018- HAZ TEMP GC RUN1 JAN 18.DTA)

EXPERIMENTAL PARAMETERS

Run Time (s): 12000
 Galvanic Corrosion Scan
 1/18/2012
 6:54:19
 Limit i (mA/cm²): 1
 Sample Period (s): 1
 Sample Area (cm²): 0.44
 Density (gm/cm³): 7.87
 Equiv. Wt: 27.92
 Init. Delay: Off
 Open Circuit (V): 1.09329

EXPERIMENTAL NOTES



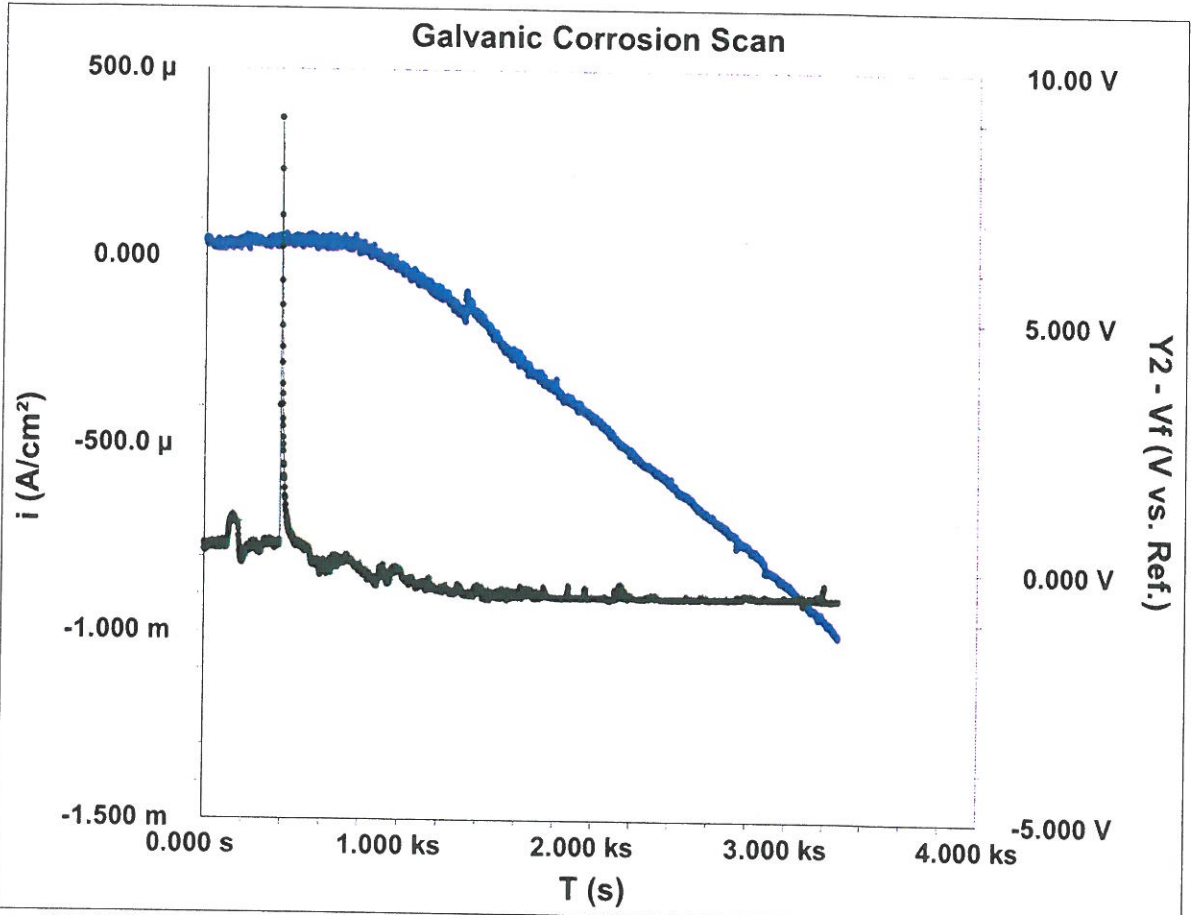
● CURVE (WELD E8018G TEMP GC DEC 27.DTA)

EXPERIMENTAL PARAMETERS

Run Time (s): 12000
 Galvanic Corrosion Scan
 12/27/2011
 6:51:54
 Limit i (mA/cm^2): 1
 Sample Period (s): 1
 Sample Area (cm^2): 1
 Density (gm/cm^3): 7.87
 Equiv. Wt: 27.92
 Init. Delay: Off
 Open Circuit (V): -0.000177

EXPERIMENTAL NOTES

DEC 26

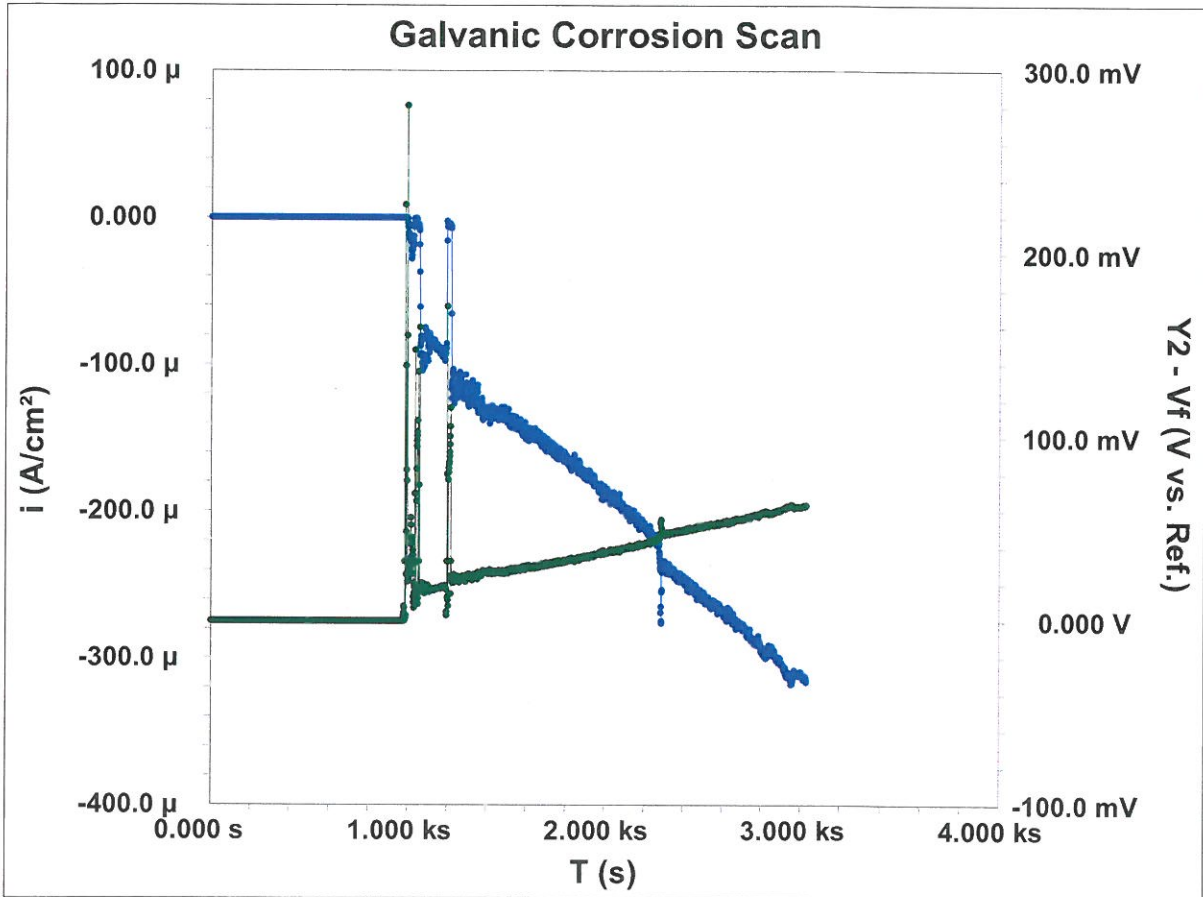


• CURVE (WELD E8018G HAZ TEMP GC RUN1 JAN 11.DTA)

EXPERIMENTAL PARAMETERS

Run Time (s): 12000
 Galvanic Corrosion Scan
 1/11/2012
 6:50:31
 Limit i (mA/cm^2): 1
 Sample Period (s): 1
 Sample Area (cm^2): 0.44
 Density (gm/cm^3): 7.87
 Equiv. Wt: 27.92
 Init. Delay: Off
 Open Circuit (V): 0.509314

EXPERIMENTAL NOTES



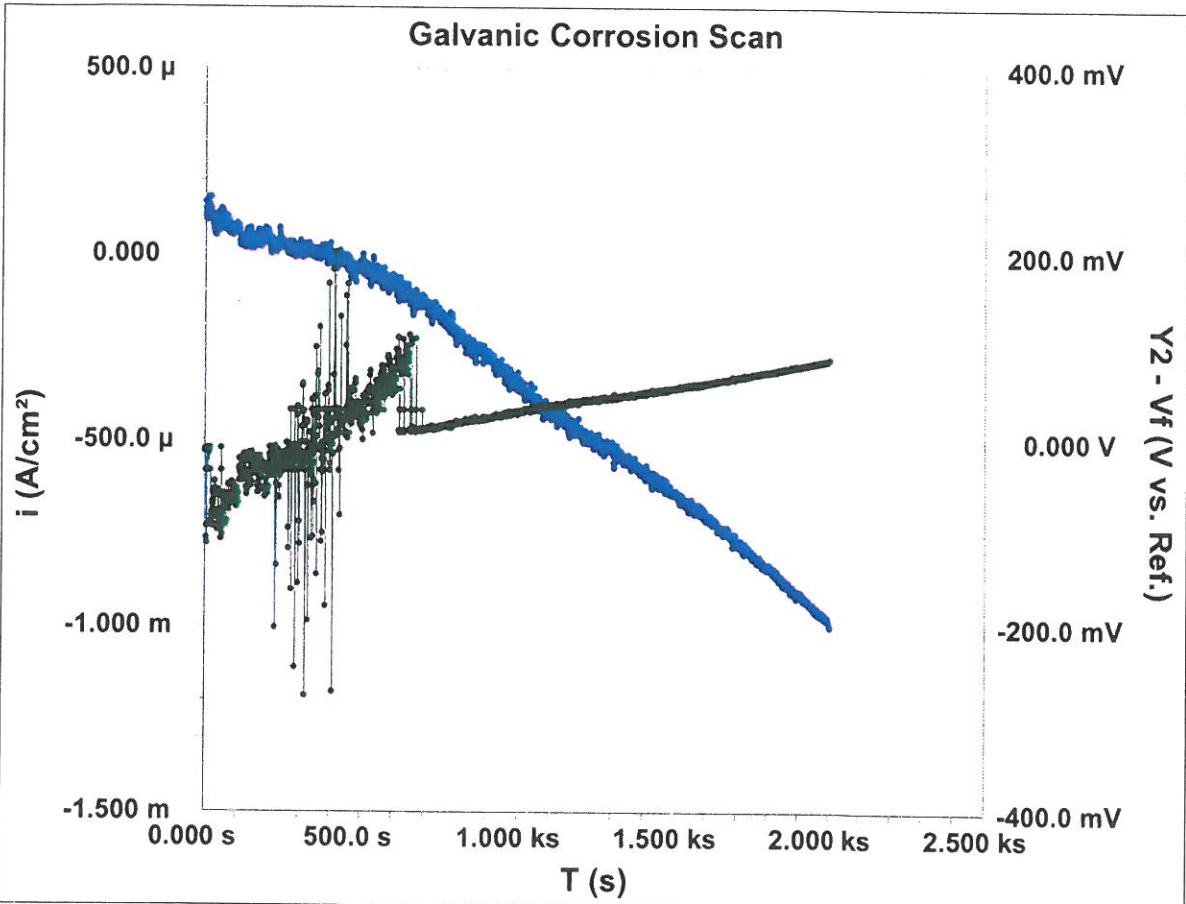
● CURVE (WELD E8018B2 TEMP GC RUN REPEAT1 DEC 26.DTA)

EXPERIMENTAL PARAMETERS

Run Time (s): 12000
 Galvanic Corrosion Scan
 12/26/2011
 7:20:56
 Limit i (mA/cm²): 1
 Sample Period (s): 1
 Sample Area (cm²): 1
 Density (gm/cm³): 7.87
 Equiv. Wt: 27.92
 Init. Delay: Off
 Open Circuit (V): 1.89471E-05

EXPERIMENTAL NOTES

DEC 26

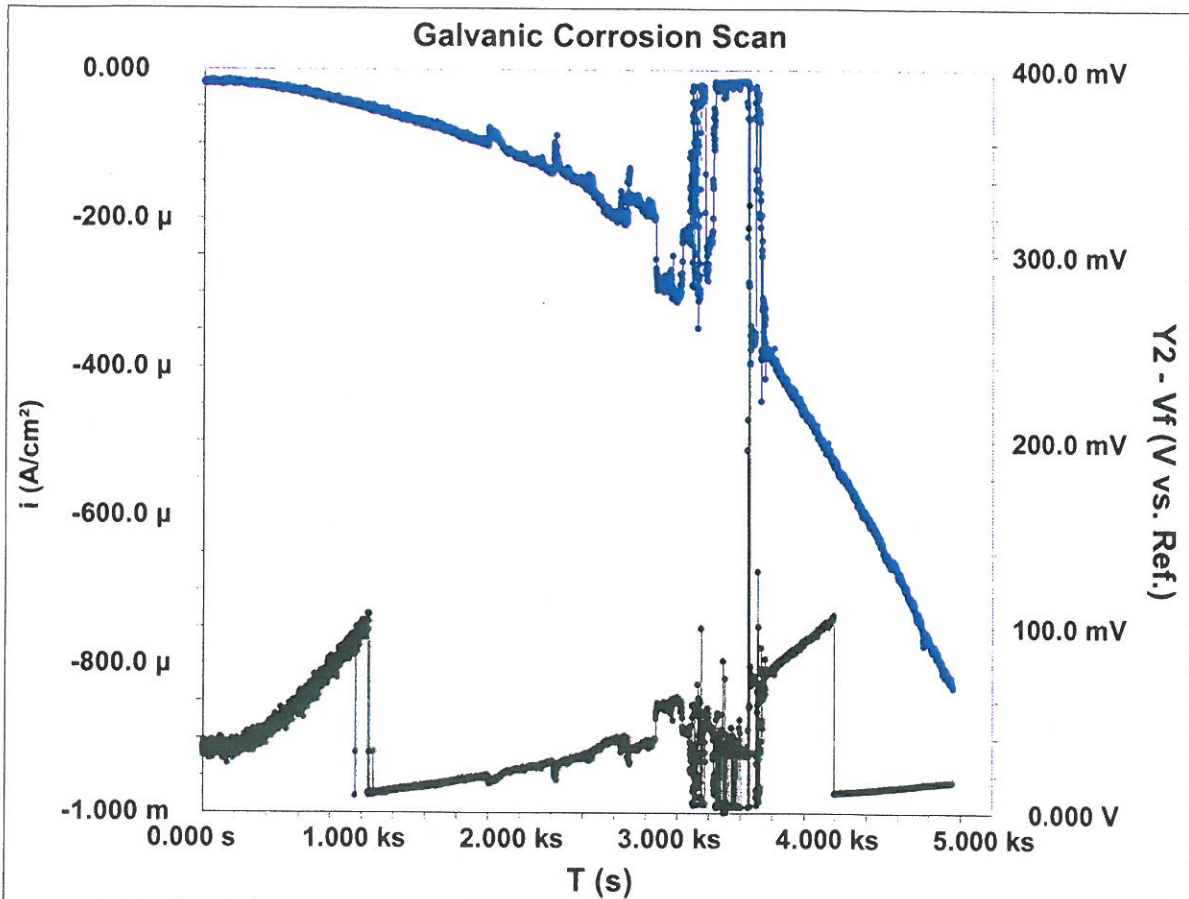


● CURVE (WELD E8018B2 HAZ TEMP GC RUN1 JAN 18.DTA)

EXPERIMENTAL PARAMETERS

Run Time (s): 12000
 Galvanic Corrosion Scan
 1/18/2012
 8:08:49
 Limit i (mA/cm^2): 1
 Sample Period (s): 1
 Sample Area (cm^2): 0.44
 Density (gm/cm^3): 7.87
 Equiv. Wt: 27.92
 Init. Delay: Off
 Open Circuit (V): 6.39336E-06

EXPERIMENTAL NOTES



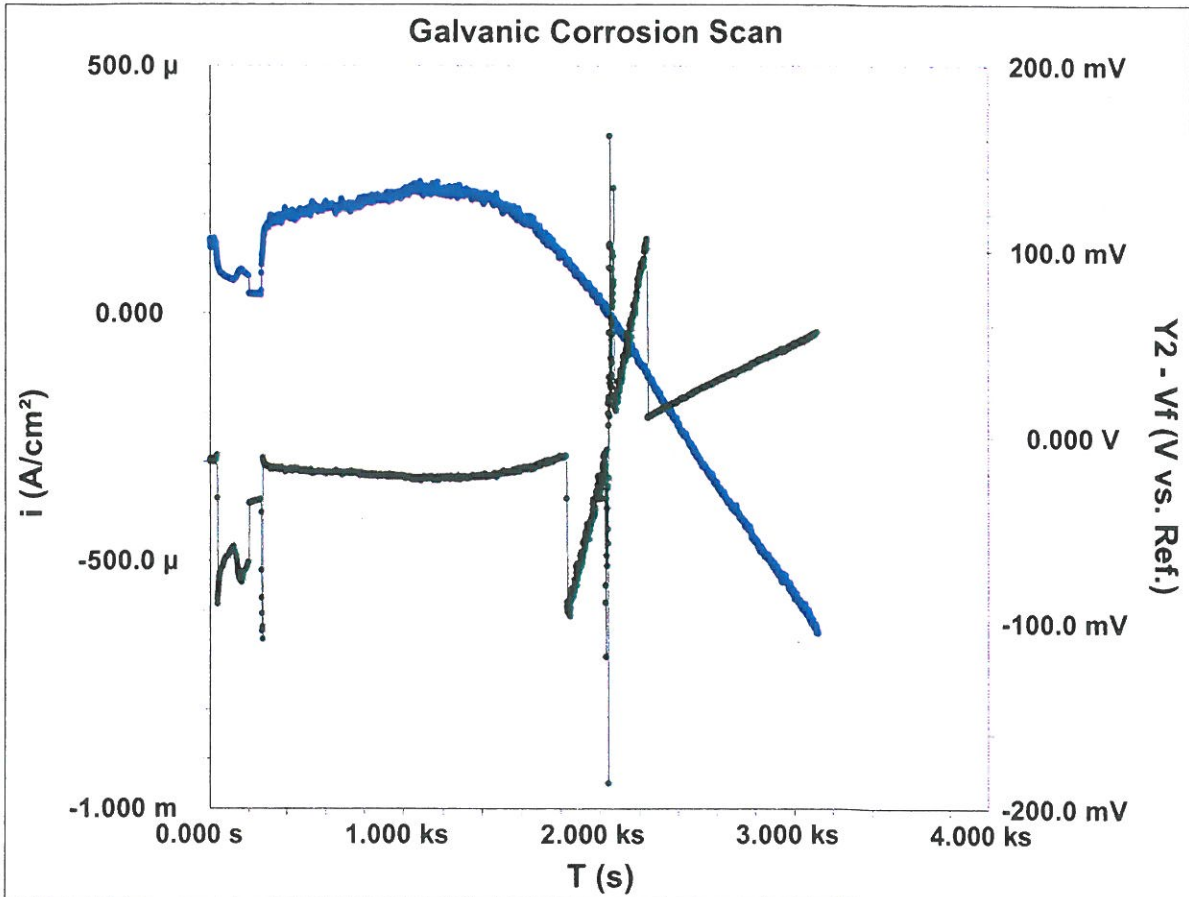
● CURVE (WELD E8018B6 TEMP GC RUN REPEAT1 DEC 25.DTA)

EXPERIMENTAL PARAMETERS

Run Time (s): 12000
 Galvanic Corrosion Scan
 12/25/2011
 7:26:47
 Limit i (mA/cm²): 1
 Sample Period (s): 1
 Sample Area (cm²): 1
 Density (gm/cm³): 7.87
 Equiv. Wt: 27.92
 Init. Delay: Off
 Open Circuit (V): -0.000158

EXPERIMENTAL NOTES

DEC 20



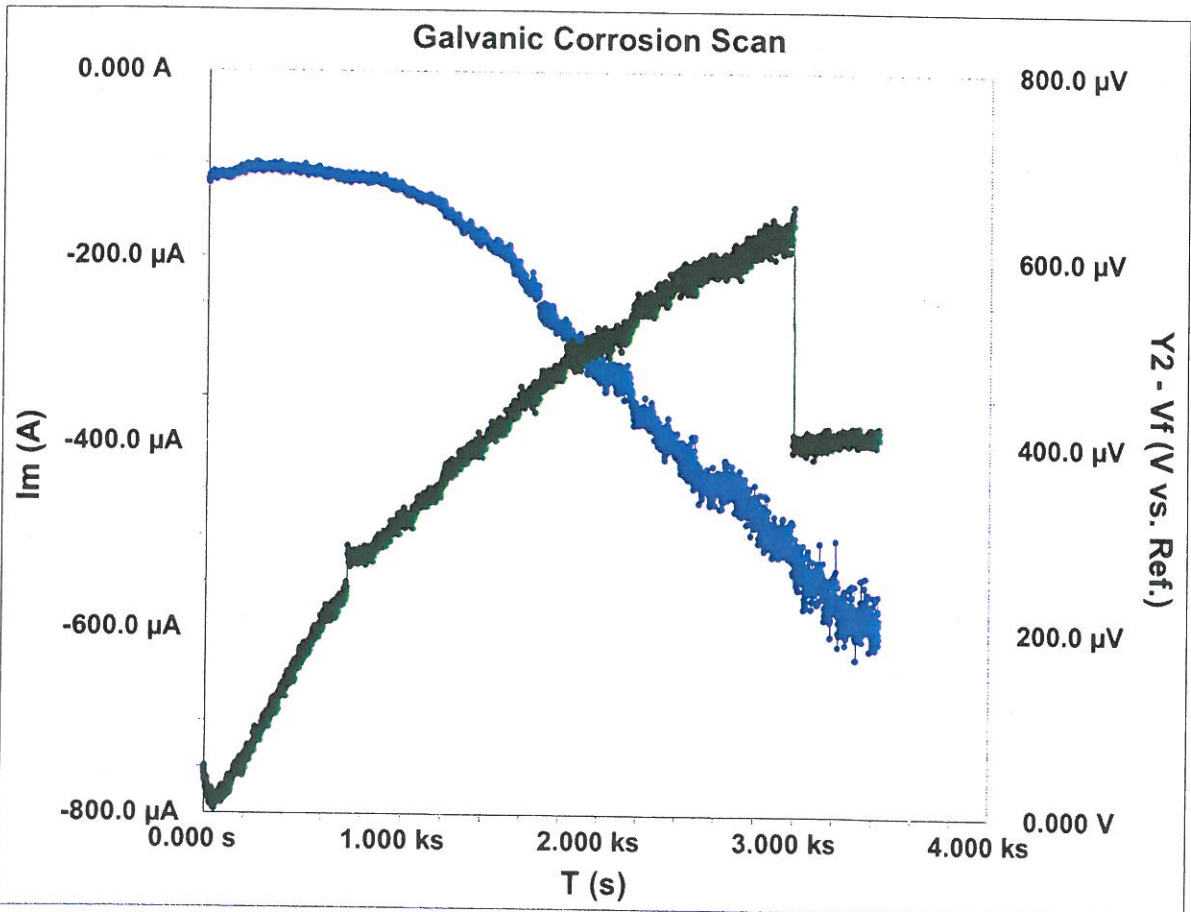
● CURVE (WELD E8018B6-REPEAT HAZ TEMP GC RUN1 JAN 18.DTA)

EXPERIMENTAL PARAMETERS

Run Time (s): 12000
 Galvanic Corrosion Scan
 1/18/2012
 9:21:25
 Limit i (mA/cm^2): 1
 Sample Period (s): 1
 Sample Area (cm^2): 0.44
 Density (gm/cm^3): 7.87
 Equiv. Wt: 27.92
 Init. Delay: Off
 Open Circuit (V): -8.9102E-06

EXPERIMENTAL NOTES

B4 – Galvanic Current Recordings at Various Temperatures with CO₂

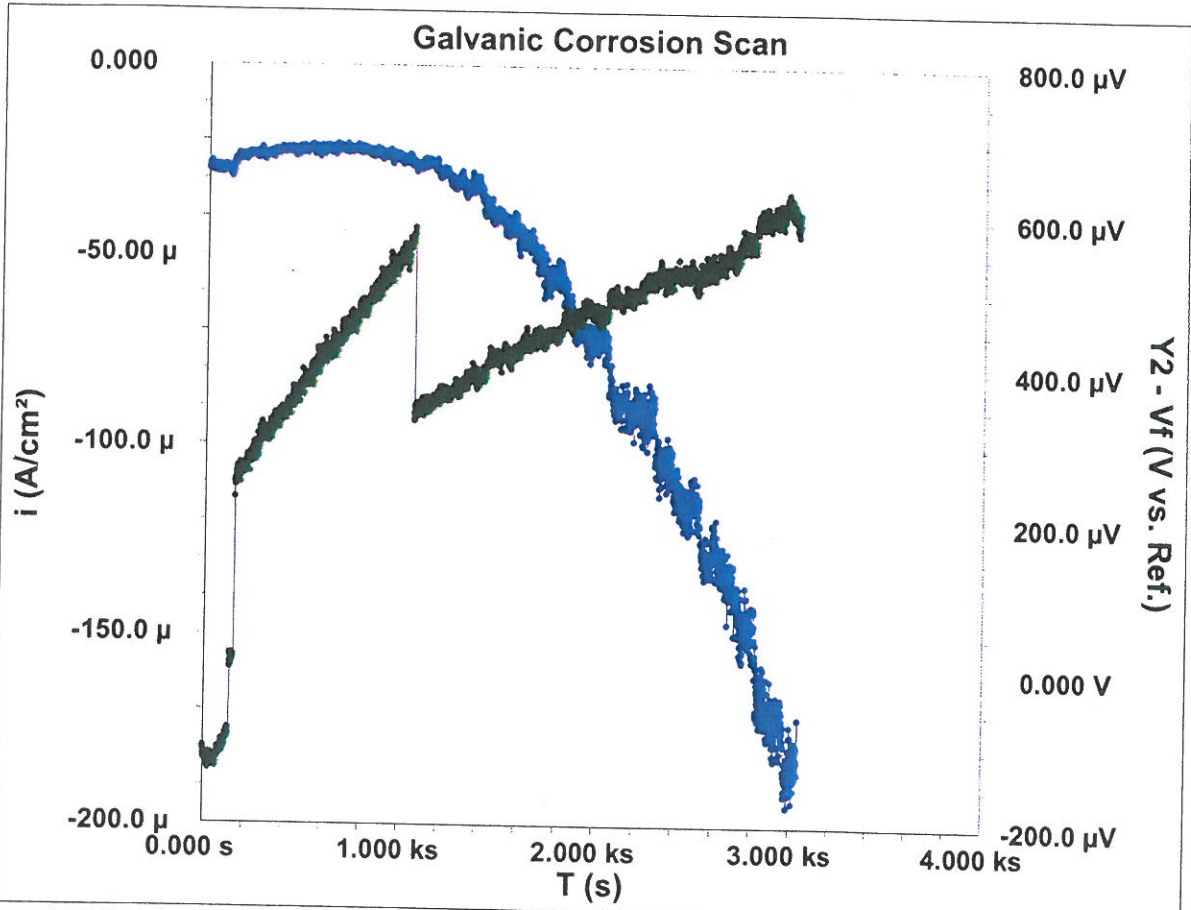


● CURVE (BM-CO2-TEMP-GC-MAY 10-run1.DTA)

EXPERIMENTAL PARAMETERS

Run Time (s): 12000
 Galvanic Corrosion Scan
 5/10/2012
 14:33:53
 Limit i (mA/cm²): 1
 Sample Period (s): 1
 Sample Area (cm²): 2.25
 Density (gm/cm³): 7.87
 Equiv. Wt: 27.92
 Init. Delay: Off
 Open Circuit (V): 0.012766

EXPERIMENTAL NOTES



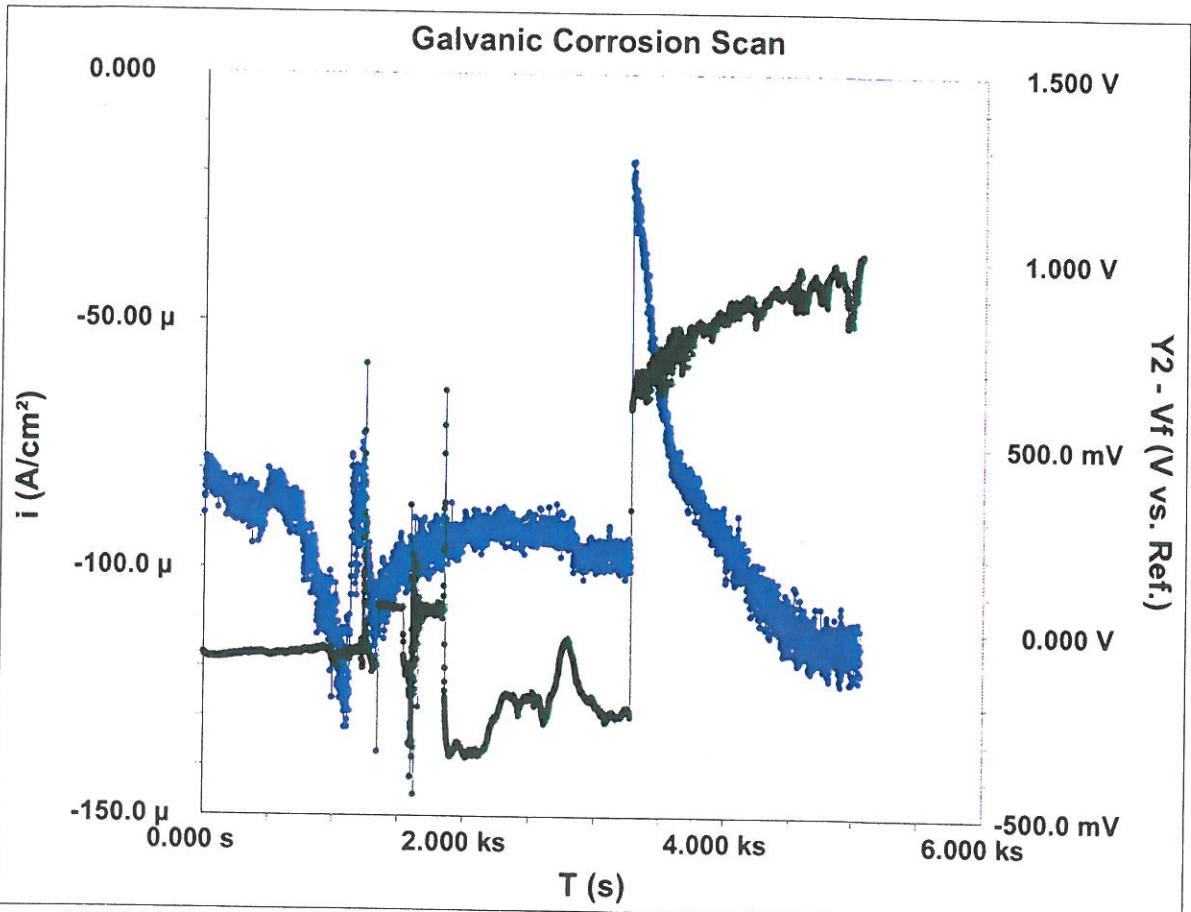
● CURVE (WELD E7018-CO2-TEMP-GC-MAY 11-run1.DTA)

EXPERIMENTAL PARAMETERS

```

Run Time (s): 12000
Galvanic Corrosion Scan
5/11/2012
15:23:30
Limit i (mA/cm^2): 1
Sample Period (s): 1
Sample Area (cm^2): 2
Density (gm/cm^3): 7.87
Equiv. Wt: 27.92
Init. Delay: Off
Open Circuit (V): 0.010202
  
```

EXPERIMENTAL NOTES

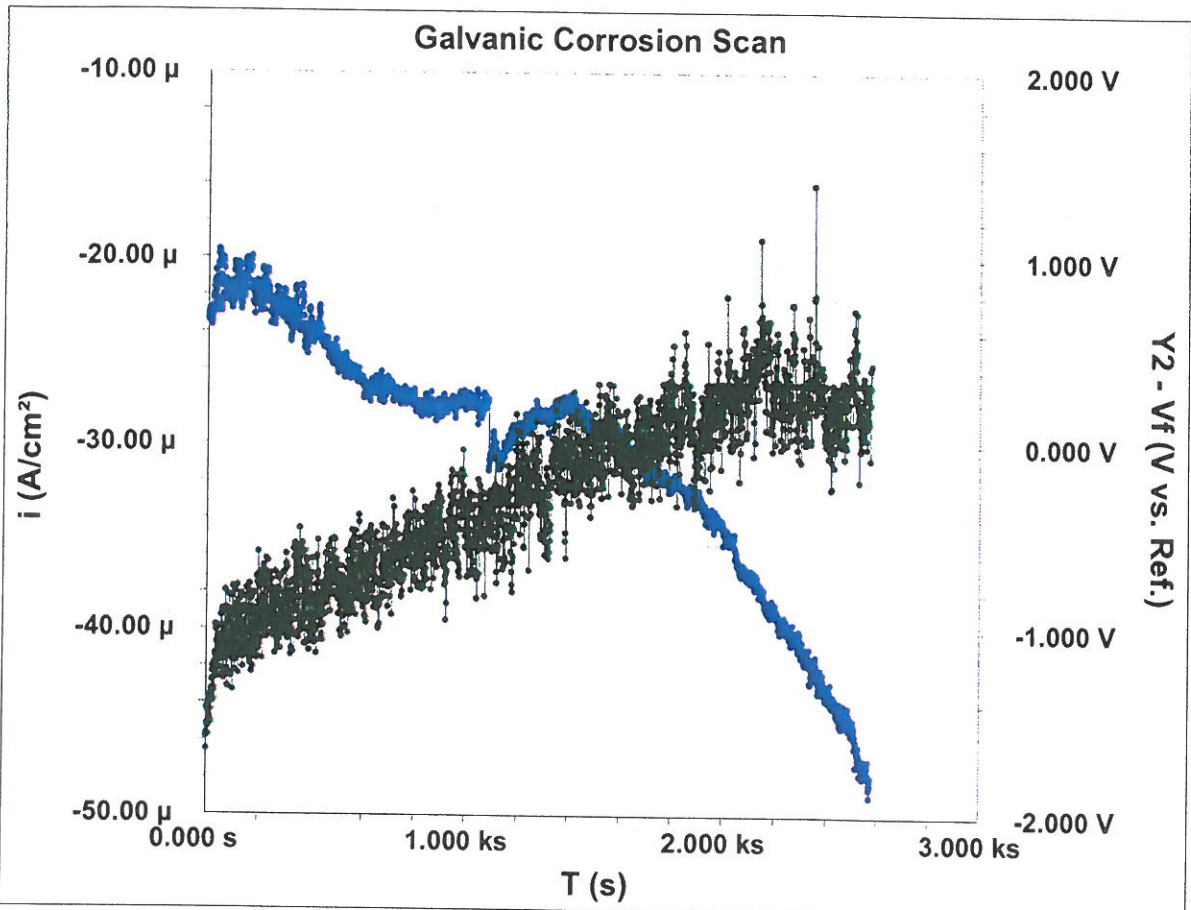


● CURVE (WELD E7018 -HAZ-GC-CO2-FEB8.DTA)

EXPERIMENTAL PARAMETERS

Run Time (s): 12000
 Galvanic Corrosion Scan
 2/8/2013
 13:20:30
 Limit i (mA/cm²): 1
 Sample Period (s): 1
 Sample Area (cm²): 0.3
 Density (gm/cm³): 7.87
 Equiv. Wt: 27.92
 Init. Delay: Off
 Open Circuit (V): -0.1188

EXPERIMENTAL NOTES

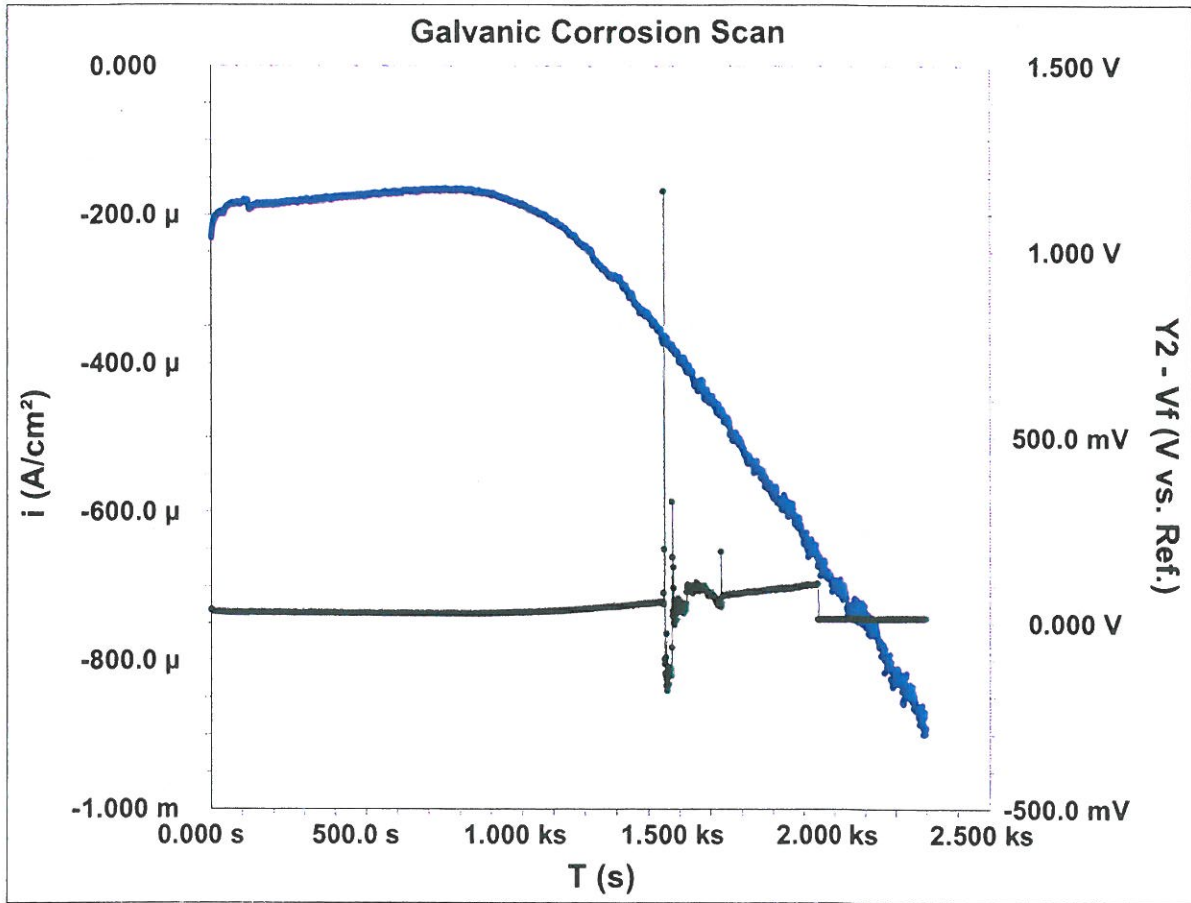


● CURVE (WELD E8018G-WELD-GC-CO2-FEB9-13.DTA)

EXPERIMENTAL PARAMETERS

Run Time (s): 12000
 Galvanic Corrosion Scan
 2/9/2013
 20:17:30
 Limit i (mA/cm²): 1
 Sample Period (s): 1
 Sample Area (cm²): 2.2
 Density (gm/cm³): 7.87
 Equiv. Wt: 27.92
 Init. Delay: Off
 Open Circuit (V): -1.72361

EXPERIMENTAL NOTES

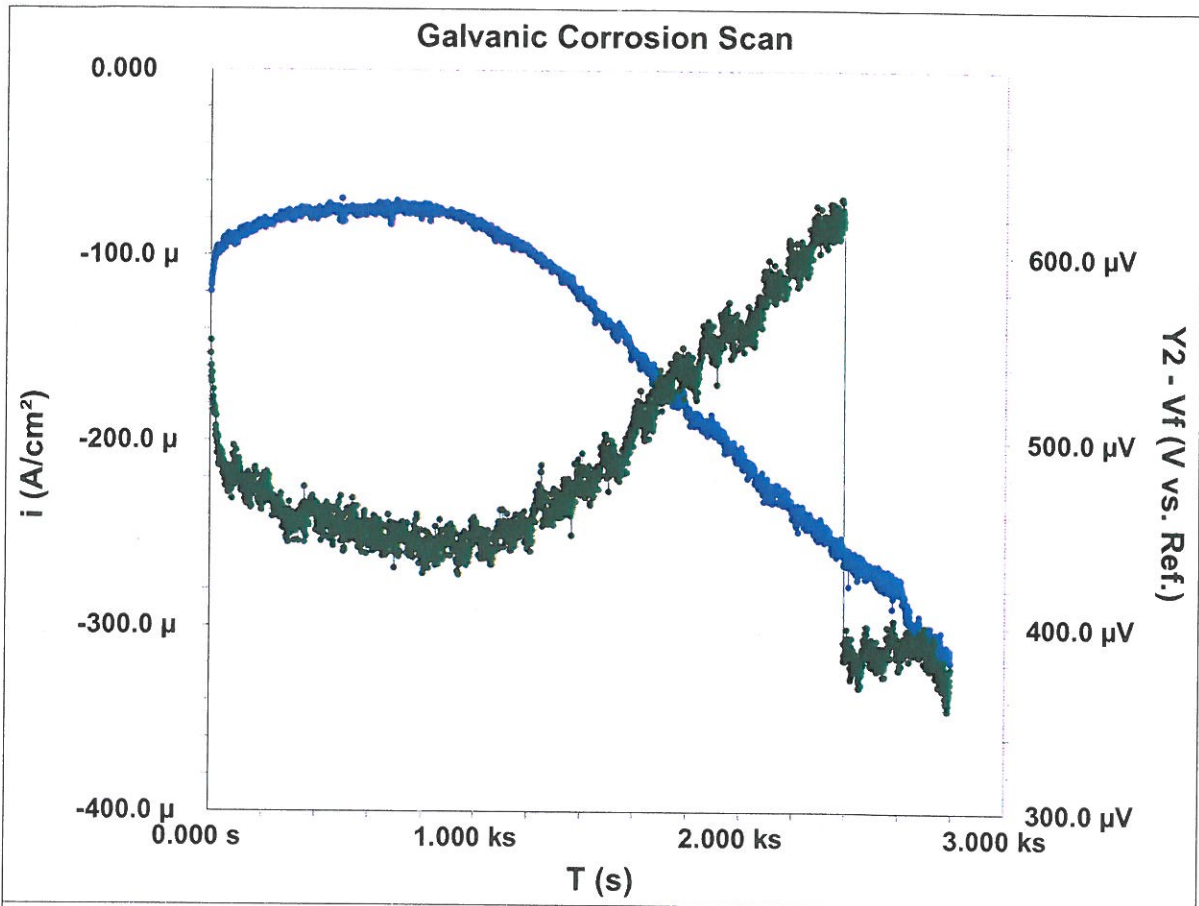


● CURVE (WELD E8018G HAZ-TEMP-CO2-GC-MAY5.DTA)

EXPERIMENTAL PARAMETERS

Run Time (s): 12000
 Galvanic Corrosion Scan
 5/5/2012
 18:42:59
 Limit i (mA/cm^2): 1
 Sample Period (s): 1
 Sample Area (cm^2): 0.8
 Density (gm/cm^3): 7.87
 Equiv. Wt: 27.92
 Init. Delay: Off
 Open Circuit (V): -0.000103

EXPERIMENTAL NOTES

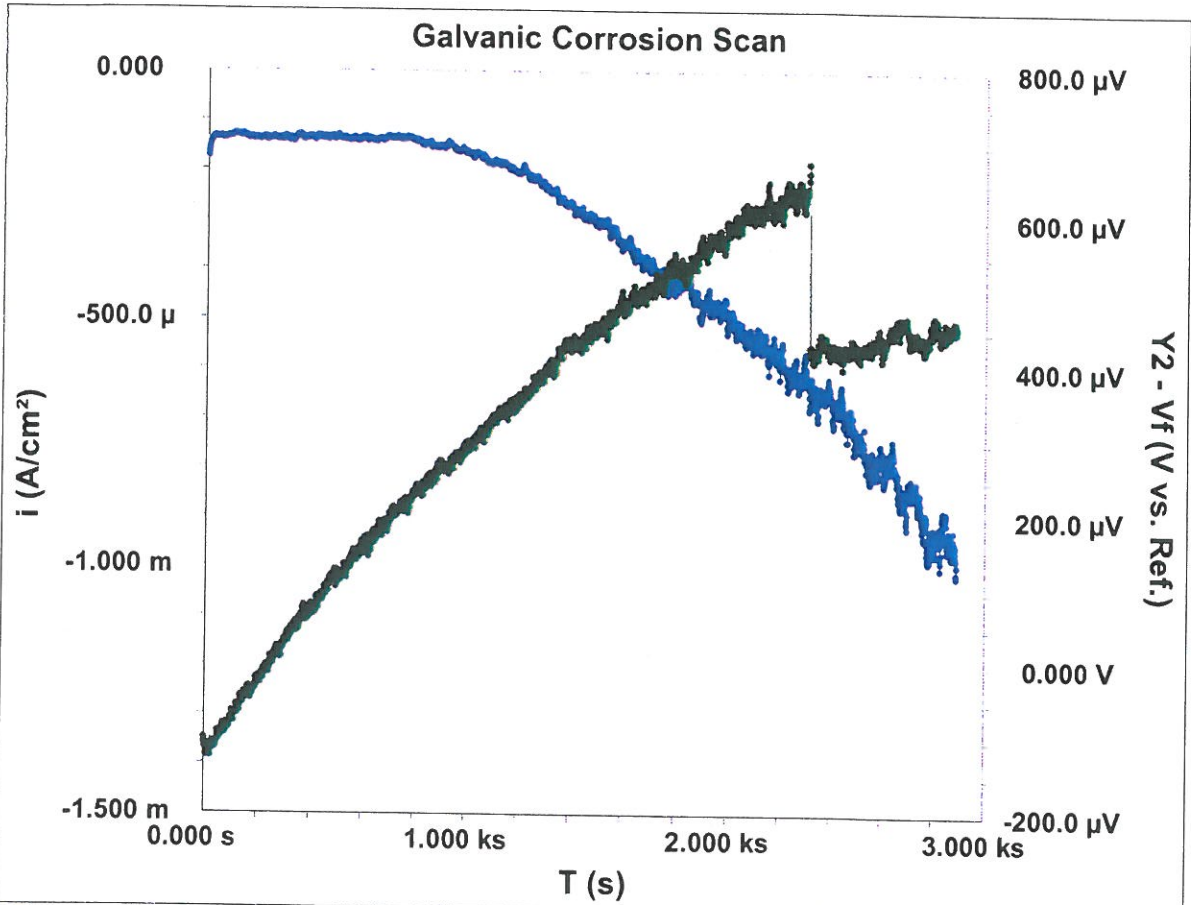


● CURVE (WELD E8018B2-CO2-TEMP-GC-MAY 11-run1.DTA)

EXPERIMENTAL PARAMETERS

Run Time (s): 12000
 Galvanic Corrosion Scan
 5/11/2012
 17:08:39
 Limit i (mA/cm^2): 1
 Sample Period (s): 1
 Sample Area (cm^2): 2
 Density (gm/cm^3): 7.87
 Equiv. Wt: 27.92
 Init. Delay: Off
 Open Circuit (V): 0.042626

EXPERIMENTAL NOTES

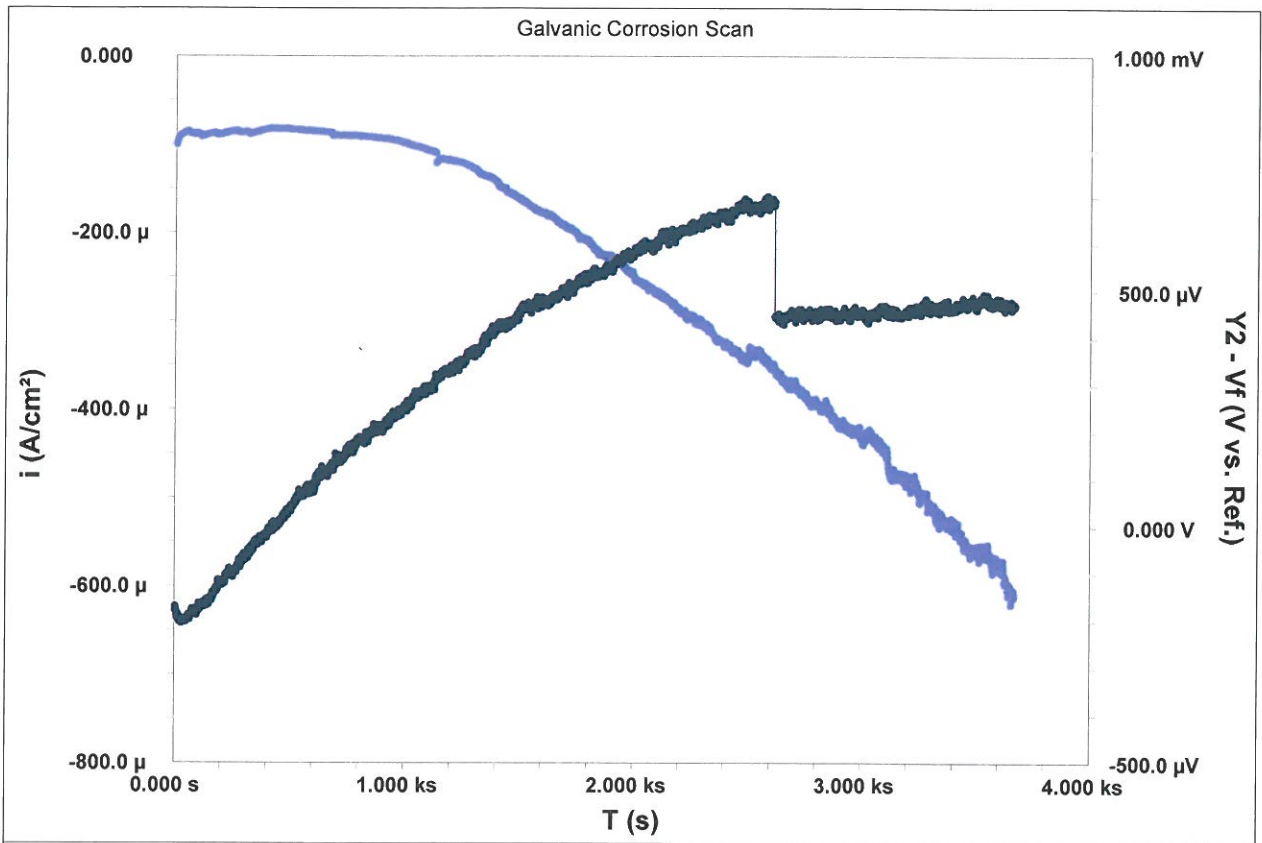


● CURVE (WELD E8018B2-CO2-HAZ-GC-MAY9-run1.DTA)

EXPERIMENTAL PARAMETERS

Run Time (s): 12000
 Galvanic Corrosion Scan
 5/9/2012
 16:52:43
 Limit i (mA/cm^2): 1
 Sample Period (s): 1
 Sample Area (cm^2): 0.8
 Density (gm/cm^3): 7.87
 Equiv. Wt: 27.92
 Init. Delay: Off
 Open Circuit (V): 0.024863

EXPERIMENTAL NOTES

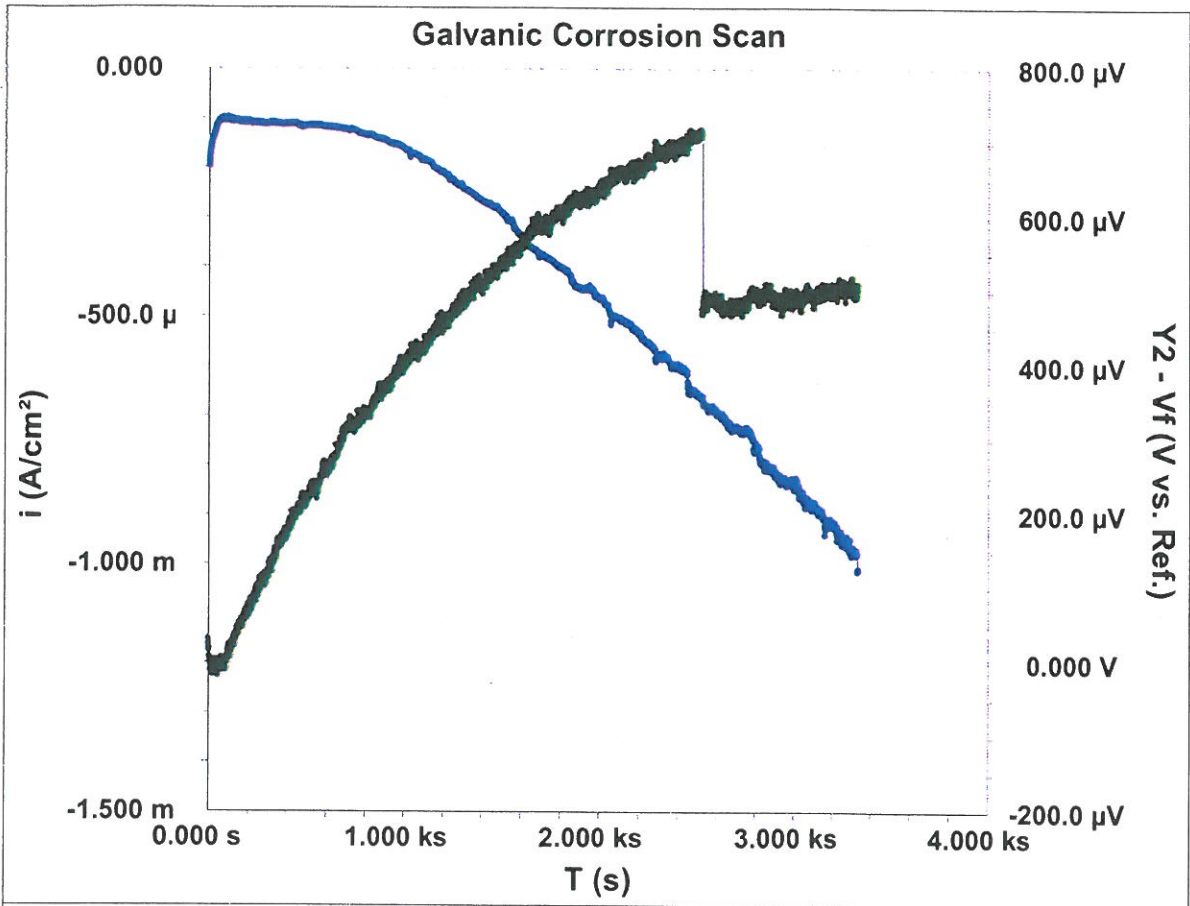


● CURVE (WELD E8018B6-CO2-TEMP-GC-MAY 12-run1.DTA)

EXPERIMENTAL PARAMETERS

Run Time (s): 12000
 Galvanic Corrosion Scan
 5/12/2012
 10:51:11
 Limit i (mA/cm^2): 1
 Sample Period (s): 1
 Sample Area (cm^2): 1.5
 Density (gm/cm^3): 7.87
 Equiv. Wt: 27.92
 Init. Delay: Off
 Open Circuit (V): 0.051517

EXPERIMENTAL NOTES



● CURVE (WELD E8018B6 REPEAT-GC-CO2-HAZ-MAY9-run1.DTA)

EXPERIMENTAL PARAMETERS

Run Time (s): 12000
 Galvanic Corrosion Scan
 5/9/2012
 11:37:54
 Limit i (mA/cm²): 1
 Sample Period (s): 1
 Sample Area (cm²): 0.8
 Density (gm/cm³): 7.87
 Equiv. Wt: 27.92
 Init. Delay: Off
 Open Circuit (V): 0.072712

EXPERIMENTAL NOTES

APPENDIX-C

POLYNOMIAL REGRESSION ANALYSIS CURVE FITTING GRAPHS

C1. POLYNOMIAL REGRESSION FOR GALVANIC CORROSION AT ROOM TEMPERATURE

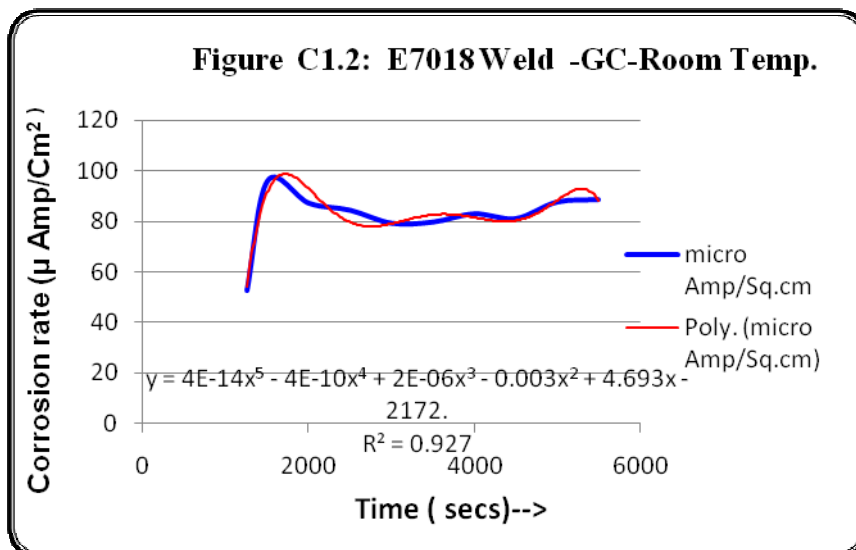
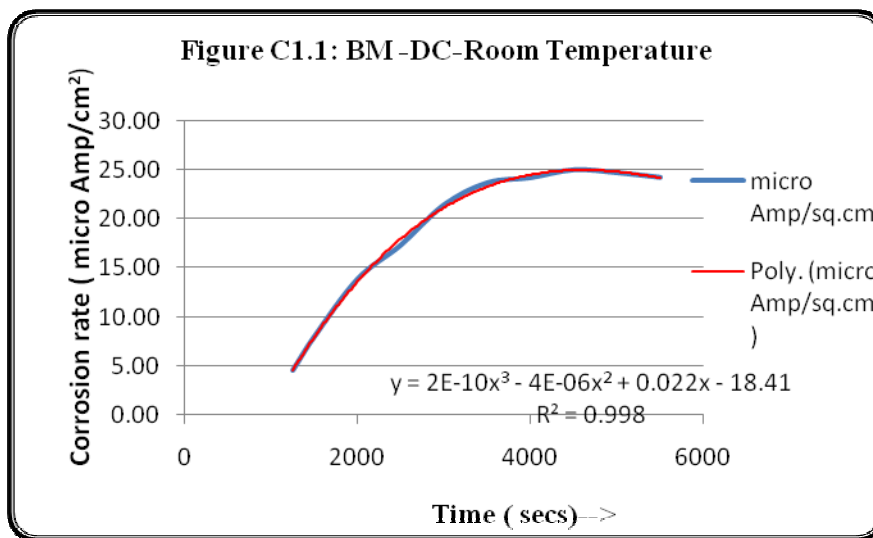


Figure C1.3: E7018 Weld HAZ -GC -Room Temp.

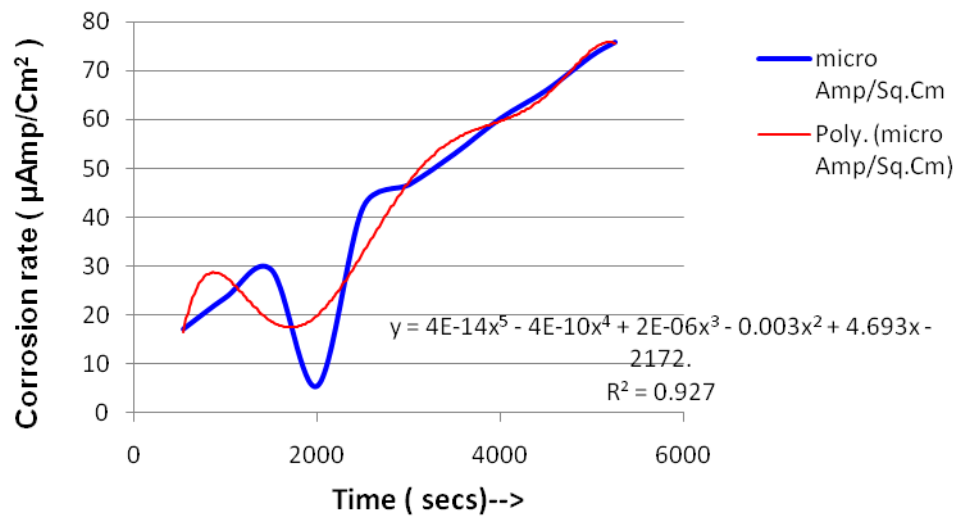


Figure C1.4: Weld E8018G -GC -Room Temp

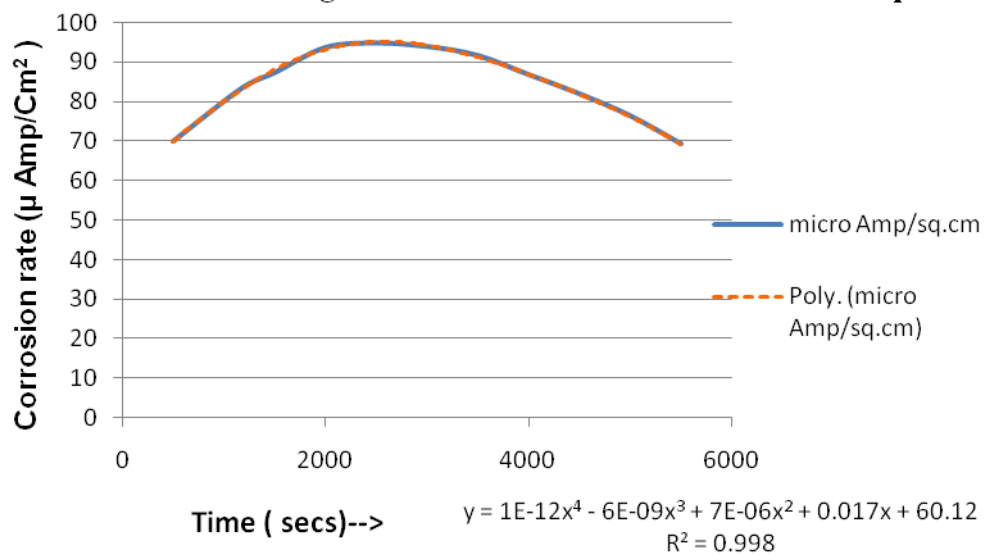


Figure C1.5: E8018G Weld HAZ-GC-Room Temp.

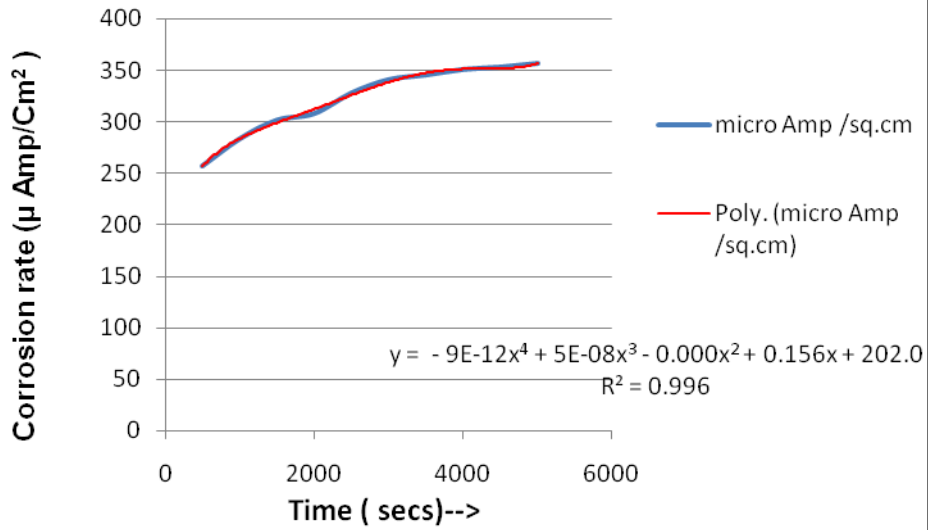


Figure C1.6: Weld E8018B2-GC -Room Temp.

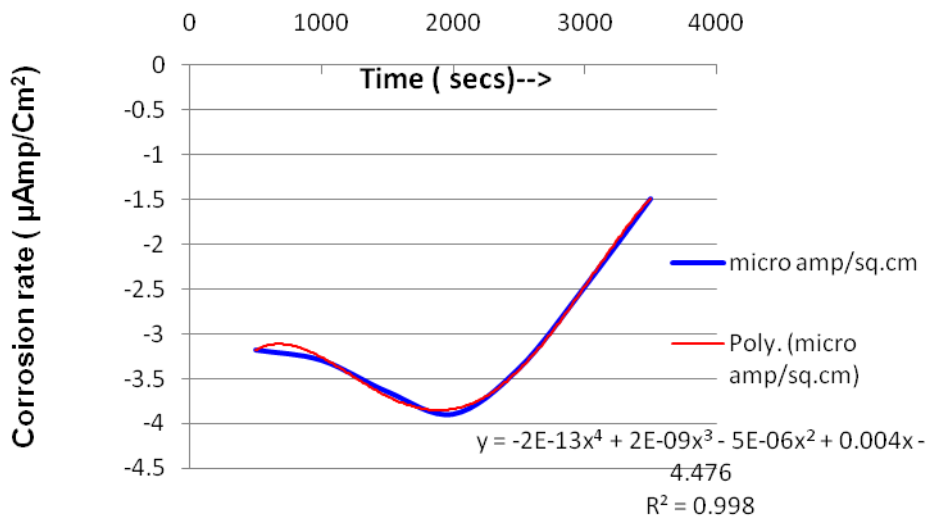


Figure C1.7: Weld No.E8018B2 HAZ -GC-Room Temp.

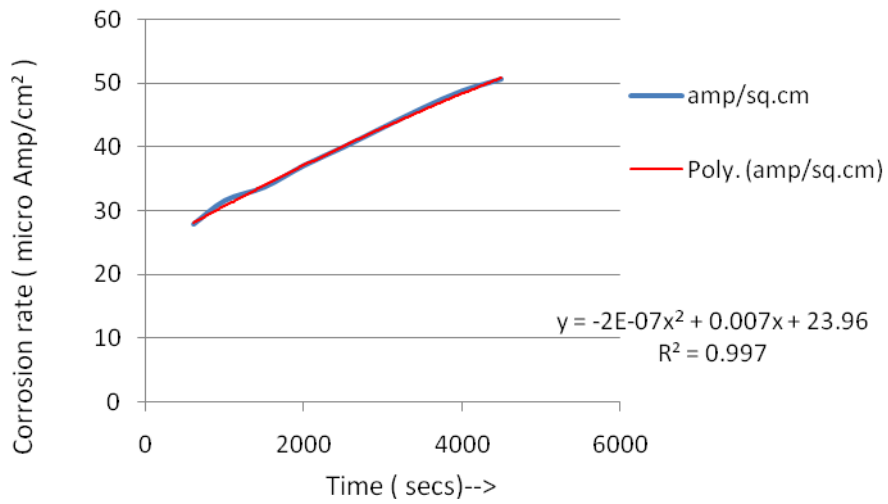


Figure C1.8: Weld E8018B6 -GC -Room Temp.

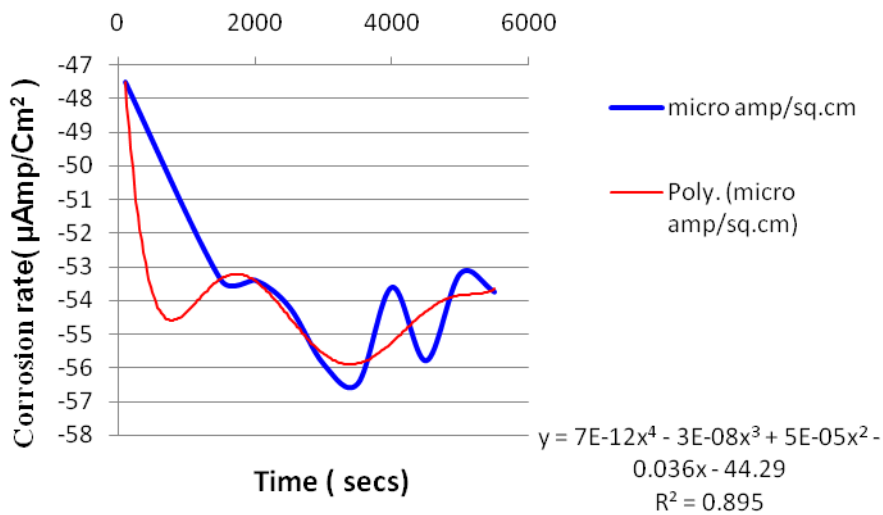


Figure C1.9: Weld E8018B6-HAZ-GC Room Temp.

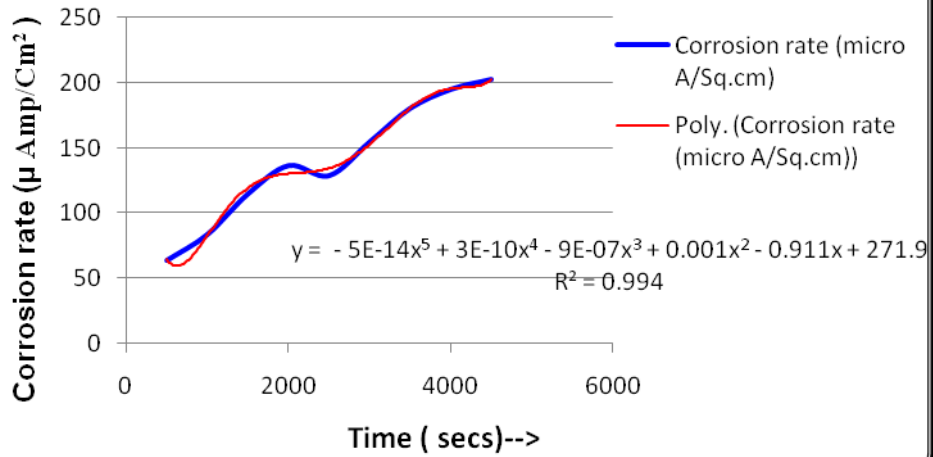
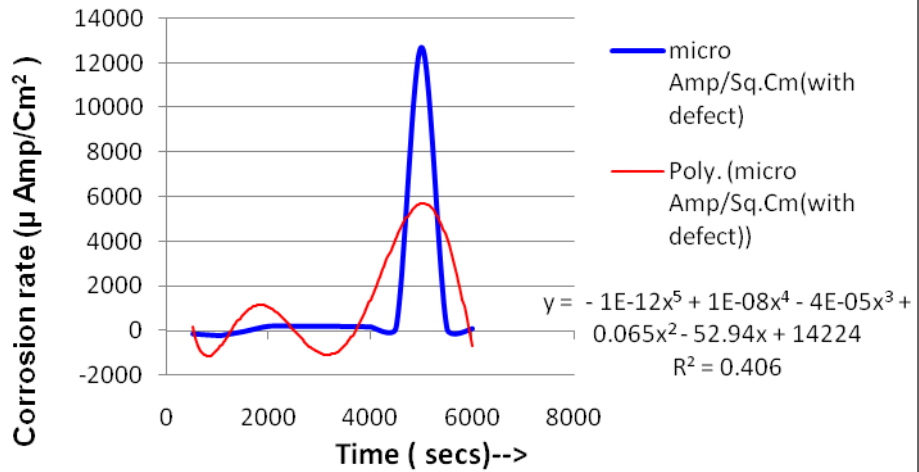


Figure C1.10: E7018 Weld HAZ GC -Room Temp.(with defect)



C2. POLYNOMIAL REGRESSION FOR GALVANIC CORROSION AT VARIOUS TEMPERATURES

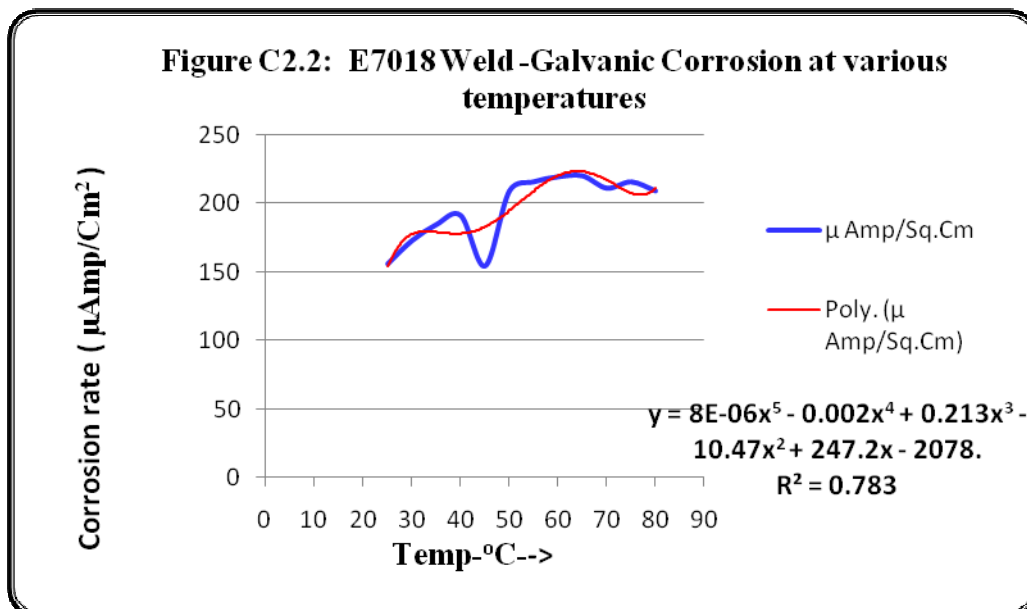
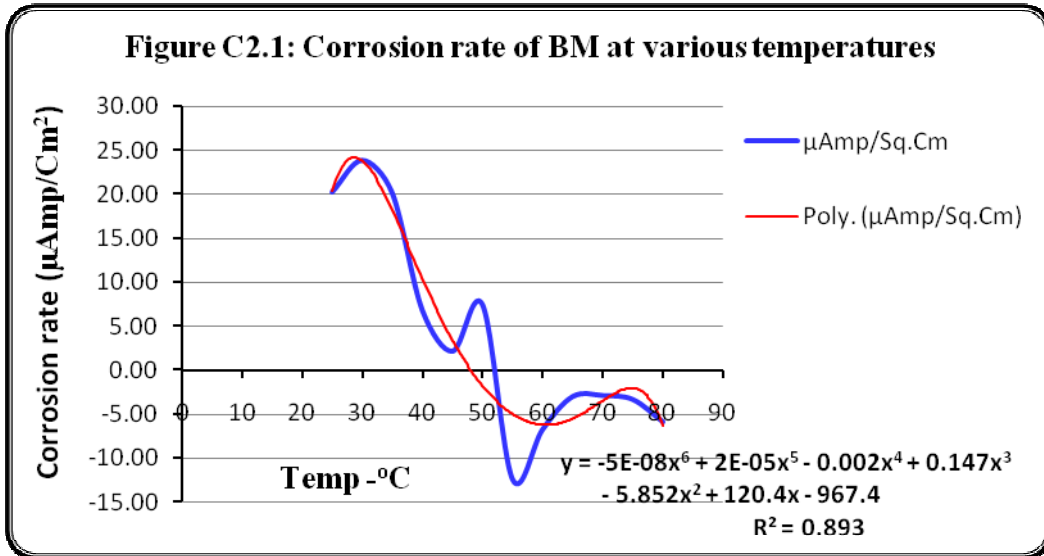


Figure C2.3: E7018 Weld HAZ -Galvanic Corrosion at Various Temp

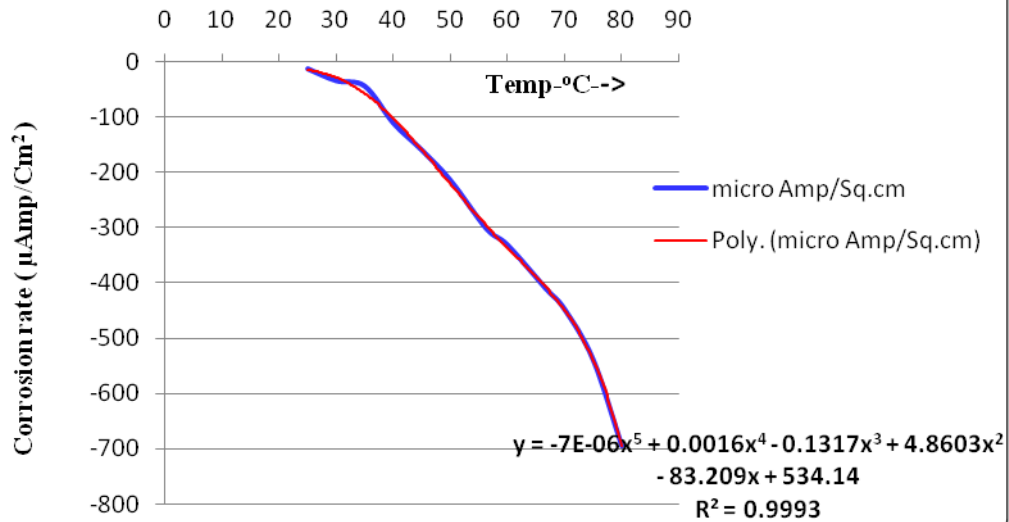
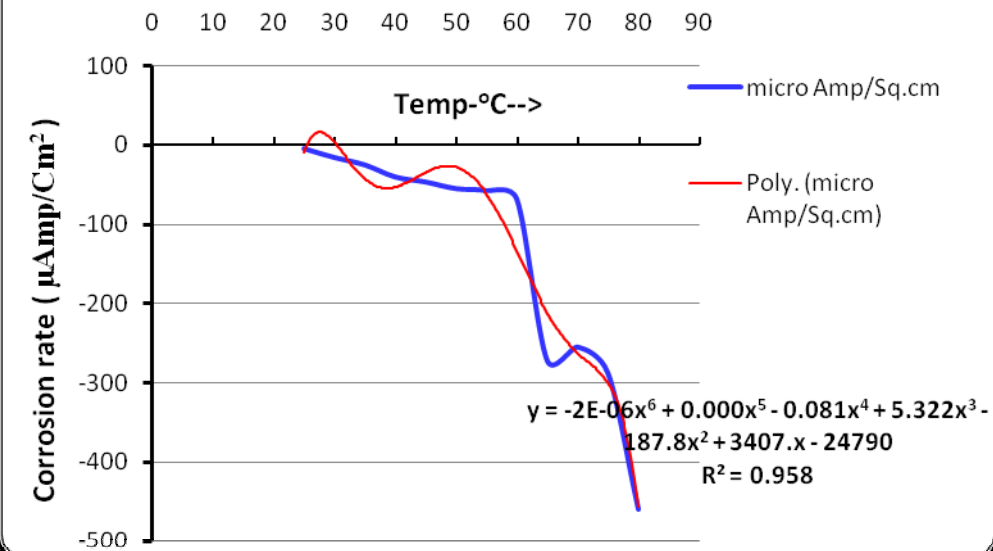


Figure C2.4: E8018G Weld Galvanic Corrosion at Various Temperatures



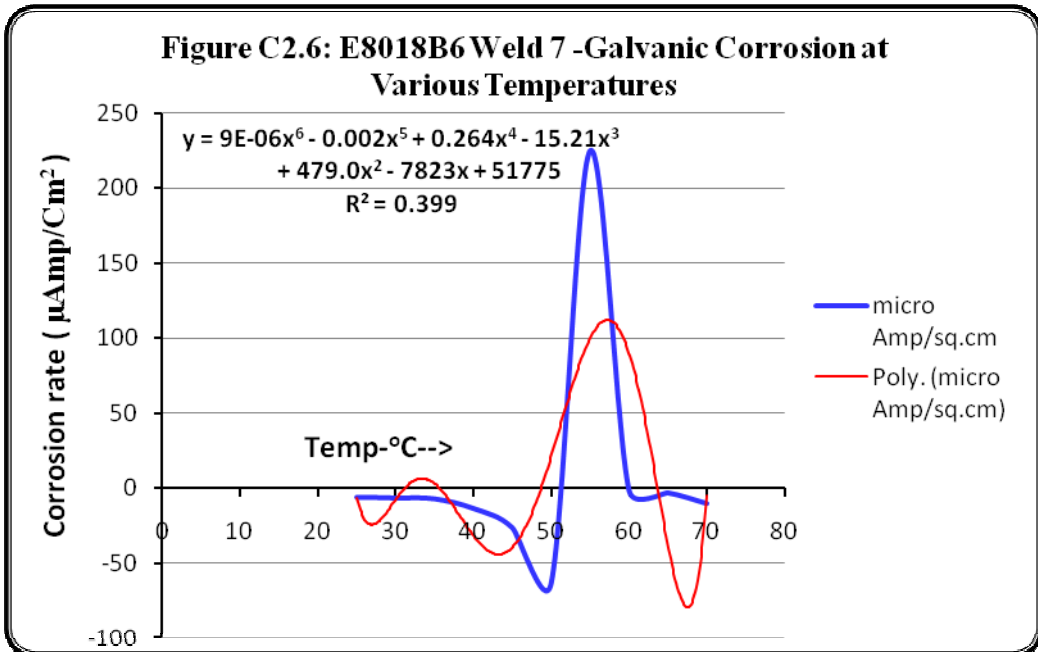
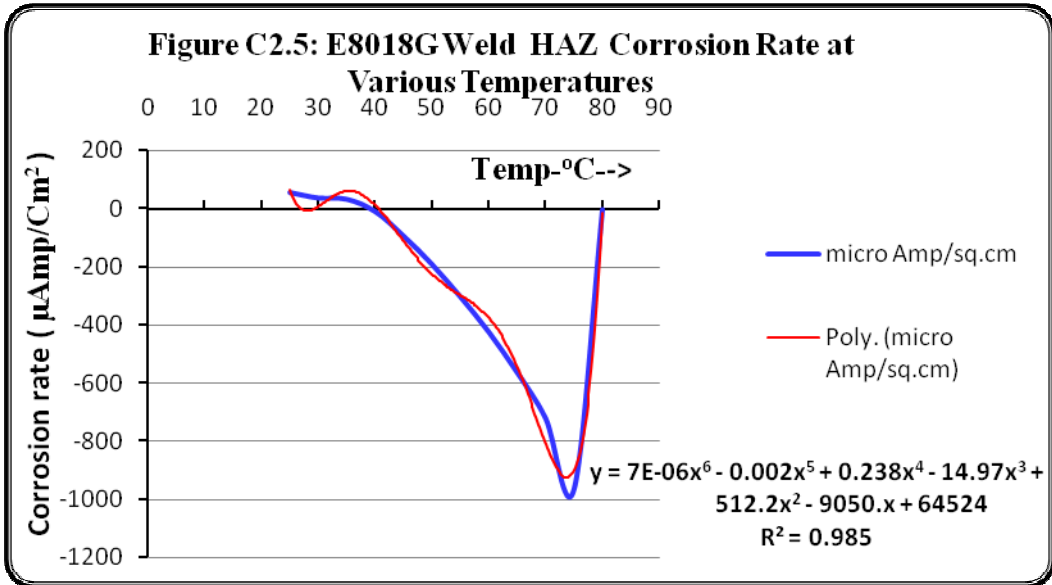


Figure C2.7: E8018B6 Weld HAZ -Galvanic Corrosion at Various Temperatures

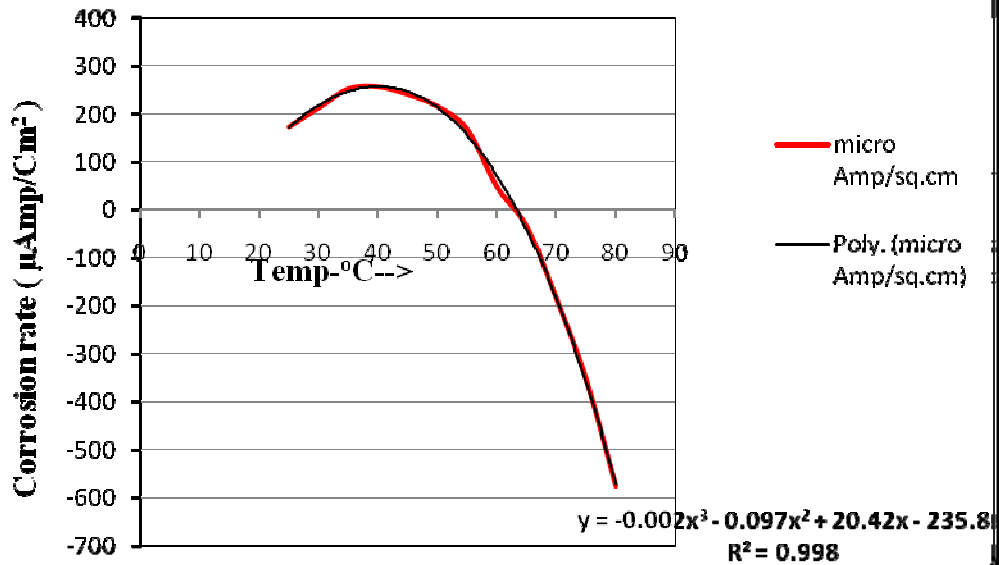


Figure C2.8: E8018B2 Weld Galvanic Corrosion at Various Temperatures

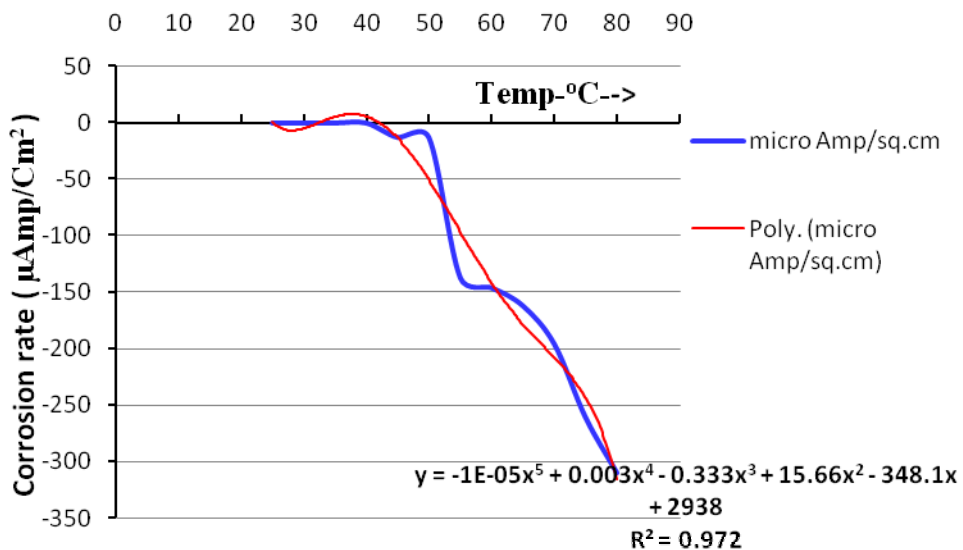
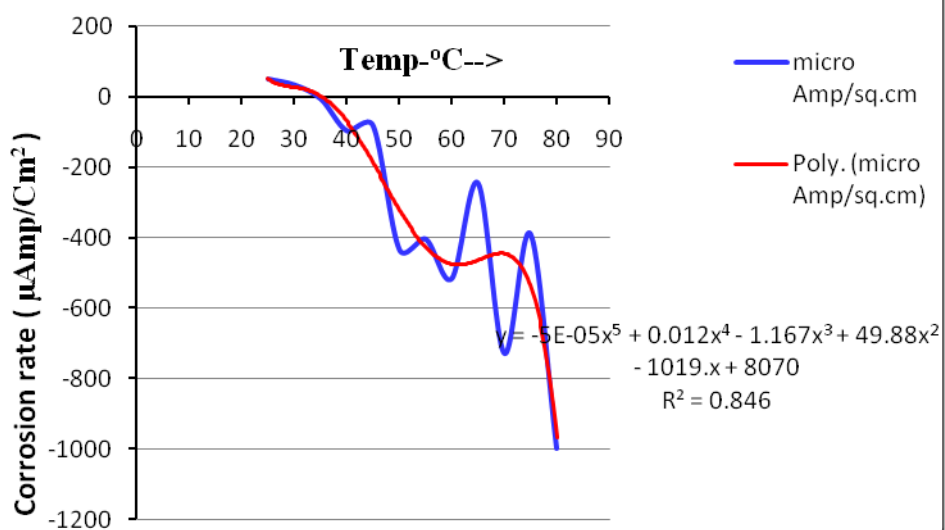


Figure C2.9: E8018B2 Weld HAZ Galavanic Corrosion at Various Temperatures



C3.POLYNOMIAL REGRESSION FOR GALVANIC CORROSION WITH CO₂ AT VARIOUS TEMP.

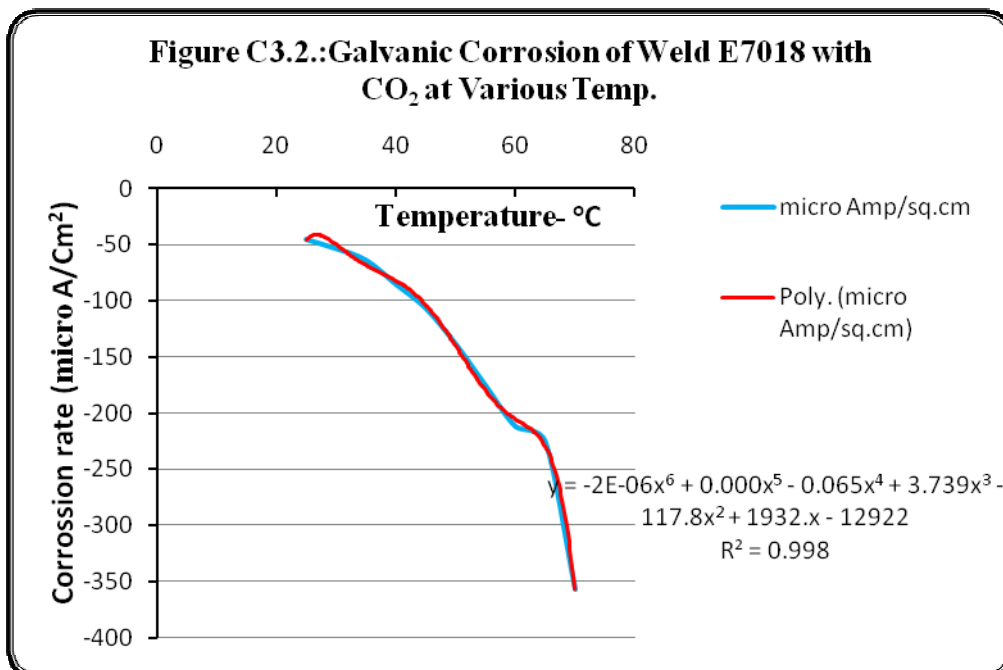
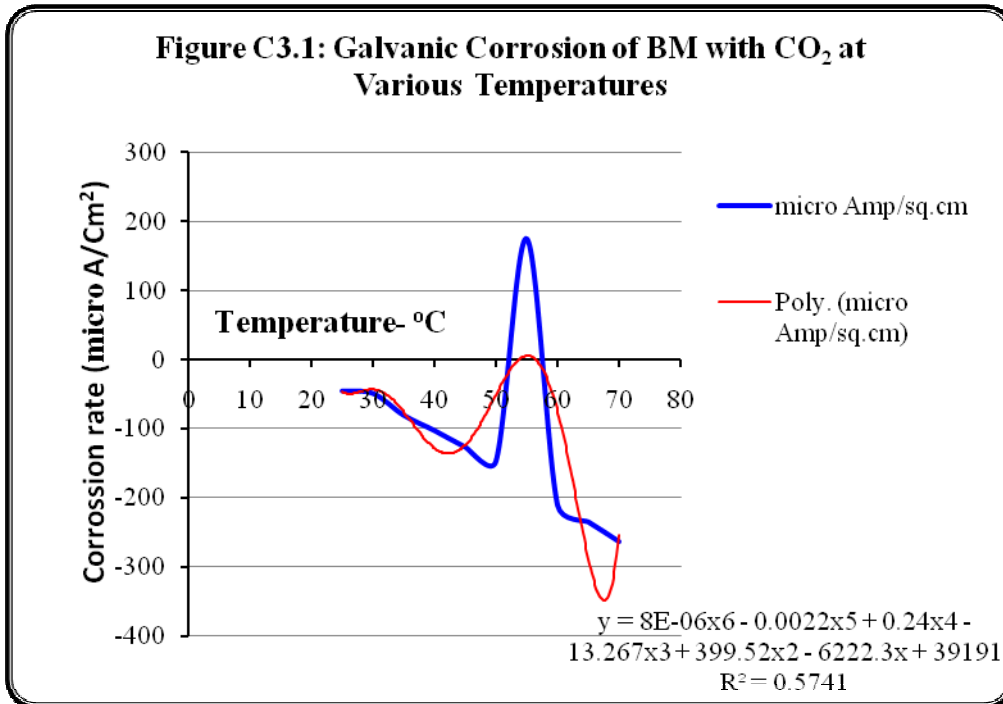


Figure C3.3: Galvanic corrosion of Weld E7018 HAZ with CO₂ at Various Temperatures

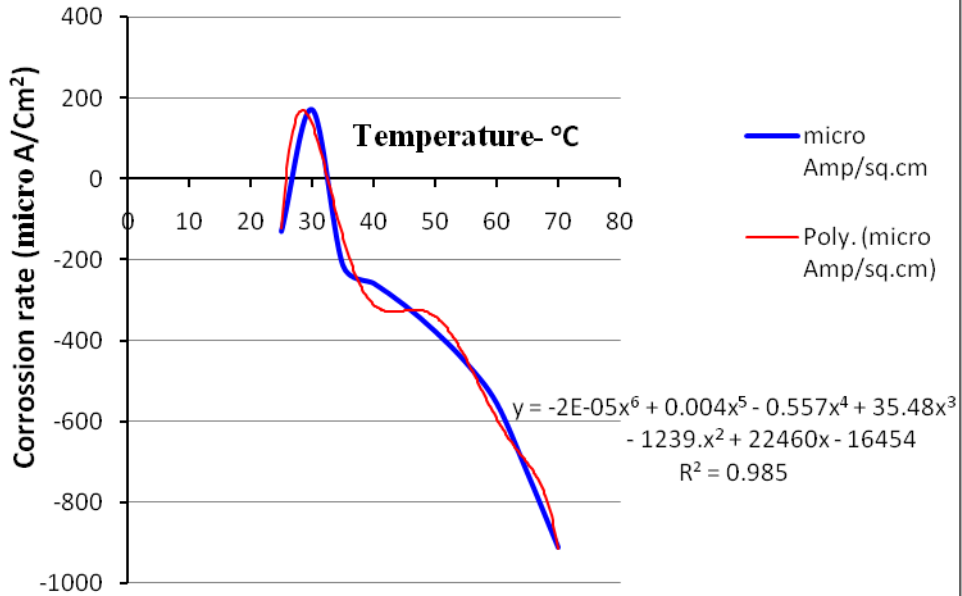


Figure C3.4: Galvanic Corrosion of E8018G Weld with CO₂ at Various Temperatures

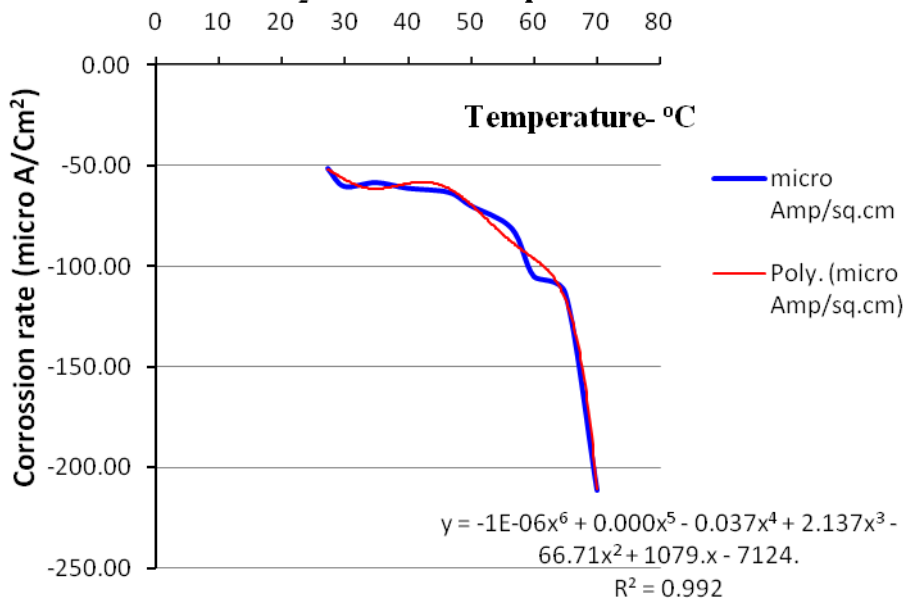


Figure C3.5: Galvanic Corrosion of E8018G Weld HAZ with CO₂ at Various Temperatures

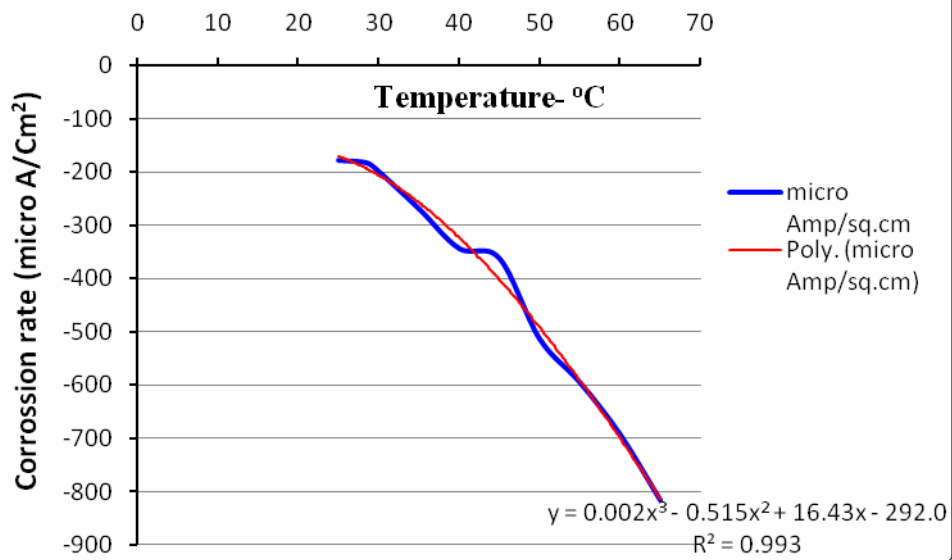


Figure C3.6: Galvanic Corrosion of E8018B6 Weld with CO₂ at Various Temperatures

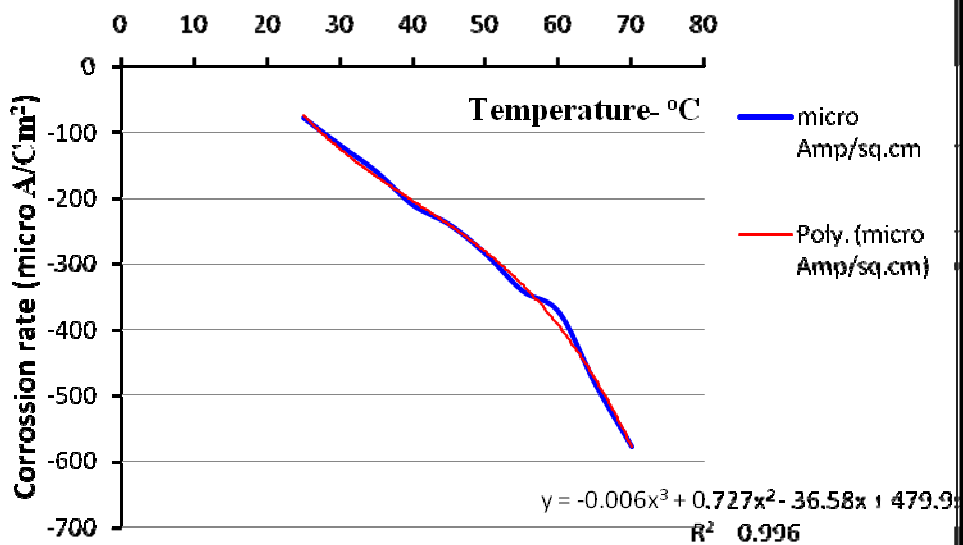


Figure C3.7: Galvanic Corrosion of E8018B6 HAZ with CO₂ at Various Temperatures

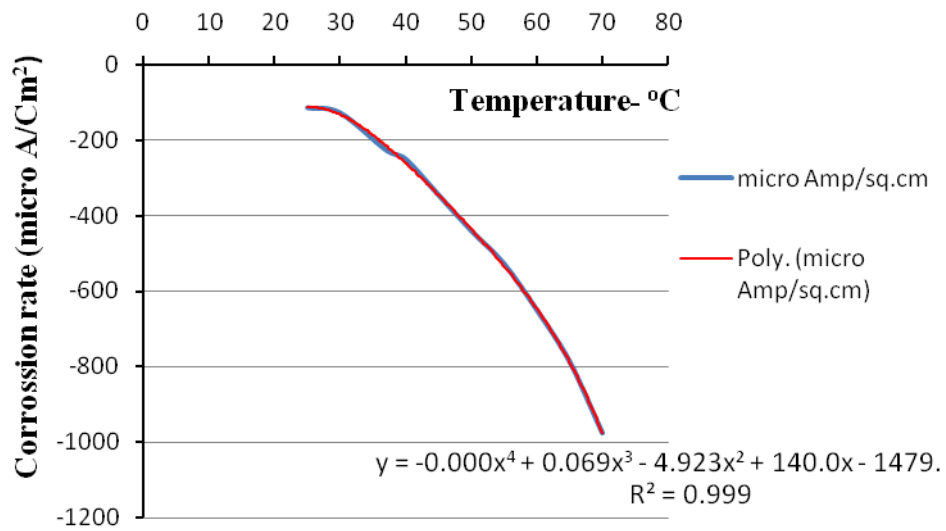


Figure C3.8: Galvanic Corrosion of E8018B2 Weld with CO₂ at Various Temperatures

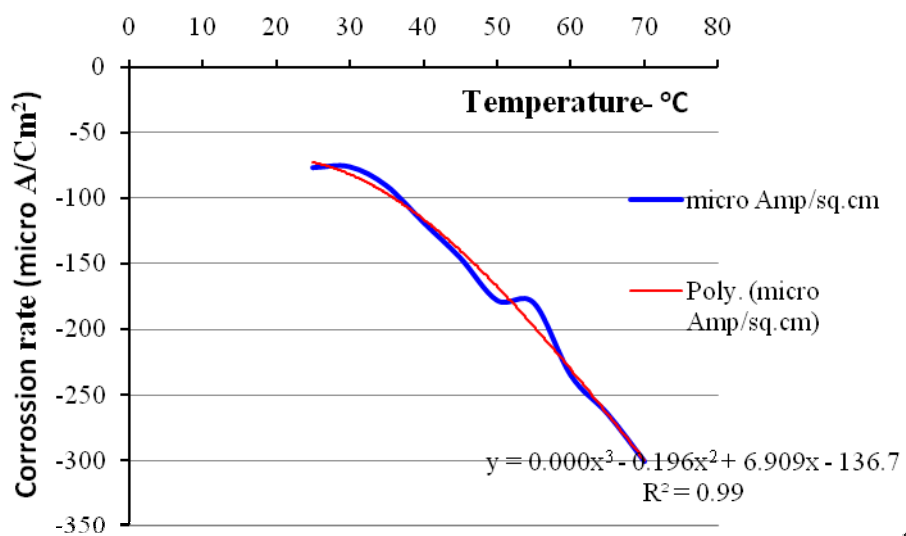
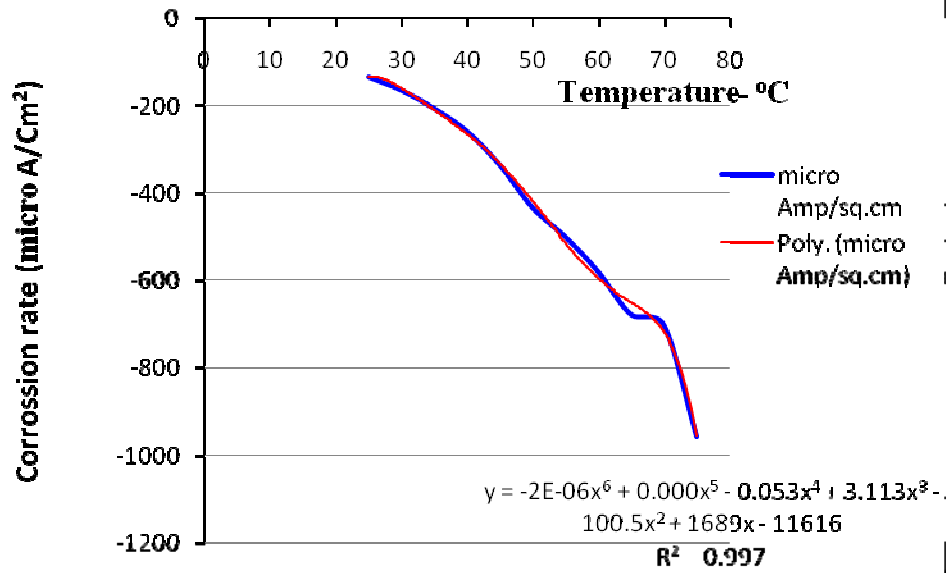


Figure C3.9: Galvanic Corrosion of E8018B2 HAZ with CO₂ at Various Temperatures



APPENDIX - E : SCHOLAR PROFILE



V. BALRAJ

EDUCATION:

1. **M.Sc.(Engg.)** : Master Degree in Welding
: Indian Institute of Science Bangalore, India.1990.
2. **B.E.(Mech.)** : Degree in Mechanical Engineering:
Madurai Kamaraj University, India.1979
3. **Diploma** : Welding Inspection Technologist
TWI / European Welding Federation, U.K.,2000

PROFESSIONAL CERTIFICATIONS

1. **NACE (USA)** : **Corrosion Specialist - P** - Cert.No.5558
Cathodic Protection Specialist- CP4.
Material Selection/Design Specialist
Protective Coating Specialist
Chemical Treatment Specialist
2. **Senior Welding Inspector: CSWIP 3.2.2:**
The Welding Institute-TWI(U.K)-C.No.1615/1
3. **ISO 9000-QMS AUDITOR:** BSI, DNV Certified.

EXPERIENCE

- 34 years of Industrial experience in Power (12 years) & OIL sector (22 years) related to Welding, Corrosion, Materials Selection and Design, Cathodic Protection design evaluation etc. Inspection/Testing, Non Destructive Testing, Coating, Quality assurance and Vendor evaluations by Technical and System audits.

TECHNICAL PAPERS PUBLISHED

1. Balraj Velu, G. Augustin, "CATHODIC DISBONDMENT TESTING – THE REALITY", *International Pipeline Coating Conference*, Dubai, April 2015.
2. Balraj Velu, Rajnish Garg, Mukesh Saxena and Paul Rostron, "WELDING CONSUMABLE ISSUES ON CORROSION OF X65QT STEEL ", *Material Performance, NACE International*, Vol.53, No.8, August, 2014.
3. Balraj Velu, Rajnish Garg and Paul Rostron, "EVALUATION OF WELD ROOT CORROSION OF X65QT MATERIAL", *International journal of Current Research*, Vol.5.Issue 04, pp871-875, April, 2013.
4. Balraj Velu et.al., "WELD METAL PROPERTIES ON CORROSION RESISTANCE OF MATERIALS FOR OIL AND GAS APPLICATIONS". *International Symposia on Joining of Materials-DEC. 2008, WRI/BHEL, Trichy, India.*
5. Balraj Velu et.al., "SURFACE TREATMENT APPLICATION IN OIL AND GAS INDUSTRY". *Surface TechWorkshop, IIT Madras- 2008.*
6. Balraj Velu, et.al., "EVALUATION OF WELD METAL PROPERTIES ON CORROSION RESISTANCE OF MATERIALS FOR OIL AND GAS APPLICATIONS", *IQPC- -4th Annual Corrosion Management Summit-Abudhabi,UAE, OCT-2009.*
7. Balraj Velu, et.al., "EVALUATION OF WELD ROOT CORROSION OF TYPE 316L STAINLESS STEEL". *Materials Performance, NACE INTERNATIONAL, USA, Aug. 2009.*
8. Balraj Velu, et.al., "FAILURE ANALYSIS OF STAINLESS STEEL PIPING IN AN OFFSHORE PLATFORM," *Materials Performance, NACE INTERNATIONAL, USA, MAY 2008.*
9. Balraj Velu et.al., "FAILURE ANALYSIS OF GLASS REINFORCED EPOXY (GRE) MATERIAL PIPING COMPONENTS". *Material performance, NACE INTERNATIONAL, USA- Feb. 2006.*
10. Balraj Velu, et.al. "EVALUATION OF SHIELDING GAS AND FLUX COMPOSITION EFFECTS ON WELD BEAD PROPERTIES", *Journal for the Joining of Materials, European Welding Institute, Vol. 4 (2) – 1992*

11. Balraj Velu et.al, "EFFECT OF SURFACE TENSION ON BEAD PROFILE FORMATION IN FLUX CORED ARC WELDING". *Symposium on Joining of Metals for 2000 AD (SOJOM) – 1991, India.*
12. Balraj Velu et.al. "STUDY ON SHIELDING GAS AND FLUX COMPOSITION EFFECTS ON WELD METAL PROPERTIES". **KEYWORDS** , *Welding Research Institute (India) Journal-, Vol. 12, No.2, 1990*
13. Balraj Velu et.al., "EFFECTS OF SHIELDING GAS AND FLUX COMPOSITION ON WELD METAL PROPERTIES." *National Welding Seminar, Bombay, India – 1990.*
14. Balraj Velu, "PULSED MIG WELDING OF STAINLESS STEEL WITH CONTROLLED METAL TRANSFER "*International Welding Seminar- Bombay, India, 1987.*